THE APPLICATIONS OF MAGNETIC METHOD IN ARCHAEOLOGICAL INVESTIGATIONS OF LEJJA PREHISTORIC SITE IN ENUGU STATE, SOUTH- EASTERN NIGERIA

By

OGAH, AREWA JAMES
B.Sc. (Physics), M.Sc. (Applied Geophysics)

PhD/Sc/08555/2006-07

Dissertation submitted to the School of Post Graduate Studies,
Ahmadu Bello University, Zaria

In partial fulfillment of the requirements for the Award of Degree of
Doctor of Philosophy in Applied Geophysics

Department of Physics, Faculty of Science
Ahmadu Bello University, Zaria, Nigeria

January, 2013

Dedication

To Mary and Praise

Declaration

I hereby declare that the work in this dissertation titled "THE APPLICATIONS OF MAGNETIC METHOD IN ARCHAEOLOGICAL INVESTIGATIONS OF LEJJA PREHISTORIC SITE IN ENUGU STATE, SOUTH-EASTERN NIGERIA" was performed by me in the Department of Physics, Ahmadu Bello University, Zaria, Nigeria, under the supervision of Prof. I.B. Osazuwa, Dr. P.O. Sule and Dr. M.K. Aliyu. The information derived from the literature has been dully acknowledged in the text and a list of references provided.

No part of this work has been presented for another degree at any institution.

_____ _____

Ogah, Arewa James

Certification

This project Dissertation titled "The applications of magnetic method in archaeological investigations of Lejja prehistoric site in Enugu State, south-eastern Nigeria" meets the regulations governing the award of the degree of Doctor of Philosophy (PhD) of the Ahmadu Bello University, and is approved for its contribution to knowledge and literary presentation.

_____ _____

Prof. I. B. Osazuwa — Date
Chairman, Supervisory Committee

_____ _____

Dr. P. O. Sule — Date
Member, Supervisory Committee

_____ _____

Dr. M. K. Aliyu — Date
Member, Supervisory Committee

_____ _____

Dr. U. Sadiq — Date
Head of Department

_____ _____

Prof. A. A. Joshua — Date
Dean, School of Postgraduate Studies

Acknowledgements

I give glory to the Almighty God for the gift of life, and for protecting me throughout the years that I have been on the road for the sake of this Degree.

I am very grateful to my major supervisor, Prof. I. B. Osazuwa who initiated the research in archaeological geophysics, and who has made huge technical contribution to the progress of the research. I appreciate you also, for devoting enough time to read and correct the original manuscript. May the Lord bless you, Sir. My second supervisor, Dr. P. O. Sule, you are highly appreciated for taking so much pain in going through this work page by page and line by line. May the Lord grant you special favour, in Jesus name. I appreciate you, Dr. M. K. Aliyu for accepting to be part of the leadership role in uniting Physics and Archaeology. Thanks for your words of encouragement. May God bless you also for being my 'land-lord'.

Dr. Kolawole M. Lawal, the man who was accessible to me for almost 24 hours, January to December of all the years that I spent in A.B.U., who gave me some ideas in numerical analysis and in computer programming, you are highly appreciated. May God bless you and your entire family. Dr. Sadiq, my Head of Department and my friend, you are highly appreciated for your understanding, assistance in one way or the other and for your concern for me and my family down home. May God also bless your own family. I appreciate you also for your wonderful words of encouragement. God bless you.

My Head of Department at the Kogi State University, Prof. S.X.K. Howusu, I appreciate you for your friendly attitude and for your understanding and assistance in one way or the other. May the Lord bless you and your family. Prof., Sir, you are more of a brother than a colleague, and may the Lord reward you for your labour of love. I also wish to use this medium to appreciate your staff, my colleagues in the Department of Physics at the Kogi State University, that you have used to assist me throughout this programme. Mr. J. Funso, Dr. Adeoye, Mrs I. Sule, Mr. S. O. Onoja, Mr. Kingsley Omatola and Mr. E. Okeme, I appreciate you all for accepting extra load from time to time as the needs arose. God bless you all.

I at this point wish to appreciate the Vice Chancellor, Kogi State University, Anyigba for approving the purchase of the proton precession magnetometer that was used for the field work. God bless you, Sir.

I wish to sincerely thank Mr. Elias Ogah, Mr. Theophilus Acholo, Mr. Robert Onubi and Master Enejo Ogah who worked tirelessly with me throughout the period of data acquisition in Lejja Community. I pray that not only will God pave way for you to also go for postgraduate studies but He will also give you the needed help to easily complete your programmes within the stipulated time. I highly appreciate every one of you.

I, at this point, acknowledge all my lecturers in the Department of Physics at the Ahmadu Bello University, Zaria for the good time spent together at seminars and for your constructive criticisms that spurred me to work harder. In this regard I appreciate you, Dr. A. Aminu, Dr. P. Akuso, The PG Coordinator, Physics Department, in person

of Dr. Y. Zakari and the Director, Centre for Energy Research and Training (CERT), in person of Dr. B. B. Dewu. Sirs, God bless you all.

I wish to highly appreciate some academic staff of the University of Nigeria Nsukka who were of great help to us before and during the period of field work. They are: (i) Dr. C. C. Opata of the Department of History who negotiated with the Community Leaders on our behalf. He never complained over my short and frequent notices requesting him to accompany me, or my exploration team, to the village throughout the period of about two years used for the field work. May the Lord reward you, Sir. (ii) Prof. J. O. Urama, the Head of Physics and Astronomy initiated my first visit to Lejja and offered all assistance necessary to keep the field work going. God bless you and your family, Sir. (iii) Dr. (Mrs) P. Eze-Uzomaka, the Head of Department of Archaeology, was in contact with us throughout the period, encouraging us and helping us to keep our gradiometer boxes in their house. May the Lord bless you and your family. We also appreciate her husband, Prof. Eze-Uzomaka for the assistance. (iv) I also appreciate Dr. P. O. Ezema for his moral support and entertainment during the period of the data acquisition.

I am indebted to some families here in Zaria who have made my stay very lively. These are (i) Dr. and Dr. (Mrs) J. Ukoje and family, (ii) My friend, Dr. E. A. Bala and family, and (iii) My 'Land-lord', Mr. Z. Ugbaje and family. May the Lord bless you all far beyond your imaginations.

I appreciate with thanks, the sponsorship provided by the Petroleum Technology Development Fund (PTDF) and the International Programmes in the Physical Sciences (IPPS), Sweden that facilitated my studies here in A.B.U., Zaria.

Finally, I appreciate my beloved wife, Mrs Mary E. Ogah, and my love, Praise, for their enduring prayers and patience. Chief S.U. Ogah, my brother and "my father", please, accept my apology for reacting lately to that which you asked me to do many years ago. The Lord will give you part of your reward here on earth, and the rest in the world to come.

ABSTRACT

The search for historic evidence in Lejja has been conducted using data acquired from sites measuring 2,160m^2, 2,030m^2 and 2,400m^2 in Uwani, Ugbelenabo and Ejuona villages respectively. The total magnetic field data and the vertical gradient of the total field data were acquired simultaneously on a regular 1 m x 1 m grid using proton precession magnetometer (Geometrics model G-856AX). The measured fields were stored in the machine's internal memory and directly downloaded into a digital computer thereby avoiding transcription errors. The total field data were reduced using polynomial fitting method for diurnal correction while regional-residual separation was done using the golden software, surfer. This method of diurnal correction is one out of the two modifications made (in the course of this study) to the existing method of land magnetic data reduction. Integrated method of interpretation was deployed using Euler deconvolution and analytic signal methods which were validated using synthetic fields. The synthetic data were generated using Rao and Babu Algorithm. Both methods of interpretation gave error margin of about ±5% with the synthetic data. Analysis of the field data from the three sites revealed that some of the artefacts still remain in situ while others have been displaced as revealed by the orientations of their anomalies. The artefacts which include furnaces, slag blocks, blooms, tuyères, fired pits, etc., are mostly found in Ejuona and Uwani villages located in south-eastern and the central parts of the community respectively. Two types of smelting furnace are suspected. These include a small type with diameter of about 1.0 metre or less mapped in Uwani, and a large one with diameter between 1.2 and 1.5 metres also mapped in Ejuona. A large mound of an estimated area of about 70 m^2 has also been mapped in Ejuona village. The spatial locations of the above ancient relics at the three sites have been obtained. A few of the relics including fired pits and fired stones suspected at the Ugbelenabo village can be found at shallow depths of between 0.62 m and 0.86 m. On the other hand, the depth of burial of the artefacts at Uwani and Ejuona villages are relatively greater than those of Ugbelenabo. The ranges are from 1.07 m to 2.09 m, and from 1.08 m to 1.82 m in Uwani and Ejuona villages respectively. Due to small sizes of the survey sites, longitude-latitude coordinates of only the origin of each site has been indicated with surface locations of the artefacts measured from this point. Excavation plans which can serve as bases for further studies have been drawn up for the three locations surveyed. It is expected that successful execution of the latter will serve as an encouragement for the practice of archaeological geophysics in the Lejja site and beyond. In addition to the polynomial fitting method mentioned earlier, single step approach of magnetic data reduction tagged, "Automatic Reduction of Magnetic Data (ARMAD)", was also introduced in the course of this study. The latter method by-passes the conventional multi-stage method of magnetic data reduction.

.

TABLE OF CONTENTS

Contents	**Page Number**
Title page	i
Dedication	ii
Declaration	iii
Certification	iv
Acknowledgement	v
Abstract	viii
Table of contents	x
List of Figures	xv
List of Tables	xix
List of Appendices	xx
CHAPTER 1	1
GENERAL OVERVIEW	1
1.1 THE SEARCH FOR ARTEFACTS	1
1.2 ARCHAEOLOGY IN SOUTH-EASTER NIGERIA	2
1.3 APPLICATIONS OF GEOPHYSICS IN ARCHAEOLOGICAL STUDIES	5
1.3.1 The Magnetic Methods in Archaeological Geophysics	6
1.3.1.1 The Technique of Soil Magnetism	7
1.3.1.2 The Magnetometer Survey Method	8
1.4 THE PRESENT STUDY	10
1.5 DESCRIPTION OF THE SITE	11
1.5.1 The Landform of the Study Area	13
1.5.2 Geology of the Study Area	14
1.6 AIM AND OBJECTIVES OF THE STUDY	15
CHAPTER 2	17
THEORETICAL BACKGROUND	17
2.1 BASIC CONCEPTS OF MAGNETIC PROSPECTING	17
2.1.1 Magnetisation in Materials	20
2.1.2 Magnetic Field Intensity	21

2.1.3 Magnetic Susceptibility 22

2.1.4 Estimate of Magnetic Effect 24

2.2 CLASSIFICATION OF MAGNETIC MATERIALS 25

2.2.1 Diamagnetic Materials 25

2.2.2 Paramagnetic Materials 25

2.2.3 Ferromagnetic Materials 26

2.2.4 Anti-ferromagnetic Materials 27

2.2.5 Parasitic Ferromagnetic Materials 27

2.2.6 Ferrimagnetic Materials 28

2.3 REMANENT MAGNETISATION IN ROCKS 28

2.4 THE GEOMAGNETIC FIELD 30

2.4.1 The Magnetic Field of Internal Origin 32

2.4.2 The Magnetic Field of External Origin
32
2.5 THE MAGNETIC ANOMALY 33

CHAPTER 3 36

DATA ACQUISITION 36

3.1 INTRODUCTION 36
3.2 INSTRUMENTATION 36
3.2.1 The G-856AX Proton Precession Magnetometer 37
3.2.2 The Features and Applications of the G-856AX Magnetometer 38
3.2.3 The Magnetometer Sensor 40
3.2.3.1 Filling the Sensor with Sensor Fluid 42
3.2.3.1 Sensor Orientation 42
3.2.4 Gradiometeter Assembly 44
3.2.5 Console Control and Display 45
3.2.6 Operating Procedures of the G-856AX 46
3.3 DATA RETRIEVAL 49
3.3.1 Computer Connection and Download 50
3.4 GETTING THE SITES AND THE INSTRUMENT
READY FOR DATA THE ACQUITION 50

3.4.1 Setting Up the Gradiometer Assembly 51
3.4.2 Site Scanning With the Magnetometer 53
3.4.3 Establishing the Grid 54
3.5 MAGNETIC DATA ACQUISITION 56
3.5.1 The Base Station 57
3.5.2 The Data Collection 58
3.6 DOWNLOADING DATA FROM CONSOLE MEMORY 60
CHAPTER 4 62
FORWARD COMPUTATION OF MAGNETIC
ANOMALY OF A 3-DIMENTIONAL BODY 62
4.1 INTRODUCTION 62
4.2 THE FORWARD METHOD 63
4.2.1 Computation of the Magnetic Anomalies 67
4.3 INVERSION OF THE SYNTHETIC DATA 71
4.3.1 Euler Deconvolution Method 70
4.3.1.1 *Application of the Euler Method to the Single-Body Model* 73
4.3.1.2 *Application of the Euler Method to the Multiple Source Models* 75
4.3.2 Analytic Signal Method 78
4.3.2.1 *Application of the Analytic Signal*
Method to the Single-Body Model 81
4.3.2.2 *Application of the Analytic Signal*
Method to the Multiple-Body Models 85
4.4 THE APPLICATION OF THE UPWARD CONTINUATION 89
CHAPTER 5 92
DATA PROCESSING AND INTERPRETATIONS 92
5.1 INTRODUCTION 92
5.2 DATA SORTING AND DESPIKING 93
5.3 DATA REDUCTION 96
5.3.1 The Diurnal Correction 97
5.3.1.1 *The Least-Squares Approach* 98
5.3.1.2 *Test of Significance of Error Improvement* 100
5.3.1.3 *Calculation of the Diurnal Variation* 104
5.3.1.4 *Graphical Display of the Diurnally Corrected Field* 104
5.3.2 Regional-Residual Separation 106
5.3.3 Automatic Reduction of Magnetic Data (ARMAD) Method 109
5.3.3.1 The *ARMAD Methodology* 110
5.4 DETERMINATION OF THE LOCATION OF THE ARTEFACTS 114
5.4.1 The Application of the Euler Deconvolution Method 113

5.4.1.1 *Determination of Optimal Window Size and Estimation*
of Shapes of Magnetic Anomaly Sources 116

5.4.1.2 *Determination of Spatial Locations of Magnetic*
Sources Using Euler Deconvolution Method 118
5.4.2 Application of Analytic Signal Method 121
5.5 SITE BY SITE DISCUSSION OF RESULTS 127

5.5.1 Uwani Site 129
5.5.2 Ugbelenabo Site 134
5.5.3 Ejuona Site 137
CHAPTER 6 142
DISCUSSION AND CONCLUSION 142
6.1 DISCUSSION 142
6.2 CONCLUSION 147
6.3 SUGGESTIONS FOR FURTHER WORK 150
R E F E R E N C E S 153
A P P E N D I X A 162
A P P E N D I X B 188
A P P E N D I X C 196

List of Figures

Contents **Page Number**

Fig. 1.1: Excavating slag prills (metallurgical debris)
in Tel Beth-Shemesh, Israel 2
Fig. 1.2: The outlook of an iron smelting furnace in Lejja
(After Eze-Uzomaka, 2009) 4
Fig. 1.3: Sketch map of Lejja Community
Showing the three survey sites 12

Fig.1.4: The landform of Nsukka area showing Lejja
(Adapted from Ofomata, 1978) 13
Fig. 1.5: Generalised geological map of Nsukka showing Lejja
(After Nwachukwu, 1978) 14
Fig. 2.1: Magnetic field at an observation P due to a current loop 18
Fig. 2.2: Electronic motion producing internal magnetic field
(a) Electron spinning about own axis (b) Electron orbiting the nucleus 20

Fig. 2.3: Magnetic dipole moment (**m**) in a volume V
(a) without external magnetic field (b) with external magnetic field **B** 21
Fig. 2.4: The geomagnetic elements X,Y and Z 31

Fig.3.1: The magnetometer accessories 39
Fig. 3.2: Magnetometer console's front panel
(All the keys except 'CLEAR' &'ENTER' are alpha-numeric.) 39
Fig. 3.3: Base station set up using tripod kit and staff section 39

Fig. 3.4: Magnetometer sensor showing various points 43
Fig. 3.5: Magnetometer sensor orientation
(a) End mounting (b) Saddle mounting 43

Fig. 3.6: Magnetic inclination of the earth's field
(adapted from G-856AX mannual) 43
Fig.3.7: The gradiometer set-up at the lower latitude 44
Fig. 3.8: Unpacking the gradiometer components at Ejuona-Lejja
The author was checking the lower sensor for dirt and proper filling of
the sensor fluid, while the field assistant was carrying the top sensor 52
Fig. 3.9: World magnetic map showing the regional field of interest
(adapted from G-856AX manual) 52
Fig. 3.10: Colour plot of field scanning at Uwani-Lejja
(highlighting anomalous zones of interest) 53
Fig. 3.11: Grid making with triangulation method 55
Fig. 3.12: Using bamboo stick pegs to mark the baseline
at Ugbelenabo site 56
Fig. 3.13: Using the marked string at the baseline in Ejuona-Lejja 56
Fig. 3.14: The pattern of the field layout showing the base
station and the bi-directional traversing 58
Fig. 3.15: The use of marked strings in forming the survey grid
(Taking magnetic measurements at Ugbelenabo-Lejja) 60
Fig. 4.1: 3-D rectangular prism 64
Fig. 4.2: Magnetic anomaly superimposed
on the single source model 68
Fig. 4.3: Calculated magnetic anomalies superimposed on their sources
(a) 3–body model (b) 4–body model 69
Fig. 4.4: Euler depth superimposed on source-anomaly map
(a) without depth filter (b) with depth filter 74
Fig.4.5: Euler depths superimposed on the
multiple-body synthetic anomaly map
(a) 3-body model (N=1) (b) 4-body model (N=1) 77
Fig. 4.6: Assessment of the shapes of the sources
by varying the structural index
(a) N = 2 (b) N = 3 77
Fig. 4.7: Analytic signal method applied to the single-source model
(a) outline of the source (b) mapping edges of the source
(C) Profile across the analytic signal anomaly for depth computation 83
Fig.4.8: Using higher order of analytic signal to compute
depth to the top of a thick prismatic body
(a) Simple analytic signal curve
(b) First-order analytic signal curve
(c) Second-order analytic signal curve 84
Fig. 4.9: Positioning analytic signal amplitudes to
locate horizontal positions of the sources 86
Fig. 4.10: Analytic signal anomaly for
the multiple-source models

(a) profile 1 (b) profile 2 (c) profile 3 (d) profile 4 87
Fig.4.11 : Stage by stage upward continuation for estimate of causative source depth
(a) Synthetic field without upward continuation (b) height of 1m
(c) height of 2m (d) height of 3m (e) height of 4m (f) height of 5m 91
Figure 5.1: Effect of data sorting on the magnetic data
(a) Raw data (b) Sorting process
(c) Appearance of well sorted data 94
Fig. 5.2: Effects of despiking on Uwani data
(a) before despiking (b) after despiking 96
Fig. 5.3: Fitting polynomial models to base station
data (Uwani site, day-1)
(B is the base station field, t is measurement time) 103
Fig. 5.4: Assessing the quality of Uwani-Lejja map after diurnal correction
(a) Before diurnal correction, (b) After diurnal correction, using
Polynomial fitting method (c) after diurnal correction, using
conventional method (1 to 4 are noise levels). 105
Fig. 5.5: Uwani field after the data reduction processes
(a) regional field (b) residual field using conventional method 109
Fig. 5.6: Evaluating performance of the ARMAD method
by comparing its resolution with those of other methods
(a) Conventional method (b) ARMAD method
(c) Gradiometer method
(Contour interval is 5 nT in all the maps) 112
Fig. 5.7: Plot of the absolute amplitudes of the anomalies comparing
ARMAD method with the conventional and gradiometer methods 113
Fig.5.8: An example of anomaly locations and Euler
solution averaging for five sources A to E (Uwani) 120
Fig. 5.9: Locations of anomalies of archaeological
interest in Uwani site (labelled 1 to 9) 120
Fig. 5.10: Maps of the edges of the magnetic sources obtained from the
analytic signal method ((a) Image (b) contour (Uwani)) 123
Fig. 5.11: Amplitude curves for magnetic source depth calculation (Uwani)
(Profiles 1 to 9 were obtained from figure 6.10b) 126
Fig. 5.12: Compering spatial locations of the sources obtained
using Euler and analytic signal methods (Uwani-Lejja)
(a) source distances along horizontal axis
(b) source distances along vertical axis (c) source depths 131
Fig. 5.13: Variation of magnetic field with altitude at the
location labelled 7 & 8 in figure 6.10a
(a) 0.0 m (b) 1.0 m (c)2.0 m (c) 3.0 m 132
Fig. 5.14: Compering spatial locations of the sources obtained
using Euler and analytic signal methods (Ugbelenabo-Lejja)
(a) source distances along horizontal axis
(b) source distances along vertical axis

(c) source depths 136
Fig. 5.15: Image plot of Ugbelenabo residual
field showing anomalies of interest 136
Fig. 5.16: Compering spatial locations of the sources obtained
using Euler and analytic signal methods (Ejuona-Lejja)
(a) source distances along horizontal axis
(b) source distances along vertical axis
(c) source depths 138
Fig. 5.17: Ejuona low-pass filtered field
showing only major anomalies 140

List of Tables

Contents	Page Number
Table 3.1 An example of the console memory stack 61	
Table 4.1 Magnetic source parameters for 3-body models	68
Table 4.2 Magnetic source parameters for 4-body models	68
Table 4.3 A portion of Euler-depth for the single-body model	75
Table 4.4 Estimating error margin in Euler solutions	76
Table 4.5 Source depth calculated with different earth models	86
Table 4.6 Sensitivity of the analytic signal method to changes in strike directions of the magnetic sources	89
Table 4.7 Variation in amplitudes of anomalies with altitude 90	
Table 5.1 Computed parameters and F_o statistics for right choice of models (Uwani site)	102
Table 5.2 Comparing anomaly amplitudes obtained using automatic reduction of magnetic data (ARMAD) method with those of conventional and gradiometer methods of magnetic data reduction	113
Table 5.3 Spatial locations of magnetic sources using Euler method at Uwani site	120
Table 5.4 Magnetic source locations using analytic signal method (Uwani)	124
Table 5.5 Mean magnetic source locations (Uwani)	133
Table 5.6 Mean magnetic source locations (Ugbelenabo)	136
Table 5.7 Mean magnetic source locations (Ejuona)	138

List of Appendices

Contents	Page Number
APPENDIX A	162
OTHER FIGURES	162
Fig. A.1: Polynomial fitting to Uwani base station data (day 2) (a) 2nd order (b) 3rd order (c) 4th order (d) 5th order	162
Fig. A.2: Polynomial fitting to Ugbelenabo base station data (day 1) (a) 2nd order (b) 3rd order (c) 4th order (d) 5th order	163
Fig. A.3: Polynomial fitting to Ugbelenabo base station data (day 2) (a) 2nd order (b) 3rd order (c) 4th order (d) 5th order	164
Fig. A.4: Polynomial fitting to Ejuona base station data (day 1) (a) 2nd order (b) 3rd order (c) 4th order (d) 5th order	165
Fig. A.5: Polynomial fitting to Ejuona base station data (day 2) (a) 2nd order (b) 3rd order (c) 4th order (d) 5th order	166
Fig. A.6: Effects of despiking on Ugbelenabo data (a) Before despiking (b) After despiking	167
Fig. A.7: Effects of despiking on Ejuona data (a) Before despiking (b) After despiking	168
Fig. A.8: Effects of diurnal correction on Ugbelenabo data (a) Without diurnal correction (b) Corrected using polynomial fitting method (c) Corrected using conventional method	169
Fig. A.9: Effects of diurnal correction on Ejuona data (a) Without diurnal correction (b) Corrected using polynomial fitting method (c) Corrected using conventional method	170
Fig. A.10: Regional-residual separation (Ugbelenabo data) (a) Regional magnetic field (b) Residual magnetic field	171
Fig. A.11: Regional-residual separation (Ejuona data) (a) Regional magnetic field (b) Residual magnetic field	172
Fig. A.12: Analytic signal amplitude curves for synthetic data with random orientations of the profiles	173
Fig. A.13: Determination of Optimal Window Size and Estimate of Shape of Magnetic Anomaly Sources (Uwani site)	176
Fig. A.14: Determination of Optimal Window Size and Estimate of Shape of Magnetic Anomaly Sources (Ugbelenabo site)	178
Fig. A.15: Determination of Optimal Window Size and Estimate of Shape of Magnetic Anomaly Sources (Ejuona-site)	181
Fig. A.16: Estimation of spatial location of magnetic sources using Euler method (Ugbelenabo)	182
Fig. A.17: Estimation of spatial location of magnetic sources using Euler method (Ejuona)	182
Fig. A.18: Edge mapping of magnetic sources (Ugbelenabo)	183

Fig. A.19: Profiles across Ugbelenabo major anomalies for depth estimation using analytic signal method 183
Fig. A.20: Analytic signal amplitude curves for depth calculation (Ugbelenabo) 185
Fig. A.21: Edge mapping of magnetic sources (Ejuona) 185
Fig. A.22: Profiles across Ejuona major anomalies for depth estimation (Ejuona) 185
Fig. A.23: Analytic signal amplitude curves for depth calculation (Ejuona) 187

APPENDIX B 188
OTHER TABLES 188
Table B.1 A portion of the Euler-depth for the 3-body models 188
Table B.2 A portion of the Euler-depth for the 4-body models 189
Table B.3 Computed parameters and F_o statistics for right choice of models (Ugbelenabo site) 190
Table B.4 Computed parameters and F_o statistics for right choice of models (Ejuona site) 190
Table B.5 A Sample of Computed Euler Depth for Uwani 191
Table B.6 A Sample of Computed Euler Depths for Ugbelenabo 192
Table B.7 A Sample of Computed Euler Depths for Ejuona 193
Table B.8 Magnetic source locations using Euler method (Ugbelenabo) 194
Table B.9 Magnetic source locations using Euler method (Ejuona) 194
Table B.10 Magnetic source locations using analytic signal method (Ugbelenabo) 194
Table B.11 Magnetic source locations using analytic signal method (Ejuona) 195

APPENDIX C 196
COMPUTER PROGRAMS 196
C.1 Synthetic Data Generator 196

C.2 Diurnal Correction Computer Program 198

C.3 Euler deconvolution computer program 200

C.4 Computer Program for averaging Euler solutions 203

CHAPTER 1

GENERAL OVERVIEW

1.1 THE SEARCH FOR ARTEFACTS

Understanding the prehistoric societies greatly requires analysis of the way people lived and interacted with themselves and their environment based on their material remains. The layout of archaeological sites and the nature of their remains can give vital clues to the way of life of the ancient civilizations. The remains, called artefacts, can be found on the ground surface (Mooketsi, 2009; Namunaba, 2009), or under soil cover (Abou and Abdel, 2007; Eze-Uzomaka, 2009). The common concealed archaeological features are furnaces and furnace fragments, pottery kilns, burnt bricks (or brick walls), fire hearths and fired soils, ceramic materials such as tiles, plates, fired clay pots and potsherds, "lost" graves and buried void space. Others are compacted earth floors such as building foundations or roads under soil cover, metal wares, iron smelting slag blocks, etc., (Clark, 1990; Johnson, 2003; Osella *et al*., 2005). A place where there are clustering of the archaeological features is called an archaeological site.

Archaeologists mostly concern themselves with retrieving such features that are of archaeological interest primarily through field survey, excavation and proper documentation of the archaeological findings. Binford (1972) described the main task of archaeology as seeking origins and tracing the history of culture. Therefore archaeological researches can result to reconstruction of the history of the prehistoric civilizations. The findings are made mostly through careful excavations of concealed features. Such practice are of diverse scales varying from as small as excavating a clay pot (or even potsherds) in a 50 cm x 50 cm pit to as large as tracing an outline of a

prehistoric human community currently under soil cover, perhaps as a result of rapid sedimentation or past natural disaster. The impact of such activity on the environment can hence vary from very small value to far more than the scaring effect of the massive excavation for metallurgical debris of Figure 1.1 (Veldhuijzen and Rehren, 2007). It is then right to say conventional archaeological prospecting is not only slow but may be destructive. To an environmentalist, it is a disruption to nature, but an archaeologist may see it as an unavoidable evil.



Fig. 1.1: Excavating slag prills (metallurgical debris)
in Tel Beth-Shemesh, Israel
(Adapted from Veldhuijzen and Rehren, 2007)

1.2 ARCHAEOLOGY IN SOUTH-EASTERN NIGERIA

The search for archaeological features in Nsukka area began in 1963, and by 1964 three sites were excavated. These included two sites in the University of Nigeria, Nsukka campus and one at Obukpa, some few kilometres to the north of Nsukka town. These initial excavations led to many archaeological surveys in the later years resulting in the discovery of forty-one abandoned villages, fourteen shrines, two iron smelting sites, two rock shelters, etc., amounting to a total of about eighty-three archaeological sites in south-eastern Nigeria (Hartle, 1975). There are therefore diverse archaeological

sites in this part of the country. Further researches have also led to discovery of additional fifteen prehistoric iron smelting sites in this region. A few examples of those within Nsukka area of Enugu State are Aku, Opi, Lejja, Orba, Umundu and Owerre Elu (Anozie, 1979; Okafor, 1993; Eze-Uzomaka, 1996). Excavation work began in most of them, particularly Aku and Opi, long before Lejja site was discovered by some staff of the University of Nigeria, Nsukka in 1980. Preliminary excavations were attempted in the same year using three different test pits from which some artefacts were recovered. Among these were furnaces and furnace remains, tuyères, clay pots and potsherds, charcoal and slag blocks (Eze-Uzomaka, 2006). After these initial findings, Lejja site was abandoned while 13 other sites out of the 17 known iron smelting sites were investigated (Anozie, 1979; Ezike, 1989). Eze-Uzomaka (2006) therefore recommended that Lejja (one of the remaining iron smelting sites) should be investigated to: (i) establish the kiln or furnace structure of the Lejja iron working culture, (ii) date the site so as to position it in the iron smelting era in Africa, (iii) document the lifestyle of the prehistoric Lejja people, etc.

These recommendations have led to researches of different types (including this one) in Lejja archaeological site. Very useful excavations were made between April and May, 2007 when two furnaces and other smelting tools were excavated at two different locations in the site (Eze-Uzomaka, 2009). From a trench measuring 2m by 2m, a fairly large circular furnace with diameter of about 1.2m was found (Figure 1.2). Other artefacts excavated were cylindrical slag block embedded in a slag pit, 7 tuyères (loaded in the furnace), pieces of charcoal and potsherds. Eze-Uzomaka (2006) gave the average diameter of the slag blocks found in the Lejja site to be between 31 and 56

centimetres. The average length and diameter of each tuyère excavated were also given as 48 and 56 centimetres respectively. In addition, Eze-Uzomaka (2006) reported that some potsherds exposed by deep gully erosion in this area were found at a depth of about 1.4 metres. It is then expected that some artefacts may be found below this depth.



Fig. 1.2: The outlook of an iron smelting furnace in Lejja
(After Eze-Uzomaka, 2009)

Undoubtedly, such research work can lead to proper documentation of the history of the people; in this case, the Igbo people and other minority tribes in south-eastern Nigeria. However, as stressed earlier, it is obvious that the conventional archaeological investigations of features under soil cover can seldom be done without much digging in the attempt to excavate the concealed artefacts (Figure 1.1). Archaeology, indeed, is destructive because as the site is dug up, it is systematically being destroyed. The method is not only slow and expensive, but may damage materials excavated beyond recovery, and once exhausted, there are no substitutes for historical records destroyed by hasty excavation (Scollar *et al*., 1986). The research may also be hampered by environmental restrictions due to its impact on the environment. While this scientific method of tracing human history is very essential, it must be applied very selectively.

For this reason, applications of relevant geophysical methods have become increasingly popular in guiding positioning of excavations in most developed and some developing countries of the world (Clark, 1990; Johnson, 2003; Godio and Torino,2005).

1.3 APPLICATIONS OF GEOPHYSICS IN ARCHAEOLOGICAL STUDIES

Geophysical methods applied in archaeology are non-destructive, and hence permitted almost everywhere. Relatively, they are cost effective and can be very rapidly employed. The methods are applied to detect and delineate subsurface features which have physical contrast with their surroundings (Tsokas and Papazachos, 1992; Piro *et al*., 1998). Archaeological geophysics (as it is called) is a means of gaining information about features under soil cover without destroying the soil matrix. The method can provide valuable information for immediate and future goals for an archaeological project. The geophysical results obtained can be integrated with other site data such as historic maps (if available) and current excavation maps to provide a site-wide context for a better understanding of site layout and boundaries. Such results can also provide basis for making decision about immediate targets for investigation and long term planning, preservation and protection of the site as a whole (Scollar *et al*., 1986).

Interestingly enough, all the cultural features mentioned earlier are capable of generating anomalies in an archaeological site due to contrast in the physical properties between them and their surrounding natural media. Such properties include resistivity, conductivity, dielectric constant, magnetisation, density, elastic parameters, etc. For example, while the presence of artefacts such as furnaces, pottery kilns and fired brick walls are revealed by the contrast in magnetisation, (or contrast in dielectric constant) between them and their host soils, the presence of filled post holes, including graves, are more easily revealed by their conductivity (and also by their dielectric constants). So because of the diverse nature of the physical properties of the archaeological remains,

different geophysical methods are applied in search of the concealed cultural features. The choice of the method to be applied is dictated by the expected target and the nature of the site. A few examples of the commonest geophysical methods applied in archaeological prospecting are DC resistivity, electromagnetic, ground-penetrating radar (GPR, or georadar) and magnetic methods (Tsokas and Tsourlos, 1997; Johnson, 2003; Osella *et al*., 2005; Martino et al., 2006). Others which are not commonly used are radiometric, microgravity and seismic methods. These methods can either be integrated, depending on availability of hardware, or applied singly, but with integrated method of interpretation.

1.3.1 The Magnetic Methods in Archaeological Geophysics

Magnetic anomalies from naturally occurring rocks and minerals are due chiefly to the presence of the most common ferrimagnetic mineral, magnetite, and its related minerals such as ulvospinel, titanomagnetite, maghemite, pyrrhotite, goethite, etc. As generalized earlier using example of geophysical methods, such anomalies exist in archaeological sites mostly as a result of contrast in magnetisation between artefacts at the subsurface and their host soils. The contrast in magnetic properties is a function of the concentration and thermal history of the magnetic mineral (particularly magnetite) grains in the cultural features relative to the mineral compositions of the surrounding natural media. That is, the amount of magnetic minerals determines the magnetic susceptibilities and hence the induced magnetisation acquired by the cultural features when they are fired. For example, many material remains of man's past such as furnaces, pottery kilns, baked bricks, tiles, clay pots and similar features compose of clay which usually contains relatively higher amount of magnetic minerals compared to

most soils formed from igneous and sedimentary rocks (Breiner, 1999; Lowrie, 2007). When the magnetite bearing clay is heated to a very high temperature (about 570^{o} C) the magnetic domains within each magnetite crystal are randomized, and when allowed to cool in the ambient geomagnetic field, many of the magnetic domains would align themselves parallel to one another creating a net magnetisation fixed with respect to the object and parallel to the earth's total field at the time of the cooling. Surface soils which also contains some magnetic minerals and were subjected to heating in the ancient human habitations must have acquired some anomalous magnetisations detectable by magnetometers or susceptibility systems. The examples above are among the factors responsible for the physical properties of the cultural features that account for the success of the magnetic methods in archaeological prospecting.

1.3.1.1 The Technique of Soil Magnetism

Enhancement of magnetic properties of surface soils by heat (particularly fire) as illustrated earlier, has been known for decades (Oldfield *et al*., 1981; Maher, 1986; Dalan and Banerjee, 1996). This enhancement accounts for the main reason that the top soils are more magnetic than the sub-soils. The acquisition of higher susceptibility, hence higher magnetization, also depends on factors such as amount of organic matter present in the surface soils, the porosity of the soils and the temperature attained during the heating (Dalan and Banerjee, 1996). The contrast in magnetisation between the topsoil and subsoil permits detection of ditches, pits and similar features that were backfilled with top soils. Backfilled areas produce positive anomalies while cultural voids (e.g., tunnels) and cavities such as tombs generate negative anomalies (Johnson, 2003; Godio and Torino, 2005).

Geophysical techniques have been developed (Clark, 1990; Crowder and Barker, 1995; Schmidt, 2007) to study magnetic susceptibilities of soils. Among these methods are the in-situ measurements of magnetic susceptibilities of soils and laboratory measurements using sensitive instruments such as the Bartington MS2 susceptibility system which consists of a meter that can be attached to one of several sensors used for either laboratory measurements (MS2B), or field measurements (MS2D, MS2F).

1.3.1.2 The Magnetometer Survey Method

In contrast to the technique of soil magnetism that measures magnetic susceptibilities of soils directly, magnetometer surveys record the magnetic fields produced by contrast in magnetisation between a subsurface feature and its host rock or soil. The magnetisation contrast could be a product of either induced magnetisation or remanent magnetisation possessed by the causative subsurface body as a result of its composite magnetic minerals.

The magnetic properties of ferromagnetic materials are also important in archaeological geophysics because of the anomalies generated by iron smelting slag blocks and other ferrous archaeological objects like farm implements, pipes and other traditional monuments. When ferromagnetic materials, known for their very strong spontaneous magnetisations, are subjected to intensive heating, their spontaneous magnetisations disappear at their paramagnetic Curie temperatures. At temperature higher than the paramagnetic Curie temperature, the susceptibility becomes the paramagnetic susceptibility with the material behaving as a paramagnetic solid and acquires an induced magnetisation in the presence of an inducing magnetic field. The

ferromagnetic materials are therefore capable of retaining both induced and spontaneous magnetisations.

Each of the archaeological features buried below the surface of the earth exhibits one, or more of the above physical properties thus building a field around itself that causes distortion in the earth's undisturbed field. The magnetometer survey method is based on detecting such anomalous fields. The principles behind this method were initially applied only to locate larger bodies such as ore deposits, geological structures, or mapping magnetic basement surfaces (Nettleton, 1976; Thompson, 1982; Telford *et al*., 1990; Blakely, 1996). In the last few decades, the method has been gaining more and more popularity in archaeological investigations (Clark, 1990; Tsokas and Papazachos, 1992; Godio and Torino, 2005; Osella *et al*., 2005), but has been applied with some cautions, because archaeological magnetic bodies are often smaller in size and are buried at shallower depths.

The magnetometer survey method is one of the most effective and one of the most universally applied geophysical methods in archaeology for two distinct reasons: (i) Many archaeological objects have distinctive and individual magnetic properties that make them prone to detection by creating anomalies on the surface of the ground. (ii) The inherent advantage of the ease of field operation of the magnetometer makes it more attractive to many researchers even though they pay dearly for this at the data processing stage. It is the primary exploration method in the search for concealed archaeological features, including concealed cultural soils, kilns or furnaces, fired clay products such as pots, ceramics and brick walls. Others are ferrous objects which

include agricultural tools and other household products, iron smelting slag blocks, etc. Depending on the level of sedimentation, these features are found in as shallow a depth as 0.3 m (Osella *et al*., 2005) to as much as a depth of about 2.0 to 4.0 metres below the ground surface (Godio and Torino, 2005; Abou and Abdel, 2007). For instance, the earlier archaeological work done in Lejja by Eze-Uzomaka (2009) has revealed that features of interest at this location may be located at depths as small as about 0.2 metre to as much as about 2.0 metre.

Ancient burned structures can show local magnetic anomalies in the range from10-1000nT. Ferrous objects, including iron smelting slag blocks can also show magnetic anomalies that range from 20 to 2000 nT. Schmidt (2007) states that anomalies higher than approximately 50 nT are normally measured over ferrous features, or over features with thermo-remanent magnetisation like kilns or furnaces. However, these values cannot be taken absolutely since they depend on both the level of magnetisation and depth of burial of the archaeological features.

1.4 THE PRESENT STUDY

The current study, focused on Lejja prehistoric iron smelting site, involves the use of detailed magnetic profiling technique at three locations in Lejja community. The sites are Ugbelenabo, Uwani and Ejuona. They were selected based on interviews conducted on the local community, the earlier archaeological study, the surface observations based on presence of blooms, and the terrain (based on the flatness of the sites). The sites are residential areas that are not only easily threatened by conventional archaeological investigations, but massive excavations are prohibited. It is therefore aimed at creating

acceptability of the archaeological research in the community and to guide archaeologists working (or intending to work) in these selected sites to precise points of excavation. It is also meant to serve as a "lead" to the practice of archaeological geophysics in the area, and anywhere in Nigeria. It would therefore pave way for long term planning of how this large prehistoric site (Lejja archaeological site) could be properly investigated to correctly document the history of the great community.

The geophysical tool adopted is magnetic method which is commonly applied in archaeology to detect and delineate shallow subsurface targets that have acquired some magnetic properties through previous heating, or have high spontaneous magnetisation, or both (Piro *et al*., 1998; Godio and Torino, 2005; Schmidt, 2007). Lejja, being an iron smelting site at which furnaces, baked clay materials in form of tools, highly fired pits or soils, etc., are expected (Eze-Uzomaka, 2006), magnetic method is therefore a valuable tool. The method has enjoyed the highest patronage in archaeological prospecting among other geophysical methods due to the fact that most ancient relics display some magnetic signals detectable by the method. It is therefore expected that such application will clearly map the positions of the artefacts in the three locations in Lejja archaeological site.

1.5 DESCRIPTION OF THE SITE

Lejja is an agrarian community made up of patches of settlements, with each family compound surrounded by sparsely thick forest. It is located at about 14 km south-west of Nsukka in Enugu State, Nigeria. Approximately, it is within longitudes $7^{o}18'$ E and $7^{o}25'$ E, and latitudes $6^{o}41'$ N and $6^{o}48'$ N. Figure 1.3 shows the three sites surveyed in

Lejja archaeological site. They are Uwani, Ugbelenabo and Ejuona sites. The Uwani site, situated at the central part of the community is located within longitudes 7°22.19′ E and 7°22.22′ E, and latitudes 6°44.40′ N and 6°44.42′ N. On the other hand, the Ugbelenabo site is located to the south-western part, within longitudes 7°19.00′ E and 7°19.04′ E, and latitudes 6°42.28′ N and 6°42.30′ N. The Ejuona site, which is in the south-eastern part of the community is found within longitudes 7°22.75′ E and 7°23.08′ E, and latitudes 6°42.74′ N and 6°42.76′ N. The altitude (measured during the field work) varied between about 350 metres above sea level in Ugbelenabo to about 454 metres above sea level in Uwani and Ejuona villages of the Lejja Community. This large community is known for its wide spread symbol of iron smelting activity. Pieces of iron (blooms) are found in most places as one moves around various villages that make up the Lejja community, a revelation of intensive prehistoric iron smelting activity. Nevertheless, apart from some slag blocks that are still visible (mostly at the village squares), the smelting furnaces and their components are no longer found on the ground surface due to sedimentations that have taken place over several decades, and may be, several centuries (Okafor, 1993; Eze-Uzomaka, 2006).

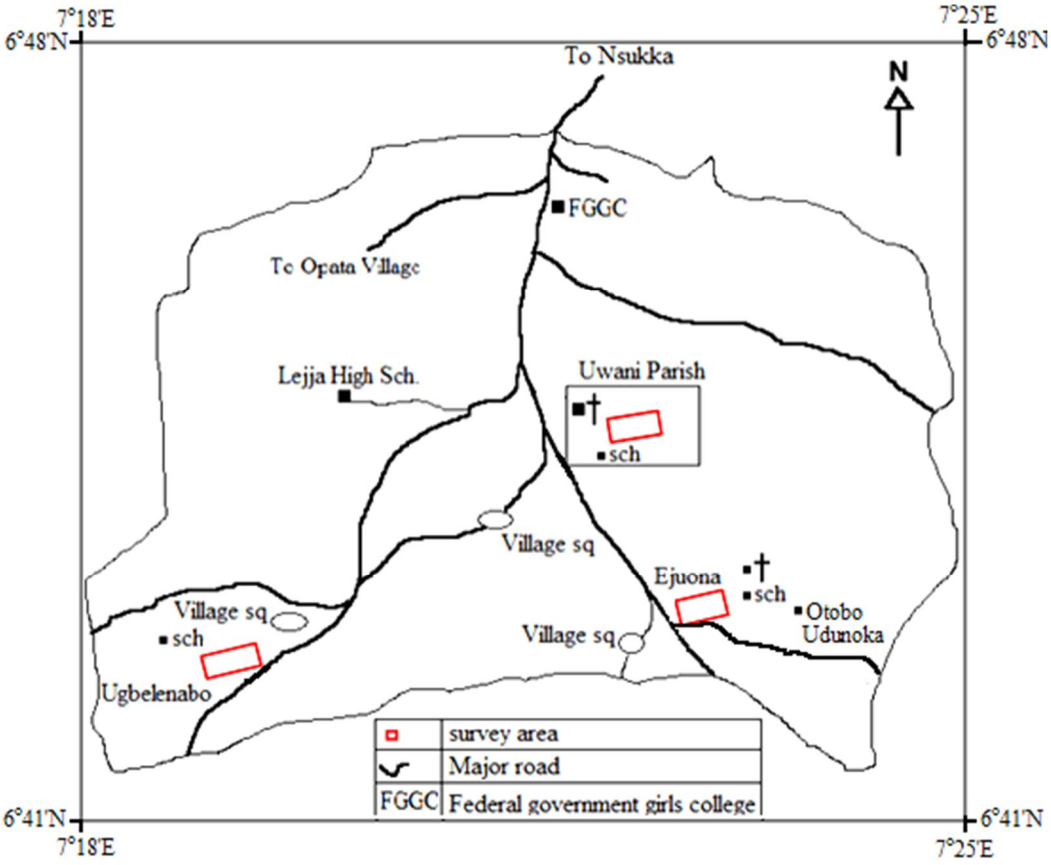


Fig. 1.3: Sketch map of Lejja Community
Showing the three survey sites

1.5.1 The Landform of the Study Area

The Nsukka area falls into four landform divisions, a western low land (Anambra plains), a plateau zone (Nsukka Plateau), an escarpment zone, and an eastern lowland (Cross River plains) (Ofomata, 1978). The study area, Lejja Community, occupies the northern sector of the north-south trending dry valley of the Nsukka plateau (Figure 1.4). The community is surrounded by steep-sided grassy hills, and as a result of extensive farming, the vegetation of the area has been reduced to derived savannah with a lot of woody species (Igbozurike, 1978; Ofomata, 1978; Eze-Uzomaka, 2006).

The plateau slopes gently towards the west at a very low angle (less than 2^{o}). It is associated with two major geological formations, the false-bedded sandstones and the upper coal measures. The plateau area is underlain with the false-bedded sandstones and the upper coal measures stand out as residuals which often rise to over 180 metres above the general ground level. The sandstone is overlain by the soil developed in the red sands formed by the weathering and ferruginization of the false-bedded sandstones.

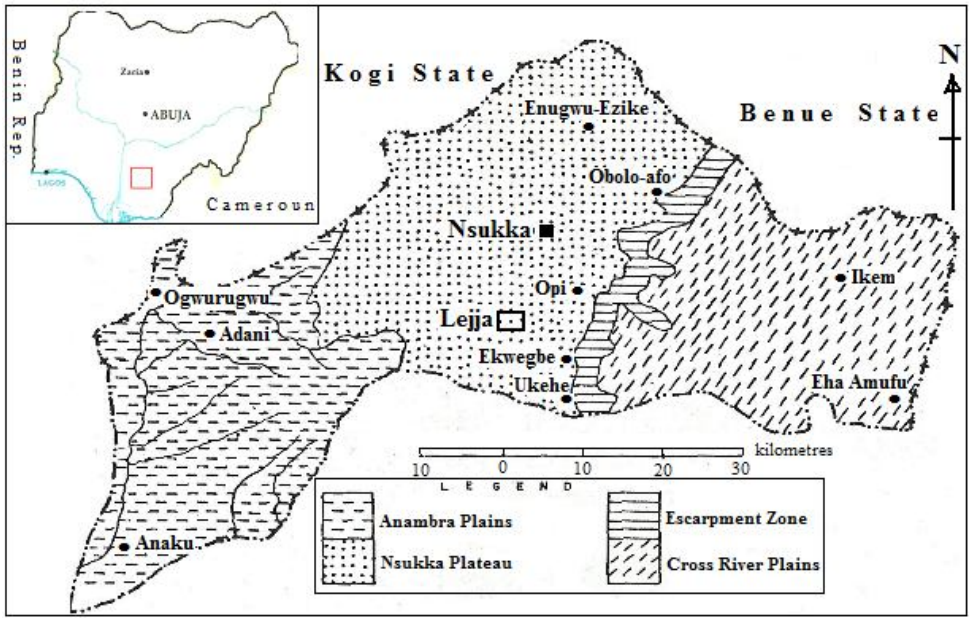


Fig.1.4: The landform of Nsukka area showing Lejja
(Adapted from Ofomata, 1978)

The red sandy soil is well drained and forms thick layer with a texture which changes from loamy sand to sandy loam with depth (Ofomata, 1978).

1.5.2 Geology of the Study Area

Lejja community, like the neighbouring Nsukka, is situated within the Eastern Nigeria sedimentary basin and is underlain by rocks which range in age from Coniacian to Paleocene (Figure 1.5). Sediments deposited within this time interval occur in four

distinct physiographic provinces, namely, the Cross-River Plains, the Escarpment, the Plateau and Anambra Plains. Nwachukwu (1978) has grouped these rocks into six formations: Awgu Shale, Enugu Shale, Mamu Formation, Ajali Sandstone, Nsukka Formation, and Imo Shale Formation. Figure 1.5 is a generalised geological map of Nsukka area showing the location of Lejja to the south-west of Nsukka, on Ajali Sandstone. The Ajali Sandstone is well exposed at some locations. It is generally a

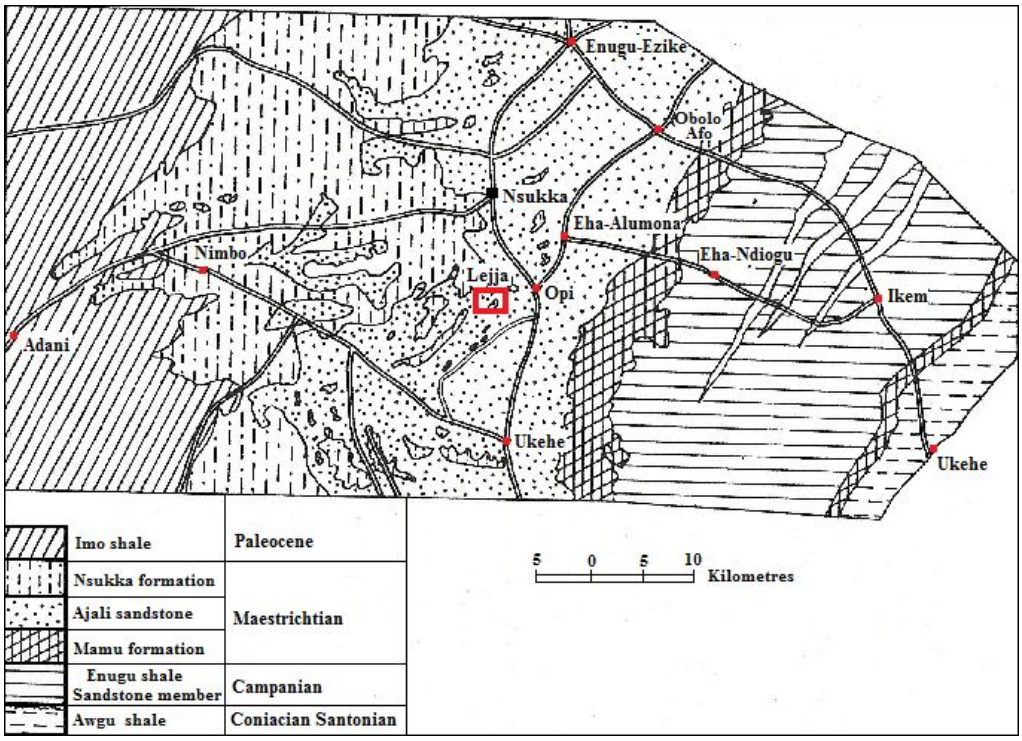


Fig. 1.5: Generalised geological map of Nsukka showing Lejja
(After Nwachukwu, 1978)

porous sandstone with occasional shale partings, unconsolidated with medium to poor sorting. Often, there is rapid alternation of coarse to fine grains in successive laminas and suggests fluctuating conditions of deposition. The sandstone is almost mono-mineralic, containing almost 95 percent of pure quartz and in lower section; that is, the white sandstone member, the quartz content may be up to 99 percent. The top of the

Ajali Sandstone is reddish in colour with haematitic stains. Occasionally, shale bands are reddish and sometimes they contain impressions of plant remains. There is also a marked absence of feldspar which has been accounted for by Nwachukwu (1978) as being caused by post-depositional changes which could have resulted in its leaching out. This is particularly significant when it is considered that the sediments are porous and will allow free movement of subsurface water that could cause such massive mineralogical leaching.

1.6 AIM AND OBJECTIVES OF THE STUDY

The aim of the study is to investigate Lejja archaeological site using the magnetic method of geophysical prospecting. The study is intended to accomplish the following objectives:

i. To determine the shape and size of the artefacts found in Lejja archaeological site. Such properties are expected to reveal part of the culture of the prehistoric Lejja Community.

ii. To determine the depths of burial that are associated with artefacts in Lejja Archaeological Site. This is because if suspected material remains of man's past must be excavated, the archaeologist must know the depth at which to dig.

iii. To determine the spatial locations of the artefacts. Such knowledge leads to precise points of excavation, thereby discouraging wild-cat excavations which are reminiscent of archaeological research, particularly in sub-Saharan Africa.

iv. Promotion of inter-disciplinary research between physics and archaeology. That is, archaeologists would see geophysical techniques as very relevant to their search for

concealed antiquities, and physicists would also take up the challenge of being partners in the application of the scientific method of tracing human history.

v. It is to serve as a pilot archaeological geophysics research in Nigeria and the West African sub-region.

CHAPTER 2

THEORETICAL BACKGROUND

2.1 BASIC CONCEPTS OF MAGNETIC PROSPECTING

A magnetic field can be produced either by a permanent magnet or by an electric current. These currents can be macroscopic as in conduction current, or microscopic such as magnetisation current (Nettleton, 1976; Blakely, 1996). Magnetic field **B** is a vector quantity and is called magnetic induction, magnetic flux density, or simply the magnetic field of a loop of current. It is convenient to think of the magnetic state of a body as resulting from elementary magnets or dipoles, each of which consists of a positive and a negative magnetic pole separated by a small distance. A bar magnet or a small filamentary current loop can usually be referred to as a magnetic dipole (Jackson, 1975; Sadiku, 1989). Using such simple basic assumption, the expression for magnetic effect of a magnetic source buried at a given depth can be estimated. For example, given the circular current loop of radius 'a' carrying current 'I' (Figure 2.1), the magnetic field at an observation point P(r,θ,□) due to the loop can be determined using spherical coordinates. Blakely (1996) expressed the magnetic scalar potential at point P as

$$V(P) = k\frac{\vec{m}.\hat{a}_r}{r^2} \tag{2.1}$$

where $k = \frac{\mu_0}{4\pi} = 10^{-7}$ Hm^{-1} in SI units, and in emu, k = 1. The magnetic moment $\vec{m}$ of the loop of figure 2.1 has the direction $\hat{a}_r$ and magnitude equal to current I times the area of the loop. That is, $\vec{m} = I\pi a^2\hat{a}_z$. The potential at P due to the current loop can therefore be expressed as

$$V(P) = k\frac{I\pi a^2 \hat{a}_z.\hat{a}_r}{r^2},$$

and resolving the magnetic moment in the $\hat{a}_r$ direction yields the potential at P given by

$$V(P) = k\frac{I\pi a^2 \cos\theta}{r^2}. \tag{2.2}$$

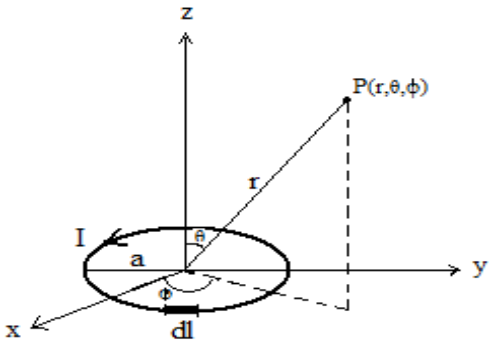


Fig. 2.1: Magnetic field at an observation P due to a current loop

One of the Maxwell's equations in static field given as

$$\nabla X\vec{B} = \vec{J}/\mu,$$

where **J** is the current density and μ is the permeability of the medium, reveals that if there is no current in the region at which measurements are made (a valid assumption in geophysics), **J**=0; that is, $\nabla X\vec{B} = 0$, and the induction field becomes irrotational. According to Helmholtz theorem (Blakely, 1996), **B** then has a scalar potential V such that

$$\vec{B} = -\nabla V, \tag{2.3}$$

where in the spherical coordinates,

$$\nabla = \frac{\partial}{\partial r}\hat{a}_r + \frac{1}{r}\frac{\partial}{\partial\theta}\hat{a}_\theta + \frac{1}{r\sin\theta}\frac{\partial}{\partial\phi}\hat{a}_\phi. \tag{2.4}$$

Substituting equation (2.2) in equation (2.3) and invoking the operator in (2.4) yields the magnetic induction field at point P given by

$$\vec{B} = k\frac{m}{r^2}(2\cos\theta\hat{a}_r + \sin\theta\hat{a}_\theta) \tag{2.5}$$

Since the magnetometer measures the magnetic field strength and not the magnetic field vector in equation (2.5), behaviour of the dipole magnetic field can be better assessed if the magnitude of the field is obtained. That is,

$$\left|\vec{B}\right| = \left(k\frac{m}{r^3}\right)\left[(2\cos\theta)^2 + (\sin\theta)^2\right]^{1/2},$$

which can be simplified to give the magnetic field strength to be

$$\left|\vec{B}\right| = k\frac{m}{r^3}\left(3\cos^2\theta + 1\right)^{1/2}. \tag{2.6}$$

Equation (2.6) reveals two major attributes of the magnetic field strength:

(i) The magnitude of the dipole field along any path extending from the dipole decreases at a rate inversely proportional to the cube of the source-sensor distance.

(ii) The magnitude depends on the angle θ, showing that the maximum field strength is obtained at the epicentre of the source, but decreases away from this central point.

The major use of equation (2.5) is not only qualitative as described by equation (2.6), but can be used quantitatively for forward modelling. For instance, a three-dimensional magnetic body can be approximated by a collection of smaller elements, adequately simple in form to possess analytical expressions for their magnetic fields. The magnetic dipole is one of the simplest examples (Bhattacharyya, 1964; Talwani, 1965; Cady, 1980; Rao and Babu, 1991; An *et al*., 2004) with which magnetic field of a body can be calculated by dividing the body into an array of small volume elements. It is assumed that each element appears at a distance as a dipole, then equation (2.5) can be used to derive the field of each dipole, and finally assuming the resultant effects of all the

dipoles which will represent the magnetic field of the three-dimensional body (Blakely, 1996).

2.1.1 Magnetisation in Materials

Any given material is composed of atoms. Each atom can be regarded as consisting of electrons spinning about their own axes (Figure 2.2a) and also orbiting the atomic nucleus (Figure 2.2b). These electronic motions give rise to internal magnetic dipoles or current loop. Such magnetic dipoles are randomly oriented in the absence of an external magnetic field; that is, the sum of the magnetic moments is zero (Figure 2.3a).

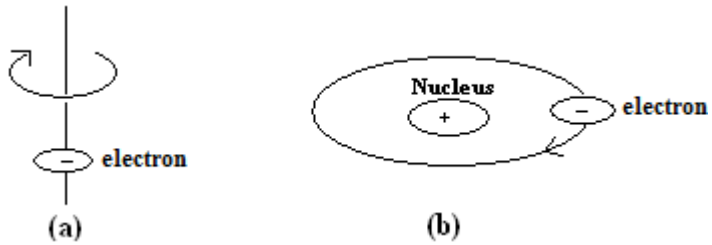


Fig. 2.2: Electronic motion producing internal magnetic field
(a) Electron spinning about own axis (b) Electron orbiting the nucleus

When an external magnetic field is applied to it (Figure 2.3b), the net magnetic moment is no longer zero since the magnetic moments of the electrons will align themselves with the external field.

The bulk magnetic properties of a volume of material can be considered in terms of the net effect of all the dipoles within the volume. Supposing that there are N atoms in a

given volume V (as in Figure 2.3b) and that the j^{th} atom has a magnetic moment $\mathbf{m}_j$, the magnetisation $\vec{M}$ can be defined as the vector sum of all the individual dipole moments $\mathbf{m}_j$ divided by the volume. That is,

$$\vec{M} = \frac{1}{V}\sum_{j=1}^{N}\vec{m}_j \qquad (2.7)$$

In SI units of measurement, the unit of magnetisation is amperes per metre (Am^{-1}), and in the electromagnetic unit (emu), it is gauss, where 1 gauss = $10^3 Am^{-1}$. A medium for which magnetisation is not zero everywhere is said to be magnetised.

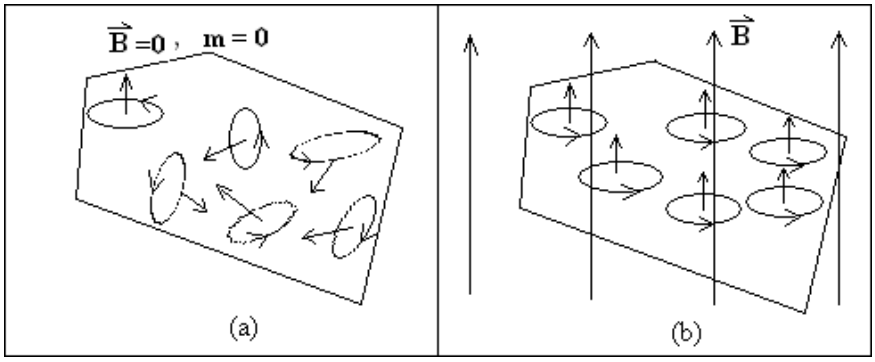


Fig. 2.3: Magnetic dipole moment (**m**) in a volume V
(a) without external magnetic field (b) with external magnetic field **B**

A small element of a magnetised material with magnetisation **M** can be considered to act like a single dipole such that **M**dv = **m**. That is, if the magnetic moment of the bulk of the material is considered, it can simply be written as

$$\mathbf{m} = \mathbf{M}V. \qquad (2.8)$$

2.1.2 Magnetic Field Intensity

One of the Maxwell's equations states that the curl of **B** is equal to the vector sum of the various forms of charge moving in the region; that is,

$$\nabla \times \mathbf{B} = 4\pi k I_t , \qquad (2.9)$$

where I_t is the sum of all the currents in the region, including the macroscopic currents $\mathbf{I}_m$, currents related to magnetisation **M**, and total displacement currents $\frac{\partial \vec{D}}{\partial t}$. That is,

$$I_t = (\mathbf{I}_m + \nabla \times \mathbf{M} + \frac{\partial \vec{D}}{\partial t}) \tag{2.10}$$

Then substituting equation (2.10) in equation (2.9) gives

$$\nabla \times \mathbf{B} = 4\pi k(\mathbf{I}_m + \nabla \times \mathbf{M} + \frac{\partial \vec{D}}{\partial t}). \tag{2.11}$$

Equation (2.11) shows that the magnetic induction **B** originates from all currents, both macroscopic and microscopic. Another type of magnetic field that is a part of **B** arises from all currents except atomic level currents associated with magnetisation. Blakely (1996) assumes dielectric properties of the region of interest to be negligible and expressed the curl of the magnetic induction as

$$\nabla \times \mathbf{B} = 4\pi k(\mathbf{I}_m + \nabla \times \mathbf{M}). \tag{2.12}$$

So in the SI units where $k = \frac{\mu_o}{4\pi}$, equation (2.12) becomes

$$\nabla \times \mathbf{B} = \mu_o(\mathbf{I}_m + \nabla \times \mathbf{M}),$$

$$\text{or} \quad \nabla \times (B - \mu_o \mathbf{M}) = \mu_o \mathbf{I}_m \tag{2.13}$$

But one of the Maxwell's equations in static field is given by Sadiku (1989) as

$$\nabla \times \mathbf{H} = \mathbf{I}_m \tag{2.14}$$

Then comparing equations (2.13) and (2.14) it is obvious that

$$\mathbf{H} = \frac{\vec{B}}{\mu_o} - \mathbf{M}. \tag{2.15}$$

H is called magnetic field intensity. It is simply magnetic induction (except for the factor μ_o) minus the effects of magnetisation. Lowrie (1997) refers to it as magnetising field. **H** has the unit of Am^{-1} in SI units, same unit as the magnetisation.

2.1.3 Magnetic Susceptibility

Some natural materials can acquire a component of magnetisation in the presence of an external magnetic field. For low-amplitude magnetic fields such as the geomagnetic field, the induced magnetisation is proportional in magnitude, and is parallel (or anti-parallel) in direction, to the external magnetic field (Blakely, 1996). This can be expressed as

$$\mathbf{M} = \chi \mathbf{H} \, . \tag{2.16}$$

The proportionality constant χ is a physical property of the material called magnetic susceptibility. It is a measure of how magnetisable a material is, or a measure of the ease with which the material can be magnetised by an external magnetic field. That is, any material that has an appreciable value of magnetic susceptibility can acquire an induced magnetisation.

The equation (2.16) emphasises the fact that if a soil or a rock that is rich in iron-oxides such as magnetite, maghaemite, pyrrhotite, or goethite (particularly magnetite) is heated above the Curie temperature of the ferrimagnetic mineral and allowed to cool in the ambient magnetic field, it has the potential to acquire appreciable thermoremanence that will be fixed in the earth material. Clay used in the construction of furnaces, kilns, making of bricks, fired pots, etc., has an appreciable amount of magnetic susceptibility because it contains some of these ferrimagnetic minerals. The temperatures at which the blast furnaces, or the pottery kilns operate (Schmidt, 2007) exceed the Curie temperatures of the ferrimagnetic minerals. Such concealed artefacts would have acquired thermoremanent magnetisation which is proportional to the magnitude, and in the same direction as that of the geomagnetic field at the time of their cooling.

From equation (2.15),

$$\mathbf{B} = \mu_o(\mathbf{H} + \mathbf{M}). \tag{2.17}$$

Substituting equation (2.16) in equation (2.17) gives

$$\mathbf{B} = \mu_o(\mathbf{H} + \chi\mathbf{H}).$$

$$= \mu_o(1 + \chi)\mathbf{H}$$

That is,

$$\mathbf{B} = \mu\mathbf{H}, \tag{2.18}$$

where $\mu = \mu_o(1 + \chi)$ is the magnetic permeability of the medium. In a vacuum, there is no magnetisation ($\mathbf{M} = 0$) so the vector fields **B** and **H** are parallel and proportional. That is

$$\mathbf{B} = \mu_o\mathbf{H}. \tag{2.19}$$

Inside a magnetisable material, as obvious from equations (2.10) and (2.12), the magnetic B-field has two sources (Lowrie, 1997). One source is external system of real currents that produce the magnetising field **H**. The other is the set of internal atomic currents that cause the atomic magnetic moments whose net alignment is expressed as the magnetisation.

2.1.4 Estimate of Magnetic Effect

The important equations so far derived can be summarised using equation (2.5). For example, substituting equations (2.8), (2.16) and (2.19) into equation (2.5) gives

$$\vec{B} = k\frac{\chi V\vec{B}_e}{\mu_o r^3}(2\cos\theta\hat{a}_r + \sin\theta\hat{a}_\theta). \tag{2.20}$$

The amplitude of equation (2.20) can be easily determined, and it is

$$\left|\vec{B}\right| = \left(k\frac{\chi VB_e}{\mu_o r^3}\right)(3\cos^2\theta + 1)^{1/2}, \tag{2.21}$$

where B_e is the earth's magnetic flux density. The highest value of $(3\cos^2\theta+1)^{½}$ is 2, which is obtained at the epicentre of the source. Using SI units where the value of k = $\frac{\mu_o}{4\pi}$, the magnetic effect at the epicentre of an archaeological feature that is under soil cover can be estimated using

$$\left|\vec{B}\right| = \frac{\chi V B_e}{2\pi r^3} \qquad (2.22)$$

where the feature has volume V, susceptibility χ, and it is buried at a distance r away from the sensor in an environment where the geomagnetic field is B_e. As shown in equation (2.22), the anomaly strength depends both on magnetisation and the depth of the buried feature. Therefore, that expression cannot be used for unambiguous characterisation of such feature. It can only be used to estimate the anomaly strength, or estimate depth if the other parameters can be estimated appropriately.

2.2 CLASSIFICATION OF MAGNETIC MATERIALS

Equations (2.3) to (2.6) of section 2.1 illustrate the dependency of magnetic behaviour of materials on the magnetic moments of its atoms or ions. There are three main classes of magnetic behaviour, based on magnetic susceptibility, which are observed in natural materials. These are the diamagnetism, paramagnetism and ferromagnetism.

2.2.1 Diamagnetic Materials

A diamagnetic material has low and negative magnetic susceptibility. Diamagnetism is a magnetic behaviour displayed by materials in which all the electron spins are paired. From the Lorentz force (Reitz *et al*., 1979; Blatt, 1992; Lowrie, 1997), it is evident that a change in the magnetic field alters the force experienced by an orbiting electron. The plane of the electron orbit is compelled to precess around the field direction. This phenomenon, called Larmor precession, is an additional component of rotation which is opposite to the orbital motion of the electron around the nucleus. As a result, a weak magnetisation proportional to the field strength is induced in the opposite direction to the applied field. The diamagnetic susceptibility is independent of temperature. It vanishes when the applied field is removed. Many rock-forming minerals such as quartz, calcite, etc., with magnetic susceptibility around -10^{-6}, belong to this group.

2.2.2 Paramagnetic Material

When some electron spins are unpaired, then there will exist some magnetic moments in the atoms or ions. The resultant magnetic moment can align with a magnetic field. Thermal energy which favours chaotic orientation of the spin magnetic moments opposes this alignment, and because it is large compared to the magnetic energy, the magnetic moments are randomly oriented if no external magnetic field is applied. When a magnetic field is applied, the magnetic moments rearrange themselves to align in the field direction. A magnetisation is then induced that is proportional to the strength (and parallel to the direction) of the applied field.

The susceptibility χ of a paramagnetic material varies inversely with temperature T as reflected in the Curie law, $\chi = \frac{c}{T}$, where the proportionality constant c is the

characteristic of the magnetic material. In solids, mutual interactions between their atoms or ions may be quite strong and paramagnetic behaviour can only be observed when thermal energy exceeds a certain threshold value at a temperature called paramagnetic Curie temperature θ. At temperature T above the paramagnetic Curie temperature, the paramagnetic susceptibility is given by

$$\chi = \frac{C}{T - \theta}. \tag{2.23}$$

The paramagnetic Curie temperature of some clay, and some rock-forming minerals such as amphiboles, chlorite, pyroxene and olivine are below room temperature (Lowrie, 1997); that is, they are paramagnetic even at room temperature. They also have magnetic susceptibility in the neighbourhood of 10^{-5} to 10^{-4}.

2.2.3 Ferromagnetic Materials

Atoms of metals such as iron, nickel and cobalt occupy lattice positions that are adequately close to allow exchange of electrons between their neighbouring atoms. This exchange involves large amount of energy (called the exchange energy of the metal) and it produces a very strong molecular field within the metal. This field aligns the magnetic moments exactly parallel to one another and thereby producing a spontaneous magnetisation M_s. A soil or a rock sample may contain thousands of tiny ferromagnetic mineral grains so that in strong magnetic fields, such a sample can acquire a magnetisation value M_i which is as high as that of a spontaneous magnetisation M_s. If the inducing field is removed, it can retain part of the induced magnetisation. This residual magnetisation is called ***remanence,*** or ***isothermal***

remanent magnetisation. When the ferromagnetic material is heated, its spontaneous magnetisation disappears at the ferromagnetic Curie temperature T_c.

2.2.4 Anti-ferromagnetic Materials

The oxygen ions usually keep the metal ions far apart in oxide crystals. This disallows the direct exchange of electrons between the metal ions. However, the exchange of electrons from one metal ion to the other is made possible through electron cloud of the oxygen ions by interaction between the magnetic spins of certain minerals. This type of indirect exchange process results in anti-parallel directions of adjacent atomic magnetic moments. This exchange results in a positive, but weak susceptibility. In such a case, remanent magnetisation is not possible. A common example of an anti-ferromagnetic mineral is ilmenite ($FeTiO_3$).

2.2.5 Parasitic Ferromagnetic Materials

When an anti-ferromagnetic crystal contains defects, vacancies or impurities, some of the anti-parallel spins are not exactly anti-parallel but are inclined at a small angle. They do not cancel out completely so a ferromagnetic type of magnetisation can result. Materials that exhibit this form of parasitic ferromagnetism have the typical characteristics of a true ferromagnetic metal, including hysteresis, a spontaneous magnetisation and a Curie temperature. An important geological example is the common iron mineral, haematite (α-Fe_2O_3), in which both the spin-canted and defect moments contribute to the ferromagnetic properties. Haematite has a variable, weak spontaneous magnetisation of about 2000 Am^{-1} and a Curie temperature of about 675^oC.

The variable magnetic properties are due to variation in the relative importance of the defect and spin-canted moments.

2.2.6 Ferrimagnetic Materials

The metallic ions in an anti-ferromagnetic material occupy the voids between the oxygen ions. In certain crystal structures, of which the most important geological example is the spinel structure, the sites of the metal ions differ from each other in the coordination of the surrounding oxygen ions. Tetrahedral sites have four oxygen atoms as nearest neighbours and octahedral sites have six. The tetrahedral and octahedral sites are occupied by divalent ions and the octahedral sites by Fe^{3+} ions. The same number of divalent ions occupies other octahedral sites, while the corresponding number of tetrahedral sites is empty. Ferrimagnetic materials exhibit magnetic hysteresis and retain a remanent magnetisation when they are removed from a magnetising field.

2.3 REMANENT MAGNETISATION IN ROCKS

The small concentration of ferrimagnetic minerals (particularly magnetite) in a rock or a soil gives it the ability to acquire remanent magnetisation. The natural remanent magnetisation has many components acquired in different ways and at different times. These can be broadly grouped into primary and secondary magnetisations.

A remanence acquired at or close to the time of formation of a rock is called primary magnetisation. Examples are thermoremanent magnetisation, acquired by igneous rocks when cooling and solidifying from the molten magma, and the remanent magnetisation acquired by a sedimentary rock during, or shortly after deposition. Remanent magnetisation acquired at a later time is called a secondary magnetisation.

This may be caused by chemical changes during weathering and erosion, or during diagenesis.

Thermoremanent magnetisation occurs when igneous rocks cool from molten magma and solidify at very high temperature (in excess of 1000^{o}C). At this temperature, there is no molecular field existing in the composite magnetic minerals such as magnetite (Curie temperature of 578^{o}C) and haematite (Curie temperature of 675^{o}C). These minerals display paramagnetic characteristic at this point with their individual atomic magnetic moments being free to fluctuate chaotically (Lowrie, 1997; Blakely, 1996). As the rock cools through its Curie temperature, the magnetisation of the magnetite grains changes from paramagnetism to ferromagnetism and a spontaneous magnetisation appears. Remanence acquired in this way is particularly stable.

Detrital remanent magnetisation is the acquisition of remanence during deposition of sediments which takes place under stable temperature. It occurs during the slow settling of fine-grained sediments containing an appreciable amount of ferrimagnetic and anti-ferromagnetic particles in the presence of an external magnetic field. In the settling process, the particles are oriented by the ambient magnetic field. This orientation is destabilised by water current that causes some hydro-mechanical forces which give rise to a declination error (Lowrie, 1997). On making contact with the bottom of the sedimentary basin, the force of gravity rolls the particles into a stable altitude, causing an inclination error. The pressure of overlying sediments during deep burial results in compacting the sediments. This compaction process can also produce further directional errors. The detrital remanent magnetisation is then finally fixed in the

sedimentary rocks during diagenesis. Varved clays exhibit this type of remanence (Telford *et al*., 1990).

Chemical remanent magnetisation (CRM) is a secondary magnetisation that takes place when magnetic minerals in a rock are chemically altered, or a new mineral is formed by some chemical actions. Lowrie (1997) gives precipitation of haematite from goethite, or from iron-saturated fluids passing through the rock as an example of the CRM. The magnetic minerals may also experience diagenetic modification or oxidation by weathering, which usually happens on the grain surface and along cracks. This process is particularly significant in sedimentary and metamorphic rocks.

2.4 THE GEOMAGNETIC FIELD

Magnetic anomalies caused by rocks and other man-made near surface features are localised effects superimposed on the normal magnetic field of the earth. For that reason, discussion of the behaviour of the geomagnetic field is necessary because of its effects on the acquisition and reduction of magnetic data, and on the interpretation of the resulting anomalies. The model of the components of the geomagnetic field shown in Figure 2.4 indicates that the total field vector **T** has a vertical component **Z** pointing downwards and a horizontal component **H** in the direction of magnetic north. The dip of the total field is the angle of inclination I which is the angle between the total field and the magnetic north. The angle between the geographic north and the magnetic north is the declination D. **T** varies from about 25000 nT in the equatorial regions to about 70000 nT at the poles (Kearey *et al*., 2002). The geomagnetic elements X, Y, and Z are recorded at magnetic observatories which are not uniformly distributed over the

earth's surface. Magnetic observatories are predominantly in the northern hemisphere. In the northern hemisphere the magnetic field generally dips downwards towards the north and becomes vertical at the north magnetic pole. In the southern hemisphere, the dip is generally upwards towards the north. The line of zero inclination is designated the magnetic equator. The magnetic equator approximates the geographic equator (Kearey *et al*., 2002).

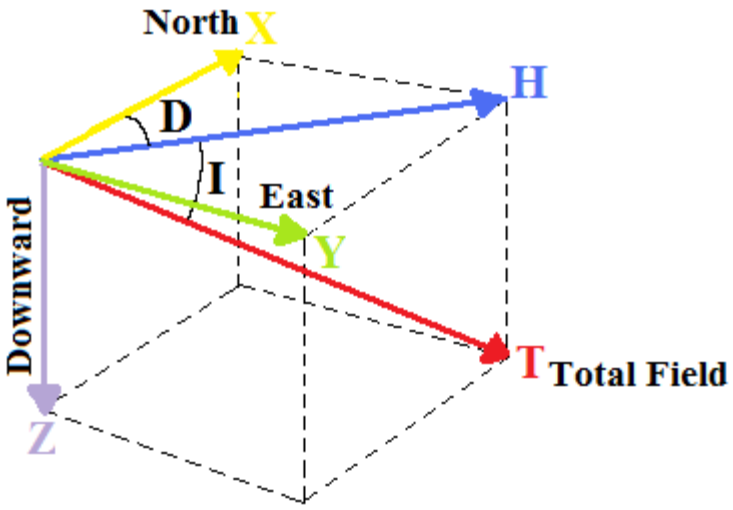


Fig. 2.4: The geomagnetic elements X,Y and Z

Repeated measurements of the main field of the earth at a fixed location reveal that the elements of the geomagnetic field are undergoing temporal changes ranging from milliseconds to millions of years. Sources of such changes which are broadly classified as external and internal are diverse in nature (Nettleton, 1976; Blakely, 1996; Lowrie, 1997). The changes most interesting to magnetic prospecting, particularly the detailed mineral and archaeological prospecting, are those associated with regional magnetic properties of the crustal rocks, and those of short-period variations caused primarily by sources of external origin.

2.4.1 The Magnetic Field of Internal Origin

The largest component of the earth's field is believed to originate from convection of liquid iron in the earth's outer core called the core field, or the main field (McElhinny, 1973; Blakely, 1996; Nabighian *et al*., 2005). The remainder, called the crustal field, originates primarily from a relatively thin outer shell of the earth (between 20 and 30 kilometres below the surface) where temperatures are below the Curie temperatures of important magnetic minerals, particularly magnetite (Fe_3O_4) and titanomagnetite (Fe_2TiO_4). Superimposed upon the crustal field may be the magnetic field produced by heat-related effects of prehistoric human habitation of an area. This may (or may not) be revealed depending on the scale of the survey. The mantle is generally considered to be nonmagnetic (Frost and Shive, 1986; Blakely, 1996) and hence the depth extent of the magnetic rocks is either the crust-mantle interface or the Curie-temperature isotherm. This field is monitored and studied using a global network of magnetic observatories and various satellite magnetic surveys (Peddie, 1983; Campbell, 1997). It has a global average of about 50000 nT (Nettleton, 1976; Telford *et al*., 1990; Lowrie, 1997). It varies with the latitude of survey area and changes slowly with time in what is known as secular variation.

2.4.2 The Magnetic Field of External Origin

Although magnetic surveys may focus on the crustal magnetic field (or the field resulting from man-made sources in the superficial layers), the magnetic field external to the earth is also very important in the surveys and must be considered. This field is the product of the interaction between the global field and magnetic fields associated

with solar wind (Campbell, 1997; Nabighian *et al*., 2005). Energetic gamma-rays, x-rays and ultra violet radiation from the sun cause ionization of nitrogen and oxygen molecules in the upper atmosphere (between heights of 50 and 1500 km) to form the ionosphere (Telford *et al*., 1990; Lowrie, 1997). Such ionization is most intense on the day side of the earth. The ionized molecules in the ionosphere release swarms of electrons that form powerful, horizontal ring-like electrical currents. As the earth rotates beneath the ionosphere, the observed intensity of the geomagnetic field fluctuates with a range of amplitude of about 10 to 30 nT at its surface within a period of 24 hours due to instabilities in the ring-currents. Such magnitude of the time-dependent event of the geomagnetic field (called diurnal variation, or daily variation) depends on the latitude at which the observations are made, and the degree of ionization of the ionosphere, which is a function of the solar activity. When the magnitude of the external field rises far beyond the above range, sometimes as much as 1000 nT, during a magnetic storm (Nettleton, 1976; Lowrie, 1997), it is normally advisable that the survey be discontinued.

2.5 THE MAGNETIC ANOMALY

As discussed in section 2.2, each grain of mineral in a rock or soil is either classified as diamagnetic, paramagnetic, or ferromagnetic. When such rock or soil is fired and allowed to cool in the earth's magnetic field, the alignment of the magnetic moments by the earth's field produces an induced magnetisation. In section 2.3, it was also discussed how each earth material containing a tiny quantity of ferrimagnetic and ferromagnetic minerals could become magnetized permanently during the formation of the rock or by later mechanism (remanent magnetisation). The total magnetisation ($\vec{M}$)

of such earth material is therefore the vector sum of the induced magnetisation ($\vec{M}_i$) and the remanent magnetisation ($\vec{M}_r$).

The magnetic field existing at any point on the surface (or near the surface) of the earth is the sum of the geomagnetic field (including internal and external fields) and the magnetisation acquired by any anomalous magnetic source within that vicinity. A total field magnetometer measures the magnitude of the total magnetic field of the earth including the field due to anomalous sources under soil cover, and magnetic noise in that environment. ***Magnetic anomaly*** can be defined as the difference between the measured (and suitably corrected) magnetic field of the earth and that which is expected from the international geomagnetic reference field (IGRF). It results from the contrast in magnetisation when subsurface materials with different magnetic properties are adjacent to each other. If $\vec{T}$ represents the total field at any point, and $\vec{F}$ is the regional field at the same point, then the total magnetic field anomaly is given by

$$\Delta T = |\vec{T}| - |\vec{F}|. \tag{2.24}$$

Let $\vec{B}$ (such as in equation 2.20) represent the perturbation of the regional field $\vec{F}$ due to some anomalous magnetic source. Then the total field is given by

$$\vec{T} = \vec{F} + \vec{B}. \tag{2.25}$$

Substituting equation 2.24 into equation 2.25 produces the total field anomaly given by

$$\Delta T = |\vec{F} + \vec{B}| - |\vec{F}|. \tag{2.26}$$

The total field anomaly is not equivalent to the magnitude of the anomalous field since ΔT in equation 2.26 is not equal to $|B|$. If the anomalous field is small compared to the ambient field, which is a good assumption in an archaeological site, then,

$$\begin{aligned}\Delta T &= |\vec{F}+\vec{B}| - |\vec{F}| \\ &\approx (\vec{F}.\vec{F}+2\vec{F}.\vec{B})^{\frac{1}{2}} - |\vec{F}| \\ &\approx (\vec{F}.\vec{F})^{\frac{1}{2}} + (\tfrac{1}{2})(2)(\vec{F}.\vec{F})^{-\frac{1}{2}}(\vec{F}.\vec{B}) - |\vec{F}| \\ &\approx \frac{\vec{F}.\vec{B}}{|\vec{F}|}\end{aligned}$$

That is, the total field anomaly is given by

$$\Delta T \approx \hat{a}_F.\vec{B},$$

where the unit vector $\hat{a}_F$ is along the regional field. Therefore if the ambient field is much larger than the perturbing field, the field produced by the anomalous magnetic source has one of its components in the direction of the ambient geomagnetic field. That component is its induced magnetisation, which is the component of interest in most archaeological sites.

CHAPTER 3

DATA ACQUISITION

3.1 INTRODUCTION

The scales of geophysical applications range from depth of 1 metre (or less) in engineering, environmental or archaeological survey (Clark, 1990; Godio and Torino, 2005; Martino *et al*., 2006) to a few (or even tens) of kilometres for crustal and upper mantle studies (Babu *et al*., 1982; Dawi *et al*., 2004). For each application, there is a limit to the depths of probe or smallest structures that can be detected, known as the resolution of the survey. In a small scale environmental survey such as the archaeological investigation, the magnetic anomaly can be as small as 0.1 nT (Scollar *et al*., 1986) requiring high resolution instruments. The artefacts are also small in size and buried at shallower depths compared to sources of magnetic field expected in oil exploration or mineral prospecting. To map such small superficial sources, the sampling rate or the line spacing must be made relatively small. The resolution of the survey is therefore a function of both the survey design and the resolution of the instrument. Full understanding of the instrument of measurement is required for successful data acquisition. Details of the instrumentation and the field work are therefore given in this chapter which is devoted to data acquisition.

3.2 INSTRUMENTATION

Since the early 1900s, many instruments have been designed (Breiner, 1999; Kearey *et al*., 2002; Nabighian *et al*., 2005) that are capable of measuring the vertical and horizontal magnetic field components, and the total magnetic field intensity. These geomagnetic elements were measured using instruments such as torsion head

magnetometer and the Schmidt vertical balance which consisted essentially of bar magnets suspended in the earth's magnetic field (Telford *et al*.,1990). Such equipment required accurate levelling and a stable platform for measurement. They were, therefore, not only time consuming but also restricted to sites on land. These sets of earlier magnetic equipment were replaced by fluxgate magnetometer which could be used to measure the same components of the field like the earlier meters, and were relatively fast and could be used on both land and sea. The fluxgate magnetometer with the highest resolution of only ±1 nT and a relatively long measuring time (about 11 seconds) compared to the modern magnetometers (with maximum of about 3 seconds) has also lost its earlier attraction. The most modern surveying magnetic instruments such as proton precession magnetometer, caesium vapour magnetometer, alkali (sodium and potassium) vapour magnetometers, etc., are, however, designed to measure only the total magnetic field and its vertical gradient with resolution of between±0.01 nT and ±0.1 nT which are higher than those of the earlier ones.

3.2.1 The G-856AX Proton Precession Magnetometer

The Geometrics G-856AX is a proton precession magnetometer. It utilizes the precession of spinning protons (or nuclei of the hydrogen atoms) in a sample of hydrocarbon fluid such as kerosene, shell sol-71, charcoal lighter fluid, n-Decane, isopar-1, etc., to measure the total magnetic field intensity, or its vertical gradient. The G-856AX proton precession magnetometer is currently the most commonly used magnetometer for both survey work and observatory monitoring (Nabighian *et al*., 2005; Kearey *et al*., 2002).

The magnetometer provides absolute readings of the total magnetic field to an accuracy of about ±0.1 nT. It has a number of advantages which include ruggedness, simplicity of operation, and has essentially no intrinsic heading error. The instrument has the disadvantage of weight, size and excess power demand which are all essential for it to have adequate signal strength.

3.2.2 The Features and Applications of the G-856AX Magnetometer

The major accessories of the G-856AX proton precession magnetometer are the console, sensor, sensor signal cable, aluminium staff (4 sections), console chest harness, two rechargeable lead-acid batteries, RS-232 data output cable, MagMap 2000 software (on CD) and application manual, also on CD (Figure 3.1). Depending on its particular configuration, the G-856AX can be a portable, or man-carried magnetometer, or a gradiometer measuring the field with two sensors, or a base station magnetometer. As a hand-carried instrument, it is operated simply by push button and an in-built digital memory stores the data when activated by another push button (using the **STORE** key), or set to do so automatically. All the operations are controlled from keys imbedded in a weatherproof membrane that comprises the magnetometer console's front panel (Figure 3.2). The key sequences for various operations have been carefully designed to provide simple yet flexible operation. For example, to store data automatically, the keys are pressed in the following sequence: **AUTO, STORE,** and **ENTER**, and any reading taken after that will be stored in the console's memory automatically. It stores over 5000 single sensor measurements, or 2500 gradiometer measurements (instrument manual). This relieves the user of the need to physically write down the data on the field, thereby

eliminating transcription errors and, most importantly, allows the use of computers to automatically record and process the data from the magnetic survey.

The G-856AX can also record data automatically at regular intervals, and can hence be left unattended to monitor diurnal changes in the earth's magnetic field (Figure 3.3).



Fig.3.1: The magnetometer accessories



Fig. 3.2: Magnetometer console's front panel
(All the keys except 'CLEAR' &'ENTER' are alpha-numeric.)

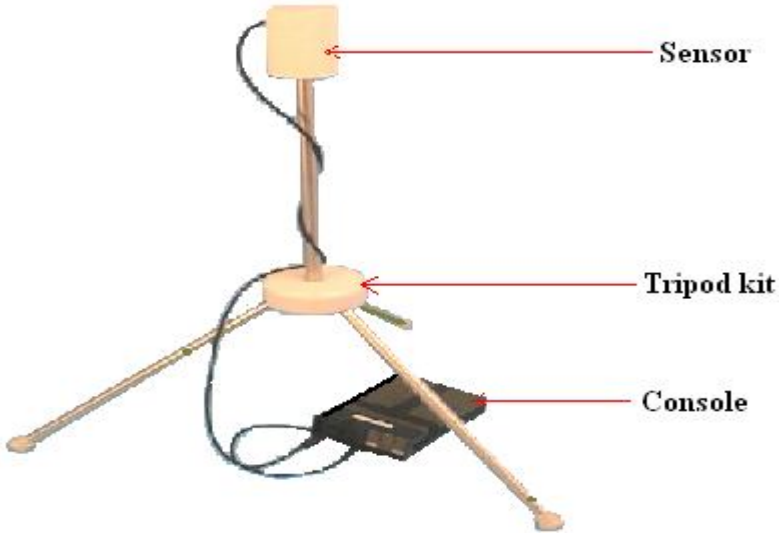


Fig. 3.3: Base station set up using tripod kit and staff section

These readings (up to 12,500) are collected at a base station and used to correct simultaneous field measurements for high accuracy surveys.

A single connector is used for the sensor signal input and data output. The output format is in the universal RS-232 protocol that is accepted by most modern computers. The interface software for downloading, profiling and gridding/contouring of data is part of the MagMap-2000 software. Physically, the G-856AX is compact and lightweight. It is weather proof and operates over a wide temperature range (-10^{o}C to 40^{o}C). It is powered by nine D-cell batteries or (more commonly) by an internal rechargeable lead acid gel cell battery.

3.2.3 The Magnetometer Sensor

The essential components of the sensor include a polarizing coil (solenoid), an hydrogen-rich liquid such as kerosene or isopar-1 (called sensor fluid) and a pick-up coil. The hydrogen nuclei (protons) in the sensor fluid have net magnetic moment (Blatt, 1992) which, coupled with their spin, cause them to precess about an axial

magnetic field (Telford *et al.*, 1976). When the sensor is placed in the earth's field, the protons align themselves in the direction of the field at that point. Depressing the **READ** key at the front panel of the console during magnetic measurements causes flow of electrical currents in the polarizing coil that is totally submerged in the sensor fluid. This current flow induces an internal magnetic field in the sensor that is much greater than the ambient geomagnetic field. This inducing field realigns the protons normal to the direction of the earth's field (about east-west direction). Releasing the **READ** key abruptly cuts off the current flow and the precession of the protons about the earth's field is detected by a second coil (the pick-up coil) as transient voltage building up and decaying over an interval of about 1 to 3 seconds.

The protons precess at an angular velocity ω (known as Larmor precession frequency) which is proportional to the magnetic field strength at the point of measurement. That is, if the earth's magnetic field strength at the measurement point is B_e, then the Larmor precession frequency is related to the field by

$$\omega = \gamma_p B_e \tag{3.1}$$

Because $\omega = 2\pi f$, where f is the precession frequency of proton, equation (3.1) can be further expressed as

$$f = \frac{\gamma_p}{2\pi} B_e . \tag{3.2}$$

where the constant of proportionality γ_p is the gyromagnetic ratio of proton, defined as the ratio of its magnetic dipole moment to its angular momentum. It has a numerical value of about 2.68 x 10^8 Hertz per Tesla. The Geometrics model G-856AX proton

precession sensor is capable of detecting the magnetic total field to an accuracy of about 0.1 nT in the earth's field of average value of about 50,000 nT.

The sensor also has some external features which include fill-port (with associated pot plug), mounting points of the sensor cable which include the electrical connection and the strain relief points (Figure 3.4). The sensor cable must be connected to the designated points using rust free hard-chromed finish (or stainless) tools such as pliers and screw drivers to avoid iron contamination. The relief point provides an extra support for the signal cable not to strain the electrical connection points. To prevent the sensor fluid from leaking out, a Teflon tape or a sewing thread must be rapped around the fill plug and carefully screwed into the fill-port.

3.2.3.1 Filling the Sensor with Sensor Fluid

In order to obtain optimum measurement results, the internal coils of the sensor must be completely submerged in any of these sensor fluids: (i) shell SOL-71, (ii) charcoal lighter fluid, (iii) n-Decane, (iv) ISOPAR-1, (v) odourless mineral spirits, and (vi) kerosene. The sensor must not be operated for an extended period without the fluid as this can damage it. Using the fill-port (Figure 3.4) a sensor fluid can be poured slowly into the sensor until it is full. The correct fluid level can be checked approximately by shaking the sensor and judging the fluid level by the degree of sloshing. Sewing thread was wrapped around the fill plug which was screwed into the fill-port and carefully tightened.

3.2.3.2 Sensor Orientation

The G-856AX sensor may be mounted on the sensor staff in either of two orientations: (i) end mounting (Figure 3.5a), so that the cylindrical axis of the sensor is parallel to the sensor staff or (ii) saddle mounting (Figure 3.5b), so that the sensor axis is perpendicular to the sensor staff. This is accomplished by screwing the sensor staff into either of the threaded receptacles in the standard (top) sensor shown in Figure 3.4. These alternative modes of mounting the sensor allow the G-856AX to be configured for use anywhere in the world. The end mounting and saddle mounting are also accommodated on the gradiometer (lower) sensor.

When making a measurement, the correct sensor orientation will be determined by the earth's magnetic field inclination in the survey area. In regions where the magnetic inclination is less than $\pm 40^{o}$, the 'white' area of Figure 3.6, the sensor should be mounted in the saddle position; that is, it is mounted so that the cylindrical axis is

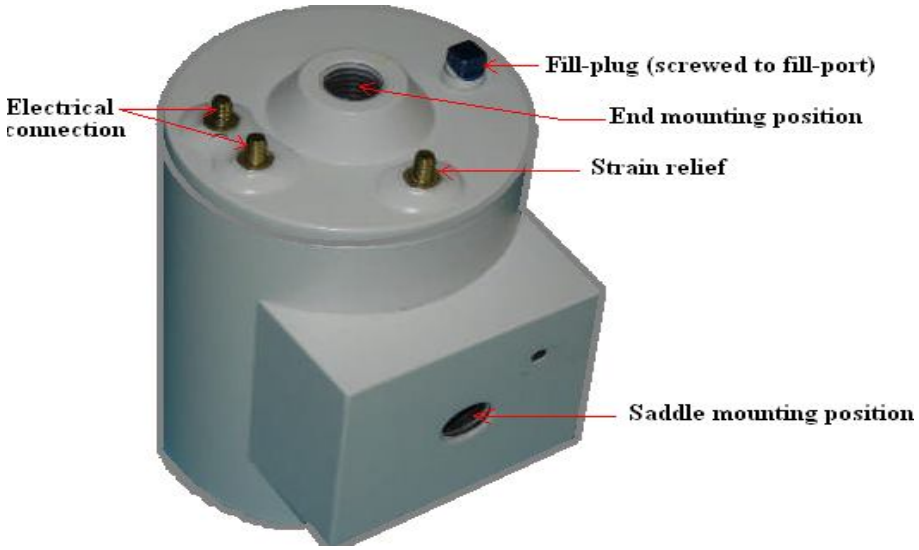


Fig. 3.4: Magnetometer sensor showing various points

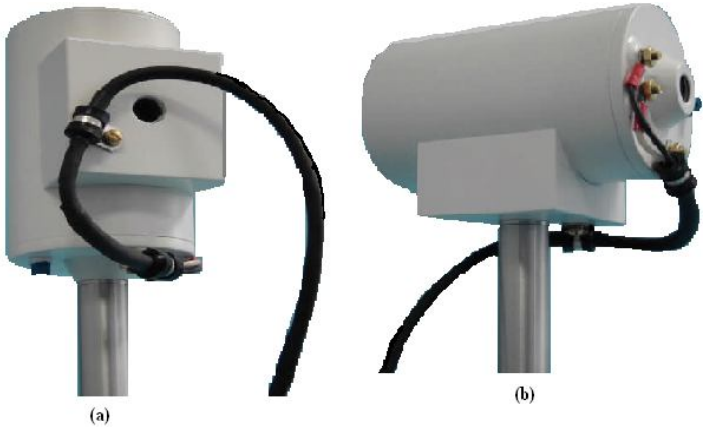


Fig. 3.5: Magnetometer sensor orientation
(a) End mounting (b) Saddle mounting

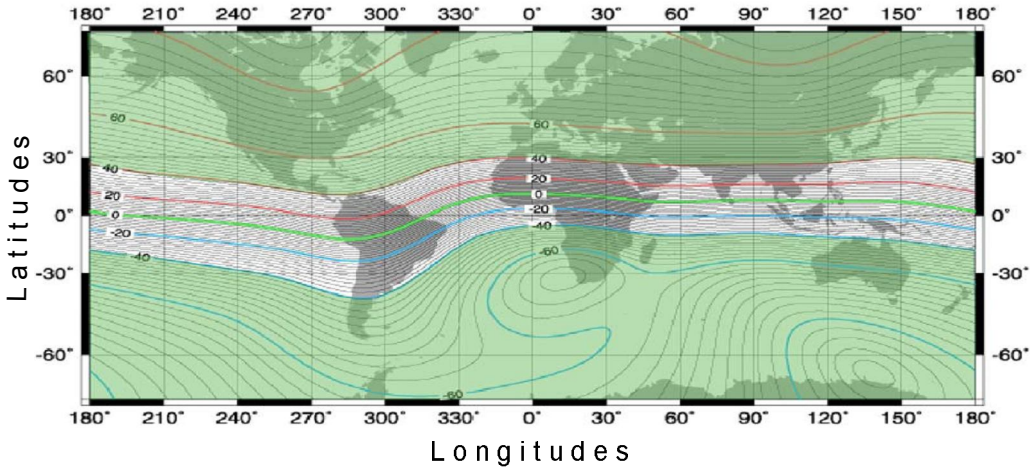


Fig. 3.6: Magnetic inclination of the earth's field
(adapted from G-856AX mannual)

horizontal. In this configuration, the sensor has a north arrow on one side. This arrow should be directed towards the magnetic north when taking measurements. Aligning the sensor this way will place the axis of the sensor's internal coils perpendicular to the earth's magnetic field (G-856AX instrument manual) and produce optimum signal (Sadiku, 1989). When surveying in regions where the magnetic inclination is greater than $\pm 40^{o}$; that is, in the 'green' region of Figure 3.6, the sensor should be mounted with its cylindrical axis vertical as shown in Figure 3.5a. This will orient the sensor for maximum signal where the magnetic field has high inclination.

3.2.4 Gradiometeter Assembly

The G-856AX gradiometer operation requires an extra set of accesssories. These items include the gradiometer sensor, lower staff adapter and upper staff adapter (not visible in Figure 3.7), two gradiometer sensor cables, and gradiometer switch. The gradiometer sensor cables are thinner than the standard sensor cable. One of the cables should be

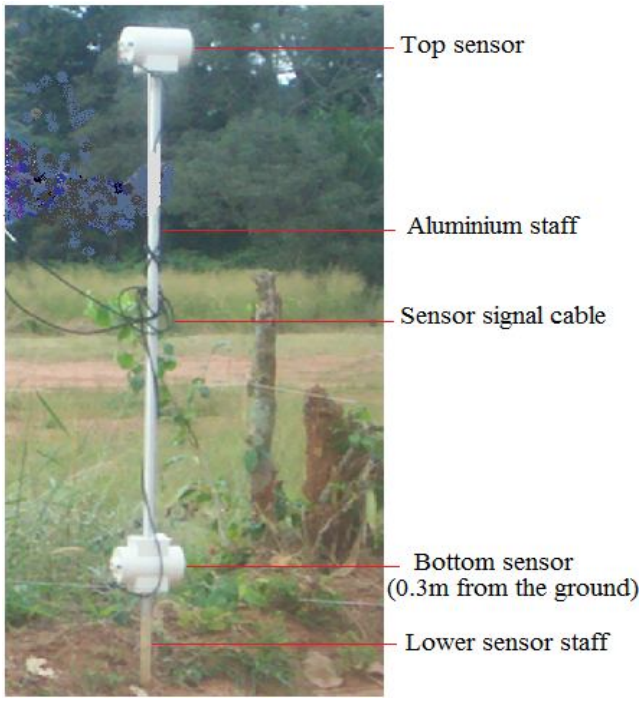


Fig.3.7: The gradiometer set-up at the lower latitude

attached to the top sensor using the stud washers and clamp. The second gradiometer sensor cable should also be attached to the bottom sensor. The two cables are then connected to the remote start switch box, which is in turn connected to the front panel of the magnetometer console. The sensors are connected to the aluminium staff as shown in Figure 3.7.

3.2.5 Console Control and Display

The console is controlled from a 12-keypad located on its front panel and shares this space with the two LED displays and sensor conector (Figure 3.2). All but two keys (**CLEAR** and **ENTER** keys) are alpha-numeric, and they are all labelled according to their functions and numeric input. The functions of the keys are summarised as follows: The **READ** key is used to take measurement of the magnetic field which is thereafter stored in the console memory using the **STORE** key. The readings stored in the memory can be accessed using the **RECALL** key which can also be used to decrement the memory location display. The **TUNE** key on the other hand is used to set the magnetometer tuning and also to display its signal strength while the **FIELD** key is used during memory recall to recover the field reading after **TIME** key has been depressed. The **SHIFT** key accesses the keys' numeric values instead of their functions. The **CLEAR** key erases a keystroke or keystroke sequence while **ENTER** key designates the end of a key sequence and transfers command to the console's processor. Others are **ERASE, AUTO** and **OUTPUT** keys which are respectively used to erase a reading (or the whole data in the memory), start and stop automatic recording/tuning, and begin output of stored data to an external device.

The LED display functions on the console are two, the **FIELD/TIME** display and **STATION/DAY** display. Each magnetic measurement taken during a survey is displayed on the **FIELD/TIME** display and goes off after about 5 seconds. This display also shows measurement time and the real time clock. The **STATION/DAY** display shows the battery voltage, the line number and the station number during field measurements.

3.2.6 Operating Procedures of the G-856AX

The internal clock of the magnetometer can be set to the Julian date and time by pressing **AUTO, TIME,** and **SHIFT** keys in sequence then followed by the figures for the date and time using the format: 'day', 'day', 'day', then 'hour', 'hour', 'hour', and 'minute', 'minute', 'minute'. This sequence is immediately followed by pressing the **ENTER key** to store the new date and time. The Julian date is the number of days since the beginning of the year. For instance, the Julian date corresponding to 30th June, 2010 is 181.

In the survey mode, the magnetometer is equipped with a means of designating the current survey line with a line number that will be stored in the console memory. Each measurement that is made in survey mode is designated by its line and station numbers. In this mode, a three-digit number indicating the line number appears in the **STATION/DAY** display when the **TIME** key is depressed. Although not all the recorded parameters are available for viewing on the displays, the G-856AX data file contains the values of the five recorded parameters for each data point. These are the field reading, the station and the line numbers, the time and the Julian date.

The magnetometer also needs to be tuned in order to provide its amplifier circuitry with the greatest signal strength and thereby providing the best sensitivity. The tuning procedure is a matter of matching the console's internal tuning frequency to the actual proton precession frequency corresponding to the local magnetic field strength (G-856AX manual). Usually, fairly accurate readings can be obtained if the magnetometer is tuned to be within 3000 nT of the local magnetic field strength which can be

approximated from the world magnetic map of Figure 4.2. This world map is overlain with contour lines showing the regional variation of magnetic field strength with position.

At the beginning of a new survey, the magnetometer should be checked for proper tuning by pressing and releasing the **TUNE** key, and if not, it should be tuned so as obtain maximum signal strength. On depressing the **TUNE** key, the **FIELD/TIME** display shows ***'SIG',*** indicating the signal strength (between **0.0** and **9.9**) in **STATION/DAY** display. This is immediately followed by appearance of ***51G*** on the **FIELD/TIME** display and ***1.7*** on the **STATION/DAY** display. After about one second, this display will be succeeded with something like ***tunE*** on the **FIELD/TIME** display. This shows the current tuning in terms of magnetic field intensity with units of 100 nT. For example, if the display shows '***330***', then 33000 nT tuning is indicated. The objective in tuning the magnetometer is to adjust the magnetometer's tuning (as indicated under ***tunE***) to obtain a reasonable signal strength (as indicated under '***SIG***'). The magnetometer tuning is done outdoors, away from power lines and any large metal object that can generate magnetic field. The procedure is, pressing **TUNE** key followed by **SHIFT** key then the three-digit number (for example **330**) then followed by **ENTER** keystroke. To know if the magnetometer is properly tuned, the **TUNE** key is pressed and held down and the signal level (between 0.0 and 9.9) is read from the **FIELD/TIME** display. A signal level lower than 3.0 indicates poor tuning and so the sensor should be checked for proper filling, else, the tuning procedure should be repeated.

In most field operations, it is necessary to set the **G-856AX** magnetometer to automatic tuning mode after a few 'good' readings have been taken. This mode helps to reduce the time required to complete data acquisition in a given site. This is done by depressing **AUTO, TUNE** and **ENTER** keys in sequence. The displays will then show ***A tunE oFF,*** and automatic tuning will be turned on. To deactivate the automatic tuning function, the console keys **AUTO**, **TUNE** and **CLEAR** are depressed in sequence. To determine the instrument's tuning mode, it suffices to press AUTO then TUNE and the **STATION/DAY** display will indicate whether the **AUTO** tune function is on or off.

Magnetic field measurements can be made after the instrument is properly tuned by depressing and releasing the **READ** key followed by the **STORE** key. These two keys are the only keys that are normally used when acquiring the magnetic data. When the **READ** key is depressed, the display will light briefly, showing '***batt 11.7***', for instance (the battery voltage), then the battery voltage will turn off after a short interval of time and the **FIELD/TIME** display will light showing a 5 or 6 digit number. This is the magnetic field reading in nano-tesla (nT). As the magnetic field appears in the **FIELD/TIME** display, another number appears in the **STATION/DAY** display such as ***001***. This is the station number. Both displays will show the readings for 5 seconds and then go off. To store the reading in the console memory, the **STORE** key should be depressed while the displays are still on. If the displays go out before the **STORE** key is depressed, the reading will be lost and the displays will show ERROR message. Otherwise the display will go out after the **STORE** key has been depressed.

The G-856AX can also be configured to store survey measurements automatically. In this mode all that is needed is to depress **READ** key in order for the console to read and store the measurement. To enable automatic storage, the **AUTO, STORE** and **ENTER** keys are depressed in sequence. To revert to the standard manual store mode, the keys are again depressed in the sequence: **AUTO, STORE, CLEAR**.

The G-856AX is also equipped with the facility that allows erasing of the last reading, the last group of readings, or the wiping out of the entire data in the console memory. To erase the last reading, the keys are depressed in the sequence: **READ, RECALL, ERASE, ERASE**. In such key sequence, the **READ** keystroke positions the memory pointer to the latest stored measurement and the **RECALL** keystroke recalls it from the console memory. Pressing **ERASE** key twice in succession while the displays are still on erases the data for this last measurement record. To erase the latest group of readings, the station number (075, for instance) where the erasure is to begin is identified, and by pressing: **RECALL, SHIFT, 075, ENTER, ERASE, ERASE** in sequence, all the readings taken between station number 075 and the last reading will be wiped out. To completely erase all the readings, the correct key sequence is: **RECALL, SHIFT, 0, ENTER, ERASE, ERASE,** and the entire data stored in the console memory will be wiped out.

3.3 DATA RETRIEVAL

Before beginning retrieval of data, the magnetometer console has to be checked to see that the batteries have sufficient energy. Failure to do this could result in incorrect or incomplete data transfer. A minimum of 9.0 volts of battery energy is required for the

data transfer. A simple test of the battery voltage can be performed by pressing the **READ** key when the sensor is not attached to the console.

3.3.1 Computer Connection and Download

The G-856AX is designed to be used with personal computer running one of the MS windows operating systems. MagMap2000 software (supplied with the instrument) should be installed in the computer. The software facilitates data download from the G-856AX and for processing the measurement results. A serial download cable is included with the G-856AX which is used to interconnect the magnetometer console's front panel connector with the serial port on a windows PC. The download cable is connected to the console's front panel connector and to the PC's serial port. Under the file menu item of the MagMap2000 software, "import G-856AX data" should be selected. A dialog box will appear that allows: (i) selection of the computer's communication port that is connected to the magnetometer, (ii) selection of the Bau rate, and (iii) setting the file name/directory for the data storage. After this information is provided, "DOWNLOAD NOW" is clicked on. Then on the G-856AX, the **OUTPUT** key and **ENTER** key are pressed in sequence and the MagMap2000 will display a dialog box that shows the progress of data transfer from the magnetometer console to the computer.

3.4 GETTING THE SITES AND THE INSTRUMENT READY FOR DATA COLLECTION

The commencement of the field work was the setting up of the magnetometer in preparation for data collection. This involved filling the sensors with the right sensor fluid, mounting the sensors on the sensor staff and connecting them to the console, and

tuning the magnetometer to receive adequate signal strength. This was followed by scanning of the site for possible magnetic anomalies, and based on such results, the dimensions and the orientations of the three sites were chosen. For each site, the coordinates of the four corners were taken using a global positioning system (GPS), and the four cardinal directions were also noted using the magnetic compass. To acquire closely spaced data at regular interval, it was necessary to create a regular grid (Clark, 1990) of the various archaeological sites. These were followed by creation of a base station within the site since total field would also be recorded. Finally, the magnetic measurements were made using the Geometrics G-856-AX gradiometer.

3.4.1 Setting Up the Gradiometer Assembly

To obtain a set of useful magnetic data from any chosen site, the magnetometer accessories must be kept free of dust or dirt as this may contaminate the sensor(s) magnetically. Since such contamination can affect the measurement result, the accessories were properly checked (Figure 3.8) and cleaned up at the beginning of every field work. The sensors were also checked for proper filling of the sensor fluid. This was to ensure that the coils of insulated wire used for signal generation in the sensor were totally submerged in the proton-rich fluid. They were then mounted on the sensor staff in the saddle position (Figure 3.5b) since Lejja archaeological site is located close to the magnetic equator where the total field is horizontal. The sensor signal cables were connected to the console's connector through the switch. The Julian date and the console time were also compared with the local ones by depressing and releasing the **READ** key, and if any difference, it was reset to match with date and the local time.

The gradiometer assembly was later checked for proper operation some distance away from buildings, power lines, vehicles and other structures that could generate significant magnetic fields. This involved depressing the **READ** key to observe if the system could read the field strength correctly. The magnetometer tuning was also checked by pressing and releasing the **TUNE** key, thereafter it might be tuned to the background of



Fig. 3.8: Unpacking the gradiometer components at Ejuona
The author was checking the lower sensor for dirt and proper filling of the sensor fluid, while the field assistant was carrying the top sensor

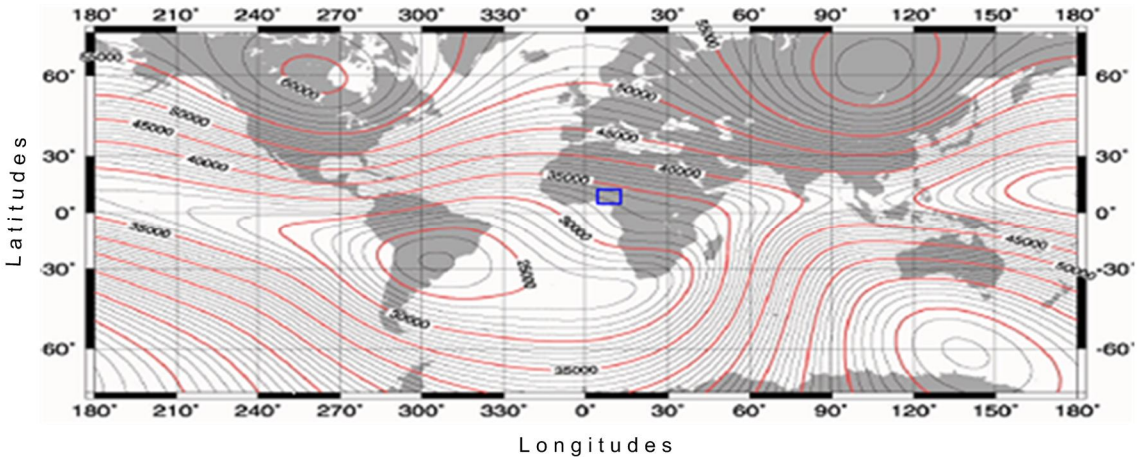


Fig. 3.9: World magnetic map showing the regional field of interest

(adapted from G-856AX manual)

33000 nT which was the geomagnetic field corresponding to the site using the world magnetic map in Figure 3.9. This was to ensure that the amplifier circuitry was provided with the greatest signal strength required to obtain the best sensitivity (Breiner, 1999).

3.4.2 Site Scanning With the Magnetometer

Random walks were made through the Lejja archaeological site to discover possible areas of iron smelting activities. The sight of a few pieces of bloom on the ground was a symbol of the smelting activity. To scan such site, the magnetic compass was first used to locate the north-south direction so as to know the correct orientation of the sensors. The magnetic readings were then taken using standard magnetometer assembly at interval of three steps which was estimated to be about 2.5 metres along the profiles which were, on the other hand, spaced three steps away from the initial route. It was certain that the routes might not be straight, neither could the data points be uniformly spaced, but contouring of such set of data using standard measurement such as data spacing of 2.5 metres and line spacing of 2.5 metres could produce a clue as to zones of high and low magnetizations within the archaeological site (Niku and Smekalova, 2002). This type of data set was acquired at Uwani, Ugbelenabo and Ejuona. These were contoured to determine the dimensions and orientations of the various sites. An example of such plot that guided the selection of the dimension of the site is shown in Figure 3.10. In such a case, there was no need for any form of data reduction. All that

33426
33156
33150
33149
33147
33146

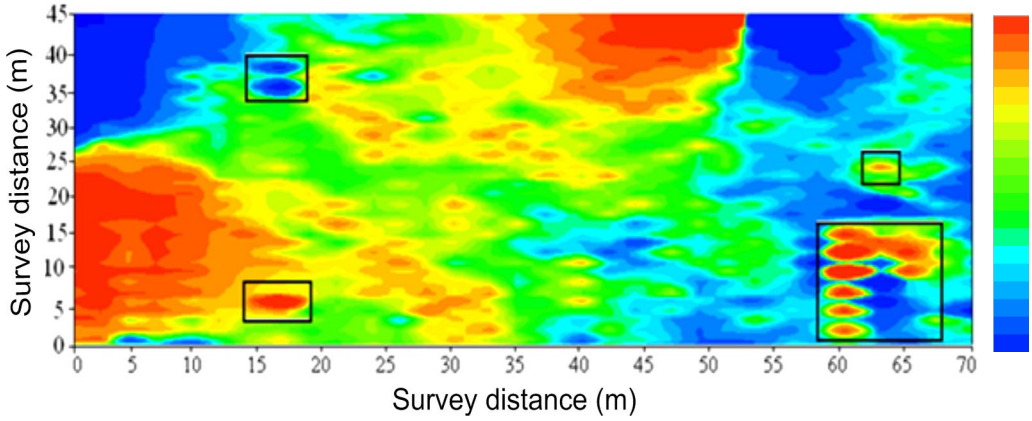


Fig. 3.10: Colour plot of field scanning at Uwani
(highlighting anomalous zones of interest)

was required was the ability to identify major events (or contour closures) not associated with features that are found on the ground surface. Some of the similar events have been highlighted in Figure 3.10.

3.4.3 Establishing the Grid

Results of geophysical surveys are interpreted by comparing readings from one area with those from other areas. The best way to achieve this, particularly when it involves dense coverage, is to take readings at regular intervals (Clark, 1990; Osella *et al*., 2005; Martino *et al*., 2006). This condition therefore called for setting up a grid for each of the sites. It is important to note that a grid once set up can be repeated since it is expected that it would be used to know the exact location of any anomalous zone.

The best way to create a grid is to locate two relatively permanent features which could be natural or cultural within the landscape that are adequately far apart to be used as a baseline by joining the two points. In the Lejja archaeological sites, both natural features (life trees) and cultural features (building and roads) were used to form the baselines which varied in length between 60 metres in Uwani and Ejuona to 70 metres

in Ugbelenabo. Grid squares of 0.5m by 0.5m were offset from each baseline along the cross-line direction using marked strings of alternate black and white colours at half metre interval. To obtain the grid line normal to the baseline, the triangulation method (Clark, 1990) with diagonal of 28.28 metres of 20 metres square right angle triangle was used (Figure 3.11). That is, each measurement was made from the origin 'O' normal to the baseline OP (based on the chosen length of the profile) to point Q (the 3rd corner of the site). To obtain the line PR, the triangulation method was also used. Joining points Q and R produced a straight line parallel to the baseline with construction error

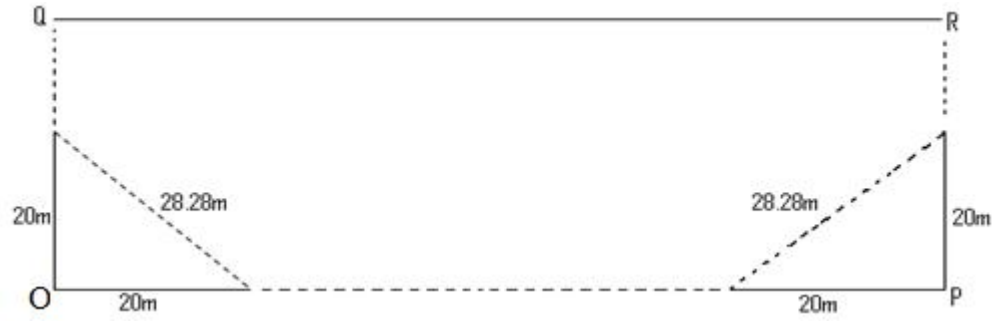


Fig. 3.11: Establishing grid with the triangulation method
(OP is the baseline)

of less than 0.12% at all the sites. The lines parallel to OQ or PR (cross lines) were the grid profiles along which magnetic measurements were made.

At the onset of the field work, bamboo stick pegs were used to line-up the baseline and the opposite line (parallel) to the baseline (Figure 3.12). The bamboo pegs were chosen since they were not magnetic, and hence could not interfere with the near surface magnetic field, making no contribution to the magnetometer readings. Their straight and hard nature also made their hammering to the ground easy, while their light weights make them easily potable. Each grid profile was marked with a peg such that a marked

string tied on a peg positioned on the baseline and the corresponding peg positioned on the opposite line served as a grid profile. This method was reliable but tedious even with three workers on site. To reduce the labour and cost, only eight pegs were later used; four pegs for the four corners of the site, and two for each of the two marked strings. The process of gridding the site was then completed by the use of four marked strings, one fixed along the baseline (Figure 3.13), the second one fixed along QR (the opposite line parallel to the baseline) while the remaining two were used as mobile strings parallel to OQ and PR. For example, if a location were to be gridded 1 m by 1 m, the mobile string 1 would be positioned 1m away from the beginning of

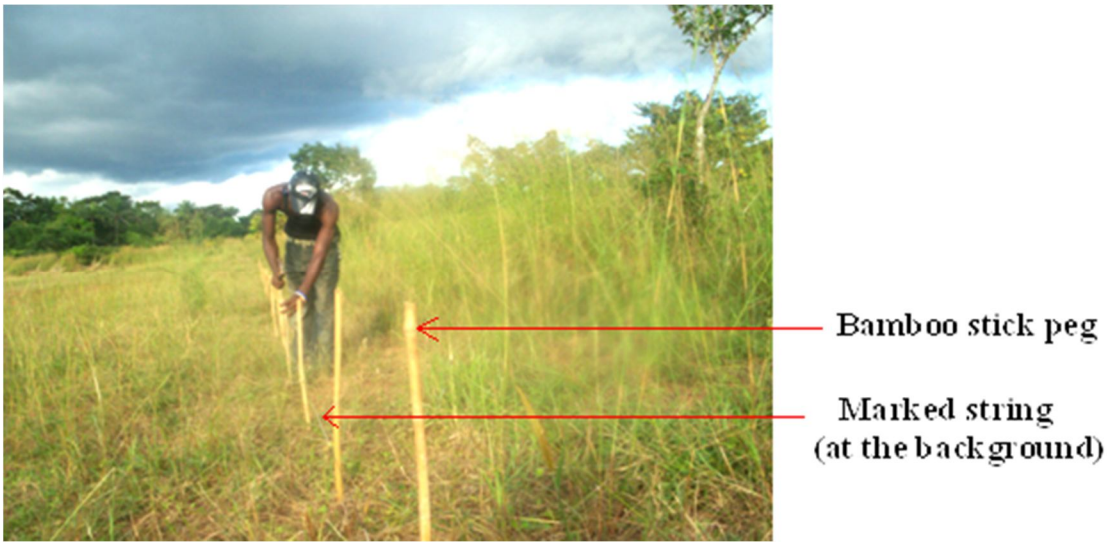


Fig. 3.12: Using bamboo stick pegs to mark the baseline
(at Ugbelenabo site)



Fig. 3.13: Using the marked string at the baseline in Ejuona site

the baseline string and the same distance away from the opposite string, while the mobile string 2 would be positioned parallel to and 1 m away from string 1.

3.5 MAGNETIC DATA ACQUISITION

Magnetic measurements acquired from the archaeological sites focus on variations in the magnetic field produced by lateral variations in the magnetization of the subsurface resulting from the presence of archaeo-magnetic sources. This expectation does not come without interference by some external magnetic sources which are the product of interaction between the global field and magnetic field associated with solar wind (Blakely, 1996; Campbell, 1997; Lowrie,1997; Nabighian *et al*.,2005). So such detailed survey, requiring high precision, must take cognisance of such external influence by incorporating some of it in the field design. Therefore, a base station had to be established at every site to pave way for the removal of diurnal effects from the acquired field data.

3.5.1 The Base Station

The earth's magnetic field varies over its surface from time to time and place to place. These changes, called ***diurnal variations*** (Telford *et al*., 1990; Nabighian *et al*., 2005), are largely due to variations in solar flare activity and the effect that solar storms have on different locations on the earth. There are several ways to remove the effects of diurnal variations (Nettleton, 1976; Breiner, 1999; Kearey *et al*., 2002). For the smaller scale archaeological applications, the use of a ***base station*** near (or within) the survey area is usually deployed (Clark, 1990). The base station can either be re-occupied at a fixed time interval throughout the survey, or after a certain number of data points, or (if the economy of the researcher allows) an instrument can record the geomagnetic field continuously at this location throughout the period of the survey. The diurnal variations can thus be subtracted from the measurements obtained from the area surveyed. In the design of the archaeo-magnetic prospecting in all the three sites, the base station was (by choice) located approximately midway between the beginning and the end point of the baseline for each of the sites. Each base station was marked with a peg so that magnetic readings could be taking at the fixed point throughout the period of the survey.

3.5.2 The Data Collection

The typical survey geometry consisted of a series of measurements equally spaced along a series of parallel lines. The lines were positioned so as to form a rectangular grid. This type of survey design ensured that the measurement points defined a grid that sampled the magnetic field strength at a uniform spatial density (Figure 3.14).

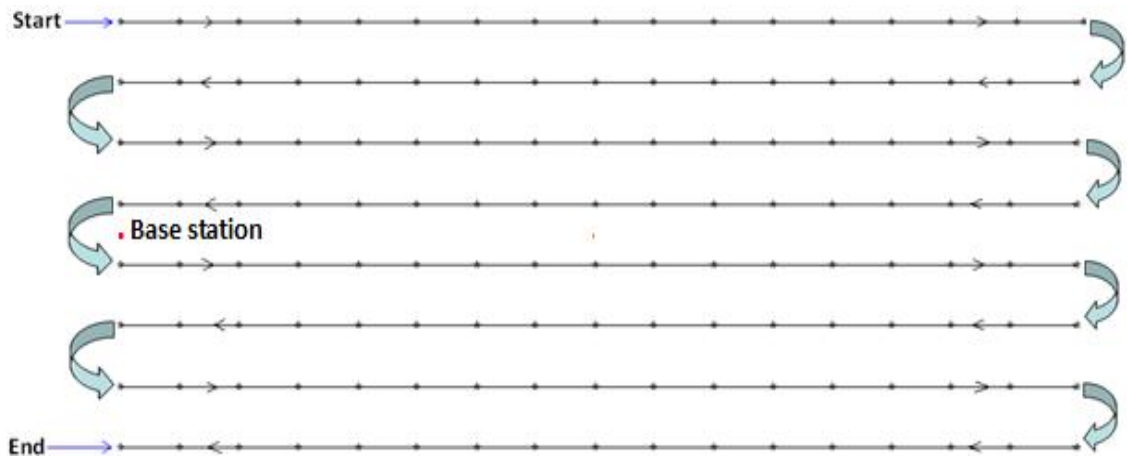


Fig. 3.14: The pattern of the field layout showing the base station and the bi-directional traversing

To begin the data collection at any site, the standard survey sensor (i.e., the top sensor) was positioned 1.25 metres vertically above the gradiometer sensor (i.e., the lower sensor). The lower sensor on the other hand, was raised only to a height of 0.30 metre above the ground. This was to increase its sensitivity to the very near-surface magnetic sources (Clark, 1990). This set up then means recording both the total field data and the vertical gradient of the total field data at the heights of 0.30m and 1.25m respectively. The line number and the station number were then set since each measurement would be designated in the console memory by its line and station numbers. When taking magnetic reading, the gradiometer assembly was positioned such that the north arrow, located on the top sensor, would point to the magnetic north. This was to ensure highest magnetic flux linkage between the geomagnetic field and the internal coils of the magnetometer sensors.

The first reading was always taken at the base station by depressing and releasing the **READ** key. Depressing the **STORE** key automatically stored the reading in console

memory. The console could also be set to automatic store mode by pressing **AUTO, STORE, ENTER** in sequence. The field magnetic measurements then commenced on the grid lines starting from a point such as labelled 'start' in Figure 3.14 and progressed in the direction of the arrow. At the end of line one, the line number would be changed to line two by pressing **TIME** key on the console followed by S**HIFT** key, then **002**, and **ENTER** key in sequence. The subsequent readings were then recorded against the new line number and the corresponding station numbers. The traversing was made in the bi-directional method; which means, if the north arrow on the sensor was pointing away from the operator of the magnetometer while taking measurements on line 1, it would be pointing to him while measurements were being made on line 2. During this period, the two field assistants would have moved string 1 over the magnetometer operator to position three at front of the swath (Figure 3.15). On reaching the end of line two, the circle would be repeated by changing the line number to 003 and taking the second base station measurement before starting the field measurements on the new line. This sequence was repeated until the entire site was covered, with every odd number line bearing extra reading at the beginning of the profile, waiting to be removed at the data processing stage. The same field procedure was repeated in all the sites.



Fig. 3.15: The use of marked strings in forming the survey grid
(Taking magnetic measurements at Ugbelenabo)

3.6 DOWNLOADING DATA FROM CONSOLE MEMORY

A good way to visualize the console memory is to think of the data as being in a "stack" of lines, where each line is made up of two parts with the first part being the ***coordinates of the data point*** while the second part is made up of time, line number and the Julian date (Table 3.1). To retrieve the data from the console memory, the RS-232 serial down-load cable was connected between the console and the serial port of an MS windows computer in which the downloading software, MagMap2000, was earlier installed. To download the data, the **OUTPUT** key was depressed and the software prompted the specification of the spacing between the discrete readings and the spacing between survey lines. After these were supplied (0.5 metre each), the program then required information on the spacing between the upper and the lower sensors. When it (1.25 metres) was supplied, followed by pressing the **ENTER** key, the program assigned a position to each reading, creating a uniform grid. It also calculated the vertical gradient (VRT-GRA) by obtaining the difference between total field recorded at the

lower sensor and that recorded at the upper sensor and dividing it by 1.25 metres (the separation of the two sensors). The information stored in the G-856AX memory, beginning with the last station number (Table 3.1), was automatically transmitted to the computer using the RS-232 serial download cable. Such data set may contain some readings (spikes) which are too high compared to the adjacent ones. Spikes which may be caused by large metal objects are removed during data processing.

Table 3.1 An example of the console memory stack

X	Y	BOTTOM-RDG	TOP-RDG	VRT-GRA	TIME	DATE	LINE	MARK
60	0	33135.2	33128.8	5.12	17:27:28	11/03/09	60	4326
60	1	33146.8	33130.2	13.28	17:27:17	11/03/09	60	4324
60	2	33132.4	33129.8	2.08	17:27:05	11/03/09	60	4322
60	3	33131.2	33128.4	2.24	17:26:55	11/03/09	60	4320
60	4	33095.8	33126.8	-24.8	17:26:44	11/03/09	60	4318
60	5	33122.2	33127.4	-4.16	17:26:33	11/03/09	60	4316
60	6	33128.8	33127.8	0.8	17:26:23	11/03/09	60	4314
60	7	33128.6	33128	0.48	17:26:13	11/03/09	60	4312
60	8	33129.6	33128.4	0.96	17:25:58	11/03/09	60	4310
60	9	33128.8	33129.2	-0.32	17:25:48	11/03/09	60	4308
60	10	33130	33129.2	0.64	17:25:37	11/03/09	60	4306
60	11	33129.8	33128.8	0.8	17:25:27	11/03/09	60	4304
60	12	33126.6	33128	-1.12	17:25:17	11/03/09	60	4302
60	13	33120.2	33127.8	-6.08	17:25:07	11/03/09	60	4300
60	14	33124.8	33126.6	-1.44	17:24:57	11/03/09	60	4298
60	15	33124.6	33125.8	-0.96	17:24:47	11/03/09	60	4296

CHAPTER 4
FORWARD COMPUTATION OF MAGNETIC ANOMALY OF A 3-DIMENSIONAL BODY

4.1 INTRODUCTION

In order to correctly interpret a set of geophysical data, mathematical boundary problems must be solved for the type of naturally occurring (or artificial) field of same nature which the field data are expected to represent. This is because inversion problem cannot exist without forward problem (Roy, 2008). Menke (1989) relates geophysical data ***d*** with the model parameters represented as elements of a vector ***m*** of a causative subsurface body in the mathematical equation given by

$$\mathbf{G}\boldsymbol{m} = \boldsymbol{d}, \tag{4.1}$$

where **G** is an n x m matrix of powers of the independent variable. Based on equation (4.1), Blakely (1996) categorised the interpretational techniques into three, and emphasised that the goal of each technique should be geared towards illuminating the spatial distribution of the sources of magnetic fields. The techniques are forward method, inverse method and data enhancement and display. The forward problem aims at obtaining the data ***d*** by assuming some values for the parameters of the model. In magnetic method, this entails theoretical calculation of magnetic anomalies from a given set of model parameters. On the other hand, the determination of the parameters of the model ***m*** from the recorded data, called the inverse method, requires calculation of one or more body parameters automatically and directly from the observed anomaly. In the data enhancement and display technique (Scollar *et al*., 1986; Piro *et al*., 1998, Piro *et al*., 2007), no model parameters are actually calculated but the anomaly is processed in some way (Blakely, 1996) in order to enhance certain characteristics of the source thereby facilitating the overall interpretation.

Section 4.2 focuses on the forward method but not in its entirety (Tsokas and Papazachos, 1992; Press *et al*., 1992; Blakely, 1996; Piro *et al*., 1998; Godio and Torino, 2005). It is aimed at generating the synthetic magnetic anomalies, and to use such fields for verification of the sensitivity and effectiveness of the FORTRAN program developed for the interpretations of the processed field data. It is, therefore, sufficient to use any forward modelling algorithm that assumes bodies of simple geometrical shapes such as prismatic bodies (Bhattacharyya, 1964; Rao and Babu, 1991), or other algorithms that are based on the assumption of irregularly shaped bodies (Talwani, 1965; Bhattacharyya and Navolio, 1975; An *et al*., 2004; Kostrov, 2007). The approach of Rao and Babu (1991) was deployed in the generation of the synthetic data mainly because of its simple approach. It was also because of its improvement on the good work of Kunaratnam (1981), based on speed of operation that has decreased the computing time by a factor of about 3 (Rao and Babu, 1991).

4.2 THE FORWARD METHOD

The theoretical magnetic anomalies for a three-dimensional model can be computed using a computer program (Appendix C.1) that has been developed in the course of this study using Rao and Babu (1991) model. The vertical sided prism model (Figure 4.1) used by these authors is a commonly used geometrical model for the three-dimensional

interpretation of magnetic anomalies. The algorithm is for fast computation of the magnetic anomalies which may be due to multiple prisms. It is a modification of Kunaratnam (1981) model made for rapid computation of the magnetic anomalies. Rao and Babu (1991) worked in Cartesian coordinates and assumed x-axis along geographic north, the y-axis along the east and z-axis vertically downwards. A point 0 on the observation plane was assumed to be the origin of the coordinate system, with observations made at grid points laid parallel to the x- and y-axes. The methodology adopted allowed the calculation of total magnetic field anomalies at any arbitrary point on the surface generated by any prismatic body. From Kunaratnam (1981), Rao and Babu (1991) obtained the following equation for the total magnetic field anomaly:

$$\Delta T(x,y,0) = G_1 \ln F_1 + G_2 \ln F_2 + G_3 \ln F_3 + G_4 F_4 + G_5 F_5 \tag{4.2}$$

where

$$F_1 = \frac{(R_2+\alpha_1)(R_3+\alpha_2)(R_5+\alpha_1)(R_8+\alpha_2)}{(R_1+\alpha_1)(R_4+\alpha_2)(R_6+\alpha_1)(R_7+\alpha_2)} \tag{4.3}$$

$$F_2 = \frac{(R_2+\beta_1)(R_3+\beta_1)(R_5+\beta_2)(R_8+\beta_2)}{(R_1+\beta_1)(R_4+\beta_1)(R_6+\beta_2)(R_7+\beta_2)} \tag{4.4}$$

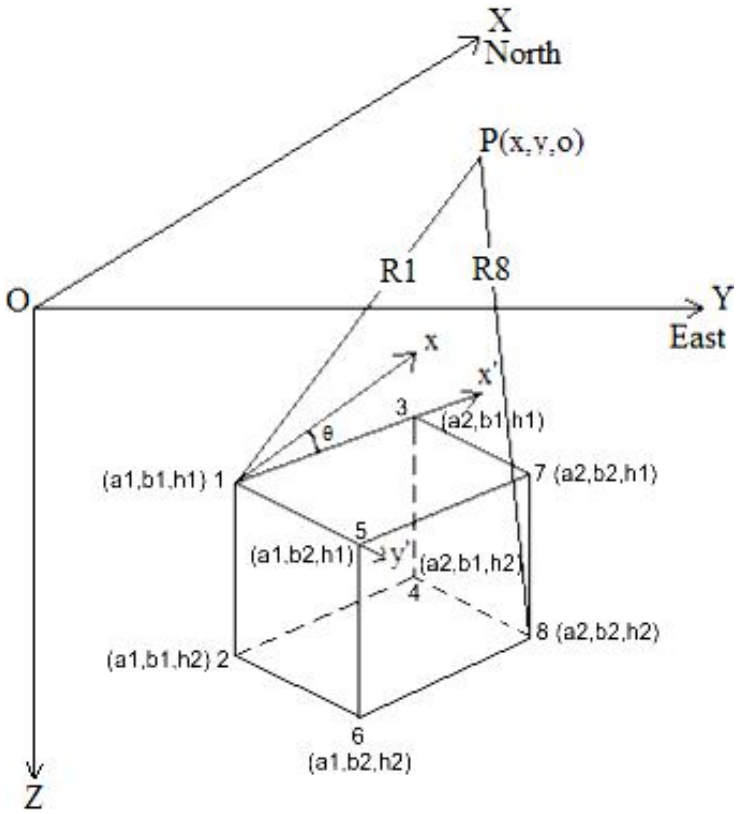


Fig. 4.1: 3-D rectangular prism

$$F_3 = \frac{(R_2+h_2)(R_3+h_1)(R_5+h_1)(R_8+h_2)}{(R_1+h_1)(R_4+h_2)(R_6+h_2)(R_7+h_1)} \tag{4.5}$$

$$F_4 = \arctan\frac{\alpha_2 h_2}{R_8\beta_2} - \arctan\frac{\alpha_1 h_2}{R_6\beta_2} - \arctan\frac{\alpha_2 h_2}{R_4\beta_1} + \arctan\frac{\alpha_1 h_2}{R_2\beta_1}$$
$$- \arctan\frac{\alpha_2 h_1}{R_7\beta_2} + \arctan\frac{\alpha_1 h_1}{R_5\beta_2} + \arctan\frac{\alpha_2 h_1}{R_3\beta_1} - \arctan\frac{\alpha_1 h_1}{R_1\beta_1} \quad (4.6)$$

$$F_4 = \arctan\frac{\beta_2 h_2}{R_8\alpha_2} - \arctan\frac{\beta_2 h_2}{R_6\alpha_1} - \arctan\frac{\beta_1 h_2}{R_4\alpha_2} + \arctan\frac{\beta_1 h_2}{R_2\alpha_1}$$
$$- \arctan\frac{\beta_2 h_1}{R_7\alpha_2} + \arctan\frac{\beta_2 h_1}{R_5\alpha_1} + \arctan\frac{\beta_1 h_1}{R_3\alpha_2} - \arctan\frac{\beta_1 h_1}{R_1\alpha_1} \quad (4.7)$$

and

$$R_1 = \sqrt{\alpha_1^2 + \beta_1^2 + h_1^2}\,, \quad R_2 = \sqrt{\alpha_1^2 + \beta_1^2 + h_2^2}\,, \quad R_3 = \sqrt{\alpha_2^2 + \beta_1^2 + h_1^2}$$
$$R_4 = \sqrt{\alpha_{21}^2 + \beta_1^2 + h_2^2}\,, \quad R_5 = \sqrt{\alpha_1^2 + \beta_2^2 + h_1^2}\,, \quad R_6 = \sqrt{\alpha_1^2 + \beta_2^2 + h_2^2}$$
$$R_7 = \sqrt{\alpha_2^2 + \beta_2^2 + h_1^2}\,, \quad R_8 = \sqrt{\alpha_2^2 + \beta_2^2 + h_2^2}$$
$$\alpha_1 = a_1 - x', \quad \alpha_2 = a_2 - x', \quad \beta_1 = b_1 - y', \quad \beta_2 = b_2 - y'$$

while

$$G_1 = EI(Mr + Nq),$$
$$G_2 = EI(Lr + Np),$$
$$G_3 = EI(Lq + Mp), \quad (4.8)$$
$$G_4 = EI(Nr + Mq),$$
$$G_5 = EI(Nr + Lp)$$

where EI is the intensity of magnetisation. L, M, N, are the direction cosines of magnetisation, and p, q, r are the direction cosines of the geomagnetic field. If the horizontal sides of the prism are not parallel to the coordinate axes, but are rotated by an angle θ with respect to the geographic north (Figure 4.1) then a new coordinate system (x',y') has to be chosen parallel to the horizontal sides of the prism. The point 0 on the observation plane remains the origin of the new (x',y') as well as old (x,y) coordinate systems. Then the (x,y) coordinates are to be replaced by the new coordinates (x',y') according equations (4.9) and (4.10),

$$x' = x\cos\theta + y\sin\theta \quad (4.9)$$
$$y' = -x\sin\theta + y\cos\theta. \quad (4.10)$$

If I and D are respectively the inclination and declination of the geomagnetic field, the direction cosines of the vector are given by

$$p = \cos I \cos(D - \theta),$$
$$q = \cos I \sin(D - \theta)$$
$$r = \sin I$$

The D and I in the study area are approximately 12^o and -10^o showing that the directional cosine r can have a small negative value but not zero. On the other hand, if I_o and D_o are the inclination and declination of the magnetisation vector, then its direction cosines are given by

$$L = \cos I_o \cos(D_o - \theta)$$
$$M = \cos I_o \sin(D_o - \theta)$$
$$N = \sin I_o$$

The complete model of the magnetic anomaly is obtained when equations (4.3) to (4.7) and their representative equations, and equation (4.8) are substituted into equation (4.2). If the observed anomalies are caused by N_b prisms, the equation for the magnetic anomaly at the field point (x,y,0) can be expressed (Rao and Babu, 1991) as

$$\Delta T(x,y,0) = \sum_{k=1}^{N_b} \Delta T_k(x,y,0) + C \,. \qquad (4.11)$$

where C represents a constant regional. Based on this anomaly model (equation 4.11), the computer program (Appendix C.1) was developed for the generation of the synthetic magnetic anomalies to be used for performance evaluation of the purchased analytic signal software and the Euler deconvolution computer program developed in the course of this study.

4.2.1 Computation of the Magnetic Anomalies

In order to simulate a typical archaeological situation, a moderate size site of 40 m by 60 m was assumed. To also give a good first trial to the methods of spatial and depth determinations, a relatively large prismatic body of 10 m by 15 m plan dimension and 2 metres thickness (300 m^3) was assumed. With assumed other source parameters such as susceptibility of 0.05, inclination and declination of -15^o and 10^o respectively of the magnetisation vector, the expected synthetic magnetic anomalies based on equation (4.2) were computed using the computer program of Appendix C.1. The results obtained were gridded and contoured so as to view the anomaly pattern. The plan view of the source was superimposed on the magnetic anomaly map (Figure 4.2) so as to assess the proper positioning of the anomaly relative to the source.

The dimensions of archaeological features expected in Lejja site (Eze-Uzomaka, 2009) are much smaller than the choice of the model made above. To obtain magnetic anomalies due to sources of similar dimensions to those expected at the archaeological site, the volumes of the sources were reduced from the 300 m^3 to as small as 0.25 m^3, but in stages. The number of sources in the model of the site (40 m by 60 m) was also increased (Tables 4.1 and 4.2). These were done in order to allow for proper evaluation of the Euler computer program already developed, and the applicability of the analytic signal software in the interpretation of the synthetic data. The reduction in sizes was

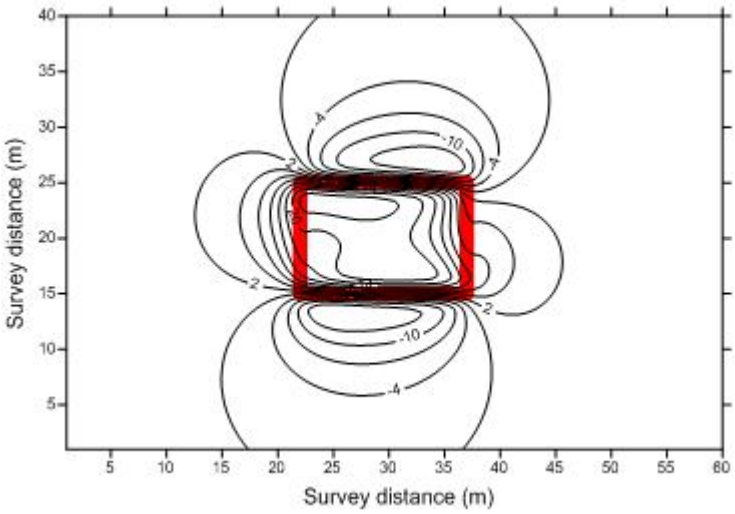


Fig. 4.2: Magnetic anomaly superimposed
on the single source model

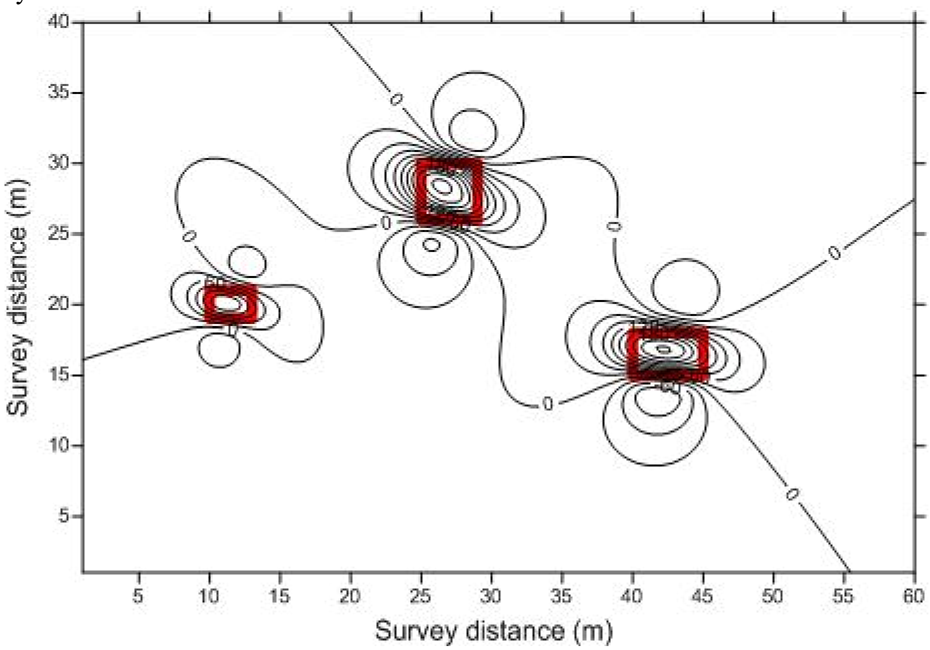
Table 4.1 Magnetic source parameters for 3-body models

S/N	a_1	a_2	b_1	b_2	h_1	h_2	i_m	d_m	susc
1	19.0	21.0	10.0	13.0	1.0	3.0	-12.0	0.0	0.5
2	26.0	30.0	25.0	29.0	1.0	5.0	-10.0	5.0	0.5
3	15.0	18.0	40.0	45.0	1.0	4.0	0.0	-10.0	0.5

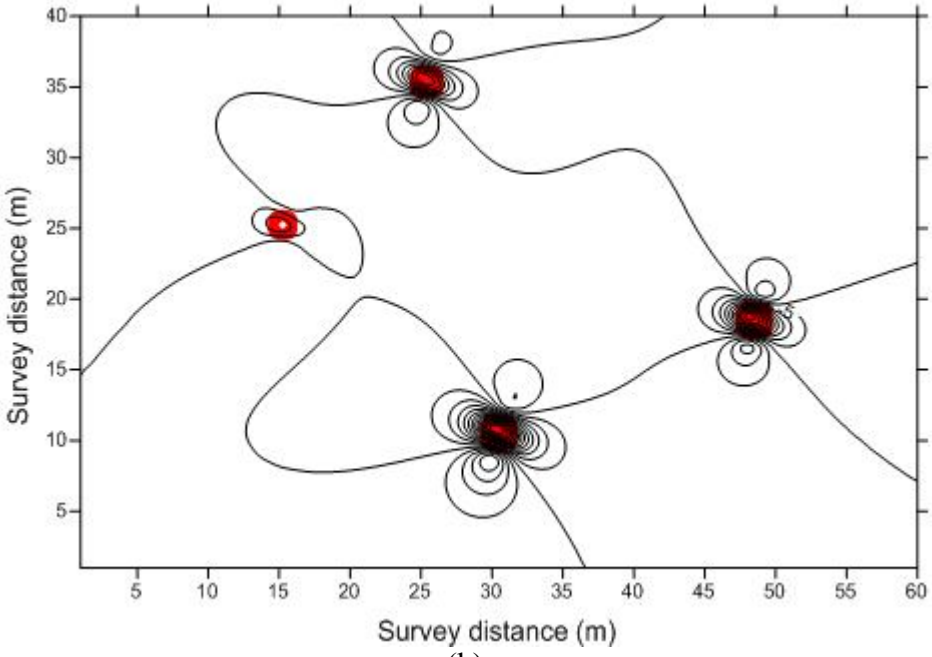
Table 4.2 Magnetic source parameters for 4-body models

S/N	a_1	a_2	b_1	b_2	h_1	h_2	i_m	d_m	susc
1	25.0	25.5	15.0	15.5	1.0	2.0	-10.0	-10.0	0.8
2	10.0	11.0	30.0	31.0	1.0	3.0	0.0	0.0	0.8
3	35.0	35.7	25.0	25.8	1.0	3.0	0.0	5.0	0.8
4	48.0	49.0	18.0	19.0	1.0	2.0	-8.0	0.0	0.8

Note: a_1, a_2, b_1, b_2, h_1 and h_2 are distances in metres corresponding with those in Figure 4.1. i_m, d_m and susc are inclination and declination of magnetisation vector and susceptibility respectively.



(a)



(b)

Fig. 4.3: Calculated magnetic anomalies superimposed on their sources
(a) 3–body model (b) 4–body model

also done to assess the limit of resolutions of the proposed techniques in interpreting archaeological magnetic field data where sources with surface area (plan view) less than about 0.30 m^2 were expected.

From the values of the horizontal coordinates a_1, a_2, b_1, b_2 (in metres), the depths to the top and bottom, h_1 and h_2 respectively (in metres), the inclination i_m and declination d_m (in degrees) of the magnetization vector, and the susceptibility, susc, of the magnetic sources (Tables 4.1 and 4.2) the synthetic magnetic fields were computed. These two sets of synthetic fields were superimposed on their sources in Figures 4.3 (a) and (b).

4.3 INVERSION OF THE SYNTHETIC DATA

Magnetic survey data are routinely interpreted by estimating source depths or locations. For this reason, many interpretation techniques such as the works of Thompson (1982), Reid et al. (1990), Hsu (2002), Keating and Pilkington (2004), etc., have been developed to enhance the estimation. A good number of such automatic interpretational methods combine source location and depth estimation. The intension here is to attempt to locate the source of the magnetic anomaly generated in the subsection 4.2.1 using two methods of interpretations, the Euler deconvolution method (Thompson, 1982; Reid *et al*., 1990) and the analytic signal method (Nabighian, 1972; Roest et al., 1992; Salem, 2005). The Euler method is very popular for computation of depths of anomaly

sources, while the analytic signal method is known for accurate mapping of edges of subsurface sources thereby giving reliable horizontal locations of the sources. The method has also proved to be effective in depth computations (MacLeod *et al.*, 1993).

4.3.1 Euler Deconvolution Method

Euler deconvolution is an automatic method used for locating the source of potential field based on both their amplitudes and gradients. The method was developed by Thompson (1982) to interpret 2-dimensional magnetic anomalies. It was extended to 3-dimensions by Reid *et al*. (1990) to be used on grid based data. Thompson (1982) assumed a magnetic dipole to be located at a point (x_o,y_o,z_o) relative to a plane of measurement (x,y) and expressed the total magnetic intensity as

$$\Delta T(x, y) = f[(x - x_o), (y - y_o), z_o]. \quad (4.12)$$

Using equation (4.12), the author expressed the Euler's equation of homogeneity as

$$(x - x_o)\frac{\partial \Delta T}{\partial x} + (y - y_o)\frac{\partial \Delta T}{\partial y} + (z - z_o)\frac{\partial \Delta T}{\partial z} = N\Delta T(x, y), \quad (4.13)$$

where $\frac{\partial \Delta T}{\partial x}$, $\frac{\partial \Delta T}{\partial y}$ and $\frac{\partial \Delta T}{\partial z}$ are the components of the anomaly's gradient in the respective directions and N is the degree of homogeneity of the anomaly ΔT. The degree of homogeneity, defined as the rate of change with distance of the field, is a parameter indicative of the source geometry and can be prescribed (Thompson, 1982; Reid *et al*., 1990). For example, Hsu (2002) assumes structural index of 3 for sphere, 2 for horizontal or vertical cylinder, 1 for thin dike, and 0 for contact or fault.

In an archaeological study where the magnetic source depths are shallow, the height of the measurement points z above the ground in equation (4.13) cannot be ignored as recommended by Reid *et al*. (1990) since they are often high relative to the source depths. On the other hand, equations (4.13) ignores the base level of the regional field B emphasized by Reid *et al*. (1990). Such assumption is valid in this study that does not cover more than 2400 m^2 in any field location. Apart from such idealized shapes characterized by specific structural indices, the method is applicable to all shapes (Reid *et al*., 1990). In an iron smelting site where furnaces are cylindrical and the iron smelting slag blocks are almost spherical in shape, the assumption of the first two shapes are very much in order. Blakely (1996) assumed ΔT_i to be the magnetic response (residual field) of any of such shapes at i-th point in the plane of the magnetic measurement due to a source located at (x_o, y_o, z_o) and replaced ΔT in equation (4.13) with ΔT_i to obtain

$$(x - x_O)\frac{\partial}{\partial x}\Delta T_i + (y - y_O)\frac{\partial}{\partial y}\Delta T_i + (z - z_O)\frac{\partial}{\partial z}\Delta T_i = N\Delta T_i. \quad (4.14)$$

If there are some ways of measuring or calculating horizontal and vertical gradients of the total field anomaly, equation (4.14) has only four unknowns: x_o, y_o, z_o and N, the first three being the location of the magnetic source. The equation (4.14) can be written in the matrix format as

$$\begin{bmatrix} \frac{\partial}{\partial x}\Delta T_1 & \frac{\partial}{\partial y}\Delta T_1 & \frac{\partial}{\partial z}\Delta T_1 \\ \frac{\partial}{\partial x}\Delta T_2 & \frac{\partial}{\partial y}\Delta T_2 & \frac{\partial}{\partial z}\Delta T_2 \\ . & . & . \\ . & . & . \end{bmatrix} . \begin{bmatrix} x - x_o \\ y - y_o \\ z - z_o \end{bmatrix} = N \begin{bmatrix} \Delta T_1 \\ \Delta T_2 \\ . \\ . \end{bmatrix} \quad (4.15)$$

for various measurement locations. Using least-squares method, the matrix equation (4.15) was solved for the three unknown x_o, y_o, and z_o for different values of the structural index N.

In the attempt to arrive at the solution of equation (4.15) (after obtaining the residual field) the following steps (Reid *et al*., 1990) were taken:

i. The residual anomaly data were gridded.

ii. The horizontal gradients, $\frac{\partial}{\partial x}\Delta T$ and $\frac{\partial}{\partial y}\Delta T$, were calculated over the gridded field using surfer package. The vertical gradients, $\frac{\partial}{\partial z}\Delta T$, were also calculated using ***MAGPICK*** (software purchased with the magnetometer).

iii. A square window of 3 x 3 grid points was chosen within the grids of gradient values and field values.

iv. For any chosen structural index (1 to 3), all points in the window were used to solve the Euler's equation (4.15) for a source location (x_o,y_o,z_o) using matrix inversion to obtain least-squares estimates. A 3 x 3 window provided nine equations from which the three unknowns and their uncertainties (standard deviations) were obtained. The solution for which the depth uncertainty was less than about 15% of the calculated depth was recorded (Reid *et al*., 1990). For a structural index of zero, Reid *et al*. (1990) recommended the solution of equation (4.13) for source position and the arbitrary offset value A which were equated to the right hand side of the equation.

v. Steps iii and iv were repeated for all possible window positions, including overlaps.

vi. A map of the solutions for each structural index was plotted at its plan (x, y) position using a symbol to indicate horizontal location (x_o,y_o) and depth z_o of the source.

4.3.1.1 *Application of the Euler Method to the Single-Body Model*

As earlier stated, the emphasis is on feasibility and validation of the developed Euler computer program, and that of the purchased processing software, MagPick (using analytic signal method), in the interpretation of the archaeological magnetic field data. A computer program (Appendix C.3) written to accomplish the task of Euler method was applied on the one-body synthetic anomaly, following the steps (iii) through (vi). Figure 4.4(a) shows the successful application of Euler deconvolution method to the model fields derived from the prismatic magnetic source. The clustering of the computed results around the magnetic source is very obvious in the figure, and indicates that there are typically many solutions (Reid *et al*., 1990; Elawadi and Ismail, 2011), virtually one for each window location. This type of result was often modified by using depth filter (Figure 4.4b). The depth filter specifies the range of acceptable results. Any computed results outside such range were rejected. This condition was imposed on the Euler depth result of Figure 4.4(b), minimising scattering of the computed source locations. Table 4.3 is a portion of the valid results of the computed depths. The mean depth is about1.03m. Compared to the model depth of 1m, this accounts for computation error of ±3%, which is lower than the present acceptable error limit of 15%.

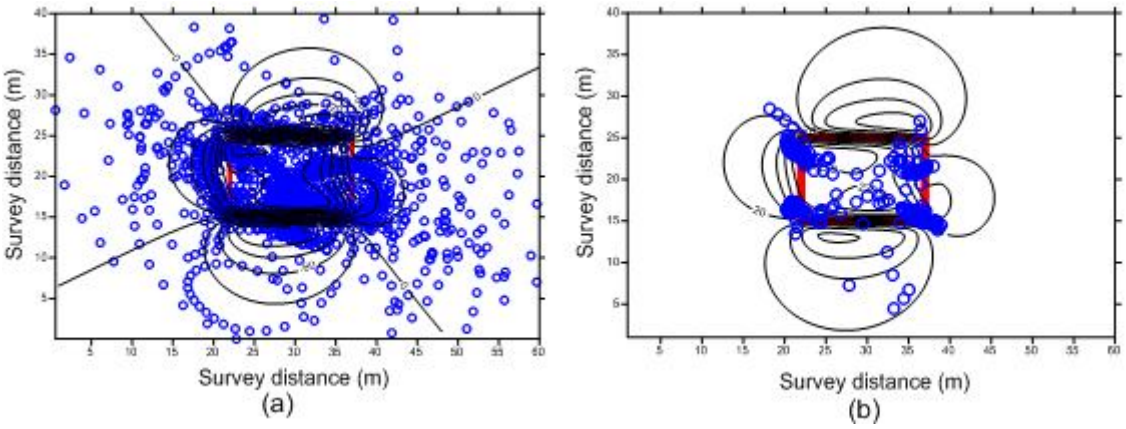


Fig. 4.4: Euler depth superimposed on source-anomaly map
(a) without depth filter (b) with depth filter

Table 4.3 A portion of Euler-depth for the single-body model

S/N	x_o(m)	y_o (m)	z_o (m)	S/N	x_o(m)	y_o (m)	z_o (m)
1	35.04558	6.71580	-0.65928	26	20.65436	16.48923	-1.45927
2	35.21452	15.72378	-0.50371	27	20.88642	16.50926	-1.34272
3	35.46637	15.51639	-0.80026	28	21.13455	16.48427	-1.19899
4	35.71565	15.72339	-0.76482	29	21.39990	16.42938	-0.99147
5	35.99043	15.44256	-1.00697	30	21.69337	16.33975	-0.69176
6	36.18660	15.89481	-0.80780	31	31.42102	17.12770	-0.80242
7	36.48000	15.53237	-1.02404	32	34.21164	16.44504	-1.07787
8	36.55624	16.26982	-0.70432	33	21.87266	16.52062	-1.56791
9	36.91207	15.71151	-0.95614	34	22.20398	16.31370	-1.08689
10	36.64889	16.81266	-0.51421	35	26.76842	15.91101	-0.92034
11	37.10457	16.20879	-0.75336	36	22.80205	15.61233	-1.60377
12	34.52502	16.11313	-0.58170	37	24.21195	14.83857	-0.96387
13	34.86730	15.85969	-1.60004	38	34.42791	5.66229	-0.85166
14	34.44518	16.30011	-0.58027	39	33.09048	8.50081	-1.45150
15	21.39562	15.09232	-0.76608	40	30.02783	17.97584	-0.75809
16	34.36552	16.45157	-0.54826	41	34.84899	20.88482	-1.36200
17	20.37511	16.10160	-1.05716	42	35.16135	20.68628	-0.98318
18	20.59206	16.18475	-0.90438	43	35.42698	20.72204	-1.42018
19	20.83618	16.21488	-0.73748	44	35.62850	20.72951	-1.67607
20	21.09900	16.21339	-0.52820	45	35.63860	20.73185	-0.74386
21	22.63557	22.15507	-1.27736	46	35.85388	20.76202	-0.96687
22	33.78912	22.35155	-1.29932	47	36.05281	20.79351	-1.11394
23	34.17153	16.57404	-0.54083	48	36.23052	20.82732	-1.20627
24	20.23615	16.28301	-1.67514	49	36.40647	20.87862	-1.26621
25	20.43279	16.42643	-1.55871	50	36.56821	20.93386	-1.29536

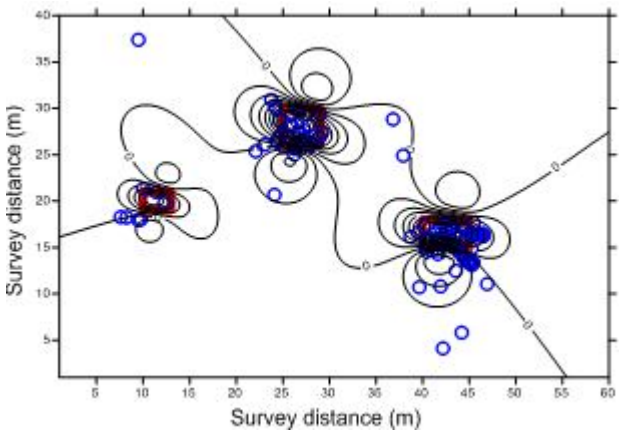
4.3.1.2 *Application of the Euler Method to the Multiple Source Models*

The horizontal locations and depths of the three sources were computed using Euler deconvolution program of Appendix C.3. A total of 69 accepted Euler depths with the corresponding coordinates of the surface locations of the sources were obtained (Figure 4.5a), giving an average depth of about 0.95 metre. As compared with a model depth of 1 metre (h_1 in Table 4.1) used in the computation of the synthetic field for all the three sources, this average depth amounts to a computational error of about ±5% of the true depth. This result, as compared with 15% error limit for acceptance of Euler depth results for field data recommended by Reid *et al*. (1990), is an indication of a reliable method to be applied to real data. A portion of the results obtained is displayed in Table B.1.

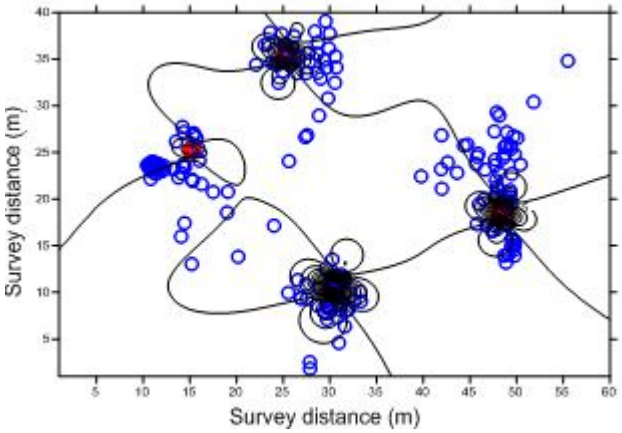
The spatial locations of the 4-body models (Figure 4.3b) were also computed using the Euler method. The table in Table B.2 shows a portion of the accepted results of the application of the Euler computer program. Mean depth of 1.03 metres was determined, which also corresponds with computational error of ±3% when compared with the model depth of 1m. The computed Euler depths were superimposed on the anomaly map (Figure 4.5b) so as to assess the various levels of the clustering of the results around the magnetic sources. Trials were made with the structural indices of 1, 2 and 3; that is, between dike, cylinder and sphere respectively (Reid *et al*, 1990; Hsu, 2002; Salem, 2005). It became obvious that the clustering occurred most with structural index of 1. This indicated that the program saw the prismatic bodies more as dikes, which was in line with theoretical expectations. In such cases, the positions of magnetic sources for both 3-body and 4-body models were adequately mapped out with minimal scattering of the results (Figure 4.5). Much scattering and fewer computed depths resulted (Figure 4.6) with the structural indices of 2 and 3 corresponding with dike and cylinder models.

Table 4.4 Estimating error margin in Euler solutions

Anomaly number	Model values			Calculated values					
	x (m)	y (m)	Depth (m)	x_c(m)	error(±%)	y_c (m)	error(±%)	depth (m)	error (±%)
1	15.24	25.21	1.00	12.44	18.37	23.78	5.67	1.00	0.00
2	25.38	35.35	1.00	26.29	3.59	35.99	1.81	1.00	0.00
3	30.50	10.46	1.00	29.79	2.33	9.37	10.42	1.00	0.00
4	48.35	18.42	1.00	48.09	0.54	18.93	2.77	1.08	8.00



(a)



(b)

Fig.4.5: Euler depths superimposed on the multiple-body synthetic anomaly map
(a) 3-body model (N=1) (b) 4-body model (N=1)

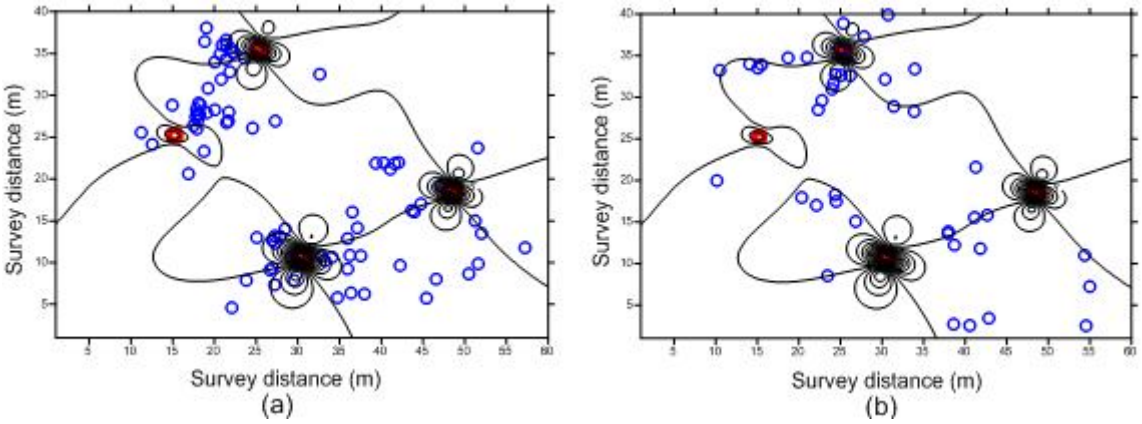


Fig. 4.6: Assessment of the shapes of the sources by varying the structural index
(a) N = 2 (b) N = 3

4.3.2 Analytic Signal Method

Analytic signal method is one of the varieties of interpretational methods that are based on the use of derivatives of the magnetic anomalies for the determination of causative source parameters such as boundaries, depths and model type (Thompson, 1982; Vallee *et al*., 2004; Salem, 2005). The method does not require knowledge of the direction of magnetisation and therefore it is useful in cases of remanent magnetisation. It was initially applied only on profile data (Nabighian, 1972; Atchuta *et al*., 1981) until Nabighian (1984) developed the relationship between the horizontal and vertical derivatives for the 3-D case (Debeglia and Corpel, 1997). The 3-D method was further developed by Roest *et al*. (1992) for the interpretation of aeromagnetic data. The

method is most important at low magnetic latitudes where reduction to the pole technique is seldom applicable due to the increase in the complexity of anomalies from the subsurface sources caused by the vector nature of the magnetic field. The amplitude of the 3-D analytic signal of the total magnetic field displays maxima over magnetic contacts regardless of the direction of magnetisation, and therefore can be used to trace the outline of magnetic bodies, particularly in archaeological magnetic survey where magnetic source-sensor distance is small (Wijns *et al*., 2005; MacLeod *et al*., 1993).

The 3-D analytic signal **A** was given by Nabighian (1984) for a potential field anomaly M as

$$A(x,y) = \left(\frac{\partial M}{\partial x}\hat{a}_x + \frac{\partial M}{\partial y}\hat{a}_y + i\frac{\partial M}{\partial z}\hat{a}_z \right), \tag{4.16}$$

where $\hat{a}_x, \hat{a}_y$ and $\hat{a}_z$ are unit vectors in the ox, oy and oz directions. Roest *et al*. (1992) showed that the amplitude of the 3-D analytic signal at location (x,y) can be expressed as

$$|A(x,y)| = \sqrt{\left(\frac{\partial M}{\partial x}\right)^2 + \left(\frac{\partial M}{\partial y}\right)^2 + \left(\frac{\partial M}{\partial z}\right)^2}, \tag{4.17}$$

where $\frac{\partial M}{\partial x}$ and $\frac{\partial M}{\partial y}$ are the horizontal gradients, and $\frac{\partial M}{\partial z}$ is the vertical gradient of the total magnetic field. The analytic signal amplitudes can be easily computed with commonly available computer software. To utilize this advantage in locating concealed magnetic sources, Nabighian (1972) derived the relationship between 2-D analytic signal amplitudes and spatial locations of magnetic sources. Such relationship was given by MacLeod et al. (1993) for the amplitude of the analytic signal over 2-D magnetic contact at depth h as

$$|A(x)| = \frac{\alpha}{\left(h^2 + x^2\right)^{1/2}}. \tag{4.18}$$

Also given for magnetic sheet (or dike) and cylinder respectively are

$$|A(x)| = \frac{\alpha}{\left(h^2 + x^2\right)} \tag{4.19}$$

and

$$|A(x)| = \frac{\alpha}{\left(h^2 + x^2\right)^{3/2}}, \tag{4.20}$$

where x is the distance along the profile and α (the amplitude factor) is given by

$$\alpha = 2M \sin d(I - \cos^2(I)\sin(D)), \tag{4.21}$$

where M is the strength of magnetisation, d is the dip of the magnetic source, I is the inclination of the magnetisation vector and D is the direction of the magnetisation.

MacLeod *et al*. (1993) have emphasized the dependency of the shape of the analytic signal on depth and have stated that the depth to the top of magnetic sources can be determined from the shape of the analytic signal anomaly. The authors then gave the relationship between depth (h) and the width $x_{1/2}$ of the anomaly at half the maximum

amplitude from equations (4.18), (4.19) and (4.20) as used by Atchuta *et al*. (1981) and Roest *et al*. (1992). The equations are:

$$x_{½} = 3.46h \quad (4.22)$$

$$x_{½} = 2h \quad (4.23)$$

and $$x_{½} = 1.533h \quad (4.24)$$

for magnetic contact, dike and cylinder respectively. By taking the second derivatives of equations (4.18), (4.19) and (4.20), MacLeod *et al*. (1993) also gave another set of equations for computing source depths based on the distance between inflection points of the analytic signal anomalies. The expressions are:

$$x_i = 1.414h, \quad (4.25)$$

$$x_i = 1.155h \quad (4.26)$$

and $$x_i = h, \quad (4.27)$$

for contact, dike and cylinder respectively. The x_i is the width of the anomaly between inflection points.

In the analytic signal technique, it is typically assumed that the causative sources are near-vertical, step-like geologic structures (Nabighian, 1972; Roest *et al*., 1992; Hsu *et al*., 1996), in which case, the analytic signal maxima are located directly over the edges of the structures. The technique has been shown to be effective in interpreting subsurface magnetic contacts (Nabighian, 1972, 1974; MacLeod *et al*, 1993; Hsu *et al*., 1998). That is, the signal amplitudes exhibit maxima over contacts, and thus, can be used to trace the outline of any magnetic body provided source-sensor separation is small (Wijns *et al*., 2005). Contact models can therefore be used to approximate most of the very near-surface structures that are encountered in archaeological and engineering surveys.

The application of analytic signal method to magnetic data is similar to reduction to the pole (RTP) procedure (Hansen and Pawlowski, 1989; Blakely, 1996) in which the anomaly is made to seat directly over its source. Since RTP is seldom applied at the low magnetic latitudes (Lawal and Osazuwa, 2004, 2007), Grant and Dodds (1972) in the development of the software called MAGMAP using fast Fourier transform (FFT) processing system, achieved a similar result that is now used in MagPick to map subsurface sources. MagPick, the processing software purchased with the magnetometer (Geometrics model G-856AX), has the facility for interpreting the magnetic data using the analytic signal technique.

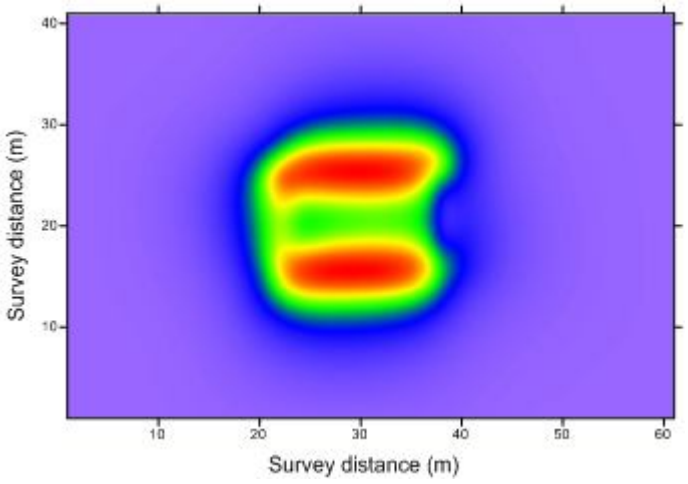
The intension at this stage was to assess and validate the analytic signal option of the multipurpose software for interpretation of the archaeological magnetic data by first applying it to synthetic magnetic data with the following objectives: (i) To estimate the computational error that might be associated with detection and mapping of magnetic sources of fairly large lateral extent, representing bloom dump under soil cover. (ii) To obtain the horizontal locations and depths to the top of sources of small sizes (e.g., between $0.25m^3$ and $2m^3$), which can approximate sizes of slag block and average-size furnace (Eze-Uzomaka, 2009). To achieve these objectives, two stages of the test were carried out. The first one was done using a single, relatively large magnetic source of volume $300m^3$ with model depth of 2m, while the second one was done using four

relatively small magnetic sources with volumes varying between 0.25m^3 and 2m^3, and model depth of 1m for all the sources (Table 4.2).

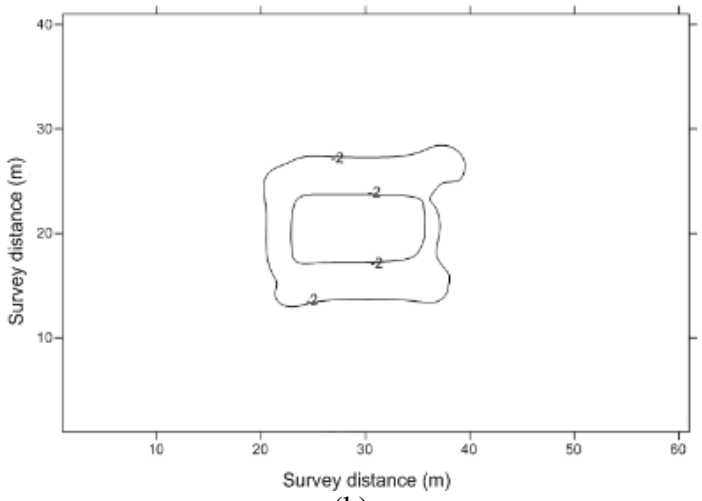
4.3.2.1 *Application of the Analytic Signal Method to the Single-Body Model*

To use the analytic signal software, the synthetic field generated (subsection 4.2.1) was first gridded using surfer package. The gridded field was then loaded into MagPick from where analytic signal amplitudes were computed. Figure 4.7 is the result of the application of the analytic signal to the synthetic field generated by the single-body model. The edges of the source are located between the two contours (Figure 4.7b). The two red patches in the anomalous area (Figure 4.7a) reflect the peaks of the analytic signal over the south and north edges of the magnetic source. The north-south trending edge of the source display very low signal amplitudes which is a reflection of the complexity of magnetic anomaly at low magnetic latitudes, because the data were assumed to have been acquired in the south-north direction at low magnetic latitudes.

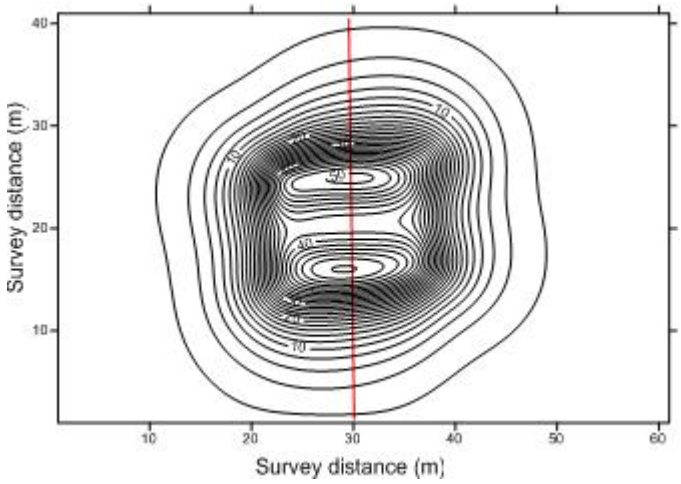
In order to calculate the depth to the top of the source using the *anomaly width at half the amplitude* method (Atchuta *et al*., 1981; Roest *et al*., 1992), a north-south profile was taken across it (Figure 4.7c) and the anomaly map was digitized. The resulting analytic signal anomaly was plotted (Figure 4.8a). The figure shows that the signal amplitude peaks over the two opposite edges of the source, the northern and the southern edges. This revealed that the depth to the top of the source was less than half width of the source (Hsu *et al*., 1998), which was in line with the model values used. To be able to compute the depth of the causative body, the first and second derivatives of the residual field were taken in stages. After each derivative, the analytic signal technique was applied (Figure 4.8 b and c) and the depth was computed. The depth obtained using analytic signal amplitudes of the first order vertical derivative of field was 2.30m accounting for computational error of about 30%. Such high percentage error required the depth calculation from the analytic signal amplitudes (Figure 4.8c) of higher order (2nd order) vertical derivative which turned out to be 2.05m, amounting to percentage error of only about 5%.



(a)

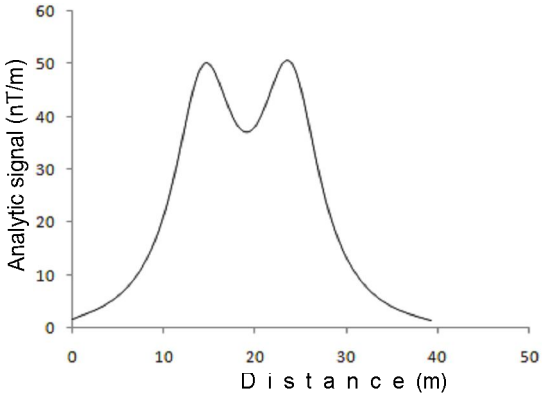


(b)

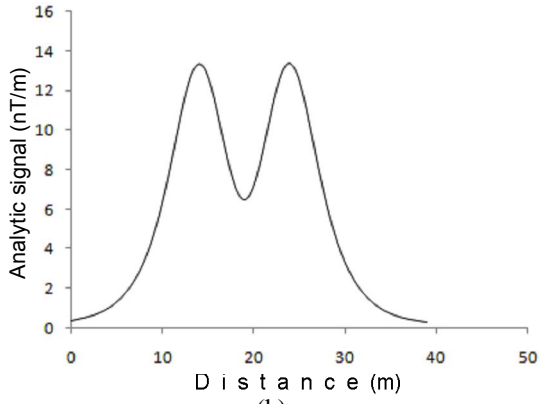


(c)

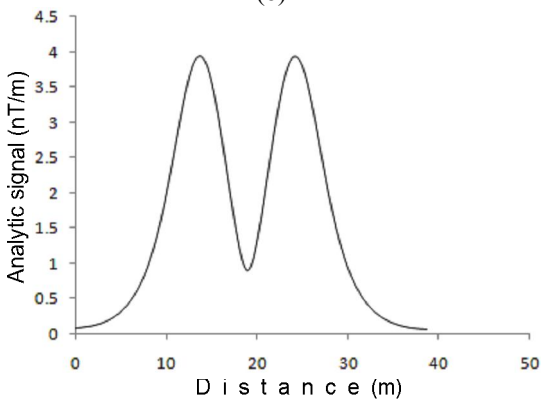
Fig. 4.7: Analytic signal method applied to the single-source model
(a) outline of the source (b) mapping edges of the source
(C) Profile across the analytic signal anomaly for depth computation



(a)



(b)



(c)

Fig.4.8: Using higher order of analytic signal to compute depth to the top of a thick prismatic body

(a) Simple analytic signal curve

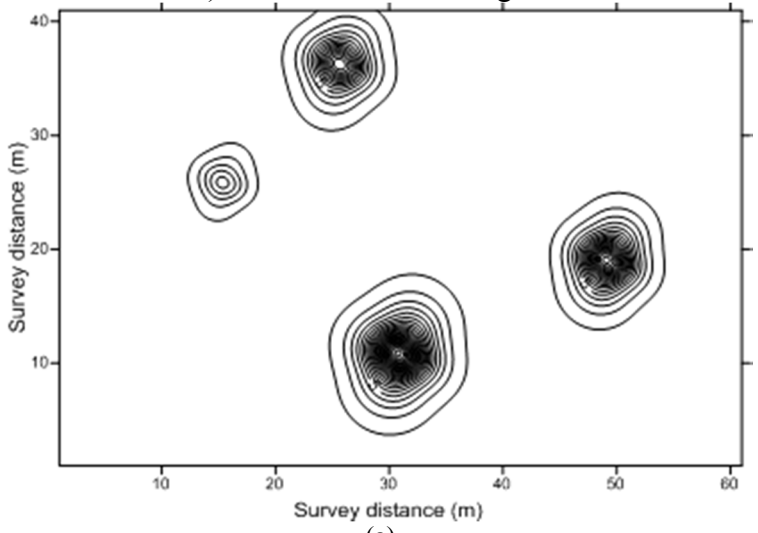
(b) First-order analytic signal curve

(c) Second-order analytic signal curve

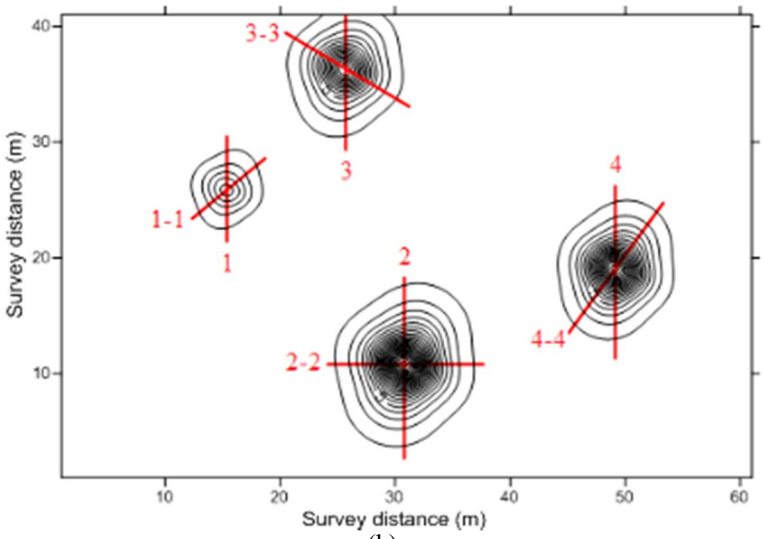
4.3.2.2 *Application of the Analytic Signal Method to the Multiple-Body Models*

As was done with the single-source model, the synthetic total field data was first contoured using the golden software (surfer) since the MagPick software uses grid files as input files. The multiple-body model grid file was then loaded in and processed using the analytic signal option of the software. The signal amplitudes computed, display maxima over the sources. In other words, contour lines of the signal amplitudes seat at the epicentroids of their subsurface magnetic sources. Figure 4.9a is a contour plot of the analytic signal amplitudes obtained with the multiple-body model data. Using this contour plot, the centre of each subsurface magnetic source was located by placing the cursor at the centre of each anomaly and migrating to a point of highest amplitude which corresponds with the epicentroid of the homogeneous source. The coordinates of each centre was then read off at the base of the surfer sheet. These values have been recorded in Table 4.6 and found to tally with the model values (Table 4.2) very reliably with computational percentage errors varying between ±0.31% and ±4.55%.

The process of depth computation began with taking profiles across the analytic signal anomalies (Figure 4.9b). The profiles numbered 1 to 4 were taken along north-south direction, making them normal to the east-west trending edges of the magnetic sources. The anomaly map was digitized using surfer digitizing facility. The digital values were plotted as analytic signal amplitudes versus distance along each profile (Figure 4.10). *Applying the width of the anomaly at half the amplitude* method, the depth to the top of the model sources were computed using contact, dike and cylinder models given by MacLeod *et al*. (1993). The depths computed for each source using the three shape models (equations 4.22 to 4.24) have been recorded against the source in Table 4.5.



(a)

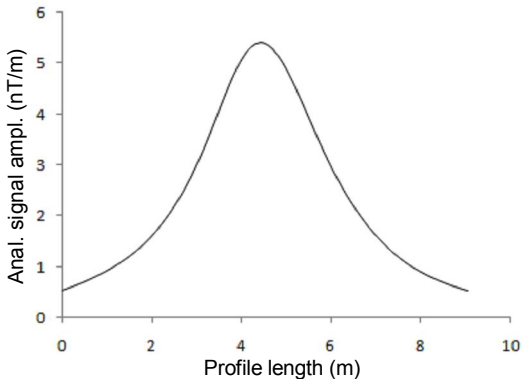


(b)

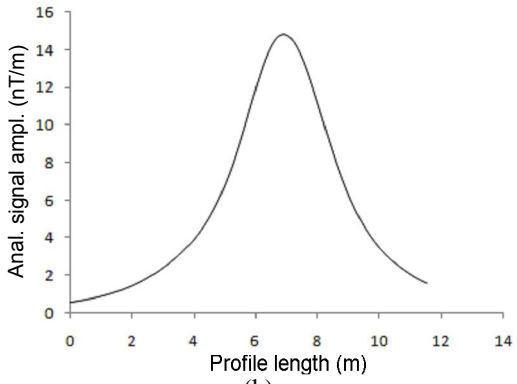
Fig. 4.9: Positioning analytic signal amplitudes to locate horizontal positions of the sources

Table 4.5 Source depth calculated with different earth models

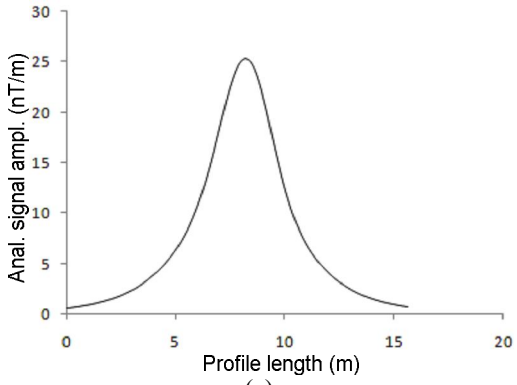
Anomaly Number	Model depth used h(m)	Depth calculated using Contact model		Depth calculated using Dike model		Depth calculated using Cylinder model	
		h(m)	% Error	h(m)	% Error	h(m)	% Error
1	1.00	0.95	±5.00	1.64	64.00	2.14	114.00
2	1.00	1.06	±6.00	1.84	84.00	2.40	140.00
3	1.00	1.03	±3.00	1.78	78.00	2.32	132.00
4	1.00	1.05	±5.00	1.82	82.00	2.37	137.00



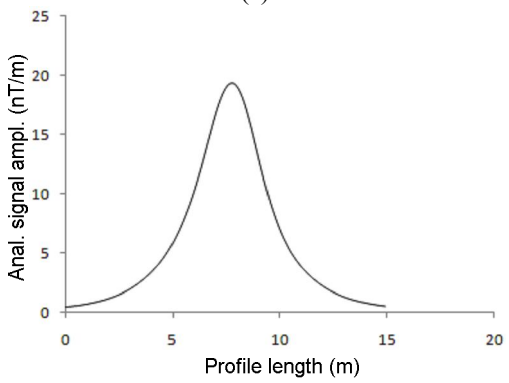
(a)



(b)



(c)



(d)

Fig. 4.10: Analytic signal anomaly for the multiple-source models
(a) profile 1 (b) profile 2 (c) profile 3 (d) profile 4

The results of the depth computations, as recorded for the single-source model, and also the multiple-source models in Table 4.5 revealed that the assumption of the contact model produced the least percentage error with the highest as ±6.00%. The minimum percentage errors using the dike and the cylinder models are ±64% and ±114% respectively. These error limits, as compared to the error limit of ±6.00% using the contact model, which was the model assumed in the computation of the synthetic magnetic field, is a confirmation of the fact that the use of wrong models can produce depths that are significantly in error (MacLeod *et al*., 1993). Therefore, the shapes of

the causative magnetic sources have to be determined prior to the application of the analytic signal method in depth determination.

Table 4.6 contains depth results that were obtained along the profiles that were taken normal to the edges of the sources. In real life situation, the strike of the magnetic sources may not be obvious due to some geological, or archaeological situations which may include ambient noise, interference from neighbouring sources, data quality, etc. To take care of the unforeseen field situations, The profiles labelled 1-1 to 4-4 (Figure 4.9b) were taken in random directions and the above procedures of depth computation were repeated using the analytic signal curves (Figure A.12) obtained from the above profiles for the depth computation. The depths obtained were favourably comparable with the model depth (Table 4.6). The h_{NS} are the depths obtained using the north-south profiles while h_{RD} are those obtained using the randomly selected profiles. The x and y are plan positions of the causative magnetic sources.

Table 4.6 Sensitivity of the analytic signal method to changes in strike directions of the magnetic sources

Anomaly	x(m)			y(m)			h_{NS}(m)			h_{RD}(m)		
Number	Model	Calc	%Error	Model	Calc	%Error	Model	Calc	%Error	Model	Calc	%Error
1	25.25	25.90	±2.50	15.25	15.38	±0.85	1.00	0.95	±5.00	1.00	0.95	± 6.00
2	10.50	11.00	±4.55	30.50	30.69	±0.62	1.00	1.06	±6.00	1.00	1.10	±10.00
3	35.35	36.42	±2.94	25.40	25.48	±0.31	1.00	1.03	±3.00	1.00	1.14	±14.00
4	48.50	49.02	±1.10	18.50	19.13	±3.30	1.00	1.05	±5.00	1.00	1.04	±4.00

4.4 THE APPLICATION OF THE UPWARD CONTINUATION

The discussion of the relevance of synthetic field in archaeo-magnetic geophysics is not complete without reference to upward continuation of the field data from one level to another. This is because magnetic data are often acquired with the magnetometer sensor very close to the ground (Clark, 1990; Godio and Torino, 2005) thereby picking even the slightest contrast in magnetisation of the very near surface materials which may not be of archaeological interest. Effects of such unwanted features (magnetic noise) are usually filtered out using upward continuation procedure (Henderson, 1970; Blakely, 1996; Nabighian *et al*., 2005).

Upward continuation is a process in magnetic (or gravity) interpretation in which the potential field data measured on a given plane are transformed to data measured at a higher elevation thereby attenuating high frequency anomalies and enhancing those of lower frequencies. That is, it is a filtering technique used for separating causative sources from different depths that have their anomalies superimposed. Blakely (1996) gives an expression for upward continuation integral as

$$U(x,y,z_o-h)=\frac{h}{2\pi}\int_{-\infty}^{\infty}\int_{-\infty}^{\infty}\frac{U(x',y',z_o)}{\left[(x-x')^2+(y-y')^2+h^2\right]^{3/2}}dx'dy', \qquad (4.28)$$

where $U(x',y',z_o)$ is the potential field at the measurement point and $U(x,y,z_o-h)$ is the upward-continued field at a height h above a measurement plane z_o ($h > 0$). That is, equation (4.28) can be used to continue data measured on a level surface to another level surface. For each point of the new surface, the 2D integral must be evaluated. This task has been described as computationally intensive by Blakely (1996) who has recommended, and mathematically demonstrated the handling of such problem in Fourier domain.

The MagPick has a package for solving equation (4.28) in the Fourier domain, and is contained in its upward continuation option. It has been envisaged that in an iron smelting archaeological site such as Lejja, there may be need for the low-pass filtering of the magnetic field data. The intension at this point is to upward-continue one of the synthetic fields in order to observe its behaviour at various altitudes as this may give some clues if such situation arises in real data. In this regard, the field generated using the 3-body model (Table 4.1) was used. The synthetic field was upward-continued in stages of 1 metre up to the height of 5 metres. At each stage, the field was contoured using surfer package (Figure 4.11) and each anomaly magnitude was measured by scanning for its highest value at the centre using the cursor and taking the amplitude reading from the base of the map. Table 4.7 shows their amplitude decay with altitude which has also been compared with their original amplitudes.

Table 4.7 Variation in amplitudes of anomalies with altitude

Anomaly number	Amplitudes of the field at altitude of:					
	0m (nT)	1m (nT)	2m (nT)	3m (nT)	4m (nT)	5m (nT)
1	65.57	37.22	17.35	9.45	NM	NM
2	107.60	72.59	38.37	19.92	11.87	8.46
3	110.02	71.70	36.60	18.50	10.92	NM

'NM' means the amplitude is no longer measurable.

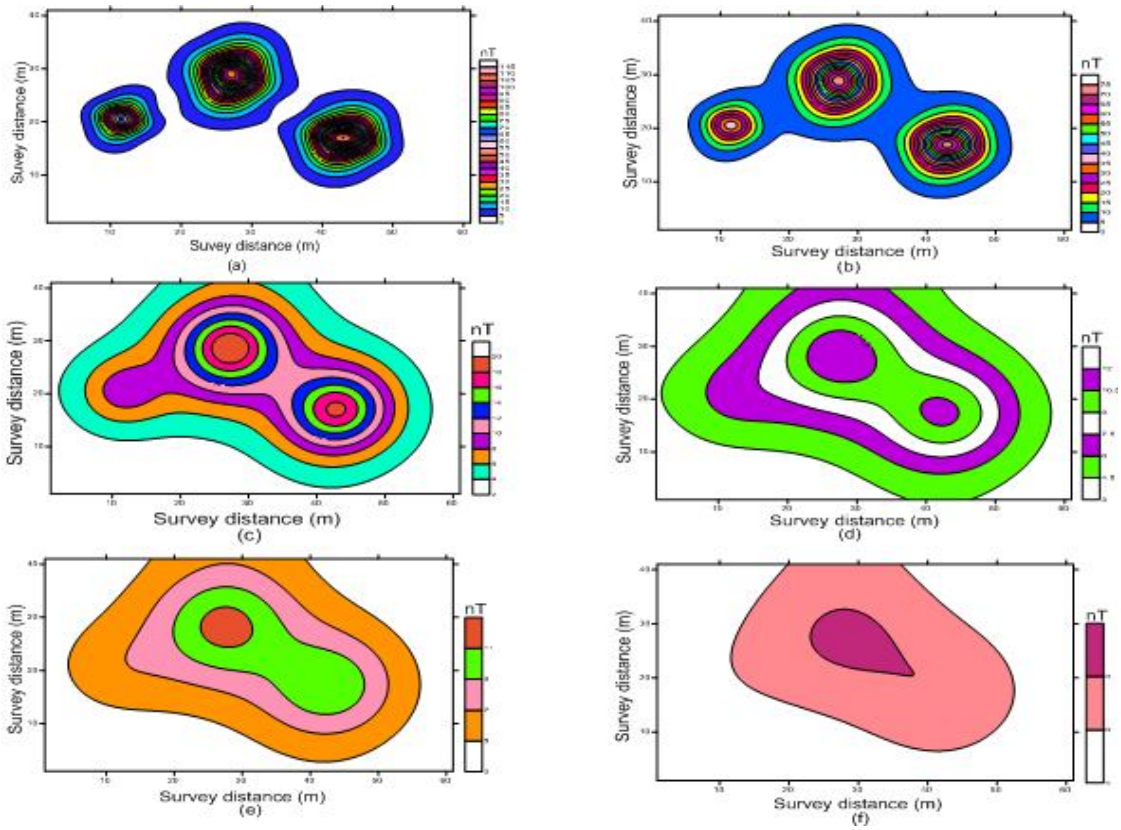


Fig.4.11 : Stage by stage upward continuation for estimate of causative source depth
(a) Synthetic field without upward continuation (b) height of 1m
(c) height of 2m (d) height of 3m (e) height of 4m (f) height of 5m

The result of the upward-continued field (Table 4.7) has revealed that at the height of 3 metres, the amplitude of the source labelled 1 has decayed to 9.45nT amounting to 14.39% of its initial value. On the other hand, that of the source labelled 3 decayed to 10.92 (about 9.93% of its initial value) at the height of 4 metres while the amplitude of the one labelled 2 decayed to 8.46 (about 7.86% of its initial value) only at the height of 5 metre above the ground surface. It is worth noting at this point that the amplitude decay of the upward-continued field with altitude is not a coincidence. It becomes obvious when Table 4.1 is compared with Table 4.7 that the height at which the magnetic field of each source disappears, leaving only a trace, (Figure 4.11) coincides with the depth of the bottom of its source. The idea derived from this observation, though still hypothetical, may influence some decisions that may be taken in the course of this study.

C H A P T E R 5

DATA PROCESSING AND INTERPRETATIONS

5.1 INTRODUCTION

Geophysical data processing includes everything done to the data between acquisition and creation of an interpretable map, profile, section, or tomograph. Such steps may include data sorting, data reduction (which includes diurnal correction and regional-residual separation), filtering, anomaly source location, depth estimation, shape, resistivity, or susceptibility determination, etc. (Nettleton, 1976; Thompson, 1982; Scollar *et al*., 1986; Telford *et al*., 1990; Loke and Barker, 1996; Tsokas and Tsourlos, 1997; Breiner, 1999; Nabighian *et al*., 2005; Salem, 2005). The aim of the data processing is to transform the raw field data into a meaningful form and to enhance the maps that delineate the concealed features whose evidence at the surface can only be weakly detected or completely obscured. In archaeological geophysics, the task is to present the final result in the form that can easily be understood and used by non-geophysicists. Therefore, such results are better presented in the image form that shows the plane view of how the artefacts are located in an archaeological site (Scollar *et al*, 1986; Godio and Torino, 2005).

The processing of the magnetic data begins with data sorting which may involve (i) ***despiking***, (ii) removing a datum (or some set of data) and shifting the entire line to cover such position (or positions), (iii) deleting an entire line, or repositioning such a line, etc. This is then followed by data reduction, which, unlike the case of gravity data processing, involves only two main steps, diurnal correction and regional-residual

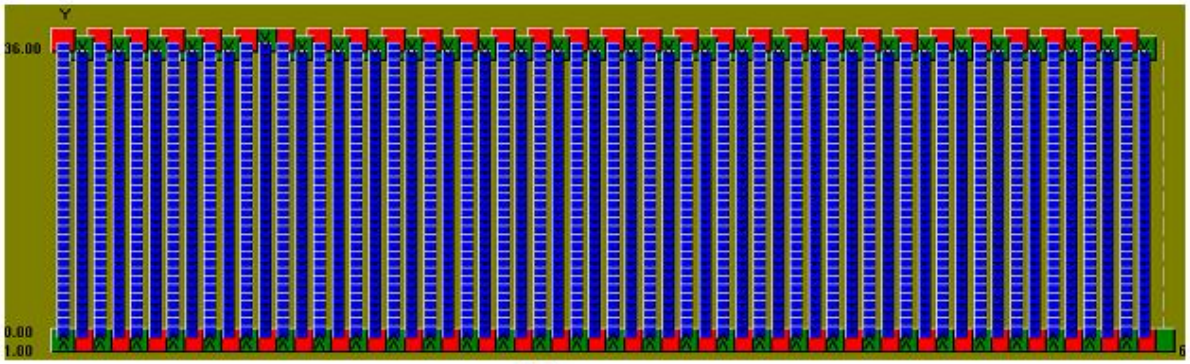
separation (Telford *et al*., 1990, Blakely,1996; Nabighian *et al*., 2005). Others are filtering, contouring, determination of depths and horizontal locations of anomalies, etc.

5.2 DATA SORTING AND DESPIKING

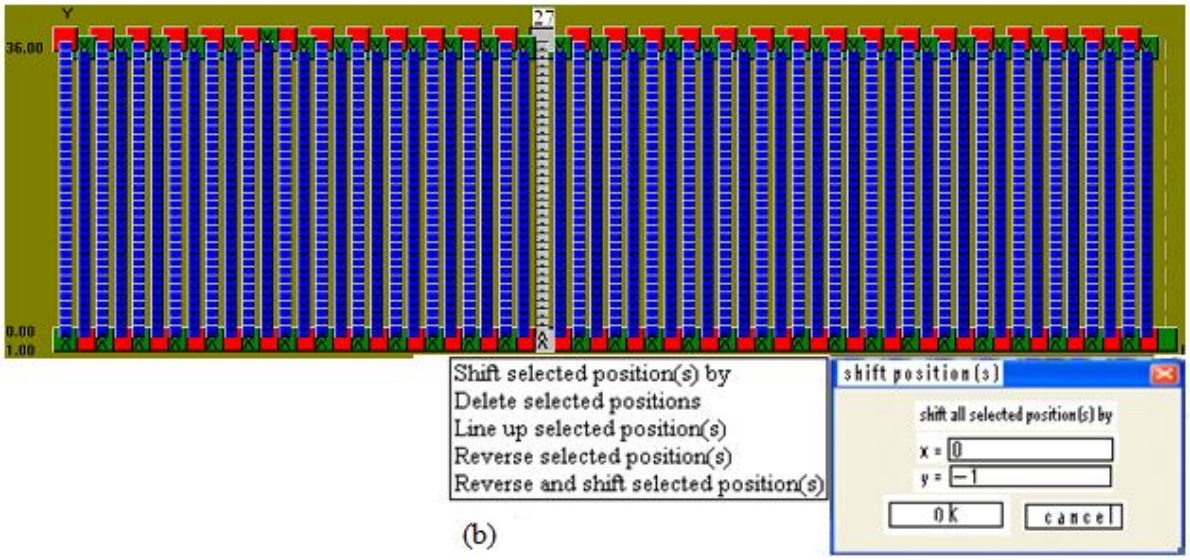
In the course of data acquisition, the base station data and the field data were collected and stored at the same location in the console memory for convenience of the field operation since there was no base station magnetometer. The price for this was paid at the stage of the data processing when a pair of 62 to 72 magnetic and time readings recorded for each base station had to be carefully located and picked out from among an average of about 13200 data. This removal of the base station data created vacancies at the beginning of every odd number line (profile) as shown in (a) and (b) of Figure 5.1. In order to disallow gaps in the data, those vacancies had to be filled by shifting each line according to the dialogue box shown in Figure 5.1b. Figure 5.1c shows the appearance of well sorted data.

Despiking is a technique used for removing readings known to be incorrect. These spikes and drop-outs (extreme values) are usually identifiable because they differ significantly from the adjacent readings. They can be caused by operating the sensor near a dead zone, under high tension lines, or over sites where there is a high accumulation of small magnetic surface clutter, and the operator is carrying the sensor just a few centimetres above the ground (G-856AX operating manual). A typical despiking session usually involves two activities. These are removal of drop-outs, and identifying and removing spikes. Drop-outs are also called zero readings which are readings that are less than the usual five digit readings. They are caused mostly by

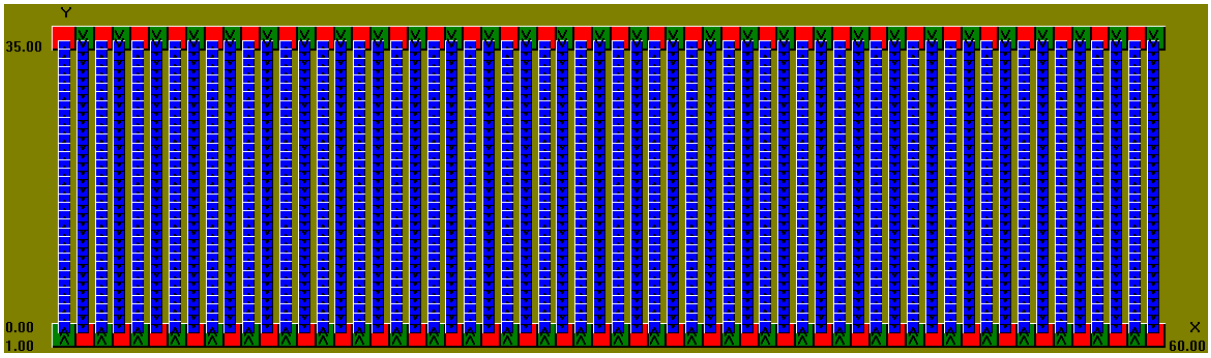
operating sensors close to very large ferrous objects; that is, the magnetometer is operated under conditions where good readings are not possible. Both drop-outs and spikes are outliers and therefore require special attention and proper handling to pave way for effective magnetic data reduction.



(a)



(b)

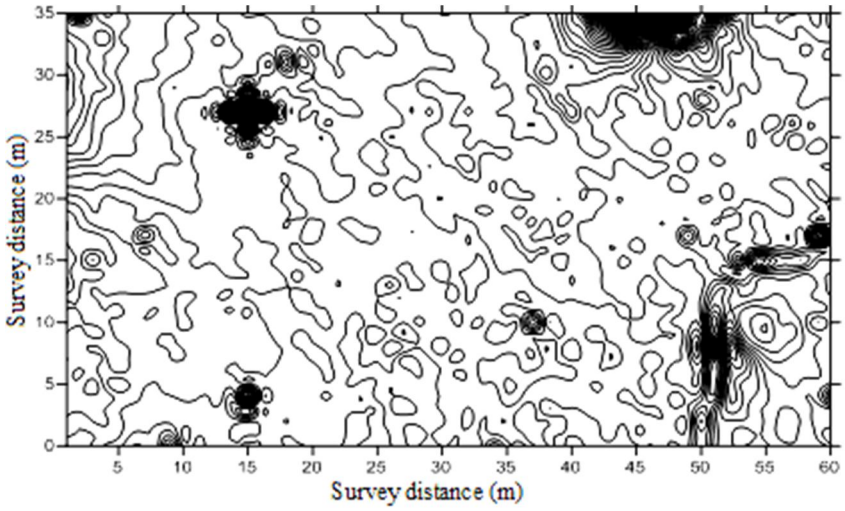


(c)

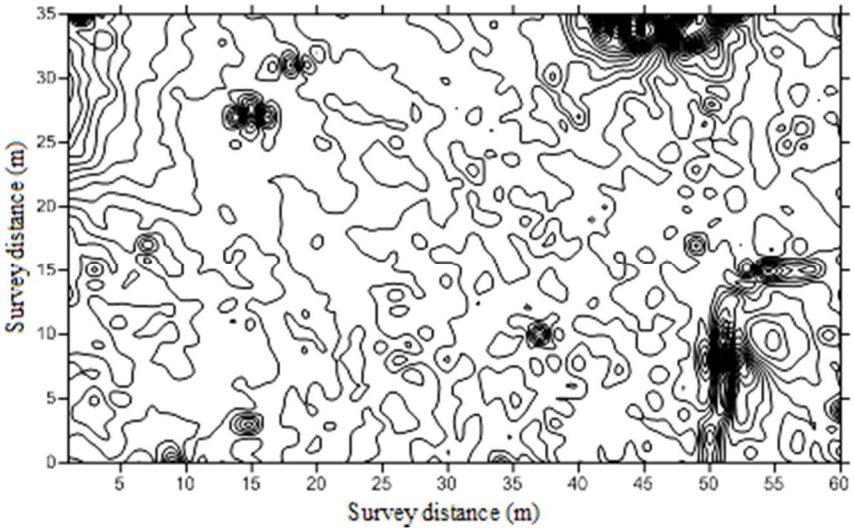
Figure 5.1: Effect of data sorting on the magnetic data
(a) Raw data (b) Sorting process (c) Appearance of well sorted data

It was discovered that some datasets contained the extreme values (the spikes). Noisy data, such as magnetic spikes and drop-outs can obscure the more subtle magnetic signatures often generated by archaeological features and must be removed by editing the data directly or by digital filtering. Preliminary contour maps of the raw data, including the extreme values, were examined in Surfer and compared with the results of the scanned fields to be sure that the spikes were indeed not archaeologically significant. The archaeological data were scanned in the spreadsheet and extreme data eliminated. The edited datasets were then gridded in Surfer, contoured, and again inspected. In a few cases when drop-outs were noticed, may be due to malfunctioning of the instrument, they were removed (using MagMap-2000 package) by selecting *"linearly interpolate drop-outs"*, which interpolates the zero readings by good adjacent ones.

The two datasets for each station (a set for each day) were combined after despiking and contoured using surfer package (version 9). This was done to be able to view the effects of despiking on the data. Figure 5.2 is a display of the differences between Uwani-Lejja raw dataset and the despiked one. Those of Ugbelenabo and Ejuona are displayed in Figures A.6 and A.7 respectively. It is obvious from Figure 5.2 that the clumsy situations created in the Uwani data at the north-west, the south-west and the eastern parts of the site by presence of spikes and drop-outs in the data (Figure 5.2a), have been resolved as depicted in Figure 5.2b. Similar obvious improvements are also recorded at some locations in Ugbelenabo and Ejuona sites after despiking (Figures A.6b and A.7b).



(a)



(b)

Fig. 5.2: Effects of despiking on Uwani data
(a) before despiking (b) after despiking

5.3 DATA REDUCTION

Unlike the gravity data, reduction of the total magnetic field data involves two main steps, namely, minimizing the effect of the solar radiation on the magnetic data (diurnal correction), and estimating and removing the regional field caused by deep-seated and distant magnetic sources not related to the sources at the horizon of interest (regional-residual separation). Removal of the two effects from the archaeo-magnetic field data is necessary to get the magnetic information into an interpretable format. As Blakely (1996) puts it, such data reduction procedure is an excellent example of enhancement of "signal" by the removal of predictable "noise".

5.3.1 The Diurnal Correction

Near-surface magnetic sources may be the focus of exploration, but because the magnetic fields external to the earth have a large effect on the magnetic measurements, the magnetic data must be corrected for the external influence (the diurnal variation).

Removal of such effect in land surveys may be done using several methods (Dobrin, 1976; Dobrin and Savit, 1988; Telford *et al*., 1990; Nabighian *et al*., 2005). The two most common methods used while acquiring total field data are: (i) use of a base station magnetometer in which magnetic readings are taken continuously and simultaneously with the field measurements for later subtraction from the field data, and (ii) returning of field magnetometer to base station for periodic measurements during the survey in order to tie the field readings to the fixed point within the survey area. The use of the first option, recommended by Geometrics 'MagMap 2000'; Lowrie, 1997, Kearey *et al*., 2002, is dependent upon the amount of funds available for the research. Due to inadequate funding of this research, it was not possible to purchase a base magnetometer and therefore the only available option was option (ii). This involved repeated measurements at the base station throughout the period of the survey.

The base station data acquired using option (ii) above are usually used to correct the magnetic field data by obtaining the difference between any two adjacent base station readings and add (or subtract) it from the field data recorded within that time interval according to the recording time of each data. This method, henceforth referred to as conventional method of diurnal correction, assumes a linear variation in the geomagnetic field within that time interval. It is actually an attempt to fit a linear curve to a set of data that is better defined by a curvilinear function. In this study, a different approach was used in correcting the field data for diurnal effect. This new method utilises the least-squares method of polynomial fitting technique to correct the archaeological magnetic field data against the diurnal effect.

5.3.1.1 *The Least-Squares Approach*

Assume that the daily variation of magnetic field strength B at any time t in a given location on the surface of the earth is represented by the regression model

$$B = c_o + c_1 t + c_2 t^2 + \ldots + c_m t^m + \varepsilon \quad , \tag{5.1}$$

where ε is the expected random error in B. The c_j's(j = 0, 1, 2, . . . , m) are the unknown constant terms called coefficients of the polynomial, or the model parameters, while m is the order of the polynomial. Therefore, the *i-th* sample of the total field taken at the fixed location (base station) at time t_i (i = 1, 2, . . . , n), can be represented as

$$\begin{aligned} B_i &= c_o + c_1 t_i + c_2 t_i^2 + \ldots + c_m t_i^m + \varepsilon_i \\ &= c_o + \sum_{i=1}^{n} \left(\sum_{j=1}^{m} c_j t_i^j + \varepsilon_i \right). \end{aligned} \tag{5.2}$$

where ε_i is the measurement error which is assumed to be uncorrelated, and n is the number of base station data. Equation (5.2) can be expressed in form of an n x m matrix. For a set of base station data, the number of equations (which is also n) usually far outnumbers the number of parameters (m) to be determined. Such problem that has no unique solution (Press *et al*., 1992; Golub *et al*., 1996; Aster *et al*., 2005) is better solved using the least-squares technique. Equation (5.2) can therefore be expressed as

$$\mathbf{G.x} = \mathbf{d}, \tag{5.3}$$

where **G** is an n by m matrix composed of the powers of the independent variable t, **x** is a column vector matrix of the coefficients (c_j) and **d** is the column vector matrix of the

data B_i. In order to obtain a square matrix, the transpose of **G** (i.e., $\mathbf{G}^T$) can be calculated. Multiplying the transpose by equation (5.3) yields

$$(\mathbf{G}^T.\mathbf{G}).\mathbf{x} = \mathbf{G}^T.\mathbf{d}. \tag{5.4}$$

Menke (1989) expands equation (5.4) as

$$\begin{bmatrix} n & \sum_{i=1}^{n} t_i & \sum_{i=1}^{n} t_i^2 & \cdots & \sum_{i=1}^{n} t_i^m \\ \sum_{i=1}^{n} t_i & \sum_{i=1}^{n} t_i^2 & \sum_{i=1}^{n} t_i^3 & \cdots & \sum_{i=1}^{n} t_i^{m+1} \\ \vdots & \vdots & \vdots & & \vdots \\ \sum_{i=1}^{n} t_i^m & \sum_{i=1}^{n} t_i^{m+1} & \sum_{i=1}^{n} t_i^{m+2} & \cdots & \sum_{i=1}^{n} t_i^{2m} \end{bmatrix} \cdot \begin{bmatrix} \hat{c}_o \\ \hat{c}_1 \\ \vdots \\ \hat{c}_m \end{bmatrix} = \begin{bmatrix} \sum_{i=1}^{n} B_i \\ \sum_{i=1}^{n} B_i\, t_i \\ \vdots \\ \sum_{i=1}^{n} B_i\, t_i^m \end{bmatrix} \tag{5.5}$$

where $\hat{c}_o$, $\hat{c}_1$, . . . , $\hat{c}_m$ are least-squares estimators of c_o, c_1, . . . ,c_m whose computational expression can be written as

$$\mathbf{x} = (\mathbf{G}^T.\mathbf{G})^{-1}.\ (\mathbf{G}^T.\mathbf{d}) \tag{5.6}$$

This type of matrix computation is relatively straight forward on a digital computer. A computer program (Appendix C.2) was adapted from Davis (1973) to compute the above parameters using equation (5.6). The base station data were first read and stored, and then sent to a series of statements which generated the sums of powers of the independent variable t necessary to fill the square matrix. As stated earlier, the n by m matrix was transposed and the product of the matrix and its transpose gave the square matrix required to obtain values of the model parameters. The fitting process used varying powers (2 to 5) of the approximating polynomials and calculated the values of the coefficients for each model. This process is the same as the minimization of the least-squares function by Montgomery and Peck (1992).

Further statistical calculations were needed to determine the best fit model out of the few candidate models (Menke, 1989; Press *et al*., 1992). This is because almost any complicated model is expected to fit data better than any less complicated one. For instance, polynomial of degree 5 is likely to fit a set of curvilinear data better than that of degree 3, or 4. The question then is how much better is this model than that of 3, or 4? Since over-fitting (adding terms that are unnecessary) can lead to ill-conditioned matrix, hence use of more complicated method of determining the coefficients, it was necessary to address the question of whether or not a fit was significantly better than the other.

5.3.1.2 *Test of Significance of Error Improvement*

Menke (1989) attempted to estimate the variance σ^2 of a data set d_i by expressing it in terms of the prediction error e_i of each model as

$$\sigma^2 = \frac{\sum_{i=1}^{n} e_i^2}{(n-p)}. \tag{5.7}$$

where the residual sum of squares SS_E is given by

$$SS_E = \sum_{i=1}^{n} e_i^2 = \sum_{i=1}^{n} (B_i - \hat{B}_i)^2 , \tag{5.8}$$

where n is the number of data, p is the number of parameters estimated, B_i and $\hat{B}_i$ are the observed and the estimated base fields respectively. If one model fits the data about as well as the other, then the variance σ_1^2 estimated from model 1 should be about the same as the variance σ_2^2 estimated from model 2. On the other hand, if model 2 gives a better fit than model 1, the estimated variance will differ in such a way that the ratio σ_1^2

$/\sigma_2^2$ will be greater than unity. If the ratio is only slightly greater than unity, the difference in fit may be entirely a result of random fluctuations in the data and therefore may not be significant (Menke, 1989). The ratios of the variances for each two adjacent models have been indicated as F_o (Table 6.1) while the estimated standard deviation (the computation error in the estimated model parameters) is denoted by σ.

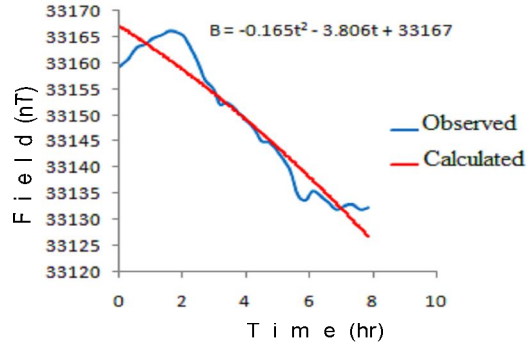
In the choice of the best-fit model for the polynomial fitting, two main standards were used. (i) A model with smaller variance was preferred to the one with larger variance, and (ii) to choose a model of higher degree, the ratio of their variances must be very significant, not less than 1.7 (Menke, 1989). Based on these criteria, the polynomial models of order 3 (day 1) and order 4 (day 2) were used to compute the diurnal correction for the Uwani site (Table 5.1). Similar choices were made for the Ugbelenabo and the Ejuona sites (Tables B.3 and B.4 of Appendix B) using the same criteria. The choice models which were used for computing the diurnal corrections have been bold-faced and underlined in all the tables.

The parameters c_j's computed and the time t_i of taking magnetic field readings at the base station were used to compute the base field for each model. The calculated and the observed fields were plotted in each case to allow visual inspection of the fit. The target was to keep the order of the polynomial as low as possible to avoid over-fitting of the model to the data (Press *et al*., 1992; Golub and Loan, 1996). After all, the so called best-fit parameters may not necessarily be the best predictor of the base station data. For example, the trial curve fittings for Uwani (day 1) displayed in Figure 5.3 reveals that Figure 5.3b does not look a better fit than Figure 5.3c. It is obvious, because the

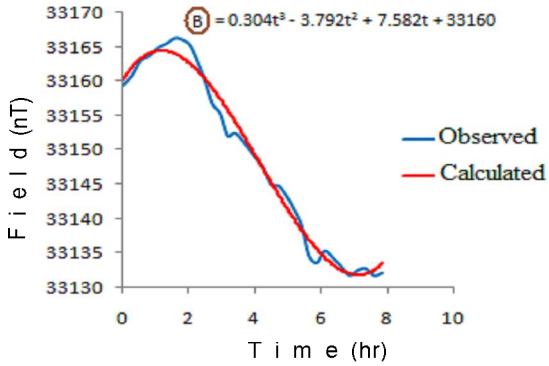
latter is more complicated than the former. Nevertheless, in terms of the model requirements particularly the ratio of the variances relative to the required lower order of the polynomial, figure 6.3b was preferred. Such plots for Uwani (day 2), Ugbelenabo and Ejuona are displayed in figures A.1 to A.5 with each choice model circled.

Table 5.1 Computed parameters and F_o statistics for right choice of models (Uwani site)

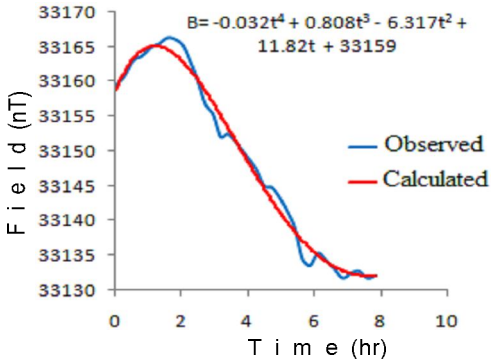
Order of Polynomial	c_o	c_1	c_2	c_3	c_4	c_5	σ	σ^2	F_o
Day 1									
2	33167	-3.81	-1.66				±3.65	13.30	
									4.94
3	33160	7.58	-3.79	0.30			±1.64	2.69	
									1.20
4	33159	11.82	-6.34	0.81	-0.03		±1.50	2.24	
									0.03
5	33158	14.72	-9.06	1.76	-0.17	0.01	±8.83	78.03	
Day 2									
2	33164	-4.80	0.04				±3.65	13.35	
									3.70
3	33157	5.78	-3.26	0.27			±1.90	3.61	
									1.73
4	33154	14.47	-8.26	1.24	-0.06		±1.45	2.09	
									0.11
5	33154	14.66	-8.43	1.30	-0.07	0.00	±4.34	18.85	


B = -0.165t² - 3.806t + 33167
Observed
Calculated
Field (nT)
Time (hr)

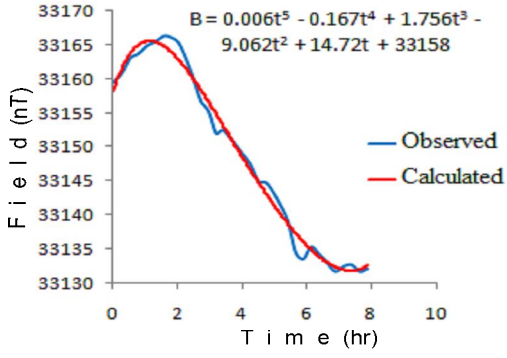
(a)


B = 0.304t³ - 3.792t² + 7.582t + 33160
Observed
Calculated
Field (nT)
Time (hr)

(b)


B= -0.032t⁴ + 0.808t³ - 6.317t² + 11.82t + 33159
Observed
Calculated
Field (nT)
Time (hr)

(c)


B= 0.006t⁵ - 0.167t⁴ + 1.756t³ - 9.062t² + 14.72t + 33158
Observed
Calculated
Field (nT)
Time (hr)

(d)

Fig. 5.3: Fitting polynomial models to base station data (Uwani site, day 1)
(B is the base station field, t is measurement time)

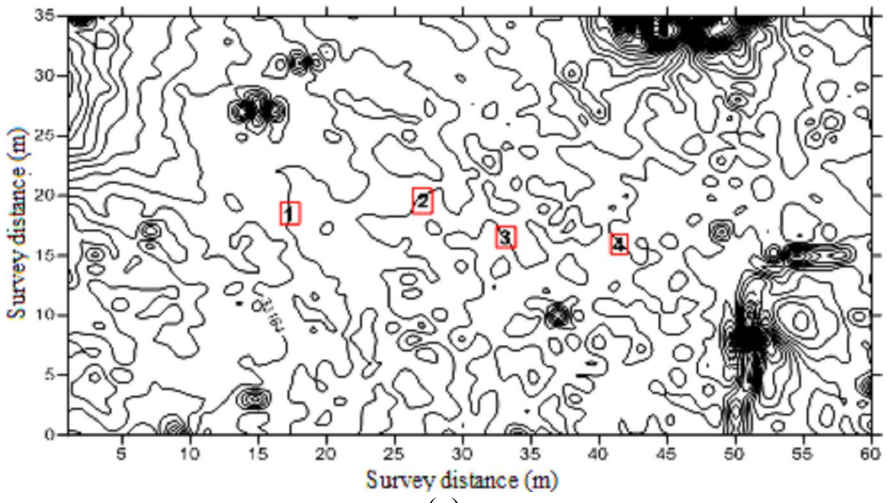
5.3.1.3 *Calculation of the Diurnal Variation*

The model selected for each dataset and the recorded time of measurements at the grid points were used to calculate the base station field with each value corresponding with exact time of an observation at a grid point. The diurnal correction to be subtracted from the field data was obtained by choosing a reference point along the time axis, preferably, the time data acquisition began at the base station. The field value corresponding with such time was taken as the constant of the polynomial model. The constant value was subtracted from the computed base field to leave the residual field values which are attributable to diurnal effect. The residual amplitudes of the base field were the diurnal corrections subtracted from the field data according to their times of measurement at the grid points. It is worth noting at this point that although the value of the constant c_o of the polynomial model may depend on the time a survey begins, the pattern and the magnitude of the earth's field for a particular day remains invariant irrespective of the time of the day a magnetic survey begins (Nettleton, 1976; Lowrie, 1997; Kearey *et al*., 2002).

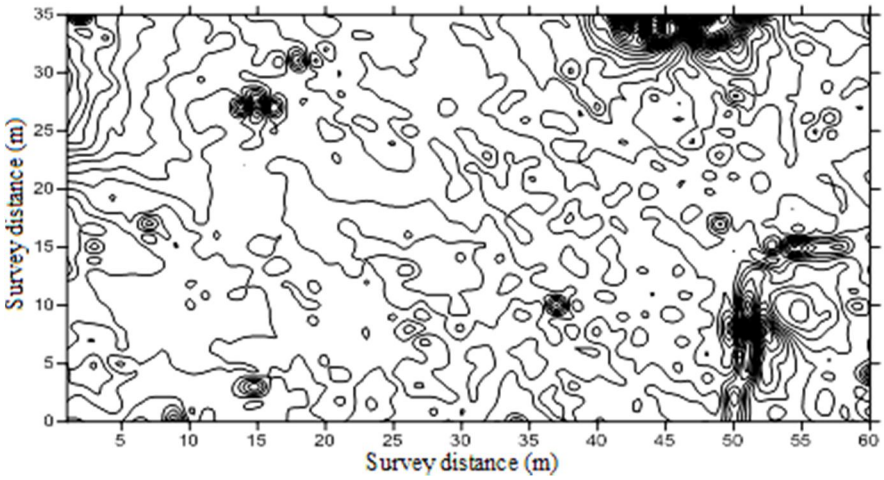
5.3.1.4 *Graphical Display of the Diurnally Corrected Field*

To view the effect of the method of diurnal correction on the field data, the diurnally corrected datasets for each of the three locations, Uwani, Ugbelenabo and Ejuona, were combined to form a single map. Each map was smoothened using spline smooth filter of the golden software's surfer version 9.0, and then contoured. The same datasets,

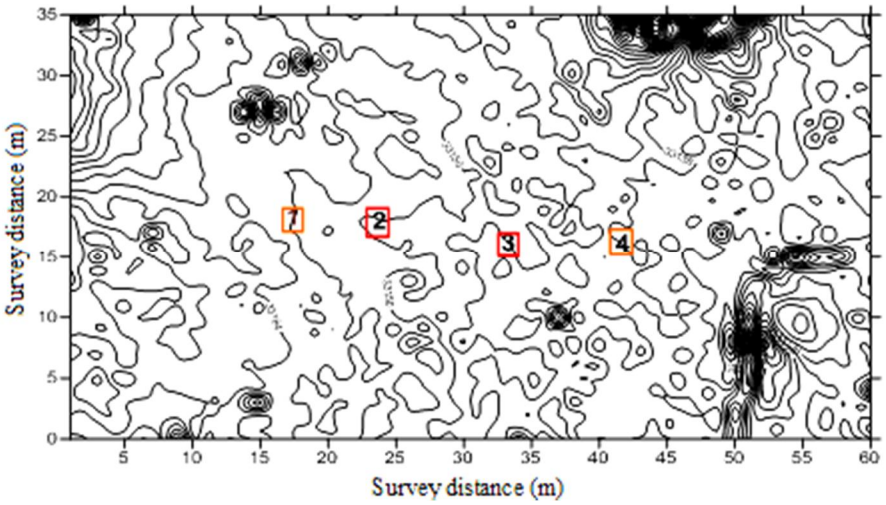
without diurnal correction, were also subjected to the same filtering process and contoured using the same contour interval of 7nT. The results displayed in Figure 5.4 show that the noise levels (labelled 1- 4) in Figure 5.4a which might have resulted from heading error have been minimised in the process of diurnal correction (Figure 5.4b).



(a)



(b)



(c)

Fig. 5.4: Assessing the quality of Uwani-Lejja map after diurnal correction (a) Before diurnal correction, (b) After diurnal correction, using polynomial fitting method (c) after diurnal correction, using conventional method (1 to 4 are noise levels).

It is also worth noting that the contour plot of the Uwani data after applying the conventional method still contains the same background noise levels, an evidence of the superiority of the polynomial fitting method over the conventional method. Those of Ugbelenabo and Ejuona are displayed in Figures A.8 and A.9. Such remarkable improvement in the quality of the data corrected using the polynomial fitting method is depicted in Ugbelenabo map (Figure A.8b). The result of the application of the conventional method of diurnal correction, as displayed in Figure A.8c, could not show such data quality. For instance, the noise levels labelled 1 to 5 in Figure A.8a (before the correction) which were filtered out using the former method could be found prominently manifesting in the data corrected with the latter method. On the other hand, there was no remarkable difference in the quality of Ejuona map after the diurnal correction using any of the two methods. This might be due to absence of heading error, or might be due to relatively higher noise level in Ejuona data which resulted from the period of the year (July) that the data were acquired (Nettleton, 1976).

5.3.2 Regional-Residual Separation

Regional-residual separation is a very important step in the interpretation of the archaeo-magnetic data. In most cases, total field magnetic anomalies of interest usually appear superimposed on a much broader anomaly which is not of interest. The broader anomaly, or regional gradient, is due to the main earth's field or relatively deep seated sources (Syberg, 1972; Blakely, 1996; Lowrie, 1997). In regional surveys, they are removed from the data using international geomagnetic reference field (IGRF) in order to better examine the anomalies of interest (Peddie, 1983; Nabighian *et al*., 2005). But in detailed surveys such as applicable in archaeological geophysics, the surface area concerned is normally so small that the IGRF is not reliable. A better approach may be to fit a polynomial surface to the diurnally corrected total field data using the least-squares method.

In the case of the archaeo-magnetic survey, a one-degree polynomial was assumed to be sufficient in fitting the surface to the data. In such a case, two auxiliary variables (say x and y) were needed. A model such as

$$d_i = m_1 + m_2 x_i + m_3 y_i , \tag{5.10}$$

was assumed. The d_i represents the data and m_1, m_2 and m_3, the model parameters. For such parameter estimation problem, a system of equation such as

$$\mathbf{Gm = d} \tag{5.11}$$

can also be used (Press *et al*., 1992; Aster *et al*., 2005) as done in case of curve fitting in subsection 5.3.1.1. The equation (5.11) has the matrix form

$$\begin{bmatrix} 1 & x_1 & y_1 \\ 1 & x_2 & y_2 \\ . & . & . \\ 1 & x_N & y_N \end{bmatrix} \begin{bmatrix} m_1 \\ m_2 \\ m_3 \end{bmatrix} = \begin{bmatrix} d_1 \\ d_2 \\ . \\ d_N \end{bmatrix}. \tag{5.12}$$

Dawi *et al*. (2004), and Aster *et al*. (2005) proved that in matrix form, the normal equation can be expressed as

$$\mathbf{G^T G m = G^T d}, \tag{5.13}$$

where $\mathbf{G^T}$ is the transpose of the matrix **G**. From equation (5.12), the products of the matrix $\mathbf{G^T G}$ is given as

$$\begin{bmatrix} 1 & 1 & . & . & 1 \\ x_1 & x_2 & . & . & x_N \\ y_1 & y_2 & . & . & y_N \end{bmatrix} \begin{bmatrix} 1 & x_1 & y_1 \\ 1 & x_2 & y_2 \\ . & . & . \\ . & . & . \\ . & . & . \\ 1 & x_N & y_N \end{bmatrix} = \begin{bmatrix} N & \sum x_i & \sum y_i \\ \sum x_i & \sum x_i^2 & \sum x_i y_i \\ \sum y_i & \sum x_i y_i & \sum y_i^2 \end{bmatrix}. \tag{5.14}$$

The right hand side of equation (5.13), $\mathbf{G^T d}$ is also given as

$$\mathbf{G^T d} = \begin{bmatrix} 1 & 1 & . & . & . & 1 \\ x_1 & x_2 & . & . & . & x_N \\ y_1 & y_2 & . & . & . & y_N \end{bmatrix} = \begin{bmatrix} d_1 \\ d_2 \\ . \\ . \\ . \\ d_N \end{bmatrix} = \begin{bmatrix} \sum d_i \\ \sum x_i d_i \\ \sum y_i d_i \end{bmatrix}. \tag{5.15}$$

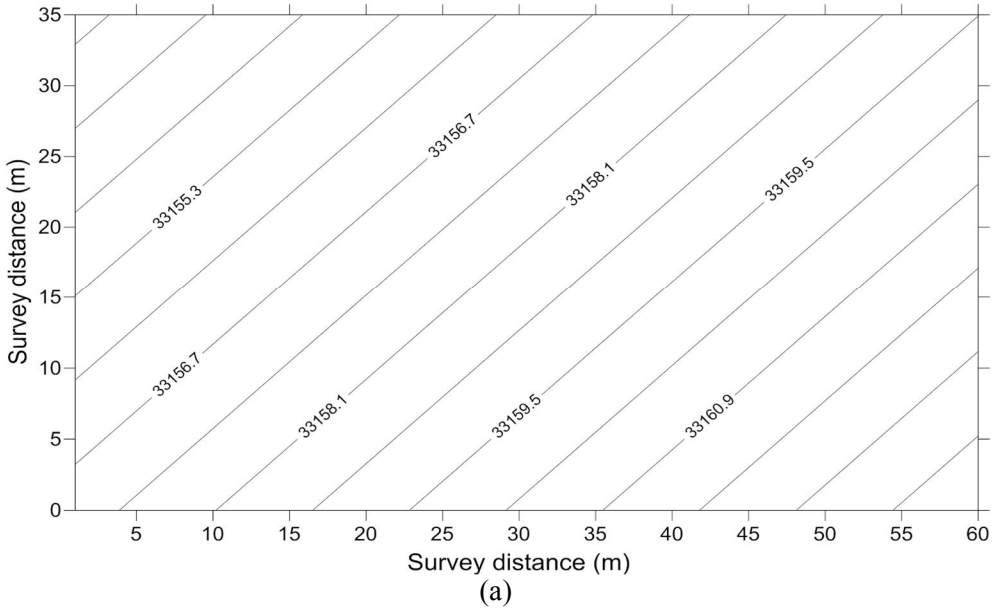
Therefore, from equation (5.11), the least squares solution is given as

$$\mathbf{m} = [\mathbf{G^T G}]^{-1} \mathbf{G^T d} = \begin{bmatrix} N & \sum x_i & \sum y_i \\ \sum x_i & \sum x_i^2 & \sum x_i y_i \\ \sum y_i & \sum x_i y_i & \sum y_i^2 \end{bmatrix}^{-1} \begin{bmatrix} \sum d_i \\ \sum x_i d_i \\ \sum y_i d_i \end{bmatrix}. \tag{5.16}$$

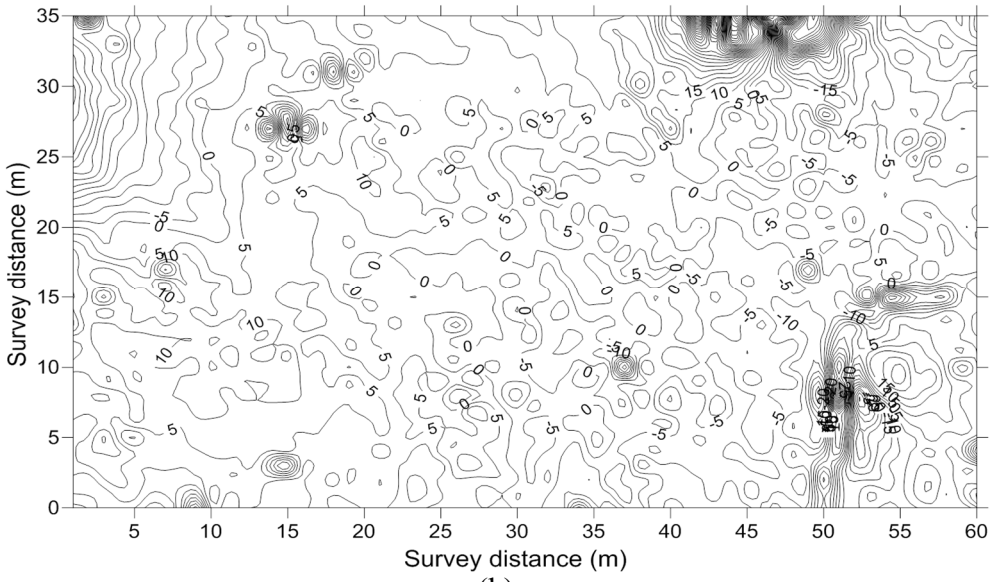
In the magnetic measurements, d_i represents the total magnetic field in nanotesla, x and y are the coordinates of the data points, while N is the total number of data points. The

parameter **m** in equation (5.16) are the coefficients of the one-degree polynomial fitted to the data. Equation (5.16) can be solved using a simple matrix inversion program (Davis, 1973; Menke, 1989). The Golden software' surfer (version 9.0) was used to obtain the polynomial surfaces. A sample plot of such a surface is given for Uwani in figure 6.5a. Figures 5.5b is the residual magnetic field of the same site. On the other hand, the regional and the residual magnetic fields of Ugbelenabo and Ejuona are displayed in Figures A.10 and A.11 of Appendix A.

In the process of repeating the procedures involved in the magnetic data reduction from one site to the other I appreciated the cumbersomeness of the dual-stage method, the diurnal correction followed by the regional-residual separation. A single step technique called automatic reduction of magnetic data (ARMAD) was later discovered in the course of this study. Although the study had gone beyond the point of discarding the data processed using the existing method, the ARMAD method was test-run with some of the field data in order to evaluate its performance.



(a)



(b)

Fig. 5.5: Uwani field after the data reduction processes
(a) regional field (b) residual field using conventional method
(Contour interval is 5 nT)

5.3.3 Automatic Reduction of Magnetic Data (ARMAD) Method

As just concluded, the conventional magnetic data reduction involving the diurnal correction and the regional-residual separation has enjoyed patronage of many researchers for decades. Different attempts and recommendations have been made to achieve a more reliable and less cumbersome method (Hoylman, 1961; Nettleton, 1976; Telford *et al*., 1990; Li and Oldenburg, 1998; Kearey *et al*., 2002) which is centred on the usual dual approach of reducing the magnetic field data. Particularly for ground magnetic survey, this has been the trend for about a century.

In the course of this study, as earlier pointed out, it was discovered that applying the two corrections separately was cumbersome and time consuming. Some errors could be introduced into the values of the estimated parameters due to the fact that the field observations might be tied to some distant datum such as the use of International

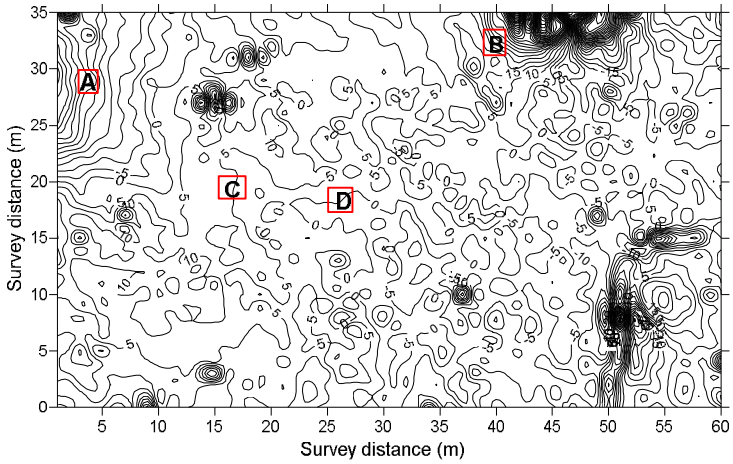
Geomagnetic Reference Field (IGRF), or fitting a low order polynomial surface to a diurnally corrected data with its procedural violations of some basic least-squares assumptions (Ojo and Kangkolo, 1997). The automatic reduction of magnetic data (ARMAD) technique is based on the understanding that results of geophysical surveys are interpreted by comparing observations at one location with those at other locations, and that the best datum (or reference point) to tie the field data to should be located within the survey area. The ARMAD technique uses the polynomial fitting method to obtain the amplitudes of the base station field corresponding exactly with the recording time at the grid stations. It ties the archaeo-magnetic field observations to those made at the base station by calculating the difference between the two observations. This simple, "arithmetic difference" is automatically the residual magnetic field, bypassing the cumbersome method of applying the diurnal correction to the field data which is usually followed by another data reduction process, the regional- residual separation.

5.3.3.1 The *ARMAD Methodology*

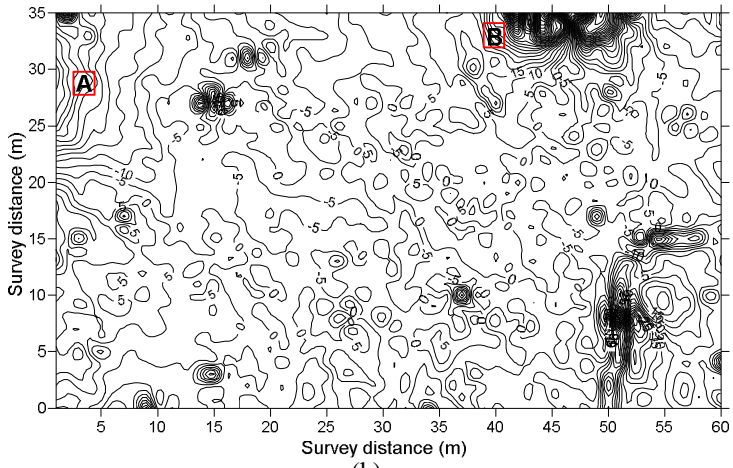
The ARMAD technique requires attention in three main areas. These are method of data collection, choice of the polynomial models to be fitted to the base station data, and correct computation of the base station field. These conditions were fully taken care of in the course of acquiring the archaeological magnetic data for the present study and in computing the diurnal corrections in the sub-section 5.3.1, and have been exhaustively discussed.

As was done in computing the diurnal correction, the base station field was computed from the base station data and the exact time of measurements at the grid points. Each

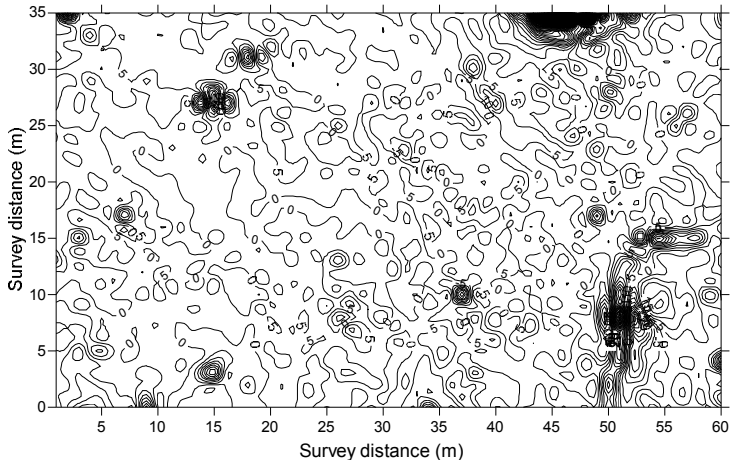
calculated base station data was then subtracted from the corresponding magnetic measurement made at a grid point. Such value is the residual magnetic field at that grid point; that is, removing both the diurnal effect and the regional field from the data automatically. That was done for all the magnetic measurements made at grid points to obtain the residual archaeological magnetic field shown for Uwani (Figure 5.6b). The performance of the ARMAD method in the reduction of magnetic field data was evaluated by comparing its result with those of the conventional (dual-stage) method of magnetic data reduction and the gradiometer method. The residual fields of Uwani obtained using all the three methods have been displayed in Figure 5.6 for visual inspection. The comparison was made qualitatively by comparing the resolutions of the three contour plots (Figures 5.6a, 5.6b and 5.6c), and quantitatively by comparing the maximum amplitudes of the residual anomalies in the three maps. The results displayed in table 6.2 indicate that the amplitudes of the anomalies obtained using the ARMAD method conform to those obtained using the gradiometer option more that those of the conventional method at almost all the selected horizontal coordinates (Figure 5.7). Because the gradiometer option is often known to give the highest resolution of any magnetic survey (Godio and Torino, 2005; Nabighian *et al*, 2005), it is right to affirm at this point that the ARMAD method, in addition to speed advantage, has higher resolution than the existing method of the magnetic data reduction. It is also obvious on



(a)



(b)



(c)

Fig. 5.6: Evaluating performance of the ARMAD method
by comparing its resolution with those of other methods
(a) Conventional method (b) ARMAD method
(c) Gradiometer method
(Contour interval is 5 nT in all the maps)

Table 5.2 Comparing anomaly amplitudes obtained using automatic reduction of magnetic data (ARMAD) method with those of conventional and gradiometer methods of magnetic data reduction

Serial number	Horizontal coord. x (m)	y (m)	Absolute amplitudes of the anomalies conventional method (nT)	ARMAD method (nT)	Gradiometer method (nT)
1	14.73	2.95	23.69	30.57	36.36
2	14.93	27.74	29.29	38.84	39.41
3	17.9	31.02	23.49	34.06	35.39
4	36.85	10.02	37.92	40.01	40.73
5	50.99	7.97	84.19	86.25	104.24
6	49.04	16.99	28.99	27.51	26.13
7	54.98	9.51	28.29	28.93	24.58
8	54.47	15.04	46.03	45.71	44.23
9	57.54	15.04	25.52	26.91	22.63

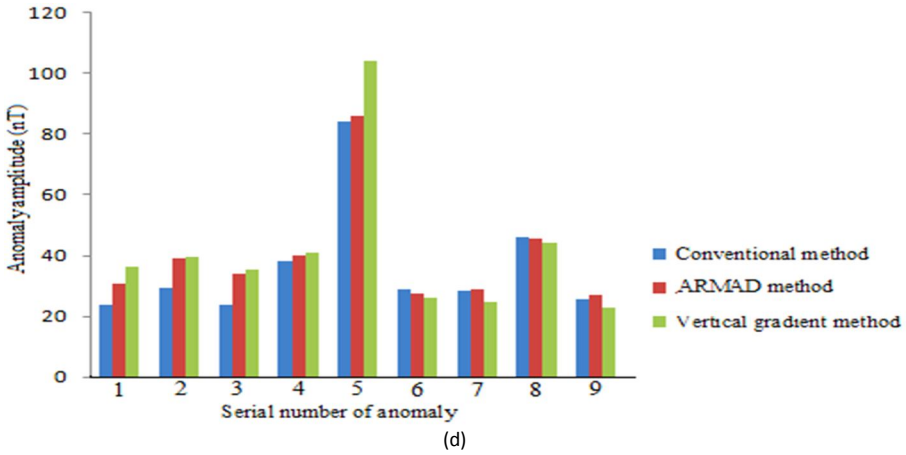


Fig. 5.7: Plot of the absolute amplitudes of the anomalies comparing ARMAD method with the conventional and gradiometer methods

visual inspection of the contour plots (Figure 5.6) that the map obtained from the application of the ARMAD method (Figure 5.6b) is comparable to that of the gradiometer method (Figure 5.6c). The noise levels labelled C and D in Figure 5.6a (result of conventional method) are suppressed in the other two maps. However, it is only the gradiometer method that was been able to filter out the noise at locations A and B that were caused by surface sources.

5.4 DETERMINATION OF THE LOCATION OF THE ARTEFACTS

Techniques using potential field derivatives to calculate the horizontal locations and depths of subsurface magnetic sources have been very attractive to many researchers (Reid *et al*., 1990; Piro *et al*., 1998; Hsu, 2002; Dawi *et al*., 2004; Godio and Torino, 2005). The most widely used among such methods are Euler deconvolution and analytic signal techniques. The main advantage of using the two techniques is that the horizontal location and the depth of burial of the causative subsurface bodies are determined independently of the magnetization direction. The theoretical backgrounds of both methods have been discussed in chapter 4. The sensitivity and effectiveness of the Euler computer program and those of the analytic signal software, for interpreting archaeological magnetic data were also validated in chapter 4 using synthetic magnetic data. The main goal in the applications of Euler and Analytic signal methods, as was earlier stressed was to point out the horizontal locations and the depths of the main features in the Lejja archaeological site so as guide the subsequent excavation in the area. Attempt was also made to first determine the shape of the suspected features so as to estimate the optimal structural index required for depth computation.

5.4.1 The Application of the Euler Deconvolution Method

The Euler method requires as inputs to the computer program, the horizontal and vertical gradients, the total (residual) field, the coordinates of the data points and the structural index. The expected outputs are the horizontal coordinates and depths to the top of the causative magnetic body, and the structural index which is also the shape

factor. As mentioned in sub-section 3.5.2, the total field data and the vertical gradient of the total field data were acquired at height of 0.30 metre above the ground surface. The horizontal gradients were then computed on each residual dataset at height of 0.3 metre using the Golden software's surfer version 9.0. The vertical gradients were measured directly in the field. These and the other parameters, the horizontal coordinates of the data points and the structural index, were used as input data to the Euler computer program.

A square window of size as small as 3 x 3 grid points (or more), within the grids of gradient values and field values, was used as a moving window through all the grid points. Within each window location, and for a specific value of the structural index N, all points in the window were used to solve the Euler equation for a source position (x_o,y_o,z_o). Due to overlapping of the moving window, there was an Euler solution for every data point. Nevertheless not all the results were expected to be recorded because there were criteria for acceptance of any result (Thompson, 1982; Reid *et al*., 1990). Among these were the structural index value and percentage of the uncertainty of the solution. The structural index that provides a small scattering of the solutions represents the optimal estimate. That is, for a computed depth to be accepted, it must have resulted from among the clustered "Euler solutions" around a suspected anomaly, and its uncertainty (standard deviation) must be less than 15% (Reid *et al*., 1990). A physical constraint also existed, and that was from the previous excavation in the area (Eze-Uzomaka, 2009) which revealed that the artefacts were found at very shallow depths, between 0 and about 1.5 metres. Surface observation of existing deep gully

erosion at Ejuona during the field work also revealed that this could be greater, perhaps up to 2 metres or more.

5.4.1.1 *Determination of Optimal Window Size and Estimation of Shapes of Magnetic Anomaly Sources*

As earlier stressed, the main focus in the application of the Euler deconvolution method was to determine the surface locations and depths to the top of anomaly sources. To achieve this objective, it was necessary to determine the structural index that gave the tightest clustering of the solutions. Since a real data set is likely to contain anomalies from various structural indices (Reid *et al*., 1990), it was necessary to solve the Euler equation for ranges of indices such as 0, 1, 2 and 3 (theoretical values for contact, dike, cylinder and sphere) at every site using the computer program of Appendix C.1, and to plot the results for each index and the corresponding window size. The maps could then be examined feature by feature and the index, and window size, which gave the best clustering of solutions, could be chosen for each feature, or a group of features. Determining the appropriate structural index was a way of estimating the shapes of the sources of the various anomalies in the three locations of the archaeological site.

Some of the relevant results obtained with various structural indices and the corresponding window sizes are displayed in Figures A.13, A.14 and A.15 of Appendix

A for Uwani, Ugbelenabo and Ejuona respectively. Assuming contact model (N=0) with varying window sizes, Euler solutions obtained in Uwani site were observed to be scattered, and not clustering around a particular point, even though many solutions were obtained. One of such solutions, using 3 x 3 grid points, has been displayed in Figure A.13. The results therefore ruled out the possibility of using contact model to interpret the data at the Uwani site. The index was therefore increased to N=1 (theoretical value for dike model), and some window sizes were used to obtain the Euler solutions. This index (N=1) displayed small scattering of the results around most of the anomalies in the site, thus representing optimal estimate for anomalies at locations A to E of Figure A.13. Indices of 2 and 3 were also experimented with giving few scattered solutions (Figure A.13). An intermediate case of N=0.5 (Reid *et al*., 1990) was also attempted to resolve the zone of complex anomalies at location F of the Uwani site. This provided solutions for the two anomalies at the location F (Figure A.13h).

The contact model applied at the Ugbelenabo site did not yield clustered solutions even with the high-resolution 3 x 3 grid nodes (Figure A.14). On the other hand, the use of dike model yielded Euler solutions that were centred mostly at all major anomalies at the site, particularly with the 3 x 3 grid nodes. Such solutions have been indicated at locations A to G of Figure A.14. It is also obvious in the same appendix that the solutions obtained with the wider window (4 x 4) of the same index, display tighter clustering at locations H, I, J and K than the corresponding locations C, D, E and F respectively. Other structural indices, 2 and 3, at this location only produced scattered solutions (Figure A.14).

In Ejuona site on the other hand, most of the anomalies were properly resolved using the contact model which gave good solution clustering at locations A to D (Figure A.15). There are many other clustered solutions at this site obtained with the same model that have not been emphasized with the reason that they may not be of archaeological interest as those of location A to D. Using dike model to obtain the Euler solutions gave enhanced clustered solutions at location E (Figure A.15). On the other hand, indices of 2 and 3 still produced many but scattered solutions at this site. The two major anomalies to the top left hand corner of the Ejuona site could only produce Euler solutions after an intermediate value of the index (N=0.5) was used. These, together with another smaller anomaly, are highlighted at locations F to H of Figure A.15.

5.4.1.2 *Determination of Spatial Locations of Magnetic Sources Using Euler Deconvolution Method*

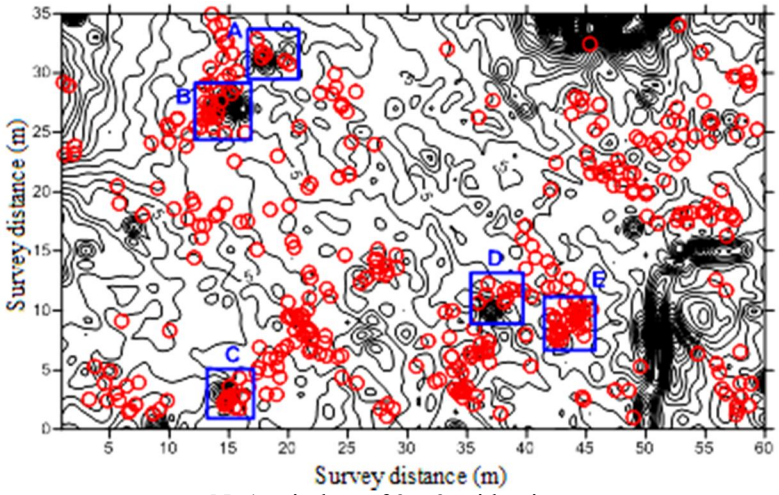
Computation of spatial locations of magnetic causative bodies were based on use of the structural indices and the window sizes that produced the smallest scattering of the Euler solutions as displayed in the Figures A.13, A.14 and A.15. All points in each moving window were used to obtain the source location (x_o,y_o,z_o) using the computer program (Appendex C.1) that is based on least-squares procedure. All such depth solutions were represented as circles at the plan location of the source. The specific locations of the magnetic sources were diffused among numerous solutions obtained at each of the three locations in Lejja archaeological site (Tables B.5 to B.7).

In an attempt to compute the locations of the sources of the anomalies labelled A to E in the Uwani site (Figure 5.8), 373 valid depth solutions were obtained based on index 1, window of 2m x 2m (3 x 3 grid points) and acceptance level of 12%. Therefore, to obtain the specific spatial location of each source, it was imperative to average all the clustered Euler solutions within the vicinities of the anomalies of interest. To do this, a computer program (Appendix C.3) was written that used the outputs of the 3D Euler depth solutions, and the coordinates of the area covered by all depth solutions for each source, as inputs. The Euler solution-averaging computer program thereby output the mean spatial locations of the sources of magnetic anomalies at each of the locations in Lejja archaeological site. The surface locations (x_o- and y_o-coordinates) and depths of burial (in metres) of the sources of magnetic anomalies in Uwani have been displayed in Table 5.3 according to the anomaly numbers indicated in the Figure 5.9. Estimated depths between 1.10 m and 2.09 m have been revealed in this site. The broad anomaly labelled 10 in Figure 5.9 resulted from a corrugated metal cover of a nearby underground water reservoir, and so did not record appreciable computed depths, even for all indices and window sizes (Figure A.13). The depth solutions for anomalies numbers 5 and 8 were obtained using the same index (N=1) as those of numbers 1 to 4, but with a different window size of 3m x 3m (4 x 4 grid points) as estimated beforehand (Figure A.13). The Euler depths were also calculated for anomalies numbers 6 and 7 using the intermediate index of 0.5 and window size of 2m x 2m (3 x 3 grid points).

On the other hand, an index of 1 was used to compute spatial locations for all anomaly sources in Ugbelenabo site, but with two different window sizes, 3 x 3 and 4 x 4 grid points, where the latter window gave less scattered Euler depth solutions at locations H

to K than the former. The depth computations for those anomalies were then based on the dike model using the 4 x 4 window. The depth computation for the rest of the anomaly sources at this site; that is, those at locations A, B and G, were done using the dike model and the higher resolution window, 3 x 3 grid points (Figure A.14). The calculated surface location (x_o,y_o) and the depth of burial (depth) of each anomaly source in metres are displayed in Table B.8 with the anomaly numbers 1 to 7 of Figure A.16 corresponding with A to G in Figure A.14.

The spatial locations of anomalies of interest, labelled A to D in Figure A.15a and A.15b, were obtained with the computer program of Appendix C.1 using the contact model (N=0). Because the solutions clustered more with dike model at location E, N=1 and high resolution window size of 3 x 3 grid points were used in obtaining the Euler



N=1, window of 3 x 3 grid points

Fig.5.8: An example of anomaly locations and Euler solution averaging for five sources A to E (Uwani)

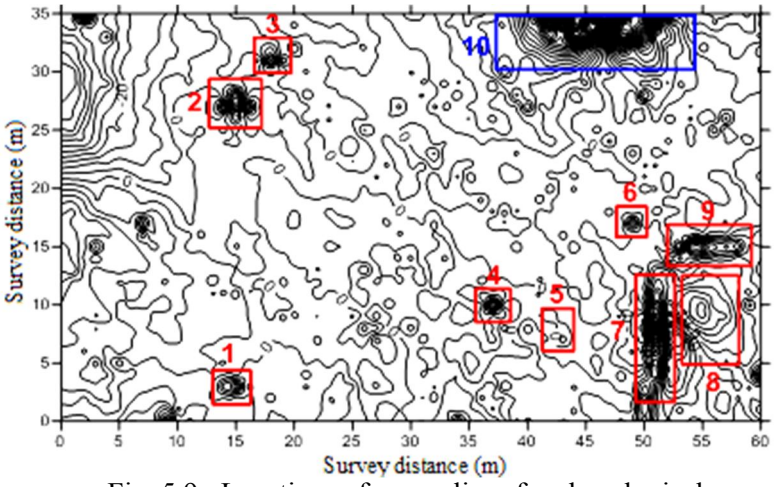


Fig. 5.9: Locations of anomalies of archaeological interest in Uwani site (labelled 1 to 9)

Table 5.3 Spatial locations of magnetic sources using Euler method at Uwani site

Anomaly No.	x (m)	error ±(m)	y (m)	error ±(m)	depth (m)	error ±(m)
1	15.35	1.84	2.71	0.33	1.16	0.14
2	13.73	1.65	26.90	3.23	1.22	0.15
3	18.46	2.22	31.53	3.78	1.10	0.13
4	37.67	4.52	11.38	1.37	1.18	0.14
5	43.30	5.20	8.17	0.98	1.11	0.13
6	50.56	6.07	17.64	2.12	1.30	0.16
7	49.55	5.95	5.29	0.63	1.54	0.18
8	51.17	6.14	8.55	1.03	2.09	0.25
9	55.92	6.71	18.01	2.16	1.57	0.19

solutions at that location (Figure A.15e). On the other hand, the Euler solutions for the anomalies at locations F, G and H were obtained using the intermediate index, N=0.5 (Reid *et al*., 1990) and the window size of 3 x 3 grid nodes (Figure A.15h). The horizontal locations and depths of the magnetic sources computed are recorded in the Table of Table B.9 according to the anomaly numbers given in the map shown in figure A.17. In all the three sites of Lejja archaeological site, including this one, the 3D Euler solutions recorded were based on the depth uncertainty (standard deviation) of less than 12 per cent.

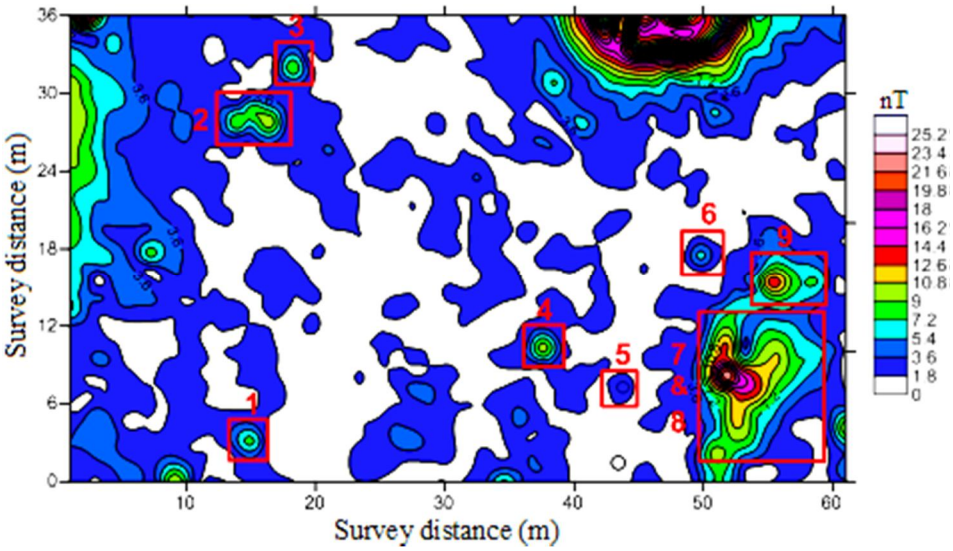
5.4.2 Application of Analytic Signal Method

The relationships between depth z_o and the width $x_{½}$ of the analytic signal anomaly at half the maximum amplitude as obtained by Atchuta *et al.* (1981) and Roest *et al.* (1992) for contact model, given as $x_{½} = 3.46z_o$ (equation 5.25), and for dike model, given as $x_{½} = 2z_o$ (equation 5.26), were used for the computation of the magnetic source depths. Where it was necessary, inflection point method was also used in the depth computation (applying equation 4.28).

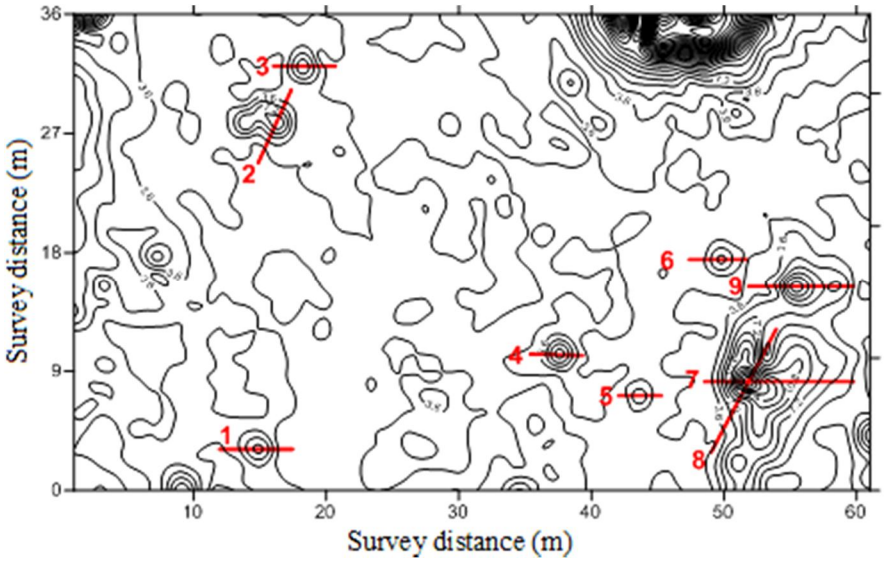
In order to use the MagPick in the depth computation, each set of the residual magnetic field data was gridded and the grid file loaded into MagPick. The analytic signal option of the multipurpose software was then used to automatically compute the horizontal and vertical gradients and thereafter obtain the analytic signal amplitudes. Because such amplitudes display maxima over magnetic contacts, they are able to map the edges of magnetic sources thereby defining the horizontal locations of the causative magnetic bodies. To define the mapped edges of the magnetic sources in Uwani archaeological site (Figure 5.4b or 5.4c), the output of the analytic signal obtained was plotted in surfer and displayed as image plot (Figure 5.10a). The map was used to estimate the boundaries of the various magnetic sources at this location of the Lejja archaeological site. It was also easy to locate the centres of the analytic signal anomalies very accurately. To implement this, a contour plot of the amplitudes of the analytic signal was made using the surfer package (Figure 5.10b). A cursor was placed at the centre of each anomaly in the map and migrated to obtain a point of maximum amplitude which corresponded with the epicentroid of the magnetic source. The x- and y-coordinates of such points were read off and recorded in Table 5.4 as the horizontal coordinates of the

centres of the sources. Using the outlines of the source given by the analytic signal technique (Figure 5.10a), the distances across the sources of interest labelled 1 to 9 were measured. The diameter of each source that did not display circular analytic signal anomaly was estimated by averaging its estimated length and width. All the measurements were done by placing the cursor at the edge of the source and taking the readings as recorded at the base of the surfer plot. The measured diameter, or distance across each causative body, has been recorded in Table 5.4.

There was also the need to calculate the depth to the top of the sources using the same contour plot of Figure (5.10b). To this end, visual inspections of the map were made to identify (where possible) the strike directions of the various magnetic sources. Profiles were then drawn normal to the strikes of the anomalies. The analytic signal map was digitized along these profiles, and the amplitudes were plotted against the distance along each profile using excel spread sheets. Such plots obtained for Uwani site are displayed in Figure 5.11 with each plot identified by its profile number. All the steps enumerated above were repeated for both Ugbelenabo and Ejuona sites using figures A.19 and A.22 respectively. The horizontal coordinates of the sources at the two



(a)



(b)

Fig. 5.10: Maps of the edges of the magnetic sources obtained from the analytic signal method ((a) Image (b) contour (Uwani))
(Coordinates of the origin: 7°22.19' E, 6°44.40' N)

locations were recorded in tables B.8 and B.9 respectively of Appendix B. The amplitude plots for both sites are also displayed in Figures A.18 and A.21 respectively.

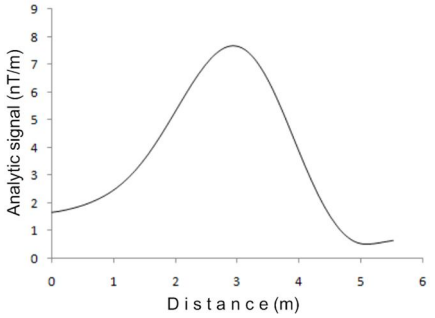
The analytic signal amplitude curves (Figure 5.11) can be used to estimate the depths of the various causative bodies by applying equations 4.22 and 4.23 for contact and dike models given in Chapter 4, where Atchuta Rao *et al*., 1981, Roest *et al*., 1992 and

MacLeod *et al*., 1993 defined the $x_{½}$ as width of the analytic signal at half the maximum amplitude. The authors recommended the use of such relationships between $x_{½}$ and the depth to the top of the magnetic source, z_o, for depth computations. The Euler deconvolution results obtained at the three sites in Lejja revealed three sources of magnetic anomalies, (i) magnetisation contacts, (ii) dike-like bodies and (iii) sources of intermediate property (N = 0.5) between contact and dike. The model type determined for each magnetic anomaly using the Euler deconvolution method was used in the analytic signal method. Excel spread sheet which was used to plot the analytic signal curves of the Figure 5.11 and those of Figures A.18 and A.21 was also used to calculate the widths of the curves at half the maximum amplitudes. Using equation (4.22), or equation (4.23), the depths to the top of the causative magnetic bodies were computed in all the three sites . In a situation that the intermediate model (N=0.5) was used, the depth to the top of the source was obtained by taking the mean of the depths calculated from equations (4.22) and (4.23). The horizontal locations of the sources, the computed depths, and estimated diameters of the magnetic sources have been recorded in Table 5.4, Tables B.10 and B.11 for Uwani, Ugbelenabo and Ejuona sites respectively.

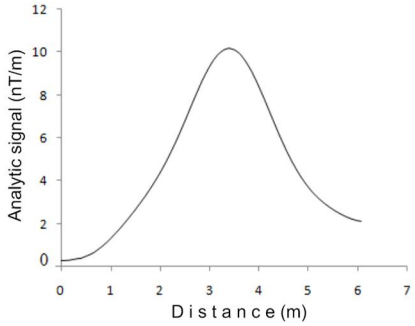
Table 5.4 Magnetic source locations using analytic signal method (Uwani)

Anomaly No.	x(m)	y(m)	depth(m)	diameter(m)
1	14.85	3.21	1.20	0.94
2	16.31	27.90	1.20	3.33
3	18.19	32.06	1.04	1.04
4	37.56	10.40	1.05	1.36
5	43.71	7.27	1.13	0.50
6	49.75	17.58	0.99	0.63
7	51.83	8.21	1.78	4.01
8	51.83	8.21	1.03	4.01

9	55.48	15.50	1.66	1.25



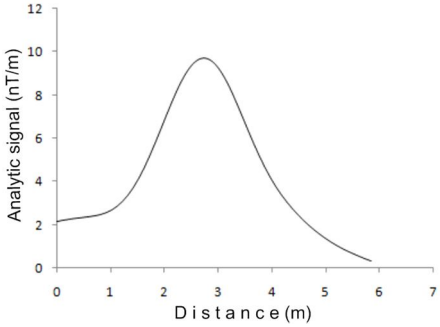
Profile 1



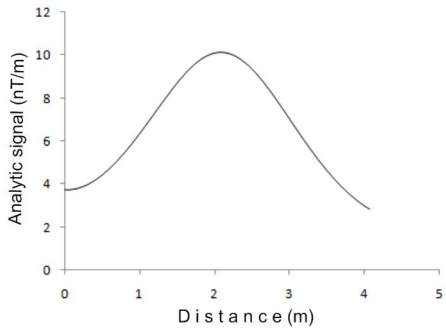
Profile 2



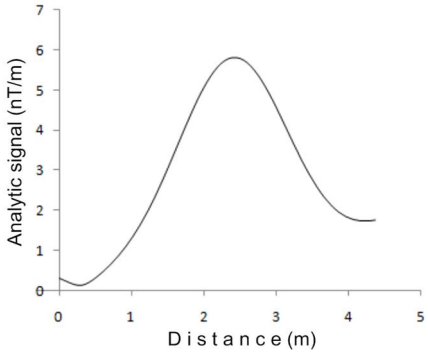
Profile 3



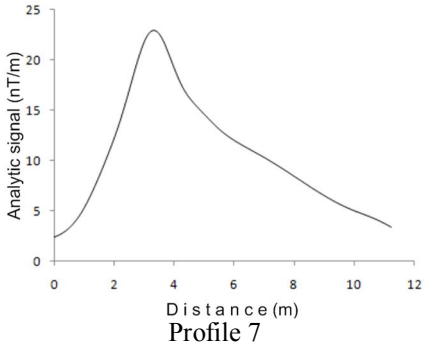
Profile 4



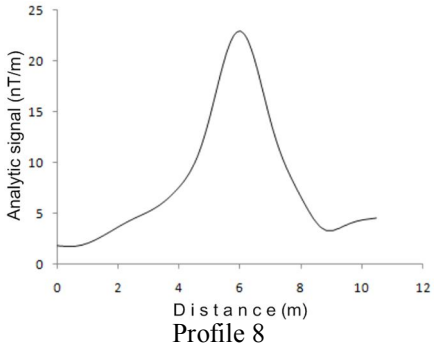
Profile 5



Profile 6



Profile 7



Profile 8

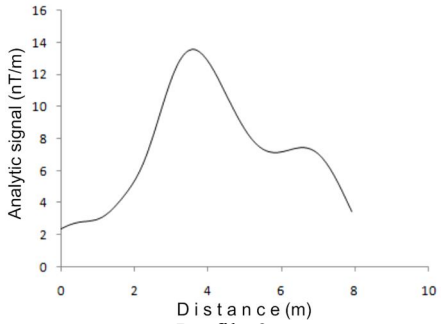


Fig. 5.11: Amplitude curves for magnetic source depth calculation (Uwani)
(Profiles 1 to 9 were obtained from figure 6.10b)

5.5 SITE BY SITE DISCUSSION OF RESULTS

Chapter 4 and this one have been concerned with the use of the Euler deconvolution and the analytic signal methods in the determination of magnetic source locations. These two widely applied techniques use the three orthogonal potential field derivatives to identify the plan locations and depths to the causative sources without reference to magnetisation direction. Therefore, in their applications, the magnetic sources were assumed to display only induced magnetisation, neglecting the effect of remanent magnetisation. Such assumption is readily acceptable in an iron smelting site such as Lejja where expected artefacts are mostly highly fired features. In all the sites, the Euler deconvolution maps have presented the derived source positions as circles at their plan positions. The optimum window size and best structural index were estimated beforehand (Figures A.13, A.14 and A.15) so as to avoid unnecessary depth computations. The correct structural index for any given feature was based on the degree of clustering of the solutions, when this could be distinguished. The valid spatial

Euler solutions obtained at a site for sources of the same structural index were sometimes very large, perhaps, in hundreds. So to obtain a reliable estimate of the plan location and depth of any magnetic source, all the clustered depth solutions within the vicinity of the source were averaged using the computer program of Appendix C.3.

As usual with the analytic signal technique (MacLeod *et al.*, 1993; Hsu *et al.*, 1998; Salem, 2005), it was assumed that the causative sources were 2D archaeological structures such as contacts, dike-like structures and cylinders. The analytic signal amplitudes were obtained from the total archaeological magnetic data by taking the square root of the sum of squared vertical and the two orthogonal horizontal first derivatives of the magnetic field. If interferences from nearby sources are minimal, such amplitudes could form bell-shaped symmetric functions (Figure 5.11, Figures A.20 and A.23) maximising over the top of each magnetic contact, with the width of the amplitude curves being related directly to the depth of the contact (MacLeod *et al.*, 1993; Debeglia and Corpel, 1997). The technique, like the Euler deconvolution technique, was utilised in locating plan positions of the magnetic contacts and estimating their depths.

The Euler deconvolution and the analytic signal methods of interpretation were meant to complement each other. They have been geared towards providing the horizontal locations, the depths of burial and possibly, the diameter or the lateral extent of the sources of magnetic anomalies. The former method has been used to estimate the shapes of the causative sources and has served as a guide in the application of the latter method. Each method has been applied separately to the three locations of the

archaeological site. In almost all cases, the choice of magnetic anomalies of archaeological interest has been based on the contour plots of the residual fields of Figure 5.4, Figures A.10 and A.11. The maps depict various magnetic anomalies which, in most cases, are in agreement with the results of the two techniques. The validity of the developed computer programs (Euler deconvolution method) and the purchased software (analytic signal method) in the interpretation of the archaeological data was demonstrated with results from synthetic data (Chapter 4). Such results are meant to serve as clues to the reliability of results obtained with the real data.

Various numerical values have been obtained for some parameters of the magnetic sources suspected to be of archaeological origin in each location. These results have been displayed in Tables 5.3 and 5.4, and in tables B.8 to B.11 of Appendix B. Nevertheless, the possibility of distorted information arising from the complexity associated with interpretation of magnetic data due to superposition of multiple magnetic sources and magnetic noise occurring from geological and cultural sources (Silva, 1986; Blakely, 1996; Ansari and Alamdar, 2009) were not ignored. For example, at some locations, certain anomalous fields resulting from power lines and surface metallic objects were superimposed on the field data while in others, the complex anomalous situations displayed had to be resolved through further analysis to be discussed shortly. The results obtained at Uwani, Ugbelenabo or Ejuona are better discussed separately.

5.5.1 Uwani Site

The maps of Figures 5.9 and 5.10 show anomalous points of archaeological interest, numbered 1 to 9. The horizontal locations and the depths of the suspected sources of the anomalies computed using the Euler deconvolution and the analytic signal methods are displayed in Tables 5.3 and 5.4 respectively. The latter table also shows an extra column containing mean distance across the corresponding sources (diameter). There are obvious close correlations in the plan locations of the causative sources obtained using the two methods as depicted in the two tables. The source depths obtained using the Euler deconvolution method, vary between 1.10 m at location 3 to 2.09 m at location 8. On the other hand, those obtained using the analytic signal method, vary between 0.99 m at location 6 to 1.78 m at location 7. The two sets of the depth results also show good correlations except for the anomaly location 8. Such large difference might have resulted from wrong orientation of profile number 7 (Figure 5.10b) which can be ascribed to inability of the analytic signal method to differentiate between the edges of the sources which, due to their close proximity, have overlapping anomalies. That is, two maxima from the two nearby parallel edges must have merged to one maximum (Atchuta *et al*., 1981; Roest *et al*., 1992; Hsu *et al*., 1998). In such situation, the analytic signal curve appears distorted. This is, perhaps, the case of the analytic signal curves of profiles 7 and 8 (Figure 5.11). The former curve is expanded while the latter is compressed at their measurement points thereby resulting in higher and lower source depths respectively than expected.

In order to clarify the correlations between the two sets of results, graphical representations of their similarities (or dissimilarities) along the horizontal direction (almost east-west), along the vertical direction (almost south-north), and the depths

have been given in Figure 5.12. The horizontal coordinates of the sources given in Figures 5.12a and 5.12b for the two methods of analysis are adequately close to be averaged to obtain the mean plan positions of the causative sources. On the other hand, because of the large contrast in the depths computed with the two methods at location 8, calculations of such mean values of depths have been avoided until a transformation method, upward continuation (Telford *et al.*, 1990; Blakely, 1996), was applied to resolve the anomalous difference. The process of upward continuation transforms the potential field measured on one surface to the field that would be measured on another surface farther from all sources. It attenuates anomalies with respect to wavelength. The shorter the wavelength, or the closer the source to the surface, the greater the attenuation. The elongated, high frequency anomaly (numbered 7) that trends about 15 degrees west of the north and is superimposed on the wider, dipolar anomaly which trends about north-south direction can be separated from the deeper body using a frequency filter. The one readily available was the upward continuation option of the processing software, the MagPick.

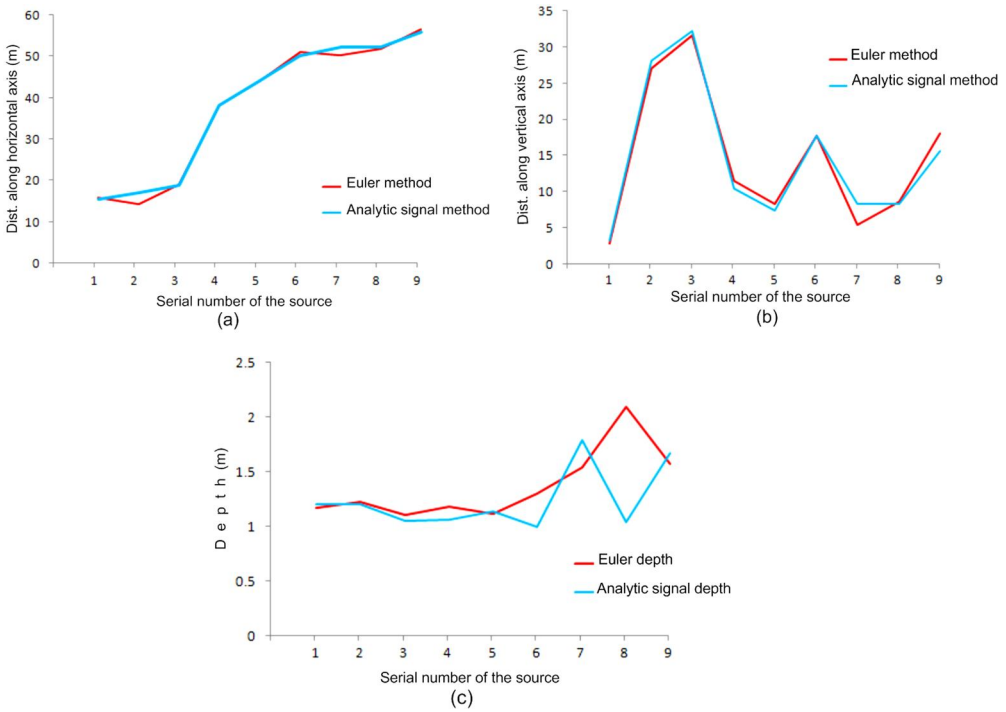


Fig. 5.12: Compering spatial locations of the sources obtained using Euler and analytic signal methods (Uwani-Lejja)
(a) source distances along horizontal axis
(b) source distances along vertical axis
(c) source depths

According to Jacobsen (1987), upward continuation of a potential field by an amount equal to the line spacing gives better resolution of the continued field than the one in which a different altitude is used. The Uwani field was therefore upward-continued in stages of 1 metre, between 1 and 3 metres. At each stage, the cursor was placed at the highest point of the anomaly produced by the source being investigated. The anomaly magnitudes and the corresponding heights of continued field were recorded and the contour plot obtained. Figure 5.13 shows slices of the coloured plots of the Uwani upward-continued fields. It was discovered that the higher frequency source was completely filtered out between the heights of 1.0 and 2.0 metres (Figure 5.13). On the other hand, the anomaly amplitude of the source number 8 depreciated from 25.76 nT at

the ground level to10.30 nT at a height of 1 m and to 1.24 nT at the height of 2 m. This accounts for about 5% of the field of the lower frequency source (location 8) remaining

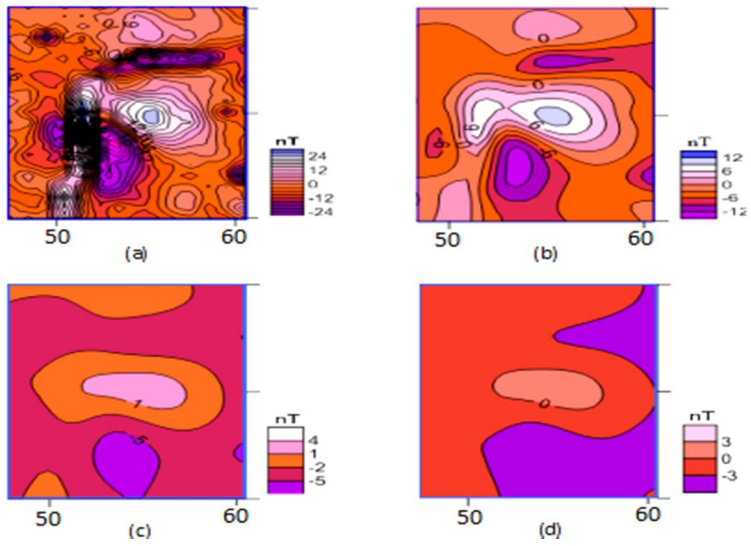


Fig. 5.13: Variation of magnetic field with altitude at the location labelled 7 & 8 in figure 6.10a
(a) 0.0 m (b) 1.0 m (c)2.0 m (c) 3.0 m

at the height of 2 metres. Further continuation produced negative field at location 8 showing that the field rarely exists beyond that height (Jacobsen, 1987). Using a mirror image of the height of continuation as demonstrated with the synthetic example (section 4.4), the Euler depth of 2.09 metres at the location 8 may be acceptable if the source is suspected to have a height a little below 1 m to about 1 m. In that case, the depth of about 2.09 m may be preferred to the analytic signal depth of 1.03 metres at the same location. Since such idea is still hypothetical, it may not be right to invoke it in taking decision over depth in the ongoing study. But the fact remains that the depth of 1.03 metres computed for the lower frequency source that is overlaid by the higher frequency source predicted to be at the depth of 1.78 metres is paradoxical. It is simply as a result of the inability of the method to separately resolve edges of the sources having superimposed anomalies. By induction, therefore, the Euler depth of 2.09

metres for the lower frequency (broader anomaly) source is preferably chosen for the source at location 8. Hence, a new table of parametric values of magnetic anomaly sources in Uwani site has been generated as given in Table 5.5.

Table 5.5 Mean magnetic source locations (Uwani)

Anomaly No.	x(m)	y(m)	depth(m)	dist. across source(m)
1	15.10	2.96	1.18	0.94
2	15.02	27.40	1.21	3.33
3	18.33	31.80	1.07	1.04
4	37.62	10.89	1.12	1.36
5	43.51	7.72	1.12	0.50
6	50.16	17.61	1.15	0.63
7	50.69	6.75	1.66	-
8	51.50	8.38	2.09	4.01
9	55.70	16.76	1.62	1.25

Figures 5.13 (a) and (b) depict the pronounced magnetic anomaly as trending almost north-south, a display of an induced magnetisation. Its signal shape (dipolar with negative towards the south and positive towards the north), based on the inclination of about -10^{o} of the geomagnetic field at the study area, also confirms that the magnetic anomaly is caused by a negative susceptibility contrast between the suspected archaeological feature and the surrounding soils. The analytic signal result also proves that the distance across the source of the anomaly is about 4 metres. The elongated anomaly superimposed on the broader anomaly (location 7) is positive and has amplitude of about 86 nT (Figure 5.9). This also shows that the nearby source of the field has negative magnetic susceptibility contrast with its host soils. The results of the two methods of interpretation have also confirmed their depth of burial to be about 1.7 to 2.1 metres (Table 5.5). It can be inferred from these that this complex area of this

site (Figure 5.10a), is most likely to be an ancient refuge dump. The causative sources at locations 1, 4, 6 and 9 display anomalies of medium amplitudes between 27 and 42 nT (Figure 5.9). The negative polarities of their anomalies confirm that they have positive susceptibility contrasts with the host soils. The results of the analytic signal and the Euler deconvolution methods also show that their diameters vary between 0.63 and 1.36 metres, and are found at depths between 1.12 and 1.62 metres. The sources number 1, 4 and 6 are, perhaps, products of a nearby smelting activity, most probably slag blocks (Godio and Torino, 2005; Piro *et al*., 2007; Eze-Uzomaka, 2009). The same reasoning goes for the anomaly source number 2, but the area (about 9 m^2) it occupies shows that it is most likely to be made up of many slag blocks. The source number 9 already described along with 1, 4 and 6 has the signal amplitude of 42 nT, the diameter of 1.36 m and buried at the depth of about 1.62 m. The medium magnetisation contrast, if compared with the analytic signal result, may allow the interpretation of this source as a small size furnace. But its actual diameter is most probably about 1 m or less with the surrounding fired soil accounting for the large-looking diameter.

5.5.2 Ugbelenabo Site

The residual magnetic map of Ugbelenabo (Figure A.10) shows many anomalous areas, but few of these seem to be of archaeological interest. A total of seven locations have been indicated and are numbered 1 to 7 (Figures A.16 and A.18). There are two other major anomalies which are not of archaeological interest because they are caused by known surface features as noticed during the field work. Among these are (i) the narrow and long northwest-southeast trending anomaly (or a set of clumsy anomalies) to the east of the site (pointed with blue arrow), and (ii) a half circular anomaly at the

southern part of the site (pointed with red arrow). The earlier feature which is made up of more or less a set of linearly arranged anomalies, is regarded as not being of archaeological interest because what seems to be an old foot path was noticed during the field work. It serves more as noise to the data, so any magnetic anomaly observed around that feature has not been considered to be of an archaeological interest. The second noisy anomaly which is at a distance of about 42 metres from the origin is an iron sign post belonging to an elementary school in the study area. It was hidden in the bush, unnoticed until the data around that area were all collected. Its magnetic noise is also superimposed on the field data as half circular anomaly at the southern part of the survey area (Figure A.10).

The applications of the two methods of interpretation, the Euler deconvolution and the analytic signal methods have produced the Euler depth map of Figure A.16 which indicates horizontal locations of the magnetic sources as circles at their plan positions, and the analytic signal image map of Figure A.18 which depicts outlines of the body edges. Using the profiles labelled 1 to 7, minus the profile for source number 3 which was not mapped by the analytic signal method, the depths to the top of the suspected sources were estimated using the relationships between depth and the width of the analytic signal anomaly (equations 4.22 and 4.23) given by Atchuter *et al*. (1981) and Roest *et al*. (1992).

Tables B.8 and B.10 are the tables of result of the plan positions and depths obtained using the Euler deconvolution and the analytic signal methods respectively. The latter table also contains an additional quantity, the estimated distance across each source.

Both the horizontal locations of the sources and their depths estimated using the two methods of interpretation are adequately correlated as depicted by Figure 5.14. For that reason, results of the two methods have been averaged and displayed in Table 5.6. Out of the seven selected anomalies, there are probably only two that are of archaeological interest. These are numbers 2 and 7 (Figure 5.15) which, not only appear to have been fired in situ, judging from the polarity of their signals, but have substantial signal

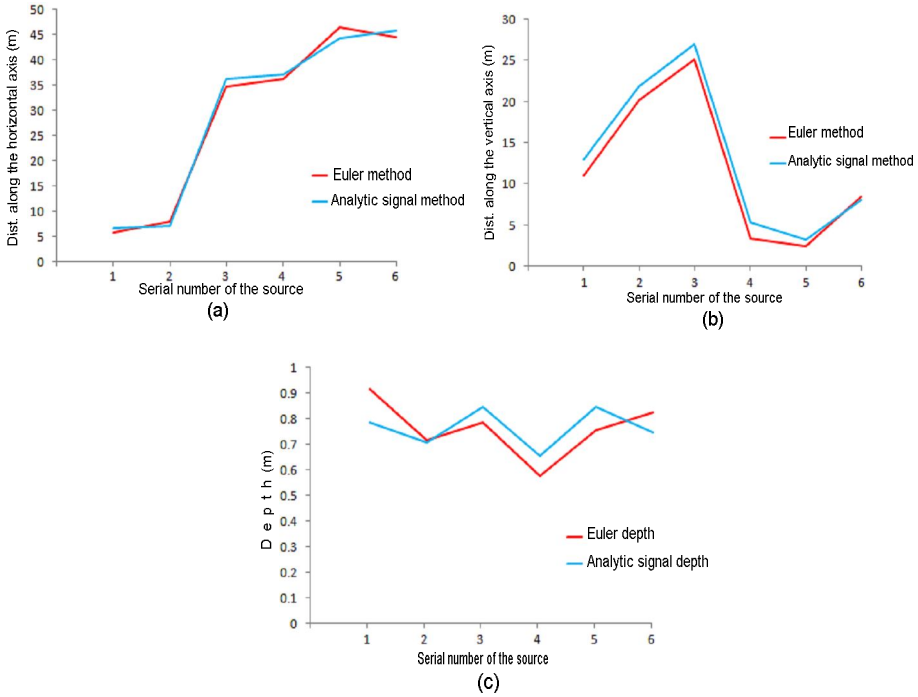


Fig. 5.14: Compering spatial locations of the sources obtained using Euler and analytic signal methods (Ugbelenabo)
(a) source distances along horizontal axis
(b) source distances along vertical axis
(c) source depths

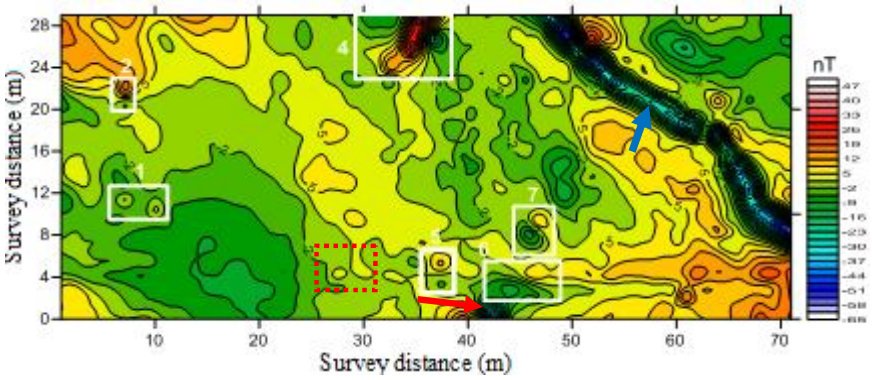


Fig. 5.15: Image plot of Ugbelenabo residual field showing anomalies of interest (Coordinates of the origin: 7°19.00' E, 6°42.28' N)

Table 5.6 Mean magnetic source locations (Ugbelenabo)

Anomaly No.	X(m)	y(m)	depth(m)	dist. across(m)
1	6.44	12.07	0.86	2.84
2	7.70	21.06	0.72	1.98
3	25.94	5.00	0.85	-
4	35.62	26.10	0.82	6.23
5	36.85	4.33	0.62	1.41
6	44.56	2.85	0.81	2.49
7	46.30	8.29	0.79	3.12

amplitudes of about 37 nT and 25 nT respectively. The same story goes for the source at location 5 except for its small signal amplitude, perhaps, not more than 10 nT. The three anomalies can be attributed to contact fire burn such as shallow fire pits. The signal shape displayed by the largest source at this site (number 4) does not make it look an archaeologically interesting source, but could be a fired stone or charcoal (furnace fuel) deposited at that location. No any other source appears attractive at that this site.

5.5.3 Ejuona Site

Ejuona is characterised with many low frequency and relatively broad magnetic anomalies, particularly the central area and the southern part (Figure A.11b). There are also a few high frequency ones, but appear to be of relatively superficial sources that may not be of archaeological interest. The anomalies suspected to be of archaeological

interest have been selected and labelled 1 to 7 (Figure A.21). For these anomalies, the Euler deconvolution and the analytic signal results have shown that they vary in depth between 0.84 and 1.88 metres (Tables B.9 and B.11). Their horizontal locations and depths computed using the two methods of interpretation correlate well enough to be averaged. In order to easily visualise such closeness, plots of the two results along the x-axis, the y-axis and the depth are given respectively in Figures 5.16 (a), (b) and (c). The Euler deconvolution and the analytic signal results did not correspond at the source numbered 7 since the former gave results for a source that was not along profile numbered 7 but for a more superficial source at a nearby location (Figures A.17 and A.22). Therefore the results displayed against the source numbered 7 in Table 5.7 were obtained directly from the analytic signal method and not mean values of the two methods.

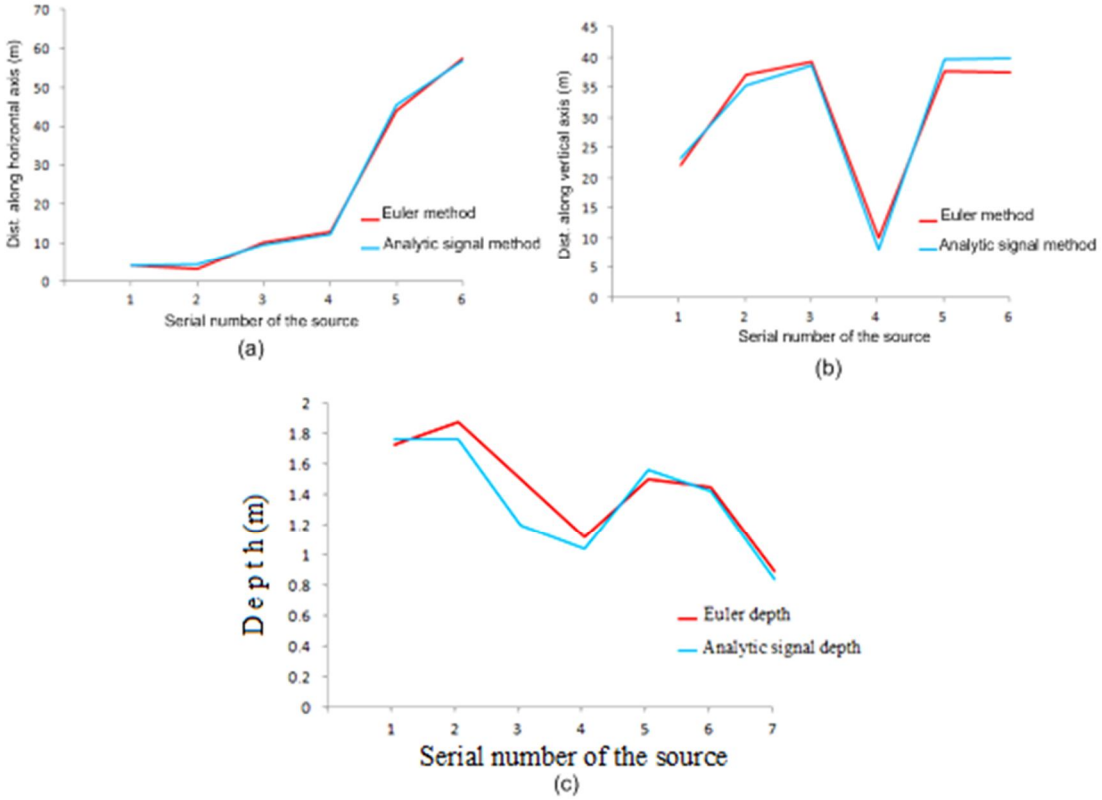


Fig. 5.16: Compering spatial locations of the sources obtained using Euler and analytic signal methods (Ejuona)
(a) source distances along horizontal axis
(b) source distances along vertical axis
(c) source depths

Table 5.7 Mean magnetic source locations (Ejuona)

Source No.	x(m)	y(m)	depth(m)	dist. across source(m)
1	4.07	22.71	1.75	6.60
2	3.78	37.28	1.82	3.07
3	9.81	39.01	1.35	1.92
4	12.53	9.16	1.08	1.04
5	44.76	38.71	1.53	1.27
6	57.06	38.66	1.45	1.27
7	54.41	27.53	1.42	3.59

There is also some contrast in depths computed at the source location 6 using the two methods. The likely cause of it, perhaps, is a small size source of high magnetisation (e.g., a bloom) buried at a relatively high depth and producing an anomaly of small diameter on the surface. For such causative source, Euler method is most likely to obtain a good depth since it utilises the vertical gradient of the field. Analytic signal method, on the other hand, can only obtain narrow bell-shape signal amplitude that leads to computation of a small depth. On that note, the results of the two methods were averaged.

The results obtained show that the north-west of the site, an area of about 20 by 20 square metres, was a major iron smelting activity area (Figure 5.17). There are a few major anomalies within this zone. They are aligned approximately in the north-south direction starting with the one of positive polarity at the southern part (indicated by the white arrow) followed by a negative polarity, high amplitude anomaly at location B. This is again followed by another anomaly of positive polarity (also arrowed) which is followed by the major one labelled A. In this area of study with geomagnetic field inclination of about -10^{o}, the above sequence is an indication of the presence of sources of magnetic field that have positive susceptibility contrasts with their host soils (Godio and Torino, 2005; Foss and McKenzie, 2009).

The compact anomaly (numbered A) is the most archaeologically interesting one in Ejuona site. It has a simple circular to elliptic shape (Figure 5.17) having moderate amplitude of about 86 nT. Application of the analytic signal method to this location

occupied by the anomaly numbered A predicts two separate sources numbered 2 and 3 in Figure A.21. The earlier source, whose centre has the coordinates (3.78,37.28), has

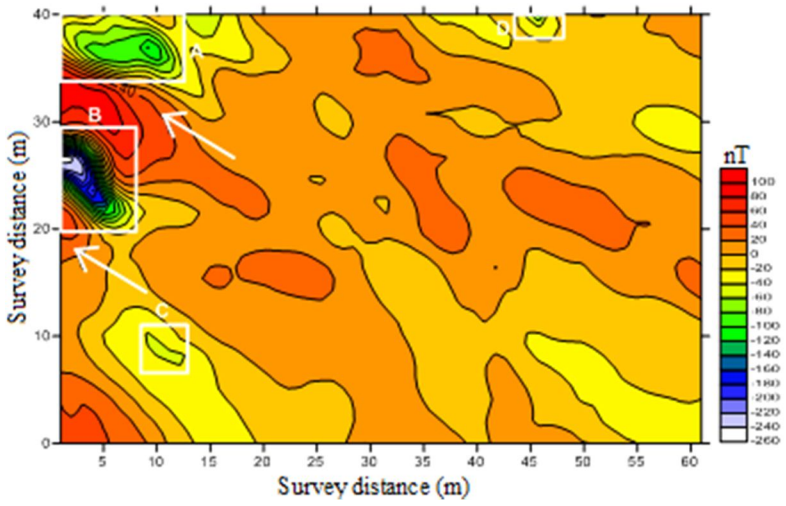


Fig. 5.17: Ejuona low-pass filtered field
showing only major anomalies
(Coordinates of the origin: 7°22.75' E, 6°42.75' N)

a diameter of about 3 metres and is buried at a depth of about 1.82 metres (Table 5.7). Immediately to the east of this is the source labelled 3 with the plan position at (9.81,39.01). It has a diameter of about 1.92 metres and buried at a mean depth of about 1.35 metres. The white background close to the latter source shows that it was not fired in situ, but perhaps, a repositioned iron smelting slag block which is suspected to be a product of a nearby smelting activity. Based on the above reasons and results of the Euler and the analytic signal methods, the magnetic source at location A is regarded as a large iron smelting furnace with surface location, (3.78, 37.28) in metres, and buried at depth of 1.82 m. The wide-looking diameter of such furnace (3 metres) may be due to long period of firing.

The second major anomaly (labelled B in Figure A.21) is an elongated, very high amplitude anomaly. Unfortunately, the full size could not be recovered. This problem was noticed at the trial contouring during the field work, but an attempt to recover the whole shape of the anomaly would mean extending the magnetic profiles to cover the main road which was not possible due to vehicular and pedestrian movements. It displays higher magnetisation than the source at location A (Figure 5.17) and occupies an estimated area of about 65 m^2 with the assumption that about 66% of it has been mapped. It can therefore be inferred from the analytic signal result that it is a mound, made up of debris such as small-size slag blocks, blooms, broken fired clay tools (e.g., tuyère), charcoal, etc., that were thrown out of the near-by furnace site and allowed to cool in the ambient geomagnetic field. The sources at points C and D (Figure 5.17) are most likely to be accounted for by the presence of such furnace debris. For example, the shape of the source at the point 6 of the analytic signal result (Figure A.21), corresponding with the anomaly location D (Figure 5.17), may be predicting an iron smelting slag block of a small diameter, perhaps, less than 1 metre and buried at a depth of about 1.45 metres.

C H A P T E R 6
D I S C U S S I O N AND CONCLUSION

6.1 DISCUSSION

A good number of artefacts that archaeologists search for are under soil cover as a result of gradual sedimentations that would have spanned over centuries, and even millennia. Such ancient relics are usually retrieved through excavations which may sometimes involve much digging. Once the antiquities are destroyed either through such hasty excavation or modern construction, there exists no substitute for the historic records. The best protection for the historic remains is to identify where they are and preserve the land for future generations to study through careful excavations or more scientific methods that will identify and study the artefacts in situ (Scollar *et al*., 1986). Although conventional method of archaeological investigations has been very productive in tracing human history, the restrictions imposed by some enlightened individuals on their immediate environments in response to international outcry for environmental protection is an added disadvantage to the age long traditional method. These and many other inherent problems associated with the conventional method of archaeological search (Clark, 1990; Eze-Uzomaka, 2009) have made the applications of geophysical methods in archaeology gain rapid popularity over the past few decades, particularly in the developed and some developing countries of the world.

The surface geophysical surveys have been applied to the problem of detecting and delineating shallow subsurface targets of archaeological origin without negative impact on the environment. A successful completion of such survey has, as a final product, a map or maps that more or less give(s) the spatial locations of the concealed features thereby guiding prospecting archaeologists to precise points of excavation. It is, therefore, surprising that such practice is almost alien to sub-Saharan Africa. It is, perhaps, due to lack of interest on the part of practising archaeologists, but most notably, the lack of awareness of the advantages of the 'new' methodology coupled with the high cost of hardware and software in the part of the world where an archaeological research seldom attracts funding.

Nigeria, particularly the southern part, is prone to relatively rapid sedimentation as a result of the country's proximity to the Sahara desert. On annual basis, the popular north-east trade wind comes with aeolian deposits that form appreciable thickness of soils after many decades. A large portion of these aeolian soils are eroded during the raining season and washed down into the river channels through surface runoff. They are redistributed by various river channels in form of alluvial soils. These deposits, in addition to the local soil formation in the south-eastern part of the country (Ofomata, 1978a) lead to the rapid rate of sedimentation in the area. That is, the historic evidences get more and more hidden from the surface as the years go by, but the history of the people must be traced. That means the archaeologists who have to dig more sporadically to excavate the artefacts are expected to face environmental restrictions if the archaic method of research is not modified.

There are about 17 major prehistoric iron smelting sites in south-eastern Nigeria (Eze-Uzomaka, 2006). In most of these, the artefacts are under soil cover and about 13 of the

them including Opi, Aku, Itoro, Umundu, etc., have already been investigated using the conventional method (Ezike, 1989; Eze-Uzomaka, 2006). The search for the artefacts in Lejja community (one of the 17 sites) using the same method, began a few years ago (Eze-Uzomaka, 2009). It is the target of this research work that such practice be discouraged in order to reduce the impact of the 'obsolete' prospecting method on the environment, and to re-streamline the research along the path of the method of archaeological geophysics. Such applications of geophysical technique are expected to be more environmentally friendly and should have no impact on the concealed features. The best of such survey method to be applied in a prehistoric iron smelting site such as Lejja, is the magnetic profiling method. Three sites, Uwani, Ugbelenabo and Ejuona were carefully selected for investigations in the Lejja community based on availability of space, flatness of the land and signs of smelting activity at sight.

The success of such survey is dependent upon some factors. These include the quality of the acquired data, the methods of data processing and interpretation, and quality of data display. To achieve the above objectives, the magnetic survey was performed on the regular 1 x 1m grid using the proton precession magnetometer (Geometrics) model G-856AX with a resolution of 0.1nT in both gradient and standard configurations. The acquired data which were automatically stored in the magnetometer memory were downloaded directly into the computer thereby avoiding transcription errors. The data reduction was done by first applying an efficient polynomial fitting method developed during this study for diurnal correction and then separating the regional and the residual using the golden software, surfer. The reduced data were later smoothened using spline smooth filter available in surfer, and then contoured for visual inspection of the magnetic anomalies. Upward continuation filter was also applied in some situations that needed to de-emphasize the effect of high frequency sources. For the purpose of correlation, the two methods of interpretation, the Euler deconvolution and the analytic signal methods were deployed after being validated using synthetic field examples.

The Euler deconvolution method is known for reliable depth computation (Thompson, 1982; Reid *et al*., 1990; Hsu, 2002). Its depth accuracy is determined by the quality of the vertical gradient and if such gradient is to be computed, low level noise and poor data quality in the original total field data will be amplified, leading to less accurate computed depths. To circumvent this, the vertical gradients of the total field data were measured with 1.25 metre sensor separation. Different structural indices and window sizes were used to determine the shape of the causative magnetic body and the optimal window size required for the Euler deconvolution results. On the other hand, the maximum values of the analytic signal amplitudes in a three dimensional plot indicate the body edges regardless of the earth's magnetic field and the direction of magnetisation. That is, the method is very handy at a low magnetic latitude area such as Lejja where reduction to the pole is not applicable (Lawal and Osazuwa, 2004). The amplitude is a bell-shaped symmetric function maximizing exactly over the top of each contact, with the width of the amplitude curve being related directly to the depth of the contact. Analytic signal method is therefore very reliable in delineating boundaries of magnetic sources (Debeglia and Corpel,1997; Godio and Torino, 2005).

The applications of these two methods at different locations in Lejja have given some impressive results about the archaeological site. Some artefacts were detected at very shallow depths, between 0.62 and 0.86 metre. Some of these features are most likely not to have been fired in situ as observed from their signal orientations. They appear to have been transported from other locations within the archaeological site. A few of them that seem to have been fired in situ have displayed low signal amplitudes showing that they may not be more than archaeological soils such as are associated with prehistoric cooking points or fire pits within the site. Such shallow rooted features are more common in Ugbelenabo at the south-western part of the community. There are indications of major iron smelting activity areas in both Ejuona and Uwani sites. In the former, it is located to the north-western part of the site, occupying an area of almost 400 m^2, while in the latter it is found at the eastern part of the site covering area of lesser extent, less than 100 m^2. The signal shapes in both sites confirm that the magnetic anomalies are caused by positive magnetic susceptibility contrasts between the archaeological features and their host soils. Their signal orientation (north-south) is also an indication of in situ firing. These results therefore suggest that there are two different types of furnace at two different sites, a fairly large one buried at the depth of 1.82 m, with surface coordinates of (3.78, 37.28) m from the origin, at the Ejuona site; and a small size one buried at the depth of 1.62 m, with surface coordinates of (55.70, 16.76) m from the origin, at the Uwani site. There also exists a large mound of furnace debris at depth of about 1.75 m, with surface coordinates of (4.07, 22.71) m from the origin, occupying an estimated area of about 70 m^2 at the Ejuona site.

Apart from the main activity areas just discussed, the applications of the two methods of interpretation indicate that not all the iron smelting slag blocks were picked from the furnace sites during and after the smelting activity. Some of them and other remnants of the smelting products and materials such as blooms, tuyère, charcoal, etc., have been detected and mapped by the methods (Figure 5.10, Figures A.18 and A.21). The spatial locations of all the artefacts mapped in the archaeological site have been recorded in Tables 5.5, 5.6 and 5.7. The records indicate that the archaeological features in Lejja which are predominantly of iron smelting in origin can be found between the depth of about 0.6 and 2.0 metres. It is also believed that with such shallow depth at some locations exposed to gully erosion, some of the furnaces can be found at the ground surface. The results are in close agreement with the previous worker, Eze-Uzomaka (2009), who predicted depth of burial of about 1.2 metres for some artefacts in Lejja.

6.2 CONCLUSION

The primary aim of the study is to use magnetic method for archaeological investigations in Lejja archaeological site so as to serve as an introduction to the use of archaeological geophysics in this site, in other sites in Nigeria and in some of her African neighbours. The geophysical survey has been conducted in Lejja using three different locations spread across the community. The data have been analysed, interpreted, and it has been discovered that the south-eastern part of the community, that is, Ejuona and perhaps Otobo Udunoka area is more promising in searching for concealed archaeological features.

Determination of the shape and size of the artefacts in Lejja was one of the objectives. The results presented have identified different types of artefacts in the community. These vary from blooms, iron smelting slag blocks, and fire pits at Ugbelenabo to small and large furnaces or mounds at Uwani and Ejuona sites of the Lejja archaeological site. Two different sizes of the furnace have been classified. The small size furnace which can be regarded as one-man business furnace with a diameter less than a metre was found in Uwani the central area of the community. The family business furnaces are relatively large, perhaps, between 1.2 and 1.5 metres in diameter and as high as about 1.5 metres. The latter was discovered in Ejuona, a village to the south-east of the community. This discovery confirms the suggestion raised by Ezike (1989) that some communities in Nsukka area might have used iron smelting as a family or community business in the prehistoric era.

At each point during the data interpretation, record of the magnetisation contrast between the archaeological features and the host soils were kept. In places that this was discovered to be very high, it was believed that the smelting activity was either prolonged at that location or the intensity of the heat was very high. Such heating effect would have generated substantial induced magnetisation in the surrounding soils whereby it may be difficult to precisely determine the diameter of the furnace since the fired soils will also contribute to the measured magnetic field at that location. The results have also confirmed that some slag blocks were mapped. This further strengthens the belief (Eze-Uzomaka, 2009) that some of the blocks were left in place after the smelting. The closer ones to the in situ furnace reveal that the slag blocks were also used as seats during and after the smelting business.

Determination of the depth to the top of the artefacts was a very serious business throughout the period of interpretation. The reason for this is that it is more difficult to obtain a reliable depth solution than to obtain the plan location of the concealed artefacts. Both the Euler deconvolution and the analytic signal methods were deployed. The Euler method is more consistent in obtaining accurate depth solutions than the analytic signal method (Thompson, 1982; Nabighian, 1984; Reid *et al*., 1990; MacLeod *et al*., 1993). In any case, the depth results obtained at most of the locations correlated well enough to permit using their mean values to represent the depth to the sources of interest. It has been discovered that most of the artefacts in the eastern part of the community, around Uwani and Ejuona villages, are buried at greater depths than those at western side, particularly far from the western dry valley. They are mostly found at depths between one and about two metres at the east while in the west, specifically at Ugbelenabo in the south-west of the community, almost all the anomalies have been found at shallow depths mostly under one metre. The reason for these can be traced to the fact that modern developments in the area (farming inclusive) has exposed the soils at the drainage channel to the west of the Nsukka dry valley to seasonal water erosion (Ofomata, 1978a). Such activity is capable of reducing the depths at which the artefacts are found. On the other hand, there are more residual hills to the east and the concealed artefacts at the foot of the hills get more deeply buried as the time rolls by.

Horizontal location of the archaeological features was one of the main objectives of the study. It has been achieved using the two methods. The applications of both the Euler deconvolution and the analytic signal methods yielded good and reliable results. The analytic signal method in particular was not only used to locate the centre of the causative sources but also used for delineation of boundaries. Source boundary maps have been produced that clearly show the plan boundaries of the artefacts at the three locations that were investigated in Lejja archaeological site. These maps can serve as guides to prospective workers in the archaeological site.

The effectiveness of the magnetic method in detecting and delineating shallow features which are of archaeological origin has been tested and found to be highly dependable. The integrated approach used was based on direct transformations, the Euler equation and analytic signal calculations. Where it was necessary to enhance the quality of the results through filtering, the appropriate filters were applied. These filters include spline smooth filter and upward continuation process. Some precautions were taken to achieve the optimal results. Among these are: (i) gridding of the field which was properly done before commencing data acquisition so as to have uniform distribution of the data (Clark, 1990), (ii) direct measurements of the vertical gradient since both low level noise and poor data quality in the original total field data can be amplified when gradients are calculated (Reid *et al*, 1990) and (iii) validation of the two methods of interpretation using synthetic field, etc.

6.3 SUGGESTIONS FOR FURTHER WORK

In the course of this study, three new research ideas were tumbled into. These include (i) Polynomial fitting method for diurnal correction (Ogah et al., 2012), (ii) A single step approach in magnetic data reduction, and (iii) Upward continuation as a means of quantifying sources of magnetic fields. The first of the three was extensively utilised during the archaeological magnetic data reduction. It was found to be very effective and is hereby recommended to researchers in near-surface geophysics who are interested in detailed surveys using magnetic and microgravity methods to test-run the method and compare with the existing method of diurnal correction.

The second method, titled ARMAD (Automatic Reduction of Magnetic Data) method, was compared with the conventional method of data reduction which usually involves correcting magnetic field data for diurnal effect to be later followed by regional residual separation. The second step of this conventional method involves the use of International Geomagnetic Reference Field (IGRF) data from observatories that may be located far from one's survey area. For a very detailed survey using data spacing as small as 25 or 50 centimetres, the calculation of such values per data point using latitude-longitude coordinates may introduce appreciable amount of errors into the data. The best datum to reduce archaeological magnetic data to is that which is within the small survey area. It is, therefore, recommended that the one step approach (the ARMAD) be experimented and used to replace the conventional method of data reduction, at least, for advantages of accuracy and reduction in computation time.

The relationship between height of continuation of potential field and depth of the causative body envisaged and experimented in the course of this study using synthetic

examples should have a good follow up research to explore its viability. The method could be very useful in quantifying subsurface magnetic or other geologic structures in combination with other depth determining techniques such Euler deconvolution or analytic signal methods if found to be reliable.

The initial intension of this study was to integrate the magnetic method with the ground penetrating radar (GPR) method in the archaeological site. That good intension failed for two main reasons: (i) Neither Ahmadu Bello University, Zaria nor Kogi State University, Anyigba has the GPR machine and we had nowhere else to borrow it. (ii) the fund available for this research was not enough to hire the machine from larger organisations where it may be available. It is therefore recommended that the GPR data be acquired from the same locations and interpreted to compare with the results obtained with the two methods of interpretation used in the present study.

An excavation plan has been documented for any archaeologist who may be interested in the study area. This will be made available and free supervision of the excavation shall be provided by the archaeologist who can get permission from the land owners to carry out excavation. At this point, we are recommending that archaeologists in Nigeria should now attempt to use this method or other archaeo-geophysical methods in Lejja and other archaeological sites in Nigeria.

R E F E R E N C E S

Abou, S. S., and Abdel, F.T. (2007). Archaeological applications of magnetic and electrical resistivity methods, south of Maryut lake – Alexandria, Egypt. *African Journal of Science and Technology (AJST), science and engineering series*, **8**: 72– 80.

An, Y., Huang, J., and Chen, Y. (2004). Forward computation of the magnetic field of a 3D body with arbitrary boundary and continually varying magnetisation. *Geophysical Prospecting*, **52**: 49 – 63.

Anozie, F.N. (1979). Early iron technology in Igbo-land (Lejja and Umundu). *West African Journal of Archaeology*, **9:** 119 – 134.

Ansari, A.H. and Alamdar, K. (2009). Reduction to the pole of magnetic anomalies using analytic signal. *World Applied Sciences Journal*, **7**: 405 – 409.

Aster, R.C., Borchers, B. and Thurber, C.H. (2005). *Parameter Estimation and Inverse Problems* (International geophysics series). Vol. 90, Academic press, Elsevier. 301 pp.

Atchuta Rao D., Ram-Babu, H.V., and Sanker Narayan, P.V. (1981). Interpretation of magnetic anomalies due to dikes: The complex gradient method. *Geophysics*, **46**: 1572 – 1578.

Babu, R.V., Achuta, R.D., Sanker, N.P.V., and Ratnam, C. (1982). Aeromagnetic survey over parts of Mahanadi basin and the adjoining offshore region, Orissa, India. *Geophysical Research bull*. **20**: 219-226.

Bhatttacharyya, B.K. (1964). Magnetic anomalies due to prism-shaped bodies with arbitrary polarization. *Geophysics*, **29**: 517 – 531.

Bhattacharyya, B. K., and Navolio, M. E. (1975). Digital convolution for computing gravity and magnetic anomalies due to arbitrary bodies. *Geophysics,* **40**: 981 – 992.

Blakely, R.J. (1996) *Potential Theory in Gravity and Magnetic Applications*, Cambridge University Press, Cambridge. 441 pp.

Binford, L.R. (1972). Archaeological Perspective. In: Binford, S.R. and Binford, L.W. (Ed) New Perspective in Archaeology, Aldine Publishing Co., USA, pp. 5 – 30.

Blatt, F.J. (1992) *Modern Physics*, McGraw-Hill, inc, 517 pp.

Breiner, S. (1999) *Application Manuals for Geometrics Portable Magnetometers,* Geometrics, San Jose, Carlifonia. 58 pp.

Cady, J.W. (1980). Calculation of gravity and magnetic anomalies of finite-length right polygonal prisms. *Geophysics,* **45**: 1507 – 1512.

Campbell, W.C. (1997) *Introduction to Geomagnetic Fields*, Cambridge University Press, Cambridge, 290 pp.

Clark, A. (1990) *Seeing Beneath the Soil: Prospecting Methods in Archaeology.* London B. T. Batsford, 160 pp.

Crowther, J. and Barker, P. (1995). Magnetic susceptibility: Distinguishing Anthropogenic effects from the Natural. *Archaeological Prospection*, **2**: 207 – 215.

Dalan, R.A. and Banerjee, S.K. (1996). Soil magnetism, an approach for examining archaeological landscapes. *Geophysical Research Letters*. **23**: 185 – 188.

Davis, J. C. (1973) *Statistics and Data Analysis in Geology*. John Wiley, New York, 550 pp.

Dawi, M.G., Tiagyou, L., Hui, S., and Dapeng, L. (2004). Depth estimate of 2-D magnetic anomaly sources by using Euler deconvolution method. *American Journal of Applied Sciences*, **1**: 209 – 214.

Debeglia, N. and Corpel, J. (1997). Automatic 3-D interpretation of potential field data using analytic signal derivatives. *Geophysics*, **62**: 87 – 96.

Dobrin, M. B. (1976) *Introduction to Geophysical Prospecting*, (3rd ed) McGraw-Hill Book Co, 630 pp.

Dobrin, M.B., and Savit, C.H. (1988). *Introduction to Geophysical Prospecting,* (4th Ed) McGraw-Hill, New York, 867 pp.

Elawadi, E. A. and Ismail, A. A. (2011). Aeromagnetic imaging of Wadi Natash volcanics, South Eastern Desert, Egypt. Internet page.

Eze-Uzomaka, P.I. (2006) Lejja iron smelting site: A proposal for excavation made to the African Archaeology Network, Kampala, 2006.

Eze-Uzomaka, P.I. (1996). Archaeological Communication in the Nsukka Area. Unpublished M.A. Thesis. University of Nigeria, Nsukka, Nigeria.

Eze-Uzomaka, P.I. (2009). Iron age archaeology in Lejja, Nigeria. *Dimensions of African Archaeology: Studies in the African Past*, **7**: 41-51.

Ezike, J.N. (1989). Traditional iron smelting and blacksmithing in Aku. Unpublished M.A. Thesis, University of Nigeria, Nsukka, Nigeria.

Foss, C. and McKenzie, K.B. (2009). Strategies to model a suite of remanent magnetisation anomalies. Paper Presented at the Austrian Socienty of Exploration Geophysicists (ASEG) Conference held at Adelaide, Februry 2006.

Frost, B.R., and Shive, P.N. (1986). Magnetic mineralogy of the lower continental crust. *Journal of Geophysical Research*, **91**: 6513 – 6521.

Godio, A., and Torino, P. (2005). Integrated data processing for archaeological magnetic surveys. *The Leading Edge*, **24**: 1138 – 1144.

Golub, G.H. and Loan, C.F.V. (1996). *Matrix Computations* (3rd edition), The Johns Hopkins University Press, 694 pp.

Grant, F.S. and Dodds, J. (1972). MAGMAP FFT processing system development notes, Paterson Grant and Watson Limited, 230 pp.

Hansen, R.O. and Pawlowski, R.S. (1989). Reduction to the pole at low latitutes by Wiener filtering. *Geophysics*, **54**: 1607 – 1613.

Hartle, D. D. (1975). *Archaeology in Nsukka area*. In: Ofomata, G. E. K. (Ed) Nsukka environment, Fourth Dimension Publishers, Enugu, Nigeria, pp. 8 – 23.

Henderson, R. G. (1970). On the validity of the use of the upward continuation integral for total magnetic intensity data. *Geophysics*, **35**: 916 – 919.

Hoylman, H. W. (1961). How to determine and remove diurnal effects precisely. *World Oil*, December, 107 – 112.

Hsu, S-K. (2002). Imaging magnetic sources using Euler's equation. *Geophysical Prospecting*, **50**: 15 – 25.

Hsu, S-K., Coppens, D. and Shyu, C. (1998). Depth to magnetic source using the generalized analytic signal. *Geophysics*, **63**: 1947 – 1957.

Hsu, S-K., Sibuet, J.C. and Shyu, C.T. (1996). High-resolution detection of geologic boundaries from potential-field anomalies: An enhanced analytic signal technique. *Geophysics*, **61**: 373 – 386.

Igbozurike, U. M. (1978). *The tourist resources of Nsukka Environment*. In: Ofomata, G. E. K. (Ed) The Nsukka Environment, Fourth Dimension Publishers, Enugu, Nigeria, pp. 470 – 478.

Jackson, J.D. (1975) *Classical Electrodynamics* (2nd edition), John Wiley and Sons, Inc, 848 pp.

Jacobsen, B. (1987). A case for upward continuation as a standard separation filter for potential-field maps. *Geophysics*, **52**: 1138 – 1148.

Johnson, W.J. (2003). Geophysical detection of graves – basic background and case histories from historic cemetries, Present at the Council for West Virginia Archaeology Spring Workshop, Charleston, West Virginia, 2003.

Kearey, P., Brooks, M., and Hill, I. (2002*). An Introduction to Geophysical Exploration.* (2nd edition), Blackwell Publishing Company, USA, 272 pp.

Keating, P. and Pilkington, M. (2004). Euler deconvolution of the analytic signal and its application to magnetic interpretation. *Geophysical Prospecting*, **52**: 165 – 182.

Kostrov, N. P. (2007). Calculation of magnetic anomalies caused by 2D bodies of arbitrary shape with consideration of demagnetisation. *Geophysical Prospecting*, **55**: 91 – 115.

Kunaratnam, K. (1981). Simplified expressions for the magnetic anomalies due to vertical rectangular prisms. *Geophysical Prospecting*, **29**: 883 – 890.

Lawal, K. M. and Osazuwa, I. B. (2004). Reduction to the pole of the aeromagnetic data of Zaria area, north central Nigeria. *Bollettino di Geofisica Teorica ed Applicata*, **45**: 89 – 95.
Lawal, K. M. and Osazuwa, I. B. (2007). A stabilization procedure for the transformation of magnetic data. *Ife Journal of Science*, **9**: 19 – 28.

Li, Y. and Oldenburg, D. W. (1998). Separation of regional and residual magnetic field data. *Geophysics*, **63**: 431 – 439.

Loke, M. H., and Barker, R. D. (1996). Rapid least squares inversion of apparent resistivity pseudo-sections by quasi-Newtonian method. *Geophysical Prospecting*, **44**: 131 – 152.

Lowrie, W. (1997) *Fundamentals of Geophysics*, Cambridge University Press, Cambridge, 392 pp.

MacLeod, I.N., Jones, K. and Dal, T.F. (1993). 3-D analytic signal in the interpretation of total magnetic field data at low magnetic latitudes. *Exploration Geophysics*, **24**: 679 – 688.

Maher, B.A. (1986). Characterisation of soils by mineral magnetic measurements. *Physics of the earth and planetary interiors*, **42**: 76 – 92.

Martino, L., Bonomo, N., Lascano, E., Osella, A., and Ratto, N. (2006). Electrical and GPR prospecting at Palo Blanco archaeological site, north-western Argentina. *Geophysics*, **71**: B193 – B199.

McElhinny, M.N. (1973) *Paleomagnetics and Plate Technonics*, Cambridge University Press, Cambridge, 357 pp.

Menke, W. (1989) *Geophysical Data Analysis: Discrete Inverse Problems (International Geophysics Series)*, Vol. 45, Academic Press, Elsevier, 289 pp.

Montgomery, D. C. and Peck, E. A. (1992). *Introduction to Linear Regression Analysis* (4th Ed) John Wiley and Sons, New York, 527 pp.

Mooketsi, C.O. (2009). Archaeological surveys in the Shashe-limpopo basin, eastern Botswana: A preliminary report. *Dimensions of African Archaeology*, **7**: 8 - 18.

Nabighian, M. N. (1972). The analytic sigal of two-dimensional magnetic bodies with polygonal cross-section: its properties and use for automatic anomaly interpretation. *Geophysics*, **37**: 507 – 517.

Nabighian, M. N. (1974). Additional comments on the analytic signal of two dimensional magnetic bodies with polygonal cross-section. *Geophysics*, **39**: 85 - 92.

Nabighian, M. N. (1984). Towards a three-dimensional automatic interpretation of potential field data via generalized Hilbert transforms – Fundamental relations. *Geophysics*, **49**: 780 – 786.

Nabighian, M.N., Grauch, V.J.S., Hansen, R.O., Lafehr, T.R., Li, Y., Peirce, J.W., Phillips, J.D., and Ruder, M.E. (2005). The historical development of the magnetic method in exploration. *Geophysics*, **70**: 33ND – 61ND.

Namunaba, I.B. (2009). Food residue analysis on prehistoric pottery from Kaya Bate site on the coastal hinterland of Kenya: New methodological applications in the Region. *Dimensions of African Archaeology*, **7**: 66 – 78.

Nettleton, L.L. (1976) *Gravity and Magnetic in Oil Prospecting*, McGraw-Hill Inc., USA, 464 pp.

Niku, O. R., and Smekalova, T. (2002). Archaeological survey and non-visible monument – the use of magnetic prospecting in outfield archaeology. *Internet page.*

Nwachukwu, S.O. (1978). The geology of Nsukka area. In Ofomata, G.E.K. (ed) The Nsukka environment. Fourth Dimension Publishers Co. Ltd, Enugu, PP. 47 – 58.

Ofomata, G. E. K. (1978). *Landforms*. In: Ofomata, G. E. K. (Ed) The Nsukka Environment, Fourth Dimension Publishers, Co. Ltd, Enugu, PP. 69 – 85.

Ofomata, G. E. K. (1978a). *Relief and Drainage*. In: Ofomata, G. E. K. (Ed) The Nsukka Environment, Fourth Dimension Publishers, Enugu, PP. 59 – 68.

Ojo, S. B., and Kangkolo, R. (1997). Shortcomings in the determination of regional fields by polynomial fitting: A simple solution. *Applied Geophysics*, **36**: 205 – 212.

Okafor, E. E. (1993). *New evidence on early iron smelting from south-eastern Nigeria*. In: Shaw T.; Sinclair P.; Andah B.; and Okoko A. (eds). The Archaeology of Africa: Food, Metals and Towns. Routledge: London, 432 – 448.

Oldfield, F., Thompson, R., and Dickson, D.P.E. (1981). Artificial enhancement of stream bed-load: A hydrogeological application of superparamagnetism. *Physics of the earth and planetary interiors*, **26**: 107 – 124.

Osella, A., de la Vega, M., and Lascano, E. (2005). 3D electrical imaging of an archaeological site using electrical and electromagnetic methods. *Geophysics*, **70**: G101 – G107.

Peddie, N.W. (1983). International geomagnetic reference field: its evolution and the difference in total field intensity between new and old models for 1965 – 1980. *Geophysics*, **48**: 1691 – 1696.

Piro, S., Sambuelle, L, Godio, A., and Taormina, R. (2007). Beyond image analysis in processing archaeomagnetic geophysical data: Case studies of chamber tombs with dromos. *Near-Surface Geophysics*, 405 – 414.

Piro, S., Samir, A., and Versino, L. (1998). Position and spatial orientation of magnetic bodies from archaeological magnetic surveys. *Annali di Geofisica*, **41**: 343 – 358.

Press, W.H., Teukolsky, S., Vetterling, W.T. and Flannery, B.P. (1992). *Numerical recipees in FORTRAN, the art of scientific computing*. (2nd edition), Cambridge University Press, Cambridge, 1256 pp.

Rao, D.B., and Babu, N. R. (1991). A rapid method for three-dimensional modelling of magnetic anomalies. *Geophysics*, **56**: 1729 – 1737.

Reid, A.B., Allsop, J.M., Granser, H., Millett, A.J. and Somerton, I.W. (1990). Magnetic interpretation in three dimensions using Euler deconvolution, *Geophysics*, **55**: 80 – 91.

Rietz, J.R., Milford, F.J. and Christy, R.W. (1979). *Foundations of Electromagnetic Theory*. (3rd edition), Addison – Wesley Publishing Company, 534 pp.

Roest, W. R., Verhoef, J. and Pilkington, M. (1992). Magnetic interpretation using the 3-D analytic signal. *Geophysics*, **57**: 116 – 125.

Roy, K.K. (2008) *Potential theory in applied geophysics*, Springer, Berlin, 651 pp.

Sadiku, M.N.O. (1989) *Elements of electromagnetics*, Sauders College Publishing, 788 pp.

Salem, A. (2005). Interpretation of magnetic data using analytic signal derivatives. *Geophysical Prospecting*, **53**: 75 – 82.

Schmidt, A. (2007). Archaeology magnetic methods. Encyclopedia of Geomagnetism and Paleomagnetism: 23–31, Encyclopedia of earth science series, Heidelberg, New York: Springer, 16 pp.

Scollar, I., Weidner, B. and Segeth, K. (1986). Display of archaeological magnetic data. *Geophysics*, **51**: 623 – 633.

Silva, J.C.B. (1986). Reduction to the pole as an inverse problem and its application to low latitude anomalies. *Geophysics*, **51**: 369 – 382.

Syberg, F.J.R. (1972). A Fourier method for the regional-residual problem of potential fields. *Geophysical Prospecting*, **20**: 267 – 282.

Talwani, M. (1965). Computation with the help of a digital computer of magnetic anomalies caused by bodies of arbitrary shape. *Geophysics*, **30**: 797 – 817.

Telford, W.M., Geldart, L.P., and Sheriff, R.E. (1976). *Applied Geophysics*, (first edition), Cambridge University Press, Cambridge, 860 pp.

Telford, W.M., Geldart, L.P. and Sheriff, R.E. (1990). *Applied Geophysics*, (2nd edition), Cambridge University Press, Cambridge, 792 pp.

Thompson, D.T. (1982). EULDPH: A new technique for making computer – assisted depth estimate from magnetic data. *Geophysics*, **47**: 31 – 37.

Thompson, R. and Oldfield, F. (1986). *Environmental magnetism*. London: Allen and Unwin, 227 pp.

Tsokas, G.N., and Papazachos, C.B. (1992). Two-dimensional inversion filters in magnetic prospecting : Application to the exploration for buried antiquities. *Geophysics*, **57**: 1004–1013.

Tsokas, G.N., and Tsourlos, P (1997). Transformation of the resistivity anomalies from archaeological sites by inversion filtering. *Geophysics*, **62**: 36 – 43.

Vallee, M.A., Keating, P., Smith, R.S. and St-Hilaire, C. (2004). Estimating depth and model type using the continuous wavelet transform of magnetic data. *Geophysics*, **69**: 191 – 199.

Veldhuijzen, H.A. and Rehren, T. 2007. Slags and the City. Early Iron Production at Tell Hammeh, Jordan, and Tel Beth-Shemesh, Israel. Internet page, 03-04-2012.

Wijns, C., Perez, C., and Kowalczyk, P. (2005). Theta map: Edge detection in magnetic data (Short Note). *Geophysics*, **70**: L39 – L43.

A P P E N D I X C

COMPUTER PROGRAMS

C.1 Synthetic Data Generator

```
                                program synthetic
c
c   Program computes synthetic magnetic data for archaeological geophysics
c   The initial parameters, declination d and inclination i of the geomagnetic
c   field and those of magnetization vector are first read in.
c   To be read in also are intensity of magnetization, ei and angle thita.
c
      dimension x(40,60),y(40,60),xp(40,60),yp(40,60),T(40,60)
c
      open(unit=5,file='inp5.txt',status='old')
      open(unit=1,file='inp1.txt',status='old')
      open(unit=2,file='inp2.txt',status='old')
      open(unit=6,file='out6.txt',status='old')
c
c   Read in values of the earth and the model parameters
c   tm=intensity of magnetization of the source, ti= angle thita
c
     read(5,*)dec,cin,demv,cimv
c
      do 500 i=1,40
      do 450 j=1,60
      T(i,j)=0.0
450   continue
500   continue
c
      do 250 n=1,2
      model=n
      if(model.gt.1)go to 20
      read(1,*)a1,a2,b1,b2,h1,h2,tm,ti
      go to 40
20    read(2,*)a1,a2,b1,b2,h1,h2,tm,ti
40    der=(dec/180.0)*(22.0/7.0)
      cir=(cin/180.0)*(22.0/7.0)
      demr=(demv/180.0)*(22.0/7.0)
      cimr=(cimv/180.0)*(22.0/7.0)
      tr=(ti/180.0)*(22.0/7.0)
c
c7    format(f4.1,1x,f5.1,1x,f4.1,1x,f5.1)
c8    format(f5.2,1x,f5.2,1x,f5.2,1x,f5.2,f4.2,1x,f4.2,1x,f5.1,1x,f4.1)
c
```

```
c      calculate direction consines for geomagnetic field
c
       dmt=der-tr
       p=(cos(cir))*(cos(dmt))
       q=(cos(cir))*(sin(dmt))
       r=sin(cir)
c
c      dl,dm and dn are direction consines of magnetization vector
c
       dmvmt=demr-tr
       dl=cos(cimr)*cos(dmvmt)
       dm=cos(cimr)*sin(dmvmt)
       dn=sin(cimr)
c
c      The constants G1,G2,....,G5 can now be computed
c
       g1=tm*((dm*r)+(dn*q))
       g2=tm*((dl*r)+(dn*p))
       g3=tm*((dl*q)+(dm*p))
       g4=tm*((dn*r)-(dm*q))
       g5=tm*((dn*r)-(dl*p))
c
c      To obtain grid values x and y, and then calculate values x' and y'
c
        do 100 ii=1,40
        do 50 jj=1,60
        y(ii,jj)=float(ii)
        x(ii,jj)=float(jj)
        yp(ii,jj)=(-x(ii,jj)*sin(tr))+(y(ii,jj)*cos(tr))
        xp(ii,jj)=(x(ii,jj)*cos(tr))+(y(ii,jj)*sin(tr))
50     continue
100    continue
c
c      The program now computes alpha, beta and distance of the source,
r,from       the  meter
c      and the functions f1 to f5 and use these values to compute the field.
c
       do 200 i=1,40
       do 150 j=1,60
       al1=a1-xp(i,j)
       al2=a2-xp(i,j)
       be1=b1-yp(i,j)
       be2=b2-yp(i,j)
       r1=sqrt((al1**2)+(be1**2)+(h1**2))
       r2=sqrt((al1**2)+(be1**2)+(h2**2))
       r3=sqrt((al2**2)+(be1**2)+(h1**2))
```

```
      r4=sqrt((al2**2)+(be1**2)+(h2**2))
      r5=sqrt((al1**2)+(be2**2)+(h1**2))
      r6=sqrt((al1**2)+(be2**2)+(h2**2))
      r7=sqrt((al2**2)+(be2**2)+(h1**2))
        r8=sqrt((al2**2)+(be2**2)+(h2**2))
       fn1=(r2+al1)*(r3+al2)*(r5+al1)*(r8+al2)
       fd1=(r1+al1)*(r4+al2)*(r6+al1)*(r7+al2)
       f1=fn1/fd1
       fn2=(r2+be1)*(r3+be1)*(r5+be2)*(r8+be2)
       fd2=(r1+be1)*(r4+be1)*(r6+be2)*(r7+be2)
       f2=fn2/fd2
       fn3=(r2+h2)*(r3+h1)*(r5+h1)*(r8+h2)
       fd3=(r1+h1)*(r4+h2)*(r6+h2)*(r7+h1)
       f3=fn3/fd3
       f41=atan((al2*h2)/(r8*be2))-atan((al1*h2)/(r6*be2))
       f42=-atan((al2*h2)/(r4*be1))+atan((al1*h2)/(r2*be1))
       f43=-atan((al2*h1)/(r7*be2))+atan((al1*h1)/(r5*be2))
       f44=atan((al2*h1)/(r3*be1))-atan((al1*h1)/(r1*be1))
       f4=f41+f42+f43+f44
       f51=atan((be2*h2)/(r8*al2))-atan((be2*h2)/(r6*al1))
       f52=-atan((be1*h2)/(r4*al2))+atan((be1*h2)/(r2*al1))
       f53=-atan((be2*h1)/(r7*al2))+atan((be2*h1)/(r5*al1))
       f54=atan((be1*h1)/(r3*al2))-atan((be1*h1)/(r1*al1))
       f5=f51+f52+f53+f54
       st1=(g1*alog(f1))+(g2*alog(f2))+(g3*alog(f3))
       st2=(g4*f4)+(g5*f5)
       T(i,j)=T(i,j)+st1+st2+320
150   continue
200   continue
250   continue
c
      do 300 ll=1,40
      do 280 kk=1,60
      write(6,9)x(ll,kk),y(ll,kk),T(ll,kk)
9     format(f5.2,1x,f5.2,1x,f10.4)
280   continue
300   continue
      stop
      end
```

C.2 Diurnal Correction Program

```
                              program polyfdiurcor

dimension A(31,2),B(5,5),tp(5),C(5)
```

```
c
      open (unit=2,file='diurin.txt',status='old')
      open (unit=3,file='diurout.txt',status='old')
c
c     array A contains base station field and time dat. array B contains
c     the terms of the coeff. matrix. array C originally contains the
c     vector of teh RHS(t&fld). It contains b after the solution.
c
      nord=4
      nord1=nord+1
c
c     first zero the array A
c
        do 20 i=1,31
        do 10 j=1,2
        A(i,j)=0.0
   10   continue
   20   continue
c
c       reading base station data
c
       do 40 i=1,31
        read(2,*)(A(i,j),j=1,2)
   40   continue
c
c       calculate sums of the least-squares solutions
c
        do 60 i=1,nord1
        C(i)=0.00
        do 50 j=1,nord1
        B(i,j)=0.0
   50   continue
   60   continue
c
        do 100 i=1,31
        tp(1)=1.0
        do 70 j=2,nord1
        tp(j)=tp(j-1)*A(i,1)
   70   continue
        do 90 j=1,nord1
        do 80 k=1,nord1
        B(j,k)=B(j,k)+tp(j)*tp(k)
   80   continue
        C(j)=C(j)+tp(j)*A(i,2)
   90   continue
  100   continue
```

```
c
c          To tell sle sub to calculate the required coefficients
c
           zero=1.0e-06
c
           do 170 i=1,5
           div=B(i,i)
           do 130 j=1,5
           B(i,j)=B(i,j)/div
   130     continue
           C(i)=C(i)/div
           do 160 j=1,5
           if(i.eq.j)go to 160
   140     ratio=B(j,i)
           do 150 k=1,5
           B(j,k)=B(j,k)-ratio*B(i,k)
   150     continue
           C(j)=C(j)-ratio*C(i)
   160     continue
   170     continue
           do 110 i=1,5
           write(3,*)C(i)
   110     continue
           stop
           end
```

C.3 Euler deconvolution computer program

```
                PROGRAM EJULER
c
c       The program reads in data from the file made up of 40 rows and 60 columns (m x
n)
c       then form matrix of coefficients (G) and the column matrix (T)
c
        dimension Dx(40,60),Dy(40,60),Dz(40,60),DelT(40,60)
        dimension GT(25,25),x(40,60),y(40,60),G(25,25)
        dimension SM(3,3),RHS(25),SRH(25),RH1(25,25),RH2(25,25)
c
        open (unit=1,file='grds.txt',status='old')
        open (unit=2,file='dims.txt',status='old')
        open (unit=3,file='EjuEul-out.txt',status='old')
c
        read(2,*)nr,nc,np,mp,SI
        do 20 i=1,nr
        do 10 j=1,nc
        read(1,*)x(i,j),y(i,j),Dx(i,j),Dy(i,j),Dz(i,j),DelT(i,j)
```

```
   10   continue
   20   continue
c
        i1=1
        i2=5
   25   j1=1
        j2=5
   30   k=0
        do 50 i=i1,i2
        SRH(i)=0.
        do 40 j=j1,j2
        k=k+1
        G(k,1)=Dx(i,j)
        G(k,2)=Dy(i,j)
        G(k,3)=Dz(i,j)
        SRH(i)=(x(i,j)*Dx(i,j))+(y(i,j)*Dy(i,j))+
      +  (0.94*Dz(i,j))+(SI*DelT(i,j))

   40   continue
   50   continue
c
c       Creating an n x n matrix out of the n x m matrix G by first creating
c       the transpose of G and multiplying the G transpose GT by G
c
        do 54 i=1,25
        do 52 j=1,5
        GT(j,i)=G(i,j)
   52   continue
   54   continue
c
c       Matrix SM (a square)is a product of GT and G
c
        do 57 i=1,3
        RHS(i)=0.
        do 56 j=1,3
        SM(i,j)=0.
        do 55 k=1,25
        SM(i,j)=SM(i,j)+GT(i,k)*G(k,j)
        RHS(i)=RHS(i)+GT(i,k)*SRH(k)
   55   continue
   56   continue
   57   continue
c
        do 90 i=1,3
        div=SM(i,i)
        do 60 j=1,3
```

```
      SM(i,j)=SM(i,j)/div
   60 continue
      RHS(i)=RHS(i)/div
      do 80 j=1,3
      if(i-j)61,80,61
   61 ratio=SM(j,i)
      do 70 k=1,3
      SM(j,k)=SM(j,k)-ratio*SM(i,k)
   70 continue
      RHS(j)=RHS(j)-ratio*RHS(i)
   80 continue
   90 continue
c
      xo=RHS(1)
      yo=RHS(2)
      if((xo.lt.1.).or.(xo.gt.60))go to 100
      if((yo.lt.1.).or.(yo.gt.40))go to 100
c
      zo=RHS(3)
c
      if((zo.gt.0.).or.(zo.lt.-2.))go to 100
c
      write(3,*)xo,yo,zo
c
  100  j1=j1+1
      j2=j2+1
      if(j2.le.60)go to 30
      i1=i1+1
      i2=i2+1
      if(i2.le.40)go to 25
c
      stop
      end
```

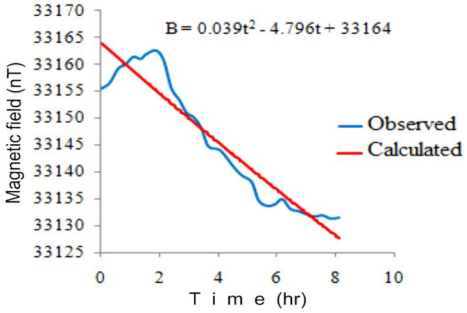
C.4 Program for averaging Euler solutions

```
                        Program AveragingEulSols
c
          Dimension x(9000),y(9000),h(9000),x1(80),x2(80),y1(80),y2(80)
c
      open (unit=1,file='Anocoord.txt',status='old')
      open (unit=2,file='EulSols.txt',status='old')
      open (unit=3,file='AvEul-out.txt',status='old')
c
      na=6
      ns=410
c
```

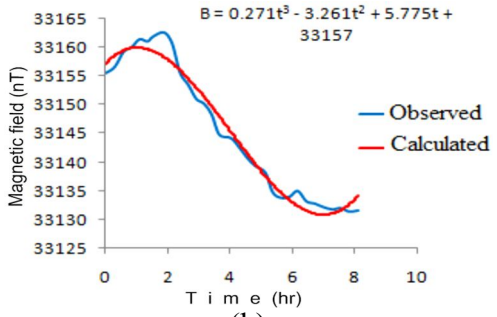
```
      do 50 j=1,ns
      read(2,*)x(j),y(j),h(j)
   50 continue
c
      do 70 i=1,na
      read(1,*)x1(i),x2(i),y1(i),y2(i)
      sumx=0.
      sumy=0.
      sumh=0.
      ncount=0
      do 60 j=1,ns
      if((x(j).lt.x1(i)).or.(x(j).gt.x2(i))) go to 60
      if((y(j).lt.y1(i)).or.(y(j).gt.y2(i))) go to 60
      ncount=ncount+1
      sumx=sumx+x(j)
      sumy=sumy+y(j)
      sumh=sumh+h(j)
   60 continue
c
      xav=sumx/ncount
      yav=sumy/ncount
      hav=sumh/ncount
      write(3,*)xav,yav,hav
   70 continue
      stop
       end
```

A P P E N D I X A

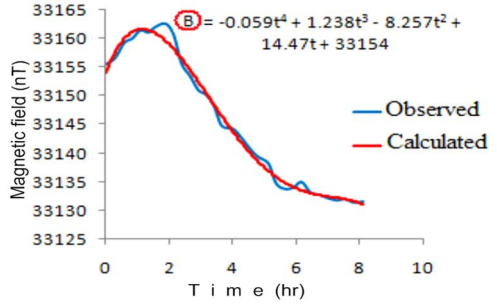
O T H E R F I G U R E S



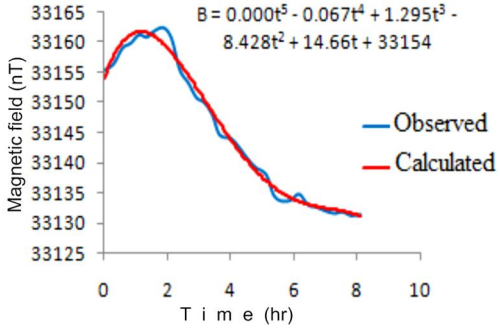
(a)



(b)

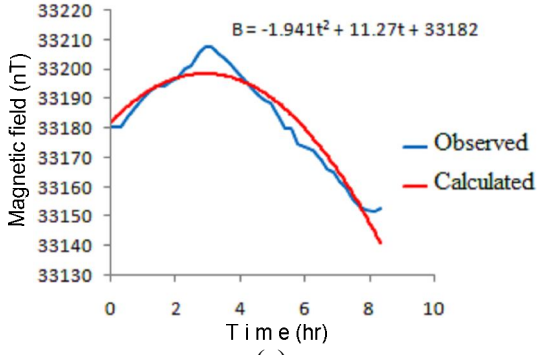


(c)

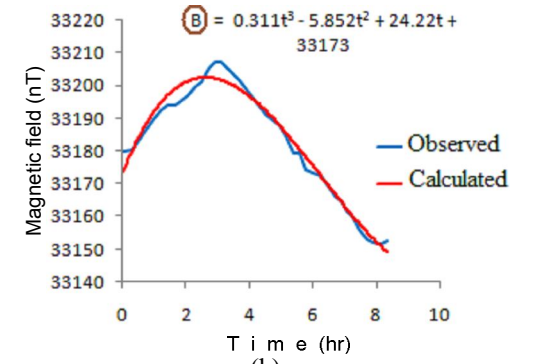


(d)

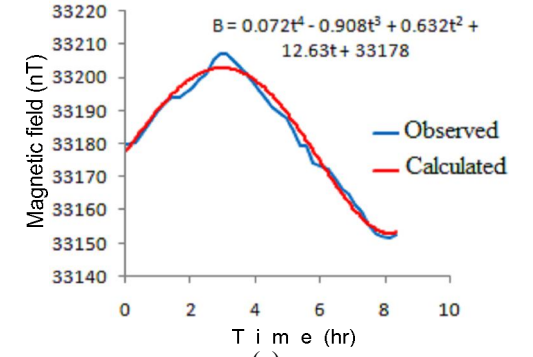
Fig. A.1: Polynomial fitting to Uwani base station data (day 2)
(a) 2nd order (b) 3rd order (c) 4th order (d) 5th order



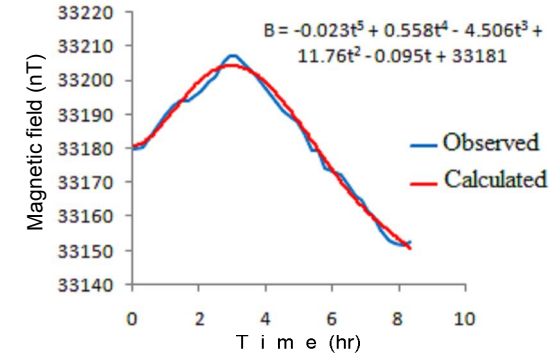
(a)



(b)

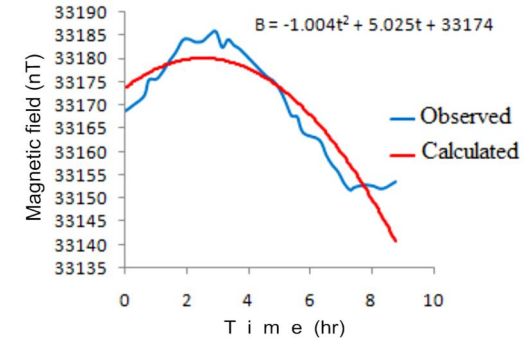


(c)

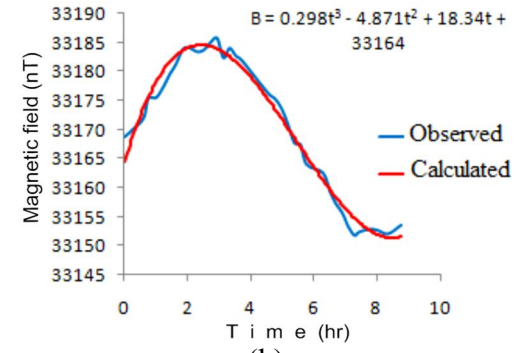


(d)

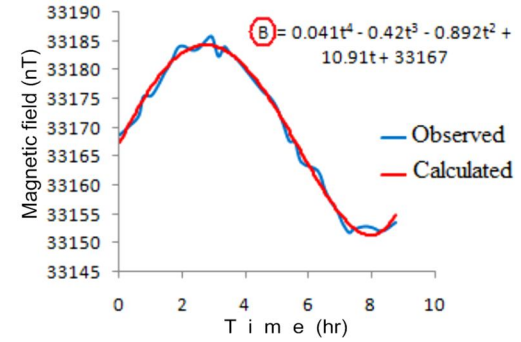
Fig. A.2: Polynomial fitting to Ugbelenabo base station data (day 1)
(a) 2nd order (b) 3rd order (c) 4th order (d) 5th order



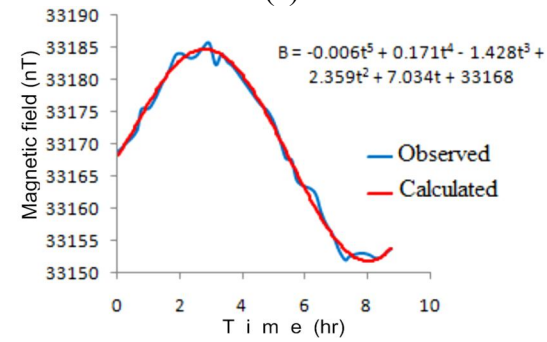
(a)



(b)

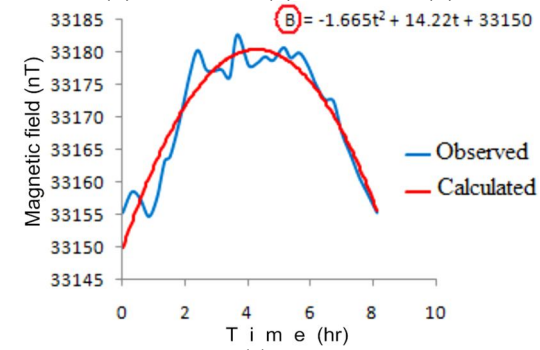


(c)

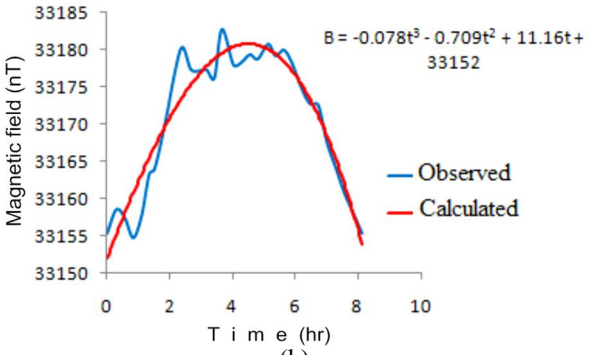


(d)

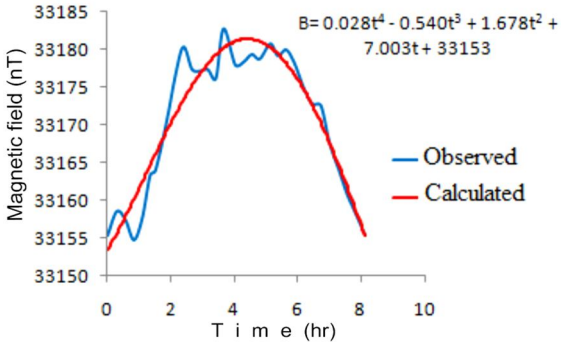
Fig. A.3: Polynomial fitting to Ugbelenabo base station data (day 2)
(a) 2nd order (b) 3rd order (c) 4th order (d) 5th order



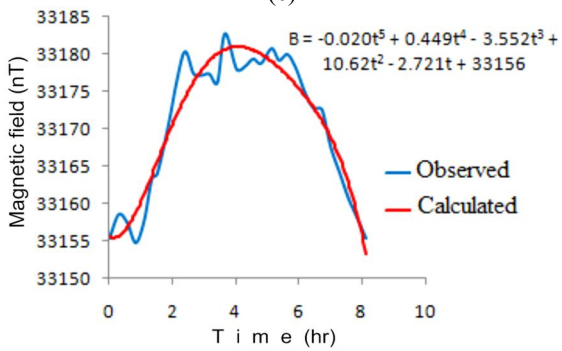
(a)



(b)

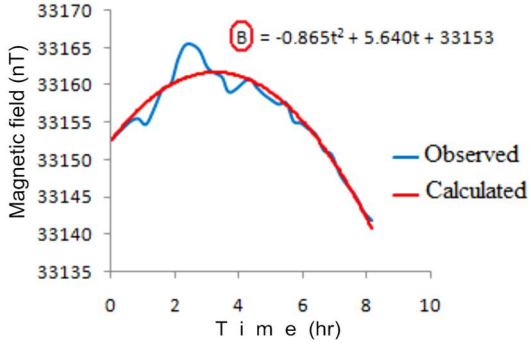


(c)

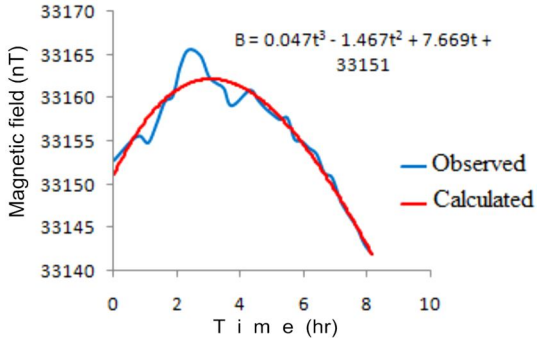


(d)

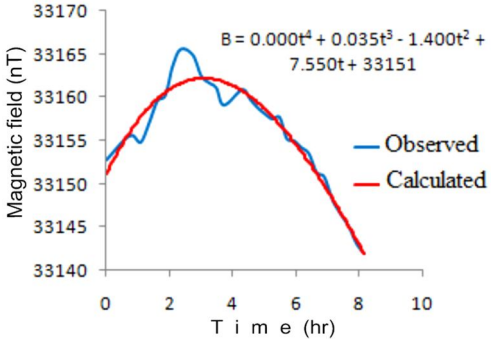
Fig. A.4: Polynomial fitting to Ejuona base station data (day 1)
(a) 2nd order (b) 3rd order (c) 4th order (d) 5th order



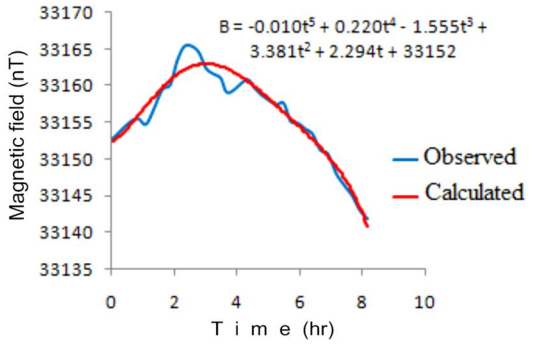
(a)



(b)

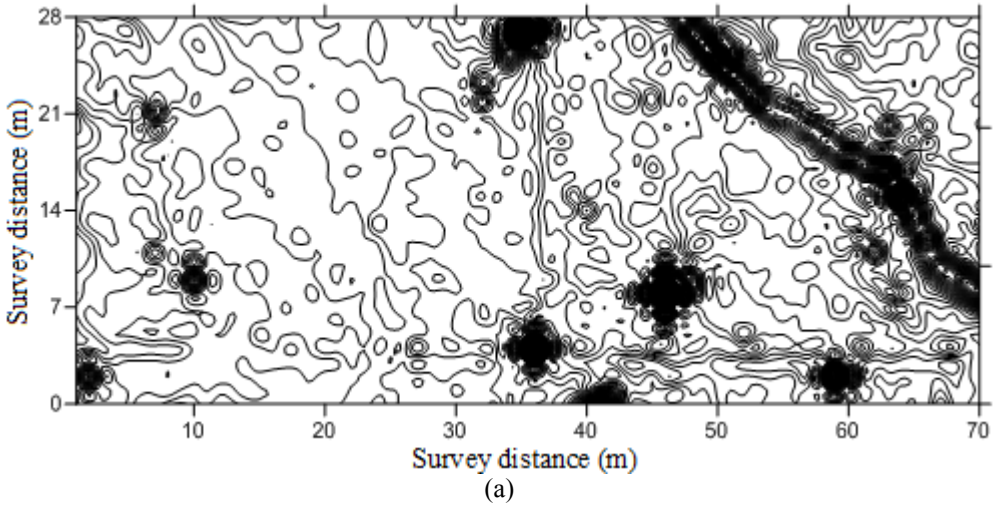


(c)

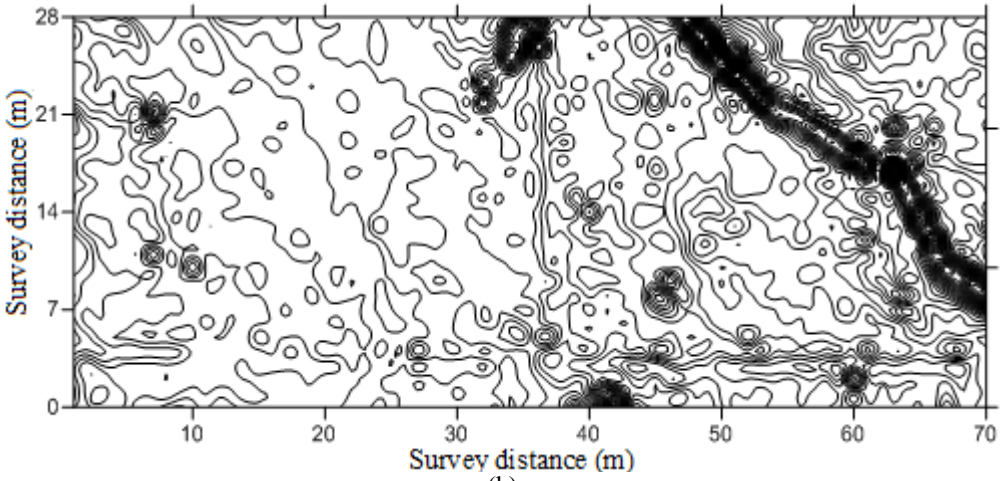


(d)

Fig. A.5: Polynomial fitting to Ejuona base station data (day 2)
(a) 2nd order (b) 3rd order (c) 4th order (d) 5th order

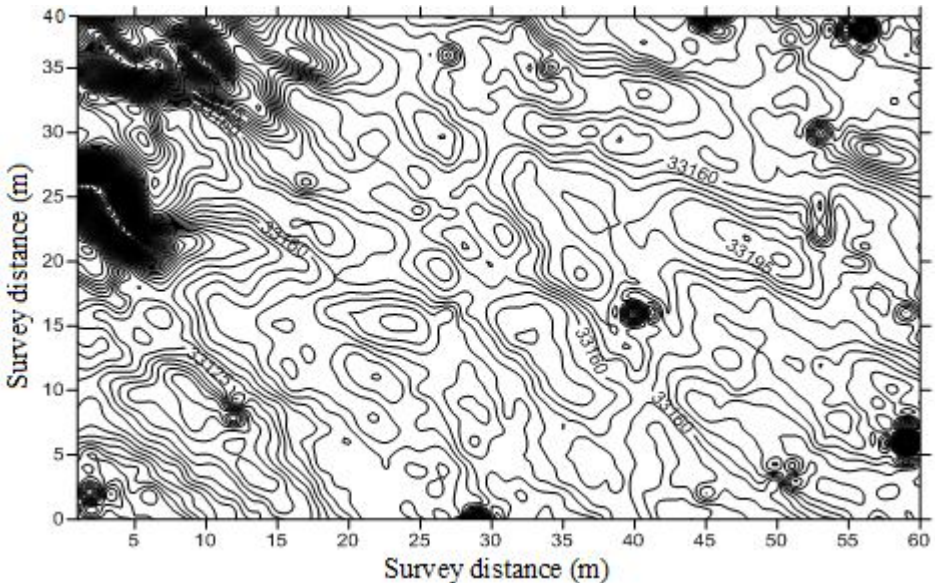


(a)

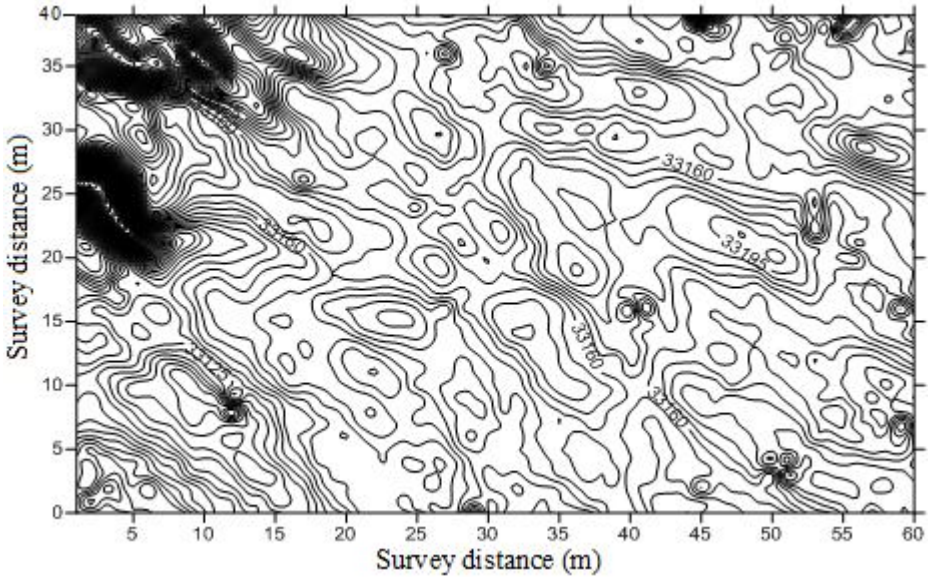


(b)

Fig. A.6: Effects of despiking on Ugbelenabo data
(a) Before despiking (b) After despiking

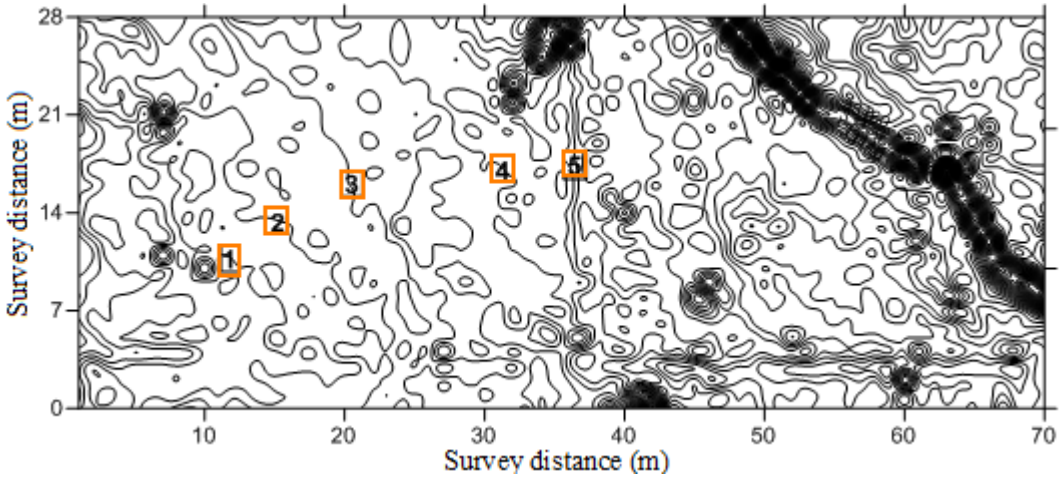


(a)

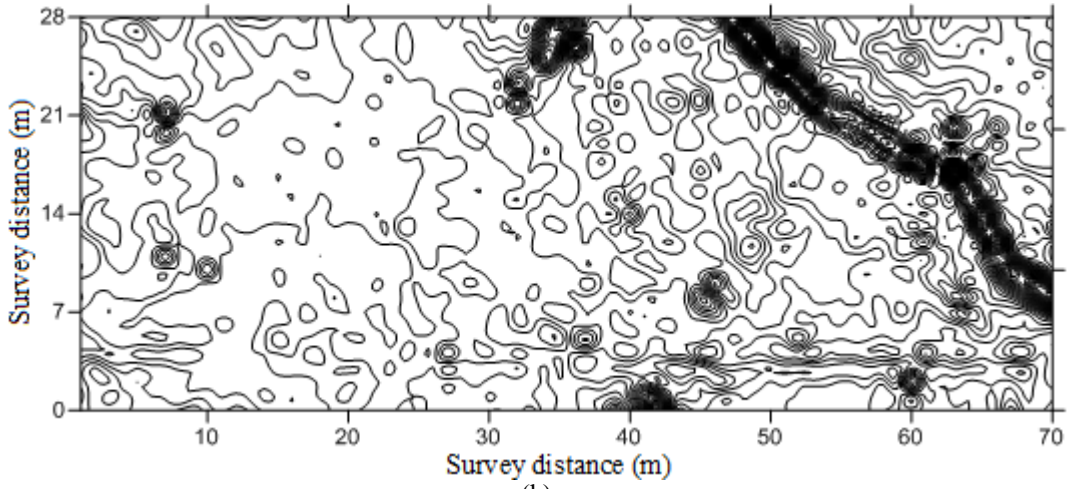


(b)

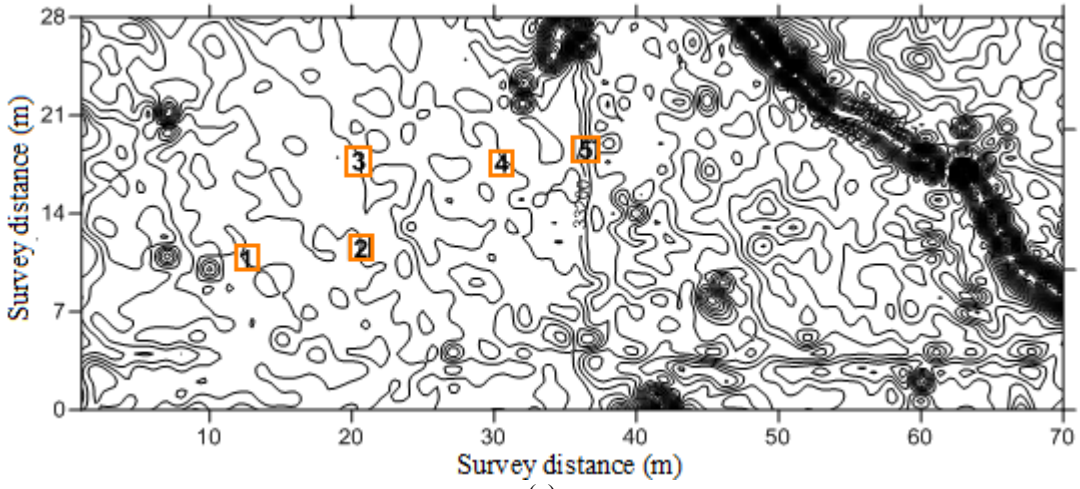
Fig. A.7: Effects of despiking on Ejuona data
(a) Before despiking (b) After despiking



(a)

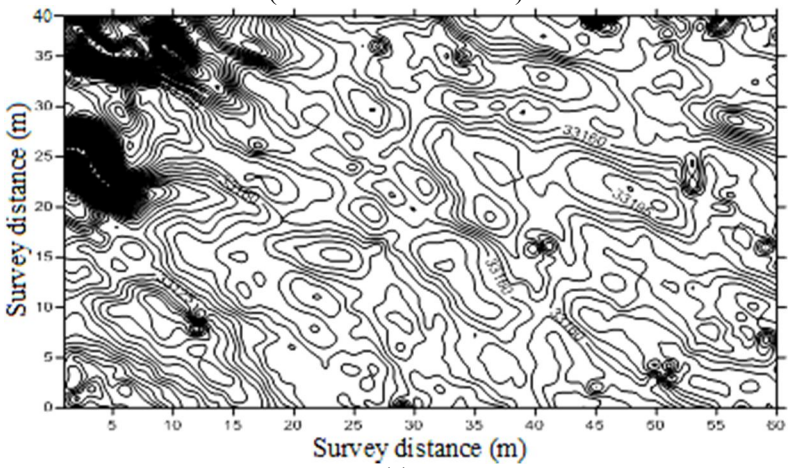


(b)

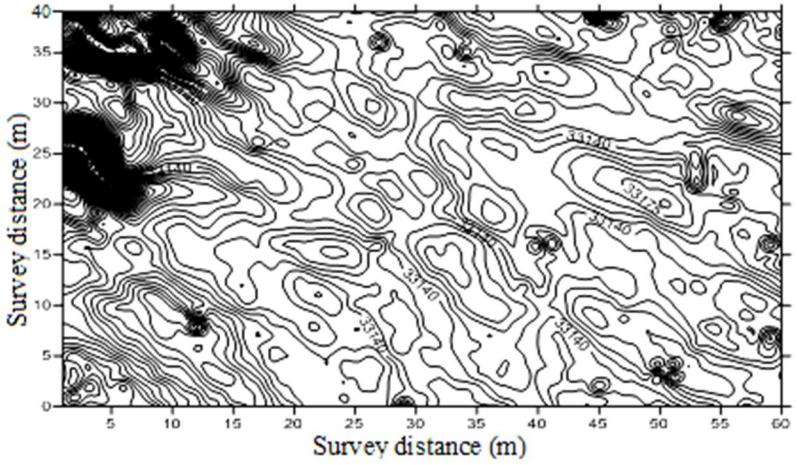


(c)

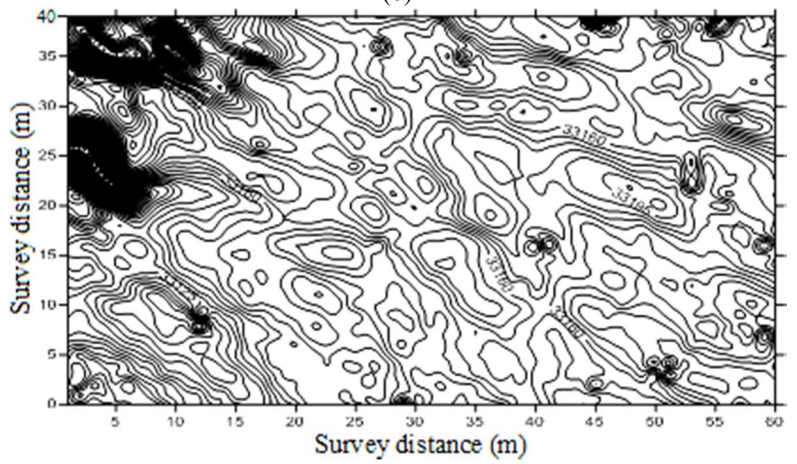
Fig. A.8: Effects of diurnal correction on Ugbelenabo data
(a) Without diurnal correction (b) Corrected using polynomial fitting method (c) Corrected using conventional method
(1 to 5 are noise levels)



(a)

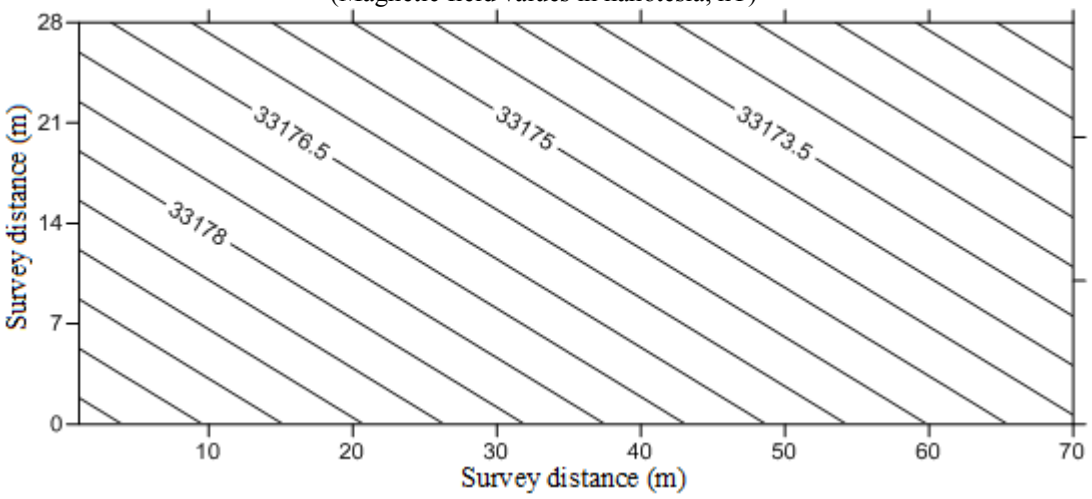


(b)

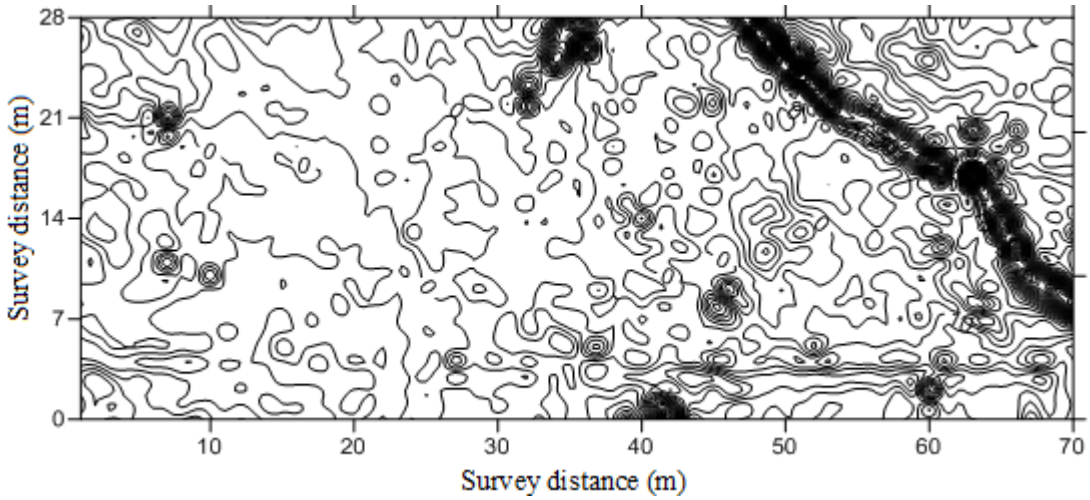


(c)

Fig. A.9: Effects of diurnal correction on Ejuona data
(a) Without diurnal correction
(b) Corrected using polynomial fitting method
(c) Corrected using conventional method
(Magnetic field values in nanotesla, nT)

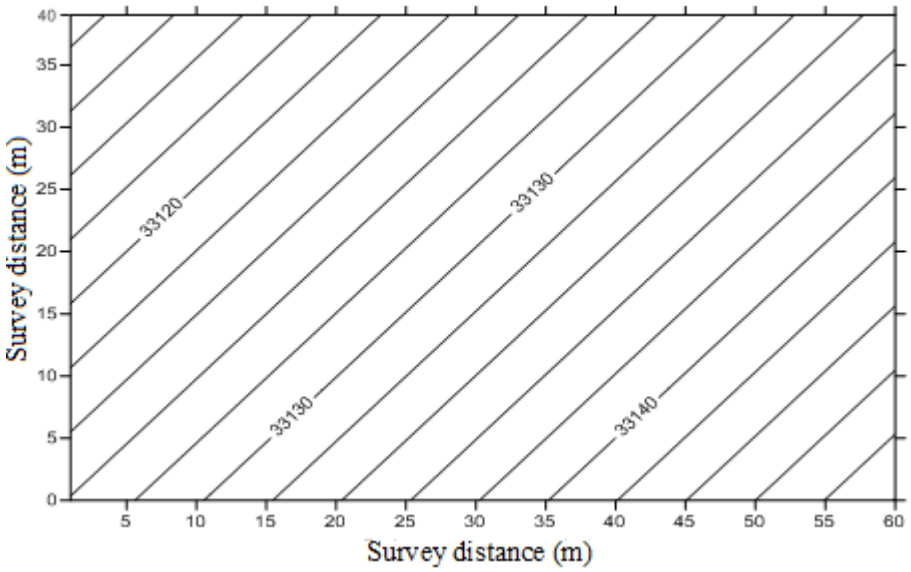


(a)

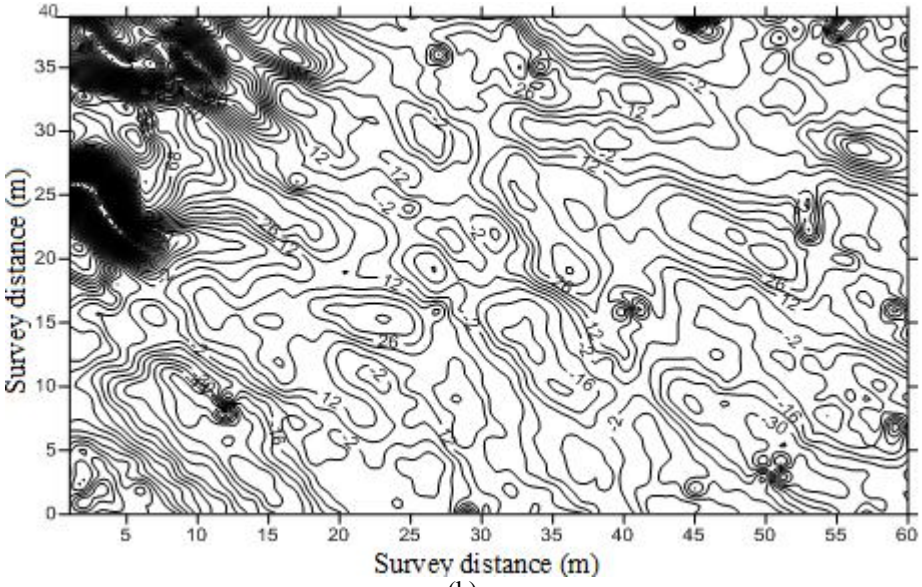


(b)

Fig. A.10: Regional-residual separation (Ugbelenabo data)
(a) Regional magnetic field (b) Residual magnetic field
(Regional field values are in nanotesla, nT)

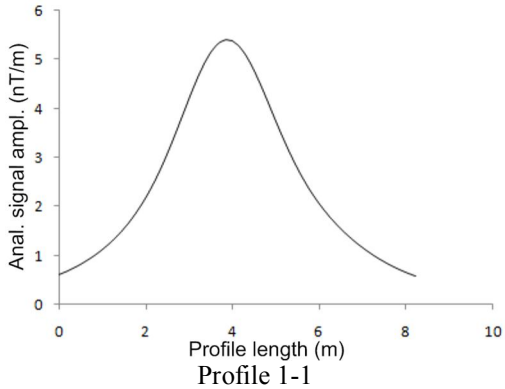


(a)

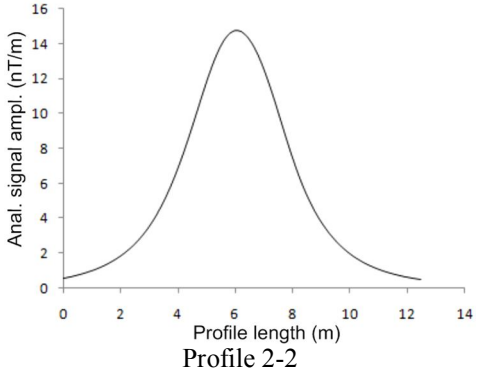


(b)

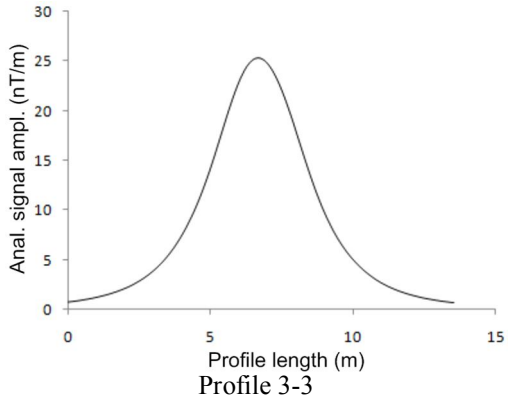
Fig. A.11: Regional-residual separation (Ejuona data)
(a) Regional magnetic field (b) Residual magnetic field
(Magnetic field values in nanotesla, nT)



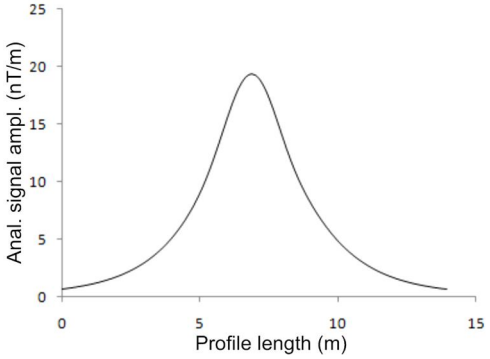
Profile 1-1



Profile 2-2

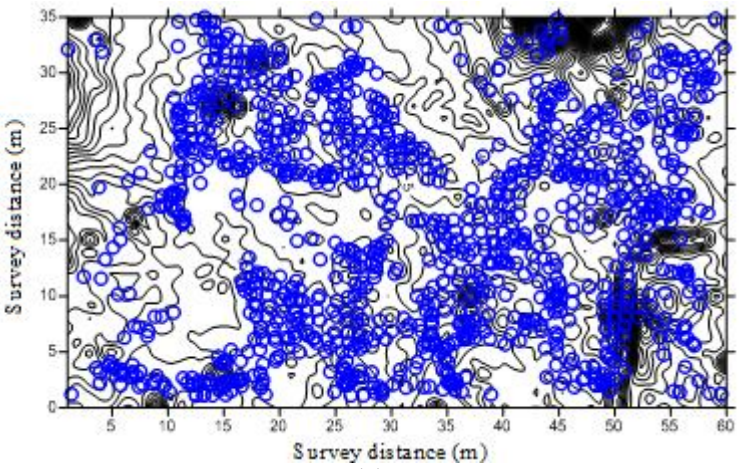


Profile 3-3

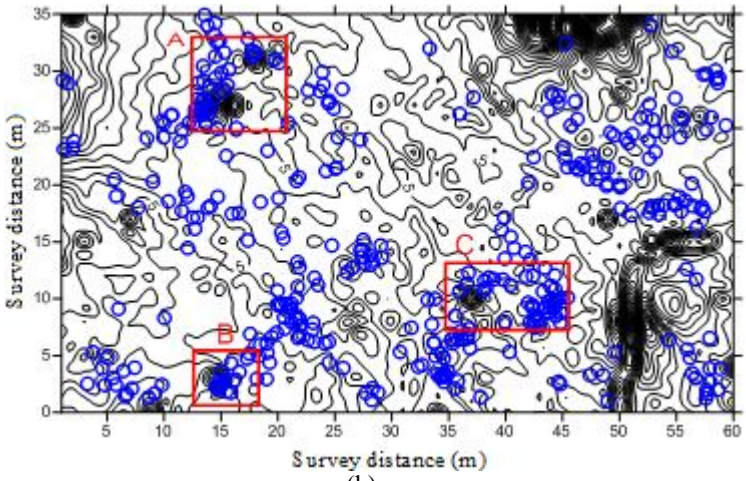


Profile 4-4

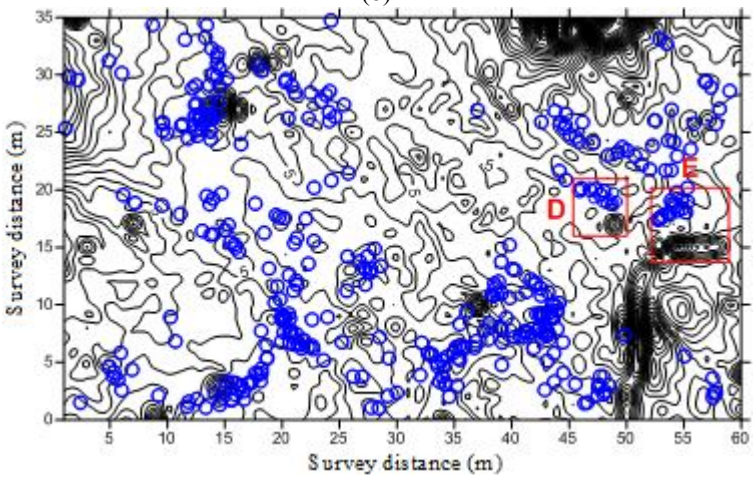
Fig. A.12: Analytic signal amplitude curves for synthetic data with random orientations of the profiles



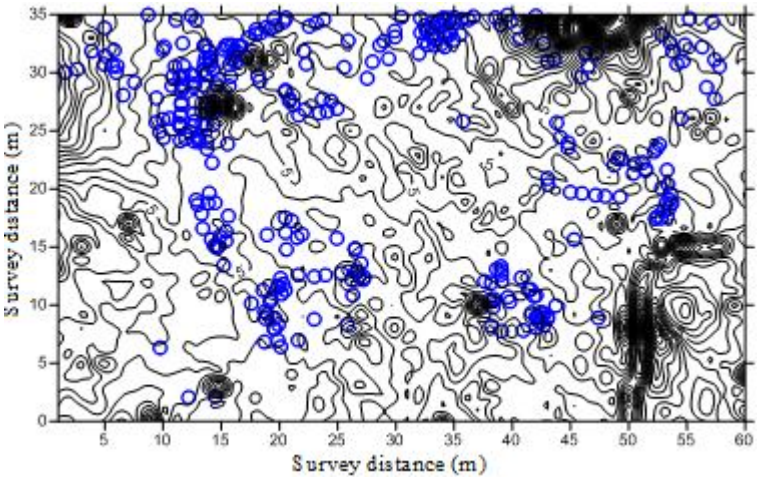
(a)


A
B
C
Survey distance (m)
Survey distance (m)

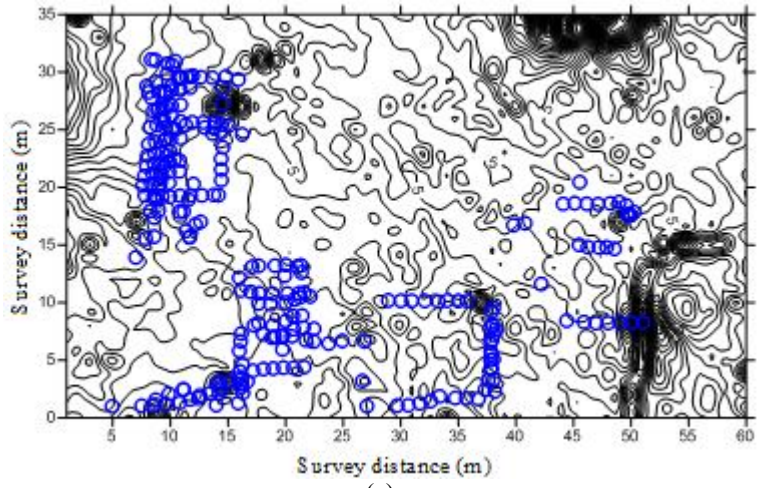
(b)


D
E
Survey distance (m)
Survey distance (m)

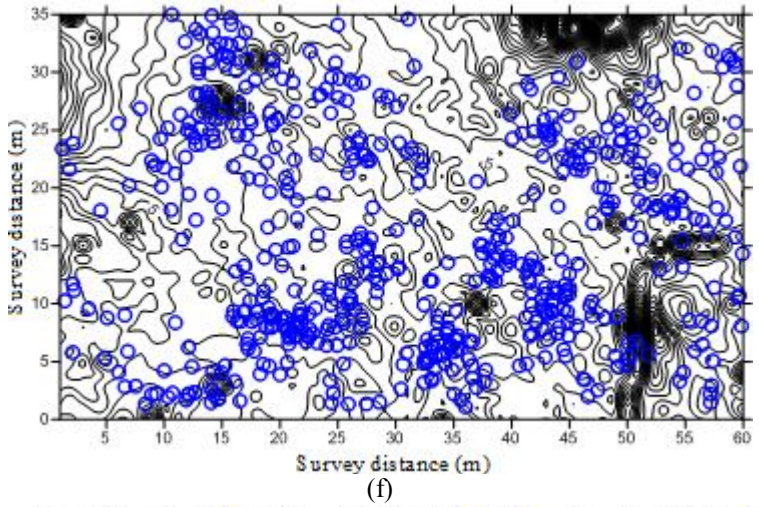
(c)


Survey distance (m)
Survey distance (m)

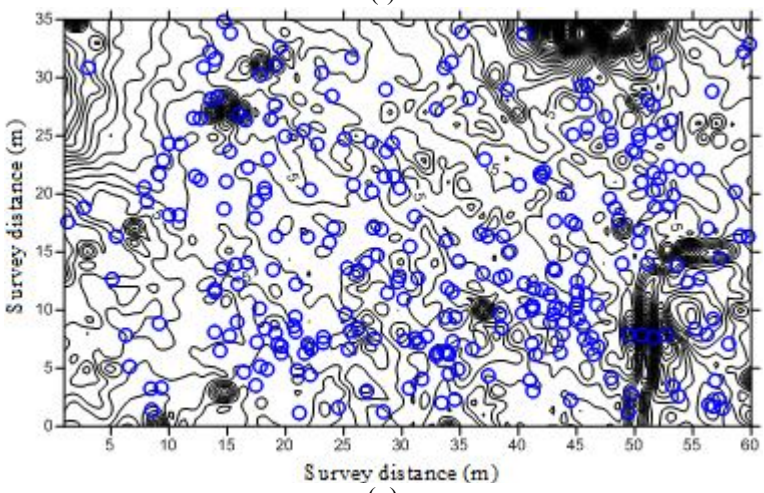
(d)


Survey distance (m)
Survey distance (m)

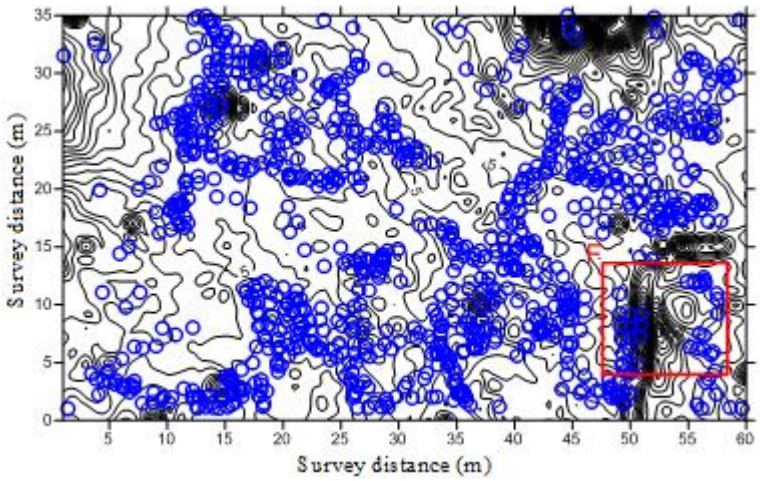
(e)


Survey distance (m)
Survey distance (m)

(f)


Survey distance (m)
Survey distance (m)

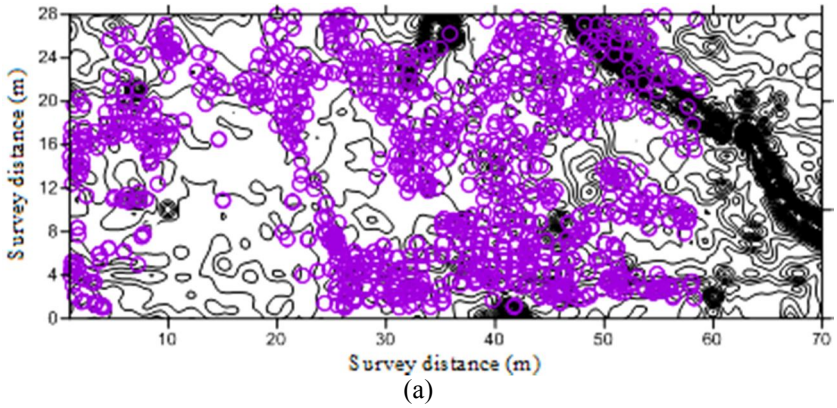
(g)



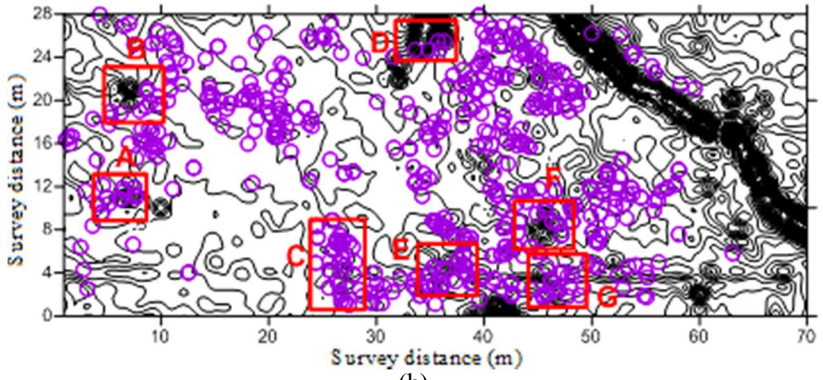
(h)

Fig. A.13: Determination of Optimal Window Size and Estimate of Shape of Magnetic Anomaly Sources (Uwani site)

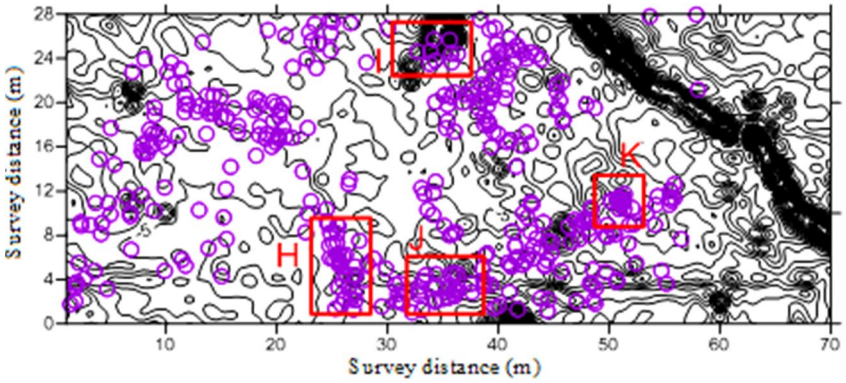
(a) N=0, 3 x 3 (b) N=1, 3 x 3 (c) N=1, 4 x 4 (d) N=1, 5 x 5
(e) N=1, 10 x 10 (f) N=2, 3 x 3 (g) N=3, 3 x 3 (h) N=0.5, 3 x 3
(e.g. 3x3 data points = 2m x 2m; N=0,1,2 and 3 correspond
to contact, dike, cylinder and sphere respectively;
(A, B, C, ..., are source positions)



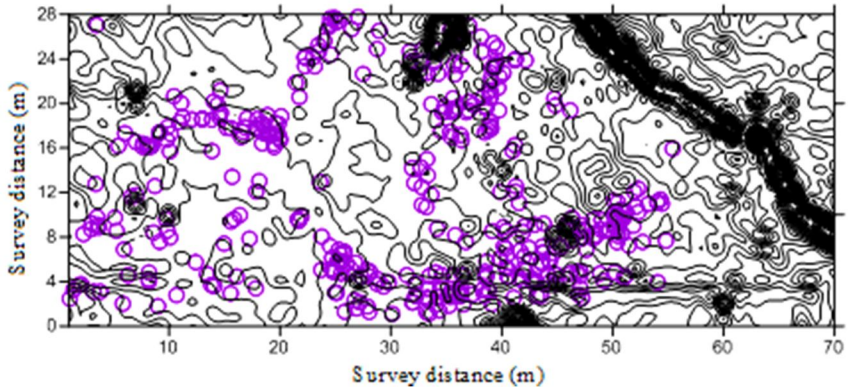
(a)


Survey distance (m)
Survey distance (m)
A
B
C
D
E
F
G

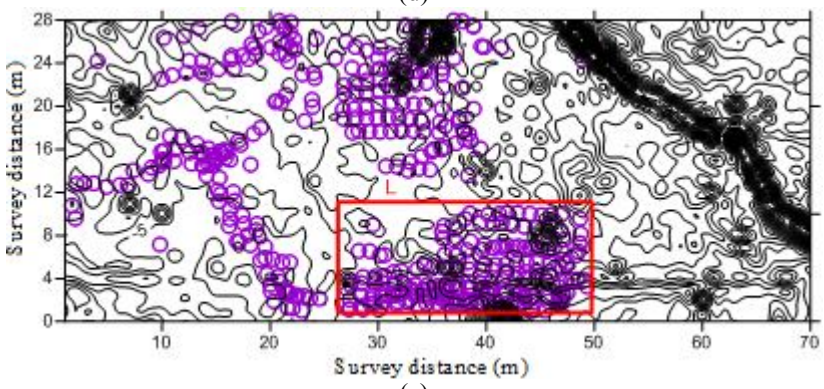
(b)


Survey distance (m)
Survey distance (m)
H
I
J
K

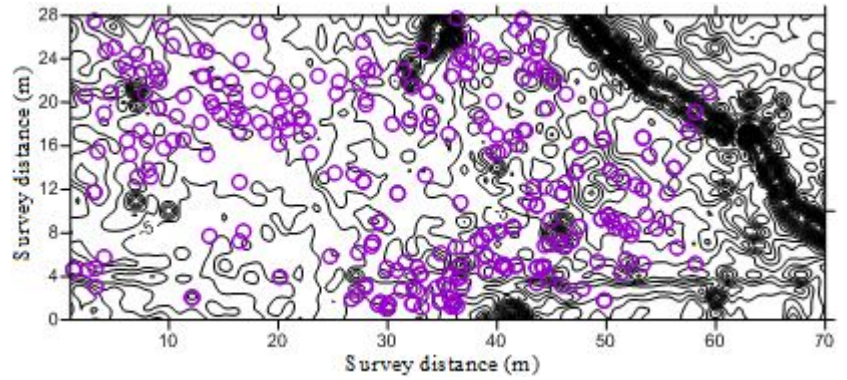
(c)


Survey distance (m)
Survey distance (m)

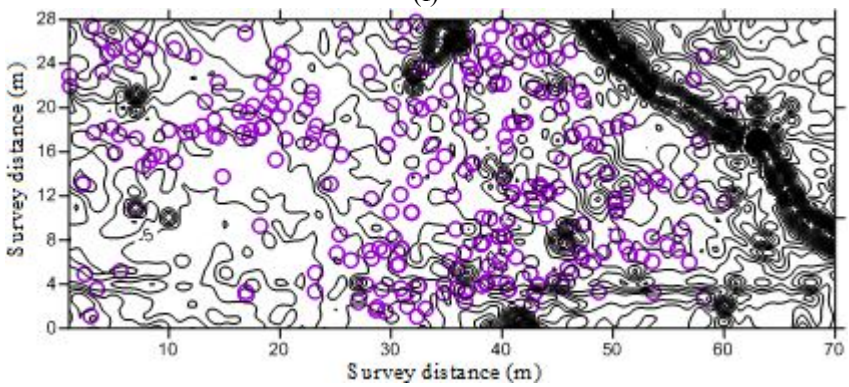
(d)


Survey distance (m)
Survey distance (m)
L

(e)



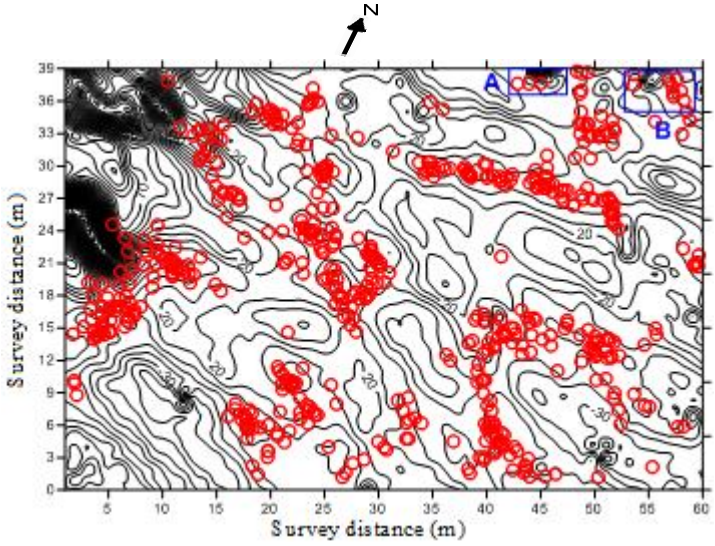
(f)



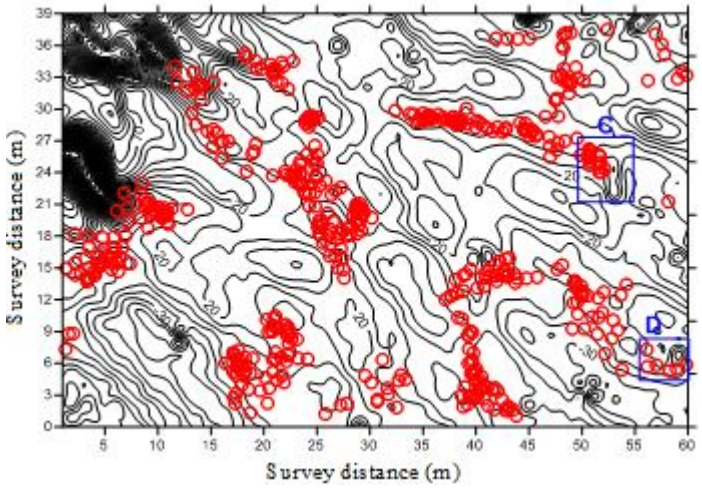
(g)

Fig. A.14: Determination of Optimal Window Size and Estimate of Shape of Magnetic Anomaly Sources (Ugbelenabo site)

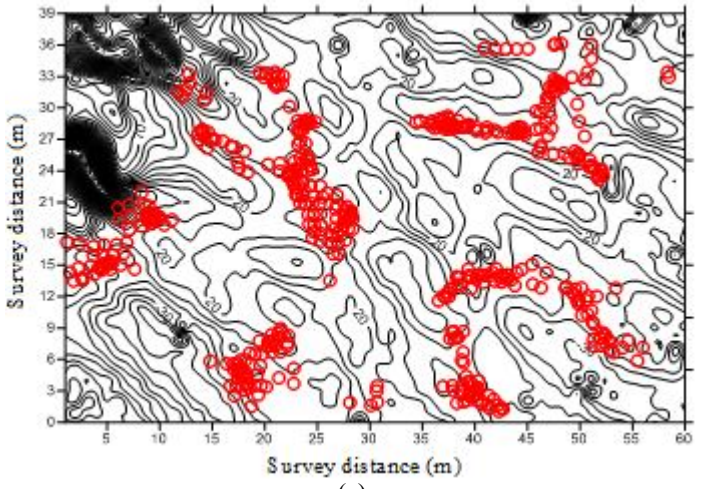
(a) N=0, 3 x 3 (b) N = 1, 3 x 3 (c) N=1, 4 x 4 (d) N=1, 5 x 5
(e) N=1, 10 x 10 (f) N=2, 3 x 3 (g) N=3, 3 x 3



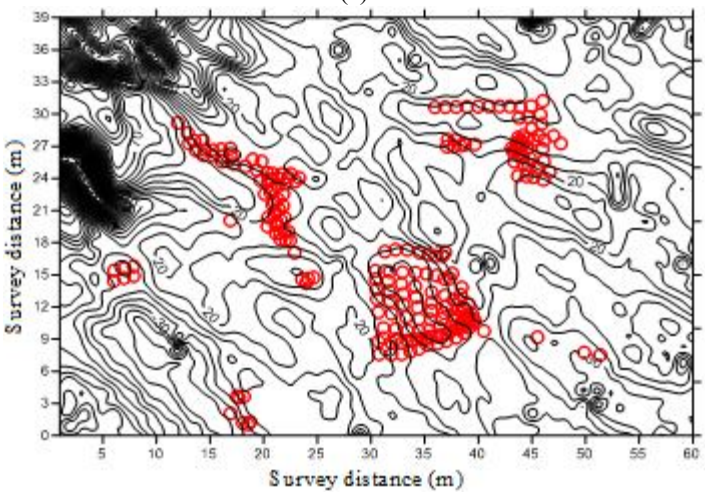
(a)


Survey distance (m)
Survey distance (m)

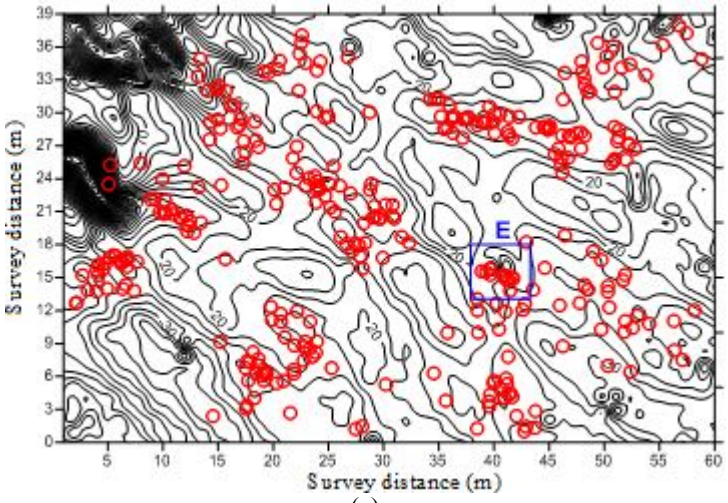
(b)


Survey distance (m)
Survey distance (m)

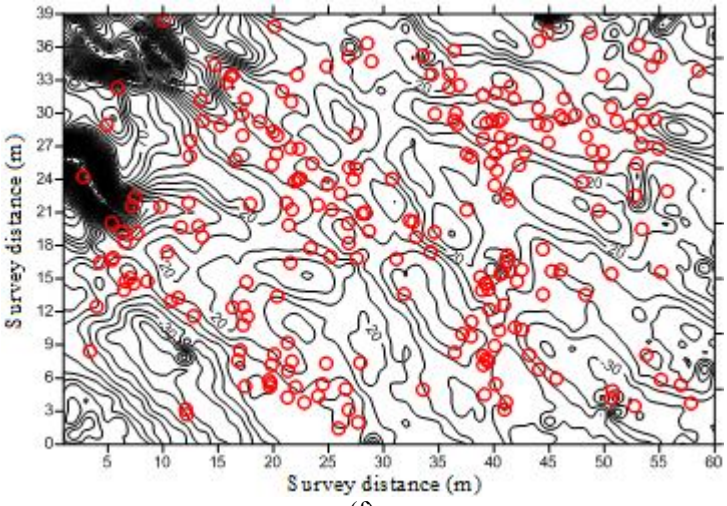
(c)


Survey distance (m)
Survey distance (m)

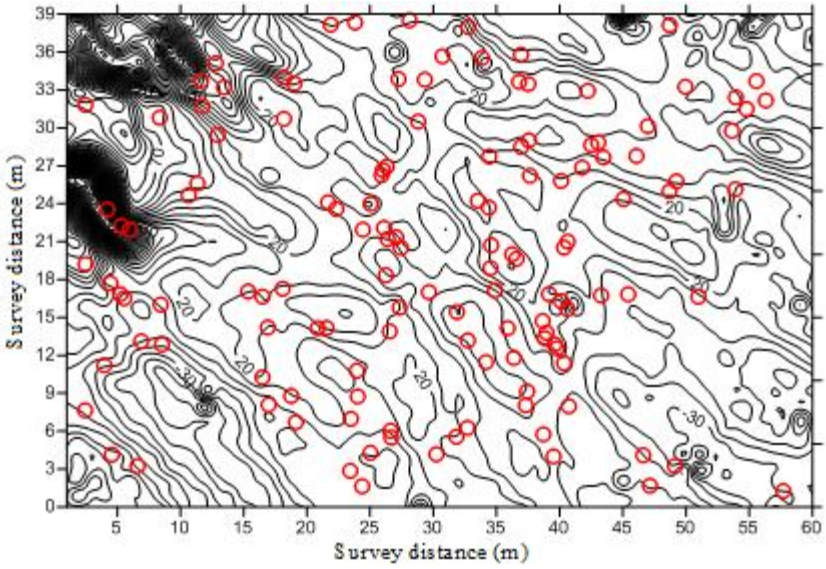
(d)


E
Survey distance (m)
Survey distance (m)

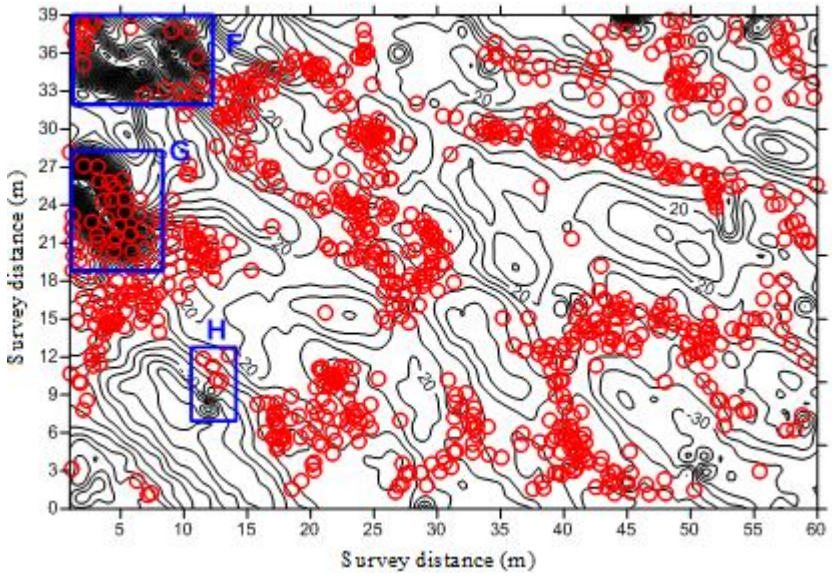
(e)


Survey distance (m)
Survey distance (m)

(f)


Survey distance (m)
Survey distance (m)

(g)



(h)

Fig. A.15: Determination of Optimal Window Size and Estimate of Shape of Magnetic Anomaly Sources (Ejuona site)
(a) N=0, 3 x 3 (b) N=0, 4 x 4 (c) N=0, 5 x 5 (d) N=0, 10 x 10
(e) N=1, 3 x 3 (f) N=2, 3 x 3 (g) N=3, 3 x 3 (h) N=0.5, 3 x 3

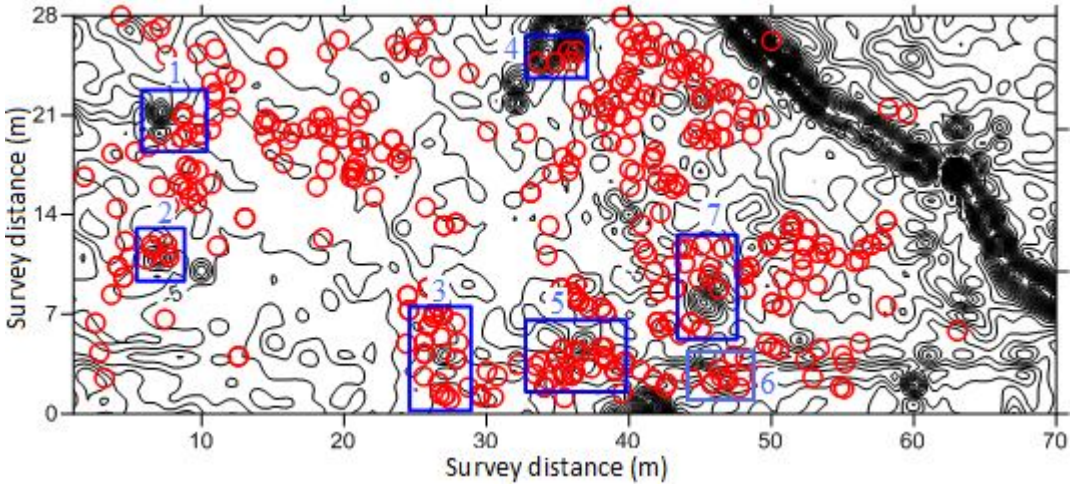


Fig. A.16: Estimation of spatial location of magnetic sources using Euler method (Ugbelenabo)

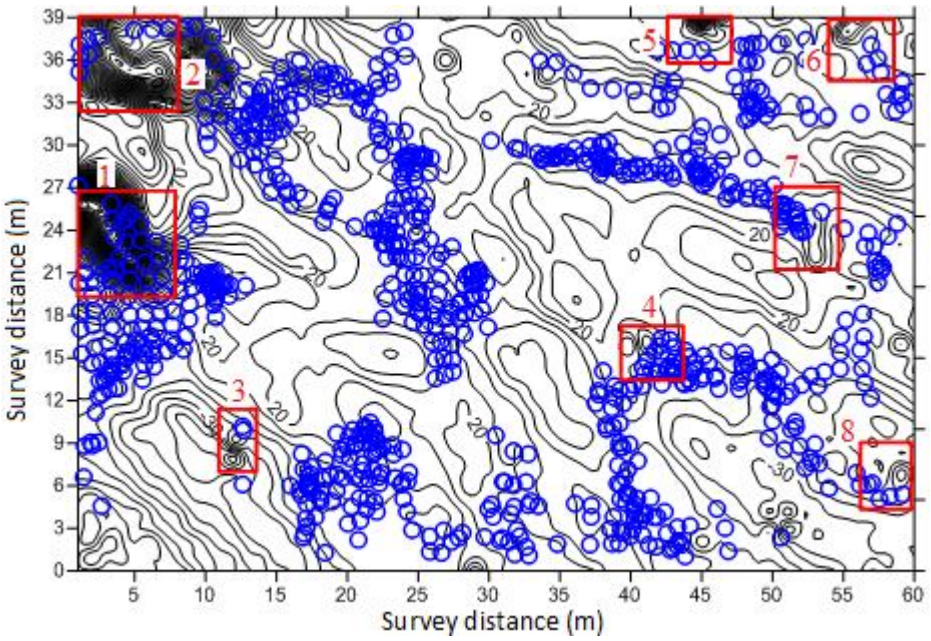


Fig. A.17: Estimation of spatial location of magnetic sources using Euler method (Ejuona)

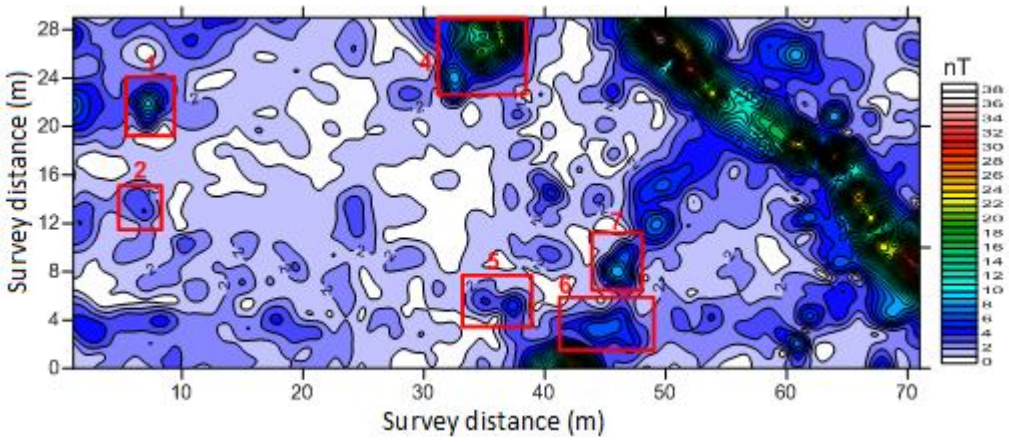


Fig. A.18: Edge mapping of magnetic sources (Ugbelenabo)

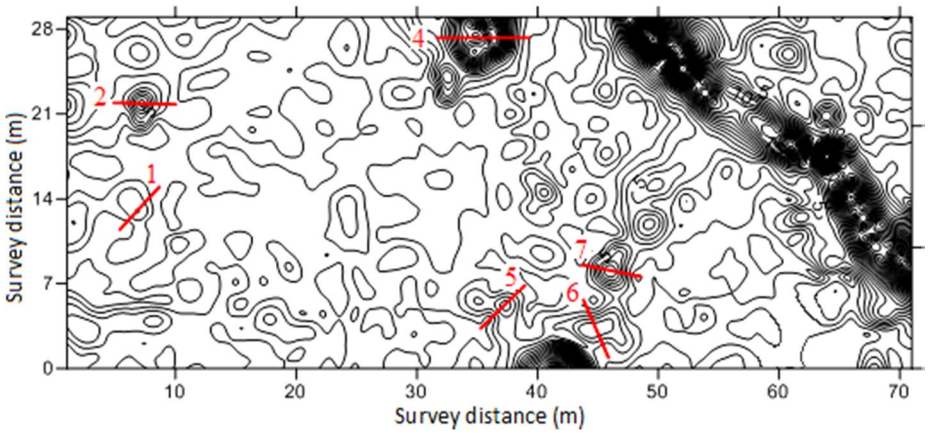
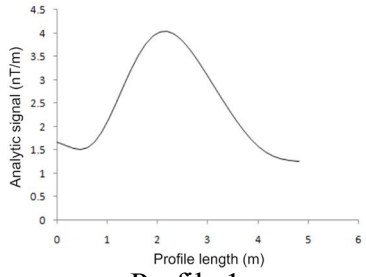
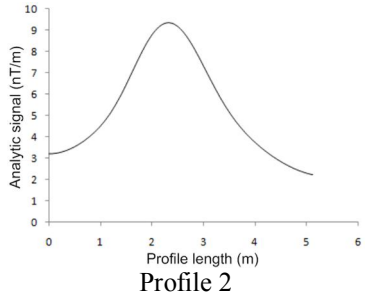


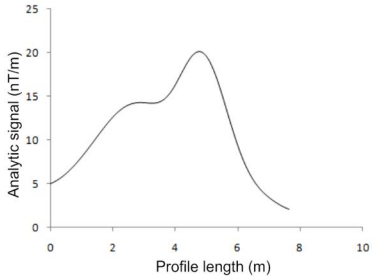
Fig. A.19: Profiles across Ugbelenabo major anomalies for depth estimation using analytic signal method



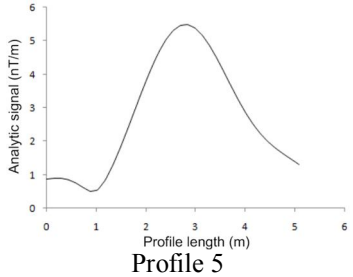
Profile 1



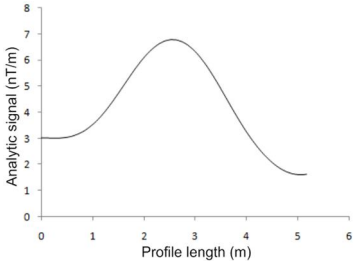
Profile 2



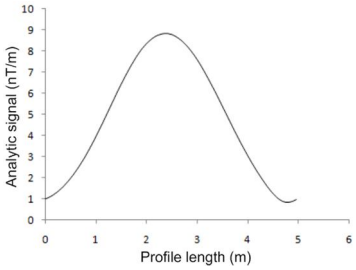
Profile 4



Profile 5



Profile 6



Profile 7

Fig. A.20: Analytic signal amplitude curves for depth calculation (Ugbelenabo)

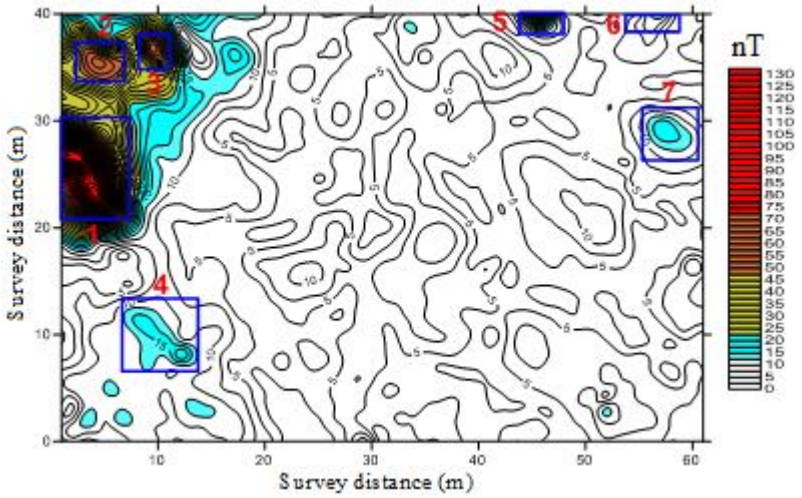


Fig. A.21: Edge mapping of magnetic sources (Ejuona)

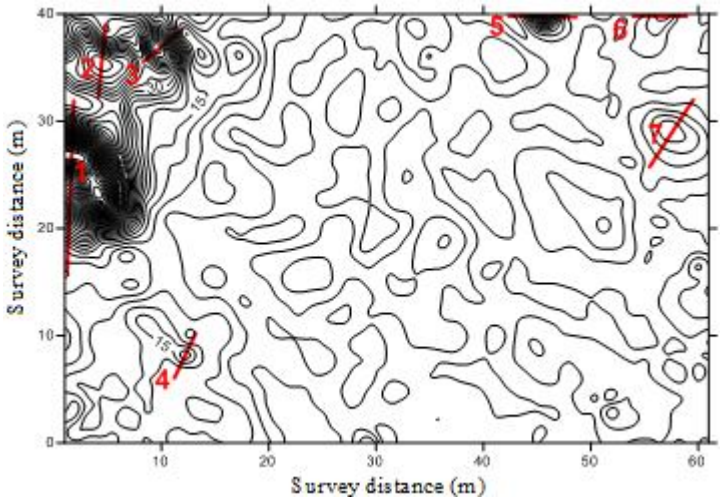
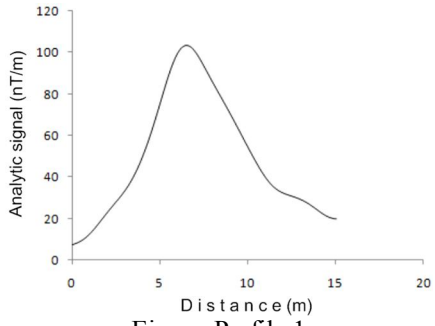
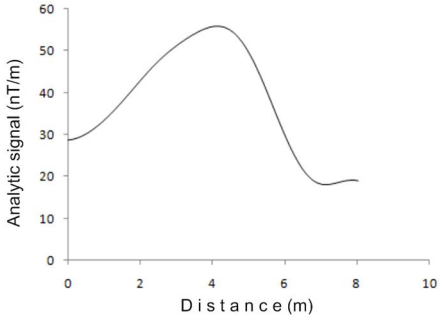


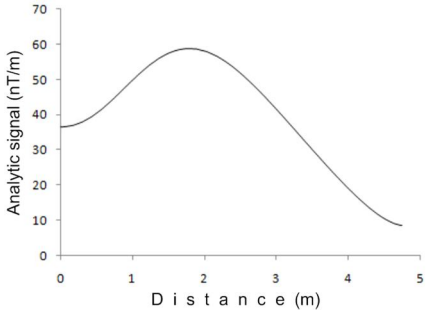
Fig. A..22: Profiles across Ejuona major anomalies for depth estimation (Ejuona)



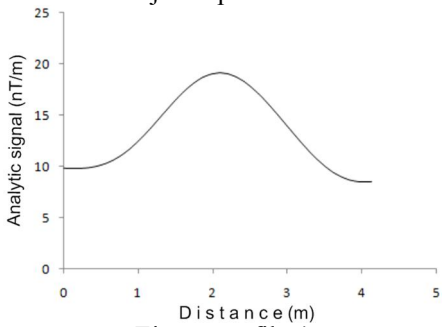
Ejuona Profile 1



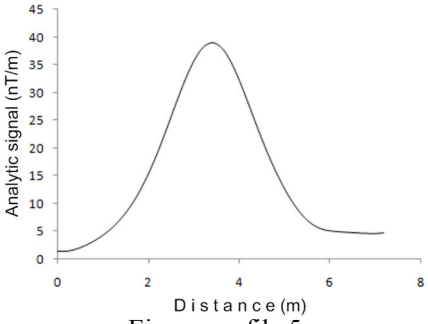
Ejuona profile 2



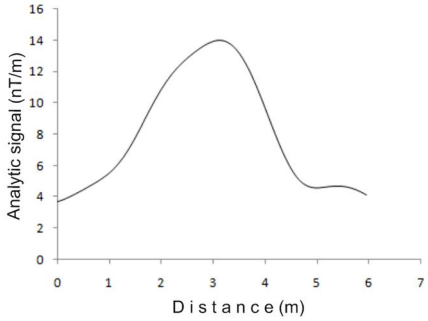
Ejuona profile 3



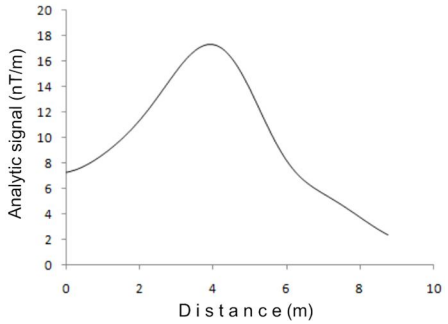
Ejuona profile 4



Ejuona profile 5



Ejuona profile 6



Ejuona profile 7

Fig. A.23: Analytic signal amplitude curves
for depth calculation (Ejuona)

A P P E N D I X B
O T H E R T A B L E S

Table B.1 A portion of the Euler-depth for the 3-body models

S/N	y_o(m)	x_o (m)	z_o (m)	S/N	y_o(m)	x_o (m)	z_o (m)
1	43.55974	12.46047	-0.23524	26	28.58724	26.23938	-1.00019
2	42.18994	4.10841	-1.70518	27	24.52444	26.82460	-0.90041
3	44.19955	5.80549	-0.11219	28	26.62321	25.94040	-1.31515
4	44.78568	13.48308	-0.01948	29	43.21665	17.14626	-1.40205
5	45.01833	13.39572	-0.38034	30	26.84154	27.34353	-0.12622
6	45.25470	13.45834	-0.51807	31	25.72871	28.21066	-0.13043
7	45.45714	13.37094	-0.72948	32	25.49085	27.06737	-1.07779
8	37.92039	24.89606	-0.62492	33	45.26128	14.88982	-0.99635
9	44.55607	13.65098	-1.10396	34	27.29593	26.90767	-1.44021
10	44.42646	13.88143	-1.20927	35	27.33612	27.55769	-1.65991
11	44.26472	14.14286	-1.22393	36	43.04092	17.13596	-1.31865
12	44.01590	14.45517	-1.06212	37	42.64968	16.63640	-0.06363
13	43.65954	14.78996	-0.81843	38	43.53876	16.44385	-0.08566
14	40.51181	15.71183	-0.63107	39	41.43249	16.51618	-1.19381
15	43.31853	15.08790	-0.86181	40	45.05182	16.54445	-1.10596
16	43.28257	15.35949	-0.06318	41	40.28867	14.99868	-0.47013
17	40.42015	14.52462	-0.30040	42	45.30478	16.49883	-0.84941
18	40.99546	14.68231	-1.47372	43	45.97329	16.39089	-1.67865
19	24.10040	20.66788	-0.54390	44	42.24396	15.57757	-1.15562
20	12.27910	19.75949	-1.87840	45	41.63448	14.28540	-0.34541
21	9.48475	17.92268	-1.86944	46	45.37681	16.41562	-0.33262
22	8.22471	18.22596	-0.63868	47	45.78648	16.35229	-0.84280
23	9.75663	18.01595	-0.87618	48	46.02801	16.34860	-1.25375
24	40.44541	15.92798	-1.97579	49	9.98500	21.34267	-1.67282
25	41.58508	15.95019	-0.51737	50	40.15232	17.31921	-1.84851

Table B.2 A portion of the Euler-depth for the 4-body models

S/N	y_o(m)	x_o(m)	z_o(m)	S/N	y_o(m)	x_o(m)	z_o(m)

1	30.96858	4.58939	-1.45410	26	47.36184	16.61945	-1.36813
2	31.73813	8.01927	-0.71753	27	49.03658	19.07167	-0.78057
3	48.86937	13.19822	-1.51327	28	10.73709	23.17076	-1.56983
4	32.56665	9.07230	-0.69863	29	11.56768	23.80080	-1.14911
5	29.64409	8.66197	-0.86011	30	10.94673	24.01020	-1.07394
6	30.98154	9.43813	-0.91894	31	11.25631	23.86000	-1.01235
7	48.67195	13.94053	-0.60797	32	11.23676	23.47395	-1.17153
8	28.60980	8.61220	-0.73063	33	11.72744	23.26992	-1.03786
9	49.03957	14.08957	-0.86681	34	16.02474	24.13335	-0.71034
10	26.89590	9.40065	-1.18187	35	13.26712	23.22784	-1.46896
11	49.53819	14.98304	-0.99548	36	14.12074	22.77505	-0.94799
12	49.56724	15.55801	-1.47168	37	12.27755	23.53412	-1.28860
13	48.77797	17.35748	-0.82105	38	14.27205	23.59040	-1.03643
14	26.55263	11.31880	-0.62314	39	48.67851	20.03664	-1.02368
15	30.84687	10.97668	-1.17580	40	45.97068	19.45398	-1.10277
16	28.91092	10.44237	-0.45771	41	48.88401	20.30346	-1.54481
17	27.5433	9.304482	-0.42997	42	15.69549	26.59318	-1.57114
18	17.49413	20.76601	-1.49561	43	25.61663	24.06896	-1.43992
19	30.10902	11.43527	-1.23792	44	15.42763	27.07591	-1.37602
20	16.25708	21.60755	-1.51339	45	26.65235	35.26476	-0.91962
21	14.47956	23.41332	-0.84876	46	24.14974	34.49236	-1.27746
22	11.36739	23.49720	-0.99814	47	26.46682	33.50520	-0.79072
23	10.53964	23.45247	-0.74431	48	28.84048	28.96338	-0.44893
24	10.42491	23.65865	-0.52510	49	29.79929	30.80015	-1.22174
25	11.11617	23.36219	-0.52969	50	49.30729	20.93132	-0.68399

Table B.3 Computed parameters and F_o statistics for right choice of models (Ugbelenabo site)

Day-1

Order of Polynomial	c_o	c_1	c_2	c_3	c_4	c_5	σ	σ^2	F_o
2	33182	11.27	-1.94				±4.92	24.24	
3	33173	24.22	-5.85	0.31			±3.08	9.47	2.56
4	33178	12.63	0.63	-0.91	0.07		±2.87	8.22	1.15
5	33181	0.10	11.76	-4.51	0.56	-0.02	±2.74	7.53	1.09

Day-2

2	33174	5.03	-1.00				±4.55	20.70	
3	33164	18.34	-4.87	0.30			±1.77	3.12	6.63
4	33167	10.91	- 0.89	-0.42	0.04		±1.32	1.74	1.79
5	33168	7.03	2.36	-1.43	0.17	-0.01	±2.29	5.23	0.33

Table B.4 Computed parameters and F_o statistics for right choice of models (Ejuona site)

Day-1

Order of Polynomial	c_o	c_1	c_2	c_3	c_4	c_5	σ	σ^2	F_o
2	33150	14.22	-1.67				±2.97	8.82	
3	33152	11.16	-0.71	-0.08			±2.88	8.29	1.06
4	33153	7.00	1.68	-0.54	0.03		±3.02	9.11	0.91
5	33156	-2.72	10.62	-3.55	0.45	0.02	±9.39	88.08	0.10

Day-2

2	33153	5.64	-0.87				±1.62	2.61	
3	33151	7..67	-1.47	0.05			±1.51	2.27	1.15
4	33151	7.55	- 1.40	0.04	0.00		±2.16	4.65	0.49
5	33152	2.29	3.38	-1.56	0.22	-0.01	±8.89	79.02	0.06

Table B.5 A Sample of Computed Euler Depth for Uwani

S/N	y_o(m)	x_o (m)	z_o (m)	S/N	y_o(m)	x_o (m)	z_o (m)
1	5.03916	4.88718	-1.38558	31	12.08723	14.44841	-1.19644

2	16.12683	2.83511	-1.20832	32	24.47589	4.38572	-1.17652
3	15.04624	3.61408	-0.50949	33	20.58776	7.37325	-1.43912
4	17.49278	5.18195	-1.19051	34	22.63869	6.36411	-0.86164
5	34.39695	3.19108	-1.16734	35	35.35333	6.06539	-1.35889
6	34.74495	3.12850	-0.75473	36	36.12418	6.43518	-1.14185
7	56.39425	3.45362	-0.58272	37	35.82191	6.38556	-1.12324
8	57.58889	1.23821	-0.57407	38	40.33421	5.32117	-1.4073
9	4.807319	2.41150	-1.35130	39	57.96338	2.69989	-0.57878
10	18.14073	2.96510	-0.91314	40	36.68089	6.88404	-1.41937
11	28.80054	1.75051	-1.09548	41	42.91325	8.14817	-1.25060
12	27.72997	1.71592	-0.55887	42	42.54212	8.04627	-0.63795
13	35.51170	2.10142	-1.17285	43	42.11842	7.91173	-0.69033
14	48.95932	1.00070	-1.34637	44	55.92156	5.53367	-1.19593
15	14.77047	2.30819	-0.55130	45	42.95017	7.61621	-1.25535
16	15.88606	1.74843	-0.74964	46	42.5345	7.45177	-0.95814
17	15.49315	1.83387	-0.99052	47	42.39061	7.69799	-1.03866
18	31.72495	7.44511	-1.02050	48	43.71200	8.72706	-1.39280
19	7.17824	2.09593	-1.33409	49	44.24066	9.10922	-1.46495
20	15.33135	2.91132	-0.90825	50	21.62944	10.07556	-1.19312
21	19.27625	4.38548	-1.48622	51	42.55505	8.49032	-0.79123
22	19.06666	5.26213	-1.37305	52	42.34866	9.20598	-0.62763
23	32.67962	4.17299	-1.29874	53	42.37031	9.43416	-0.65978
24	39.92893	7.97589	-0.97889	54	21.04388	9.34164	-0.97363
25	49.54513	5.28578	-1.46071	55	39.76765	11.67977	-0.61271
26	35.23747	6.45524	-1.33519	56	41.97068	9.64222	-0.72164
27	36.10785	7.19622	-0.98060	57	43.72713	9.75833	-1.48059
28	35.56421	8.49122	-1.04008	58	44.24809	9.64156	-1.23451
29	58.84892	3.83653	-0.91691	59	20.73138	9.55584	-1.48218
30	57.91788	6.54354	-1.46269	60	38.13573	11.58020	-1.05243

Table B.6 A Sample of Computed Euler Depths for Ugbelenabo

S/N	y_o(m)	x_o (m)	z_o (m)	S/N	y_o(m)	x_o (m)	z_o (m)
1	26.97513	1.69037	-1.18979	31	46.27136	2.26667	-1.34514
2	28.23793	1.28856	-0.21799	32	43.84000	2.07762	-0.51246
3	26.72470	1.26601	-0.28745	33	41.18926	2.99655	-0.10812
4	29.64334	1.17542	-0.47937	34	54.88162	2.01767	-1.18817
5	30.59966	1.13676	-0.29208	35	49.22414	2.06252	-1.31114
6	37.28677	2.76960	-0.53733	36	2.843409	4.24245	-0.64266
7	48.74072	2.34072	-0.82298	37	24.29520	4.74433	-0.40238
8	50.24073	3.81387	-1.18509	38	26.41219	5.12325	-0.48159
9	47.23445	2.71449	-1.27142	39	28.02372	4.80620	-1.05901
10	48.94035	3.34380	-0.21486	40	31.77255	3.57893	-0.89006
11	61.05418	4.85031	-1.43856	41	34.03006	2.29708	-1.51128
12	53.70820	3.86071	-0.50518	42	35.31750	2.89753	-0.40501
13	56.36289	4.19252	-0.84078	43	35.97783	2.95345	-0.21741
14	26.05654	5.51419	-0.28658	44	38.14962	4.04679	-1.11157
15	26.49459	2.14996	-1.33371	45	43.48068	5.26175	-1.47022
16	29.81645	2.80856	-1.20826	46	52.32313	2.83899	-1.24558
17	35.37227	1.29765	-0.96497	47	50.26469	4.54345	-0.37416
18	34.70420	2.26272	-0.85666	48	23.16071	7.65530	-0.49584
19	34.16909	3.11193	-0.52721	49	35.26212	4.64800	-0.33988
20	38.24406	4.12223	-0.64992	50	36.18195	4.54219	-0.28558
21	39.60433	3.18769	-0.28823	51	5.801547	8.86897	-1.08659
22	39.62688	1.54645	-1.14672	52	26.09289	7.20121	-0.68525
23	46.72478	2.34842	-0.25494	53	25.74000	6.13235	-1.33854
24	46.57509	2.46664	-0.34974	54	48.29289	9.04700	-0.35605
25	45.91730	2.40255	-0.33388	55	50.05267	7.42960	-0.73552
26	55.53098	3.25709	-0.66003	56	50.80547	7.23879	-0.81044
27	26.57066	1.71842	-1.15661	57	2.23090	6.51220	-0.41098
28	35.28701	3.73046	-0.89865	58	24.30940	4.79456	-0.16394
29	38.38432	3.61407	-0.71424	59	25.84872	7.05868	-0.68617
30	39.56683	3.55709	-1.31001	60	24.63951	7.22688	-1.30292

Table B.7 A Sample of Computed Euler Depths for Ejuona

S/N	y_o(m)	x_o (m)	z_o (m)	S/N	y_o(m)	x_o (m)	z_o (m)
1	2.66968	4.57394	-1.97306	31	16.89337	2.35412	-1.29748
2	18.42976	1.28125	-1.37030	32	17.15191	3.13071	-1.15597
3	30.74448	2.15486	-1.50216	33	17.74690	3.78744	-0.71360
4	30.92385	2.31149	-1.50904	34	20.04143	3.33035	-1.33919
5	32.60716	1.68643	-1.35055	35	20.92361	3.55627	-0.87933
6	39.17514	1.93408	-1.20513	36	24.58158	2.88700	-1.74836
7	39.96432	2.43928	-0.53330	37	25.81352	2.44152	-1.70974
8	41.26934	1.83455	-0.60171	38	26.78972	2.84180	-1.70233
9	42.78605	1.48117	-0.57429	39	27.85721	2.33190	-1.23141
10	43.83651	1.03138	-0.72315	40	29.68358	2.39207	-1.51427
11	16.97512	2.62772	-1.32008	41	31.81127	1.17418	-1.62720
12	17.07449	3.70081	-1.55127	42	32.81089	1.08204	-1.73413
13	20.78152	2.19349	-1.38464	43	32.16830	2.43619	-1.99151
14	25.82556	1.34881	-1.16498	44	37.21353	3.81650	-1.72092
15	26.64743	1.27257	-1.73941	45	38.52327	2.96811	-0.71469
16	27.35273	2.04787	-1.45508	46	39.30506	2.92379	-0.70302
17	31.42041	2.04664	-1.74013	47	40.12630	2.91507	-0.73473
18	30.28021	3.81780	-0.75786	48	40.64393	3.56612	-0.78157
19	29.95345	4.35237	-0.73052	49	42.54662	2.65570	-0.89145
20	31.94554	2.90453	-1.47838	50	43.58459	1.84765	-0.59334
21	34.82211	1.90046	-1.81751	51	43.36420	2.12238	-0.76278
22	37.12174	1.85293	-1.95574	52	46.64866	3.02004	-1.87523
23	38.66959	1.91650	-1.15762	53	50.59597	2.35291	-1.92797
24	39.43145	2.68525	-0.45367	54	59.19598	5.39624	-0.83829
25	40.81792	2.54144	-0.32307	55	56.74261	6.07372	-1.55273
26	41.78533	1.70451	-1.08361	56	17.13250	4.73232	-1.40015
27	42.96180	1.61435	-0.87746	57	18.05197	5.10467	-0.16367
28	43.24336	1.81960	-0.83280	58	18.13851	4.93125	-0.06770
29	46.87776	1.38988	-1.56061	59	18.92700	4.88834	-1.00727
30	1.407836	6.60412	-1.01367	60	20.28923	4.52849	-0.94778

Table B.8 Magnetic source locations using Euler method (Ugbelenabo)

Anomaly number	x (m)	error ±(m)	y (m)	error ±(m)	depth(m) (m)	error ±(m)
1	6.04	0.72	11.09	1.33	0.92	0.11
2	8.19	0.98	20.20	2.42	0.72	0.09
3	25.94	3.11	5.00	0.60	0.85	0.10
4	34.87	4.18	25.17	3.02	0.79	0.09
5	36.35	4.36	3.39	0.41	0.58	0.07
6	44.60	5.35	2.49	0.30	0.76	0.09
7	46.62	5.59	8.52	1.02	0.83	0.10

Table B.9 Magnetic source locations using Euler method (Ejuona)

Anomaly number	x (m)	error ±(m)	y (m)	error ±(m)	depth (m)	error ±(m)
1	4.11	0.49	22.08	2.65	1.73	0.21
2	3.11	0.37	37.13	4.46	1.88	0.23
3	10.10	1.21	39.20	4.70	1.50	0.18
4	12.91	1.55	10.09	1.21	1.12	0.13
5	43.93	5.27	37.62	4.51	1.50	0.18
6	57.37	6.88	37.42	4.49	1.45	0.17
7	51.56	6.19	25.78	3.09	0.89	0.11

Table B.10 Magnetic source locations using analytic signal method (Ugbelenabo)

Anomaly number	x (m)	y (m)	depth (m)	error ±(m)	dist. across source (m)
1	6.83	13.04	0.79	0.11	0.48
2	7.20	21.91	0.71	0.10	1.22
3	-	-	-	-	-
4	36.36	27.02	0.85	0.12	3.28
5	37.34	5.26	0.66	0.09	0.95
6	44.51	3.20	0.85	0.12	2.01
7	45.97	8.06	0.75	0.10	1.22

Table B.11 Magnetic source locations using analytic signal method (Ejuona)

Anomaly number	x (m)	y (m)	depth (m)	error ±(m)	dist. across anomaly(m)
1	4.02	23.33	1.76	0.24	6.60
2	4.44	35.42	1.76	0.24	3.07
3	9.52	38.82	1.20	0.08	1.92
4	12.15	8.23	1.04	0.14	1.04
5	45.58	39.79	1.56	0.21	1.27
6	56.74	39.90	1.42	0.12	1.27
7	57.25	29.27	0.84	0.15	3.59